

DOCTORAL THESIS

Microbial Interactions with Inanimate Solid Surfaces: A Methodological Approach

Merilin Rosenberg

TALLINN UNIVERSITY OF TECHNOLOGY
DOCTORAL THESIS
6/2022

Microbial Interactions with Inanimate Solid Surfaces: A Methodological Approach

MERILIN ROSENBERG



TALLINN UNIVERSITY OF TECHNOLOGY

School of Science

Department of Chemistry and Biotechnology

This dissertation was accepted for the defence of the degree 28/02/2022

Supervisor:

Prof Angela Ivask
Institute of Molecular and Cell Biology
University of Tartu

Co-supervisor:

Dr Kaja Kasemets
Laboratory of Environmental Toxicology
National Institute of Chemical Physics and Biophysics

Associate Prof Vambola Kisand
Institute of Physics
University of Tartu

Opponents:

Prof Joanna Verran
Department of Life Sciences
Manchester Metropolitan University

Associate Prof Niilo Kaldalu
Institute of Technology
University of Tartu

Defence of the thesis: 29/03/2022, Tallinn

Declaration:

Hereby I declare that this doctoral thesis, my original investigation and achievement, submitted for the doctoral degree at Tallinn University of Technology has not been submitted for doctoral or equivalent academic degree.

Merilin Rosenberg

signature



European Union
European Regional
Development Fund



Investing
in your future

Copyright: Merilin Rosenberg, 2022

ISSN 2585-6898 (publication)

ISBN 978-9949-83-794-6 (publication)

ISSN 2585-6901 (PDF)

ISBN 978-9949-83-795-3 (PDF)

Printed by Koopia Niini & Rauam

TALLINNA TEHNIKAÜLIKOOL
DOKTORITÖÖ
6/2022

Mikroobide interaktsioonid tahkete eluta pindadega: metoodiline käsitus

MERILIN ROSENBERG



Contents

List of Publications	6
Author's Contribution to the Publications	7
Introduction	8
Abbreviations	9
1 REVIEW OF THE LITERATURE.....	11
1.1 Microbial lifestyles	11
1.1.1 The biofilm life cycle	13
1.2 Antimicrobial surfaces.....	15
1.2.1 Interactions between antimicrobial surfaces and microbes.....	15
1.2.2 Antimicrobial mechanisms of metal-based surfaces	17
1.2.3 Antimicrobial surface testing	20
2 AIMS OF THE STUDY.....	27
3 MATERIALS AND METHODS	28
4 RESULTS AND DISCUSSION.....	29
4.1 Bacterial biosensors in rapid in situ screening of copper-based antibacterial surfaces (Publication I).....	30
4.2 <i>In situ</i> biofilm viability staining with propidium iodide (Publication II).....	32
4.3 Antimicrobial and antibiofilm properties of solid surfaces coated with nano-ZnO or nano-ZnO/Ag (Publications III, IV).....	35
5 CONCLUSIONS	38
References	39
Acknowledgements.....	54
Abstract.....	55
Lühikokkuvõte.....	57
Appendix	59
Publication I	59
Publication II	79
Publication III	107
Publication IV	129
Curriculum vitae.....	153
Elulookirjeldus.....	155

List of Publications

The list of author's publications, on the basis of which the thesis has been prepared:

- I **Rosenberg M**, Vija H, Kahru A, Keevil C W, Ivask A
Rapid in situ assessment of Cu-ion mediated effects and antibacterial efficacy of copper surfaces.
Scientific Reports, 2018; 8(1).
DOI: 10.1038/s41598-018-26391-8
- II **Rosenberg M**, Azevedo N F, Ivask A
Propidium iodide staining underestimates viability of adherent bacterial cells.
Scientific Reports, 2019; 9(1).
DOI: 10.1038/s41598-019-42906-3
- III Visnapuu M, **Rosenberg M**, Truska E, Nõmmiste E, Šutka A, Kahru A, Rähn M, Vija H, Orupõld K, Kisand V, Ivask A
UVA-induced antimicrobial activity of ZnO/Ag nanocomposite covered surfaces.
Colloids and Surfaces B: Biointerfaces, 2018; 169: 222–232.
DOI: 10.1016/j.colsurfb.2018.05.009
- IV **Rosenberg M**, Visnapuu M, Vija H, Kisand V, Kasemets K, Kahru A, Ivask A
Selective anti-biofilm properties and biocompatibility of nano-ZnO and nano-ZnO/Ag coated surfaces.
Scientific Reports, 2020; 10(1).
DOI:10.1038/s41598-020-70169-w

Author's Contribution to the Publications

- I I participated in experimental design, performed experimental work, analysed the data, and participated in writing the manuscript.
- II I designed and performed the experiments, analysed the data, and wrote the manuscript.
- III I designed and performed the antimicrobial experiments, analysed the data, and participated in writing the manuscript.
- IV I designed and performed the biofilm experiments, analysed the data, and wrote most of the manuscript.

Introduction

Increasing urban population density, affordable international transport and global production chains have increased the risk of potential pathogen spread from person to person and via high-touch surfaces in public spaces or high-risk applications over long distances. Increase in antibiotic-resistant nosocomial infections at health care facilities as well as risk of potential food-borne pathogen contamination in food and feed industry have also significantly raised the need to widen the means to reduce potential pathogen carryover. One of the solutions that could passively decrease the spread of pathogens is installing antimicrobial materials (*e.g.*, solid surfaces, surface coatings, textiles) at the critical points of cross-contamination such as handrails, doorknobs, countertops, keyboards, furniture *etc.* Antimicrobial materials are widely marketed as consumer products but have not yet dominated the market nor are massively applied where they could be of most use.

One of the reasons of moderate use of antimicrobial surface applications is the hardship of justifying the higher price of materials with reliable application-appropriate efficacy data. Although such data is legally needed to support antimicrobial claims on commercial products, relevant methodology is largely lacking, and protocols deeply rooted in laboratory practice or more elaborate standardized tests not tailored to specific applications are still widely used. These shortcomings are mostly caused by two main reasons. Firstly, the use of methods that rely on liquid exposure of active agents to bacterial cultures and cannot be directly adapted to 2D surface testing. Secondly, most methods specifically developed for surface testing are optimized for best case scenario of antimicrobial action and cannot be easily adapted to different real-life use conditions.

The purpose of the current thesis was to characterize the interactions occurring between microbes and novel multimodal antimicrobial surfaces thereby contributing to targeted improvement of antimicrobial surface design as well as to adapt and optimize antimicrobial surface testing methodology.

As a result of the study, new methods have been developed and existing ones critically evaluated highlighting novel limitations to widely used approaches. Applying the gained knowledge, the antimicrobial properties of the metal-based photocatalytic surfaces were characterized in depth.

This thesis has been published as 4 peer-reviewed scientific articles. The results have been presented at the following international science events: Functional materials and Nanotechnologies-2017 (Tartu, Estonia, 2017; paper III), ASM Biofilms (Washington, DC, USA, 2018; paper II), FEMS2019 (Glasgow, UK, 2019; paper II), FEBS3+ (Riga, Latvia, 2019; paper II), Eurobiofilms (Glasgow, UK, 2019; paper II), several meetings and conferences of the COST AMiCI network (2017-2020; papers I-IV).

Abbreviations

AATCC	The American Association of Textile Chemists and Colorists
ANOVA	analysis of variance
ASTM	ASTM International, an international standards organization
ATP	adenosine triphosphate
BPR	Biocidal Product Regulation
BSA	bovine serum albumin
c-di-GMP	cyclic diguanosine monophosphate
CFU	colony forming unit
CLSM	confocal laser scanning microscopy
DIN	The German Institute for Standardization
DNA, eDNA	deoxyribonucleic acid, extracellular DNA
DNAse I	deoxyribonuclease I
<i>e.g.</i>	<i>exempli gratia</i> ; for example
ECHA	European Chemicals Agency
ECM	extracellular matrix
EPA	Environmental Protection Agency
EPS	extracellular polymeric substances
ESKAPE	antimicrobial-resistant ESKAPE pathogens <i>i.e.</i> <i>Enterococcus faecium</i> , <i>Staphylococcus aureus</i> , <i>Klebsiella pneumoniae</i> , <i>Acinetobacter baumannii</i> , <i>Pseudomonas aeruginosa</i> , <i>Enterobacter</i> spp.
<i>et al.</i>	<i>et alia</i> ; and others
<i>etc.</i>	<i>et cetera</i> ; and so forth
EU	European Union
FBS	fetal bovine serum
FDA	fluorescein diacetate
Fig.	Figure
<i>i.e.</i>	<i>id est</i> ; that is
ISO	International Organization for Standardization
JIZ	Japanese Industrial Standard
LB	lysogeny broth, also known as Luria–Bertani medium
Log	logarithm; used here to denote logarithm with base 10
MBC	minimal bactericidal concentration
MBEC	minimum biofilm eradication concentration
MIC	minimum inhibitory concentration
NA, eNA	nucleic acid, extracellular nucleic acid
NIH	National Institutes of Health
NP	nanoparticle

PBS	phosphate buffered saline
PI	propidium iodide
RH	relative humidity
RNA	ribonucleic acid
ROS	reactive oxygen species
SAF	surface-associated amyloid fibers
UVA	ultraviolet A radiation
VBNC	viable, but not culturable

1 REVIEW OF THE LITERATURE

In the following chapters literature relevant to the microbial lifestyles, surface-related antimicrobial strategies and testing methods of antimicrobial surfaces are reviewed to give an overview of how the multidisciplinary field of antimicrobial surface development and efficacy assessment relates to the broader context.

1.1 Microbial lifestyles

Microbes can either exist in free-living planktonic form such as many liquid cultures in classical microbiology or cellular aggregates forming biofilms at various air-liquid, liquid-solid or solid-air interfaces, on biotic or abiotic surfaces. Planktonic and biofilm lifestyles of microbes from the same clonal origin can result in remarkably different physiological profiles and tolerance to environmental stresses and *vice versa*, environmental factors can trigger biofilm formation or dispersion. Biofilms are microbial communities presenting in various forms from small aggregates of a few cells adhering to each other to complex surface-associated syntrophic communities (Fig. 1 and (West et al., 2006)). These communities are relatively protected from their immediate environment by self-produced extracellular matrix (ECM), low metabolic activity and structural as well as physiological heterogeneity as compared to more homogenous planktonic cultures (Stewart & Franklin, 2008; Stoodley et al., 2002). Complexity and heterogeneity build niches favoring different modes of interaction between community members and with the surrounding environment. Costerton *et al.* have defined biofilms simply as matrix-enclosed bacterial populations adherent to each other and/or to surfaces or interfaces and in their complexity compared them to tissues of eukaryotic organisms (Costerton et al., 1995). Etymology of the term biofilm since the first studies in the 1930s is recently well reviewed by Flemming *et al.* (Flemming et al., 2021).



Figure 1. An image by a Leiden University microbiologist Shraddha Shitut (with permission) depicting human and microbial communities using various materials to build a hospitable environment creating niches favoring different modes of interaction between community members and with the surrounding environment. Much like human cities or termite mounds biofilms seem to represent J. S. Turner's "extended physiology" in niche construction theory (Laland et al., 2016; J. S. Turner, 2000) at a microscale. Comparing biofilms to human cities nicely illustrates the dynamic heterogeneity of the systems and has also been used by others (Paula et al., 2020; Watnick & Kolter, 2000).

Where there is a surface, there is a biofilm. Biofilm is the naturally occurring predominant microbial lifestyle. It is estimated that up to 80% from the total of 1.2×10^{30} bacterial and archaeal cells on earth live in biofilms (Flemming & Wuertz, 2019) with majority of the remaining planktonic cells found in pelagic oceanic habitats. Similar tendency is estimated to be true in medical field with up to 80% of human bacterial infections being caused by biofilms (NIH, 2002; Römling & Balsalobre, 2012) among which the antimicrobial-resistant ESKAPE pathogens *i.e.* *Enterococcus faecium*, *Staphylococcus aureus*, *Klebsiella pneumoniae*, *Acinetobacter baumannii*, *Pseudomonas aeruginosa*, *Enterobacter* spp. (Pendleton et al., 2013) have proved to be the most challenging to treat. The term biofouling is used to address formation of undesirable biofilms causing economic and/or medical damage in engineered environments or on biointerfaces. Measures to counteract biofilm formation include using antifouling surface materials as well as cleaning agents, soluble biocides, and antibiotics. Therefore, surfaces with antimicrobial activity preventing biofilm formation seem like a desirable tool in decreasing the bioburden on communal surfaces and pathogen carryover by fomites. Nonetheless, based on data in the peer-reviewed literature database Scopus, most publications about bacteria and archaea disregard biofilms (Fig. 2). Therefore, also methods for studying microbes in general as well as pathogenic species largely rely on results generated in planktonic cultures creating an unprecedented bias in our understanding about microbiology.

Regarding antimicrobial efficacy testing using planktonic cultures one has to acknowledge that some amount of biofilm is always present in the system depending on the organism and volume to surface ratio of the vessel used. The amount of biofilm included in the viability endpoint measured depends partly on the liquid manipulation procedures as nicely visualized by Kragh *et al.* (Kragh et al., 2019). Therefore, hereinafter the term **antimicrobial** is used in a broader meaning denoting both action against planktonic and biofilm-residing organisms while the term **antibiofilm** is used for strategies specially targeting biofilms.

As the biofilm lifestyle is more relevant to biofouling of surfaces it is reviewed in more detail in the next chapters.

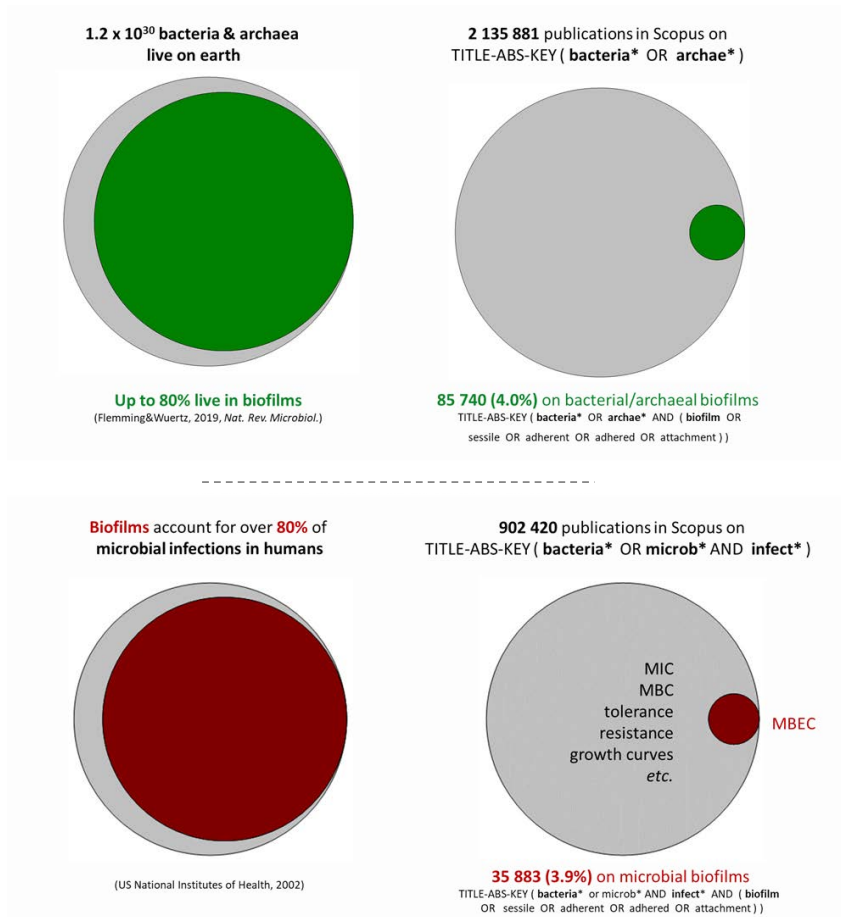


Figure 2. Estimated proportions of microbes living in biofilms and infections caused by biofilms (left column) versus proportion of scientific literature about biofilms in the field (right column). Data retrieved in September 2021.

1.1.1 The biofilm life cycle

The biofilm life cycle is a dynamic cyclic process of attachment, maturation, and dispersion (Fig. 3), including the much-studied planktonic phase. Generally, formation of surface-bound biofilms starts with reversible attachment of cells to the substrate which is mainly driven by physical factors (*e.g.*, surface charge, hydrophobicity, shear stresses). Reversible physical interaction with the surface is followed by community-orchestrated irreversible attachment, microcolony formation, ECM production, growth, maturation and active dispersion in response to local environmental cues (Rumbaugh & Sauer, 2020).

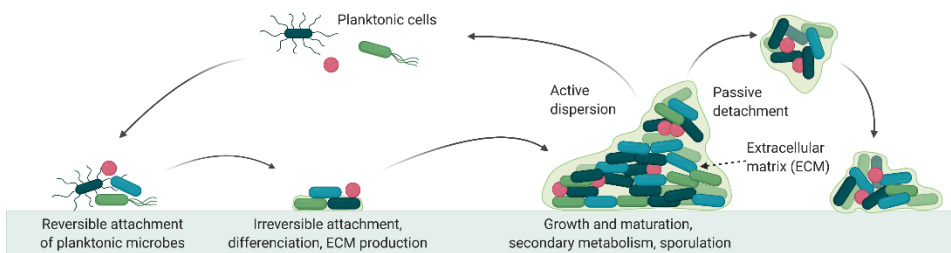


Figure 3. The biofilm life cycle. Surface colonisation is started by reversible attachment of microbial cells to the surface mainly due to physical forces followed by active process of irreversible attachment, differentiation and start of production of the extracellular matrix (ECM). The biofilm physiology is established during growth and maturation of the biofilm while balancing between syntropic relations and predation, responding to environmental cues etc. The majority of biofilm-residing microbes can either passively disperse e.g., due to shear stress or physical erosion and continue as a biofilm or disperse actively in a regulation-controlled manner by releasing planktonic cells. These planktonic cells can spread and form new biofilm aggregates. Interventions to the process could target prevention of attachment, destruction of biofilm biomass or signalling for dispersion.

Bacteria tend to form biofilms in response to commonly occurring physical and chemical stress factors such as nutrient limitation, light exposure, desiccation, extreme temperatures, pH or salt concentration etc., but also in response to sublethal exposure to antimicrobials (Linares et al., 2006; Penesyan et al., 2020) possibly largely via general stress response and c-di-GMP second messenger signaling (Hengge, 2009; Jenal et al., 2017). Due to generally lower metabolic activity, secondary metabolism, encapsulation into the ECM etc. the formed biofilms can have magnitudes of order higher tolerance towards stressors, including common chemical treatments (Ceri et al., 1999; Olson et al., 2002). Compartmentalization and spatially heterogeneous natural selection in a mature biofilm also contributes to antibiotic resistance development and transfer (France et al., 2019; Olsen, 2015) as well as producing antibiotic-resistant bacteria that are more fit and not easily outcompeted in the absence of the drug (Santos-Lopez et al., 2019). It has been recently demonstrated that biofilms can also act as a reservoir for antimicrobial resistance elements (Røder et al., 2021).

General understanding of the extracellular polymeric substances (EPS) in the biofilm matrix has changed in time from the sugar-based slime concept (Costerton et al., 1978; Limoli et al., 2015) to include other biopolymers such as several proteins, surface-associated amyloid fibers (SAFs) and critical dependence on extracellular DNA (eDNA) in biofilm formation (Flemming & Wingender, 2010; Seviour et al., 2019; Taglialegna, Lasa, et al., 2016; Whitchurch, 2002). The latter is not only important in surface-bound biofilms but also in aggregates more resembling chronic biofilm infections (Alhede et al., 2011) suggesting that eDNA has a more universal role in biofilm development. The general importance of eDNA in early phases of biofilm development is evident as many early monospecies biofilms of both Gram-positive and Gram-negative bacteria are eradicated or substantially impaired by DNase I treatment (Okshevsky & Meyer, 2015). DNase has also been suggested to be used as an antibiofilm strategy (Swartjes et al., 2013). Negatively charged eDNA can interact with positively charged ECM components (e.g., Pel polysaccharide in *P. aeruginosa* biofilms) forming structurally important interaction (Jennings et al., 2015). eDNA itself as well as DNA-binding proteins

in the biofilm ECM could be promising targets for biofilm eradication strategies (Novotny et al., 2021). Recent findings also begin to shed light to structural heterogeneity and possible functions of extracellular nucleic acids. For example, Thomas Seviour *et al.* recently showed that the ECM of *Pseudomonas* species contains extracellular DNA and RNA, including non-canonical DNA structures collectively contributing to ECM elasticity (Seviour et al., 2021) and Buzzo *et al.* demonstrated that it is the left-handed nuclease resistant Z-DNA that is abundant and structurally important in biofilm ECM of several bacterial species (Buzzo et al., 2021). eDNA has also been demonstrated to interact with SAFs possibly further enhancing biofilm formation (Fernández-Tresguerres et al., 2010; Schwartz et al., 2016; Van Gerven et al., 2018). However, not all amyloid fibers have the same effect. While SAFs participate in biofilm formation and are structural components of the biofilm ECM (Gallo et al., 2015; Oli et al., 2012; Romero et al., 2010; Schwartz et al., 2012, 2016; Taglialegna, Lasa, et al., 2016; Taglialegna, Navarro, et al., 2016), introduction of exogenous amyloid fiber forming peptides can inhibit biofilm formation by *Streptococcus mutans*, *Streptococcus sanguis*, *S. aureus*, *Escherichia coli* and *Candida albicans* (Chen et al., 2020) and may possess bactericidal properties (Bednarska et al., 2016).

1.2 Antimicrobial surfaces

Antimicrobial surfaces have been proposed to prevent the spread of potentially pathogenic microbes that can be carried over by solid surfaces (Boyce, 2007; Otter et al., 2011, 2015; Weber et al., 2010) and remain viable or infectious on surfaces for relatively long periods of time ranging from days to months depending on the microbial species and ambient conditions (Kramer et al., 2006).

1.2.1 Interactions between antimicrobial surfaces and microbes

Antimicrobial surfaces, designed to prevent surface colonization and/or kill the microbes can achieve antimicrobial activity in various ways (Adlhart et al., 2018) including physical mechano-bactericidal interaction (Linklater et al., 2021) but can be broadly divided into four main categories depicted on Figure 4:

- **anti-adhesive** surfaces (*e.g.*, superhydrophilic and superhydrophobic surfaces, nanopatterned and biomimetic surfaces acting via inhibition of microbial attachment);
- **contact-killing** surfaces (covalently bound active agents, *e.g.*, quaternary ammonium compounds acting upon direct contact between the microbe and the surface);
- **biocide releasing** surfaces (*e.g.*, metal surfaces, antibiotic releasing surfaces, acting via local or long-distance release of biocides)
- **photocatalytic/self-cleaning** surfaces (mainly TiO₂, ZnO)
- or combination of the former resulting in **multimodal** surfaces.

Choice of surface type and active agent depends on the application and environment where the surface is to be used. The latter are also important to consider when assessing the antimicrobial efficacy of any given surface application.

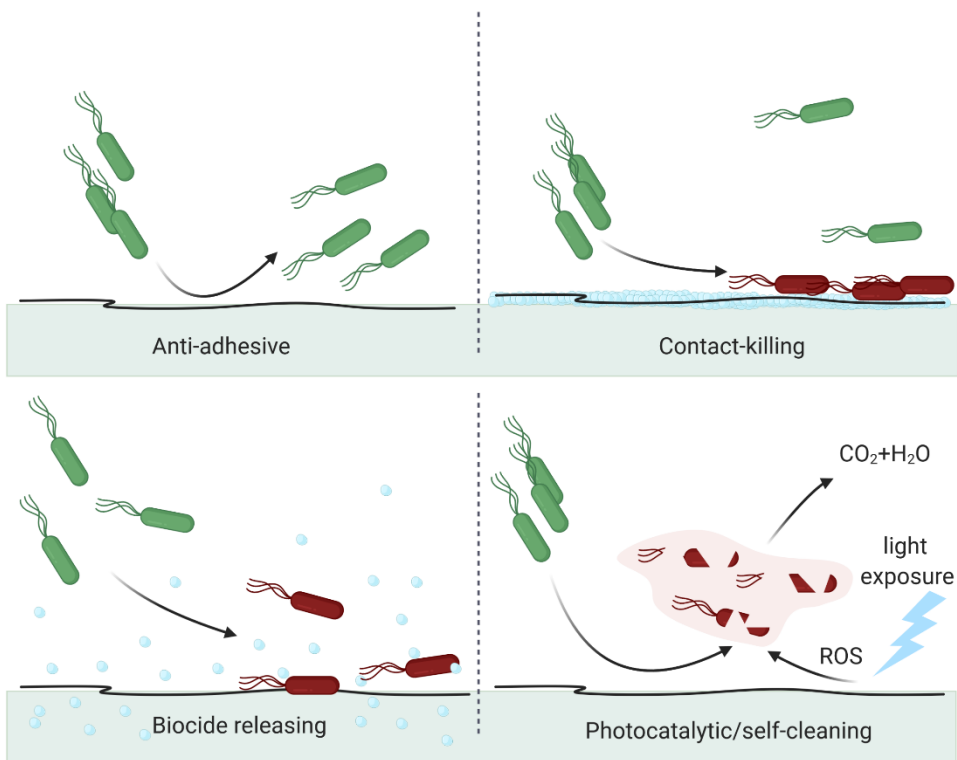


Figure 4. Main antimicrobial surface types. Viable bacteria are depicted in green, dead in red.

Release-based metal surfaces are the most used historically in both marine antifouling (copper, organotin compounds) and everyday use items such as cooking utensils (silver spoons and water storage vessels, copper pots) and doorknobs to even early invasive medical applications (e.g., copper alloy plates to mend broken bones (Mitchell, 2016) or a quite exceptional case of using flattened silver coin to replace parts of the human skull (Barillo & Marx, 2014)). With the recent ban on ecotoxic organotin compounds in marine applications, re-emergent interest in copper and zinc is increasing in the field while silver and antibiotic releasing surfaces are still most researched for invasive medical applications (Rosenberg et al., 2019).

Although release of the active agent from surface application into the surrounding environment could contribute to chemical pollution, it could also achieve higher antimicrobial efficacy. Infectious biofilms tend to appear as small aggregates generally less than 100 μm in diameter (Bjarnsholt et al., 2013) and in case of implant-associated infections can reside not only directly on the surface of the implant but in the surrounding tissue (Jensen et al., 2017). Such microbes may be inactivated by release-based surfaces in invasive medical applications, favouring their use over contact killing surfaces.

While many of the possible antibiofilm strategies imply chemical treatment and/or physical removal of an already existing biofilm, biofilm formation inhibition is feasible to be achieved through targeted surface material development. Prevention, as opposed to eradication, also abrogates the need to remove the residual biomass that could be a substrate to *de novo* biofilm formation. Such surfaces could be either physically

anti-adhesive, contact-killing or biocide releasing in design thereby either preventing attachment of viable microbes or also killing planktonic microbes near or at the surfaces.

Effective chemical treatment of established biofilms is notoriously harder to achieve than inactivation of planktonic microbes. For example, minimum biofilm eradication concentration (MBEC) of widely used antibiotics towards pathogenic microbes can be up to 1000 times higher than their minimum inhibitory concentration (MIC) towards planktonic cultures (Ceri et al., 1999; Olson et al., 2002). Metal-based antimicrobial applications on the other hand are especially promising, as they have proven to be effective against both planktonic and biofilm communities in similar concentrations (Harrison et al., 2004). Therefore, the focus of the following chapters is directed towards metal-based surfaces.

1.2.2 Antimicrobial mechanisms of metal-based surfaces

Precise biocidal mechanisms of metal toxicity that form the basis of their antimicrobial properties are not completely understood but are known to require interaction between free metal and either membrane-bound or cytosolic cellular target. Two of the major targets for metal toxicity are protein function impairment by interactions with sulfhydryl (SH) groups and displacing essential metal cofactors (Hodgson, 2010). Although different metals ions share the described general targets, their affinity can vary. For example, heavy metal affinity to SH groups has been demonstrated to decrease in the following order: $\text{Hg}^{2+} > \text{Ag}^{+} > \text{Cu}^{2+} > \text{Ni}^{2+} > \text{Zn}^{2+}$ (Vieira et al., 1997). Considering antibacterial applications, one must evaluate not only antibacterial activity of the metal but also toxicity to non-target organisms, precluding, for example, the use of mercury in most antimicrobial applications. Along with the use of elemental metal or metal salts as antimicrobials, one novel approach is the use of metal-based nanoparticles (NPs) that due to their large surface area exhibit relatively high antimicrobial activity. The antimicrobial properties of metal-based NPs can be mainly attributed to the release of metal ions (Slavin et al., 2017) and electrostatic NP-cell interactions (Kim et al., 2007) resulting in high local concentration of metal ions due to large surface area of nanoparticulate matter, direct membrane damage (Gogoi et al., 2006; Su et al., 2009) and in some cases emergence of damage by abiotic reactive oxygen species (Jin & Jin, 2021; Yoshida et al., 1993).

The general nature of the main targets of metal toxicity allows for a multifaceted antimicrobial attack on cellular functions while acquiring true resistance to excess metal ions, many of which are essentially needed micronutrients, is complicated if not impossible. For example, about a third of all enzymes need metal cofactor for proper function (Andreini et al., 2008). Plasmid and chromosomally encoded metal tolerance or resistance, depending on definition, has been described (Hobman & Crossman, 2015; Silver & Phung, 1996, 2005; R. J. Turner et al., 2020) resulting in either prevention of toxic metal ion uptake, efflux of excess metal ions, metal ion sequestration or oxidation-reduction to change redox state of metal ions. Metal tolerance is most often found as well as can be employed where it is physiologically relevant. Therefore, environments rich in respective metals (Haferburg & Kothe, 2010) making soil and polluted environments such as ore mining and agricultural runoffs or communal waste water systems a reservoir for genetic elements carrying metal tolerance. It has been recently shown that tolerance mechanisms of metal NPs and respective ions can be mechanistically different. For example, motility-enhanced tolerance can be acquired towards Ag NPs but not Ag ion (Stabryla et al., 2021).

Higher metal tolerance, when encoded by multiresistance plasmids could potentially unfavourably co-select for antibiotic resistance in sublethal metal concentrations (Baker-Austin et al., 2006; Bazzi et al., 2020; Pal et al., 2017). Whereas in other cases metals could contribute synergistically to antibiotic treatment (Habash et al., 2017; Morones-Ramirez et al., 2013; Pietsch et al., 2021) with implications in wound care or invasive medical device-associated infections highlighting the need to carefully weigh risk and benefit in the use of antimicrobial metals in any given application.

1.2.2.1 Silver-based antimicrobial surfaces

Silver is a naturally occurring and contrary to copper and zinc a biologically non-essential metal. To this day silver is the most exploited active ingredient in antimicrobial surface applications in both commercial use and prevalence in academic literature followed by copper and zinc (Rosenberg et al., 2019). Antimicrobial silver has been historically used in infection prevention long before Louis Pasteur, Robert Koch and the Germ Theory of disease. Historical applications of silver mainly focus on water storage and disinfection, battlefield surgery and burn wound care (Barillo & Marx, 2014; Lemire et al., 2013).

The antimicrobial activity of silver is classically mainly attributed to the interaction of Ag^+ ions with the thiol groups of proteins impairing DNA replication, the respiratory chain and proton motive force (Bragg & Rainnie, 1974; Dibrov et al., 2002; Feng et al., 2000; Holt & Bard, 2005; Lemire et al., 2013) resulting in systemic damage and death. Silver is presumed to hijack copper-transport systems to enter cells (Ghandour et al., 1988; Odermatt et al., 1994; Solioz & Odermatt, 1995), but as the element is not required for cellular processes, cells generally also lack well-tuned mechanisms to export or detoxify silver. Recent advances in omics have suggested narrower initial targets for Ag^+ toxicity, for example primarily damaging multiple enzymes in glycolysis and tricarboxylic acid cycle leading to metabolic divergence to the reductive glyoxylate pathway and suppressing the cellular oxidative stress responses eventually resulting in systemic damage and death in *E. coli* (Wang et al., 2019). Due to rapid adsorption to surrounding surfaces, high reactivity with thiol groups in proteins and formation of insoluble salts in the presence of chloride, sulphite and phosphate, silver toxicity is rapidly neutralized by organic matter and salt in biological systems (Behra et al., 2013; Xiu et al., 2011). Interestingly, it has been recently suggested that tolerance towards ionic and nanoparticulate silver could be mechanistically different with the latter affected by bacterial motility (Stabryla et al., 2021).

Optimal conditions for silver toxicity in surface applications seem to be similar to the ones that favour growth of human-associated microbes, *i.e.* at 35°C and 95% relative humidity (RH) whereas copper retains its antibacterial activity also at room temperature and dry conditions (Michels et al., 2009) that are more representative of indoor high-touch surfaces.

1.2.2.2 Copper-based antimicrobial surfaces

Copper has a long history as an anti-infective material (Borkow, 2012; O’Gorman & Humphreys, 2012), has been used in marine antifouling applications (Rosenberg et al., 2019) and is still deployed in water safety (Stout & Yu, 2003). Copper-based applications stand out among other antimicrobial surfaces by having demonstrated antimicrobial field-use benefits in actual health-care settings (Salgado et al., 2013; Sifri et al., 2016; von Dessauer et al., 2016; Zerbib et al., 2020).

From biological point of view, copper is a trace element required in many enzymatic processes involving redox chemistry (Karlin, 1993) but is harmful to cells in excess. Antimicrobial properties of copper are mainly attributed to redox chemistry, Fenton-type reactions and generation of reactive oxygen species resulting in lipid peroxidation (Yoshida et al., 1993), membrane damage (Nan et al., 2008) and DNA fragmentation (Warnes et al., 2010) as well as protein damage via thiol-disulphide chemistry (Vieira et al., 1997) and replacement of other metal cofactors of proteins (Macomber & Imlay, 2009). Oxidative DNA damage seems to be a secondary effect after membrane damage and mainly periplasmic ROS attack (Macomber et al., 2007) in Gram-negative bacteria but could beneficially contribute to reducing potential horizontal transfer of genetic elements coding antibiotic resistance and metal tolerance.

Bacteria, fungi and viruses are inactivated on copper-based surfaces within minutes to hours (Borkow, 2012; Dauvergne et al., 2020; Grass et al., 2011) in dry test conditions resulting in shorter inactivation times and higher cellular copper uptake (Santo et al., 2011) suggesting a direct contact-killing based mechanism of action. The fact that contact killing is largely reduced by Cu(I) and Cu(II) chelators (Santo et al., 2008) adds to the already common understanding that antimicrobial activity of copper is mediated by copper ions in water environment and the same could be true in (semi-)dry test conditions.

1.2.2.3 Zinc-based antimicrobial surfaces

Zinc is an essential micronutrient that is incorporated into 4-10% of proteins across the domains of life (Andreini et al., 2008) but it also possesses a dose-dependent antibacterial activity at higher concentrations. Zinc toxicity towards microbes is mainly attributable to deactivation of proteins via thiol-disulphide chemistry (Harrison et al., 2009; Lemire et al., 2013) and protein binding or metal replacement (*e.g.*, manganese starvation (Couñago et al., 2014; McDevitt et al., 2011)) resulting in impaired energy metabolism (Hosler et al., 2006; Mills et al., 2002; Ong et al., 2015), higher susceptibility to reactive oxygen species (ROS) (Eijkelkamp et al., 2014) and eventually loss of membrane potential and membrane permeabilization. Zn tolerance in higher than physiological concentrations has been demonstrated to depend on microbial species. *C. albicans* and *P. aeruginosa* were less sensitive to Zn toxicity than *E. coli* or *S. aureus* (Pasquet et al., 2014).

Zinc has also been studied in the context of biofilms. Antibiofilm properties of Zn-based applications could partially be attributed to Zn toxicity to bacteria above physiological concentrations but in addition other biofilm-specific mechanisms could be involved. It has been proposed that sublethal Zn or Ag concentrations could inhibit biofilm formation by interfering with quorum sensing (Al-Shabib et al., 2016; García-Lara et al., 2015; Gómez-Gómez et al., 2019; Zähringer et al., 2013) or affect amyloid fibril formation (Huma et al., 2020; Yarawsky et al., 2020).

Antimicrobial action of ZnO nanomaterials is a combination of mostly Zn²⁺ ion release and ionic toxicity described above but also electrostatic attraction and NP adsorption to cellular material as well as light-induced ROS generation resulting in inactivation of proteins, disruption of energy metabolism, lipid peroxidation and membrane damage, DNA damage and disruption of replication (Jin & Jin, 2021; Sirelkhatim et al., 2015). Nano-specific effects damage bacterial cell membranes and downregulate genes associated with managing oxidative stress in *S. aureus* as well as upregulate genes associated with cation efflux in *E. coli* and *P. aeruginosa* and inhibit biofilm formation by

E. coli, *S. aureus* and *P. aeruginosa* (Brayner et al., 2006; Dutta et al., 2012; J.-H. Lee et al., 2014; L. J. Lee et al., 2005; Pati et al., 2014; Seil & Webster, 2011) among other microbes.

Internalization on ZnO NPs by endocytosis-incapable prokaryotes (Brayner et al., 2006) as well as abiotic ROS generation in dark conditions (Hirota et al., 2010; Lakshmi Prasanna & Vijayaraghavan, 2015) still remain debatable.

1.2.2.4 Photocatalytic antimicrobial surfaces

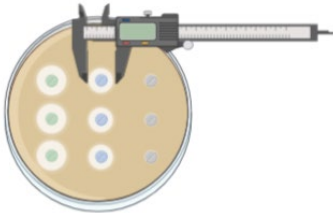

Some antibacterial metal oxides also act via light-induced generation of ROS and general organic matter degradation, including microbial cells. The most popular antimicrobial photocatalyst is TiO₂ but also ZnO is widely used (Sirelkhatim et al., 2015). The fact that photocatalysis not only kills the microbes but also results in photooxidation of cellular debris (Joost et al., 2015), referring to the possibly extended efficacy of such self-cleaning surfaces. In case of ZnO, photocatalysis under UVA illumination is combined with ionic toxicity in all lighting conditions allowing multimodal applications.

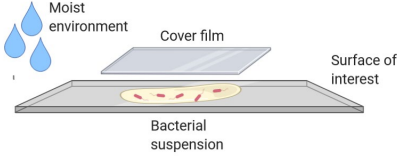
Photocatalytic activity of light-activated surfaces (*e.g.*, TiO₂, ZnO, Fe₂O₃, ZnS, FeS₂) is based on their ability to excite the electrons from valence band to conduction band creating electron–hole pairs after absorbing photons with high enough energy to exceed the band gap energy of the material (Friehs et al., 2016). The electrons (e⁻) and holes (h⁺) can either recombine or reduce/oxidize surface-adsorbed O₂ and H₂O to produce ROS (*e.g.*, superoxide anion O₂^{-•} and hydroxyl radical •OH). The highly reactive ROS can partially or completely degrade organic contaminants including microbes. Doping, composites with noble metals and heterostructures are used for better charge separation to restrain e⁻/h⁺ recombination (Zaleska-Medynska et al., 2016) or overcome the restriction of a large band gap via surface plasmon resonance (Linic et al., 2011) and in both cases enhance photodegradation.

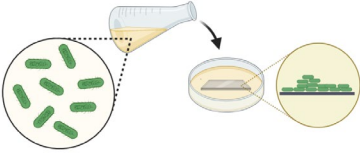
1.2.3 Antimicrobial surface testing

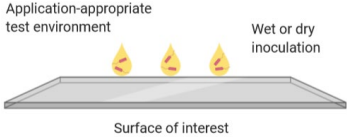
To assess efficacy of an antimicrobial surfaces, one must consider material properties as well as the many variables encountered during the proposed end use of the product and choose or design an application-appropriate testing protocol. Methods used to assess antimicrobial surface efficacy, can be broadly divided into five categories described in Table 1. This division is based on test formats with similar advantages and limitations to better highlight the challenges in deciding between diffusion-based, suspension-based, thin layer, antibiofilm and simulated use methods.

Table 1. Testing methods of antimicrobial surfaces and their advantages and disadvantages as perceived by the author.

<h2 style="text-align: center;">Diffusion-based methods</h2> <p>Endpoint measured:</p> <ul style="list-style-type: none"> • extent of growth inhibition zone <p>Surface types:</p> <ul style="list-style-type: none"> • release-based surfaces only 	<p>Advantages:</p> <ul style="list-style-type: none"> • fast and inexpensive • suitable for solid surfaces and textiles, porous and non-porous surfaces • no specific equipment needed in addition to standard microbiology lab setup <p>Disadvantages:</p> <ul style="list-style-type: none"> • does not simulate end use • qualitative or only semi-quantitative • only evaluates growth inhibition by released active ingredient and not bactericidal properties • dependent on diffusion efficiency and water-solubility of different active ingredients • growth agar itself might inactivate some active ingredients. <p>Examples: ISO 20645, AATCC 30, AATCC TM147, DIN EN 1104,</p>
<h2 style="text-align: center;">Suspension methods</h2> <p>Endpoint measured:</p> <ul style="list-style-type: none"> • viable count of suspended microbes <p>Surface types:</p> <ul style="list-style-type: none"> • release-based surfaces 	<p>Advantages:</p> <ul style="list-style-type: none"> • fast and inexpensive • anti-adhesion properties can be analyzed in the same system in parallel • liquid environment composition can be adjusted • no specific equipment needed in addition to standard microbiology lab setup <p>Disadvantages:</p> <ul style="list-style-type: none"> • does not simulate end use • quantitative, but large volume to surface ratio decreases sensitivity <p>Examples: ASTM E2149</p>
<h2 style="text-align: center;">Large surface area methods</h2> <p>Main endpoint measured:</p> <ul style="list-style-type: none"> • viable count of microbes retrieved from the surfaces <p>Surface types:</p> <ul style="list-style-type: none"> • release-based surfaces • contact killing surfaces • photoactive surfaces • multimodal surfaces 	<p>Advantages:</p> <ul style="list-style-type: none"> • quantitative, standardized and generally reproducible, if strictly followed • low volume to surface ratio maximizes microbe-surface interaction • available for both solid surfaces and textiles • can be modified to also test viruses <p>Disadvantages:</p> <ul style="list-style-type: none"> • elaborate methods • do not simulate end use: very humid and warm ($\geq 90\%$ RH; 35-37°C) test

 <p>Moist environment</p> <p>Cover film</p> <p>Surface of interest</p> <p>Bacterial suspension</p>	<p>conditions and/or unrealistically long exposures (18-24 h for textiles and solid surfaces, 4-8 h for photoactive materials)</p> <ul style="list-style-type: none"> • surface hydrophobicity/hydrophilicity can complicate testing (Perez-Gavilan et al., 2021) • modifications to the standards prone to be influenced by microbial physiology (Wiegand et al., 2018) • cell retrieval methods have to be adjusted to suit each surface type of interest • method modifications may make it impossible to fulfill pass criteria of standard tests and cause problems with testing service providers • generally, no biologically meaningful lower threshold of antimicrobial activity is provided <p>Examples: ISO 22196/ JIS Z 2801/ ISO 21702, ISO 27447, ISO 20743/JIS L 1902/ISO 18184, AATCC TM100, Petrifilm methods</p>
---	---

<h2 style="text-align: center;">Adhesion-based & biofilm methods</h2> <p>Main endpoints measured:</p> <ul style="list-style-type: none"> • amount of biomass (crystal violet assay) • microscopy (live/dead staining, biovolume, morphology, etc.) • viable count (harvesting and culturing) <p>Surface types:</p> <ul style="list-style-type: none"> • anti-adhesive surfaces • multimodal surfaces 	<p>Advantages:</p> <ul style="list-style-type: none"> • endpoints can be tuned to anti-adhesive and biofilm claims <p>Disadvantages:</p> <ul style="list-style-type: none"> • elaborate methods • hard to achieve relevance to end use conditions • often specialized and/or expensive equipment and/or respective services needed (flow reactor or flow cell systems, confocal and/or electron microscopy etc.) • anti-adhesive approaches that prevent surface colonization by potential pathogens are not compatible with several logs kill criteria required by legislation in some fields of application • standardized biofilm methods use viable count as a single endpoint disregarding biomass • often poor reproducibility due to biologically complex system • viable, but not culturable (VBNC) microbes and extracellular DNA could cause discrepancies between cultivation and live/dead staining based endpoints <p>Examples: various published protocols as well as several ASTM standard methods (<i>e.g.</i>, E2196, E2562, E2647, E2799, E2871, E3321)</p>
---	--

<h2>Simulated use methods</h2>	
<p>Main endpoints measured:</p> <ul style="list-style-type: none"> • viable count of microbes retrieved from the surfaces • ATP bioburden assays • microscopy methods • other methods justified to substantiate an antimicrobial claim under specific conditions <p>Surface types:</p> <ul style="list-style-type: none"> • release-based surfaces • contact killing surfaces • anti-adhesive surfaces • photoactive surfaces • multimodal surfaces <div style="text-align: center;">  <p>Application-appropriate test environment</p> <p>Wet or dry inoculation</p> <p>Surface of interest</p> </div>	<p>Advantages:</p> <ul style="list-style-type: none"> • quantitative methods simulating end use • different testing approaches can be combined • free choice of relevant microbes, inoculum density, contact time • inoculation methods include dry or semi-dry inoculation of materials e. g. spraying, swabbing, microdroplets, printing • testing in ambient conditions or controlled environment (humidity, temperature) • simulated soiling and drying possible • simulated cleaning and wear possible • methods of inoculation and cell retrieval have to be adjusted to suit each proposed application and surface type of interest <p>Disadvantages:</p> <ul style="list-style-type: none"> • expensive and elaborate methods needing consultations, method modifications, pilot tests and planning in cooperation with service provider • might need specific equipment (e.g., climate chambers, spray systems) • method modifications may make it impossible to fulfill pass criteria of standard tests <p>Examples: Interim EPA methods (EPA, 2020a, 2020b) and their predecessors issued for testing copper surfaces including the widely used and modified sanitizer surface method ; suggested simulated splash and print-inoculation method concepts in EU BPR (ECHA, 2018); examples from the literature (Knobloch et al., 2017; McDonald et al., 2020; Ojeil et al., 2013)</p>

1.2.3.1 Standardized protocols and legislative requirements

In the recent European Union legislation, the Biocidal Product Regulation (BPR, Regulation (EU) 528/2012) requires that efficiency testing of products with antimicrobial claims are not only tested using standard protocols but also in application-appropriate and field conditions to demonstrate efficacy of treated articles in end use. Guidance on efficacy testing is methodologically vague and asks for testing approaches tailored to the specific claim to be used to assess antimicrobial efficacy of treated articles (ECHA, 2018), including surfaces and textiles. While Appendix 4 lists required pass criteria for biocides to be in the range of 4-5 log reduction during a scale of seconds to an hour, only at least 3 log kill tested in a range of times during 5 min to 1 h is required of treated articles with example claims to protect human or animal health (Table 9 (ECHA, 2018)). Although tailored approach is required, the only thorough method suggestion is to adapt the ISO 22196 (ISO, 2011) (Table 1) to application-specific conditions with basic concepts of

simulated splash and semi-dry inoculum printing to simulate hand contact only schematically illustrated.

The ISO 22196 standard method is adopted from the Japanese industrial standard JIS Z 2801 and is to this day the only international well-standardized quantitative approach for industrial antimicrobial solid surface testing. A very similar standard method covering both solid surfaces and textiles, ISO 27447 (ISO, 2019b), is used for photocatalytic materials while different textile-specific protocols are described for non-photoactive textiles (ISO 20743 (ISO, 2013) for antibacterial and ISO 18184 (ISO, 2019a) for antiviral textiles). In practice, also the ISO 13697 (ISO, 2015) designed to evaluate microbicidal efficacy of chemical disinfectants used on non-porous surfaces has been applied to study surfaces with antimicrobial properties without the use of additional chemical disinfectants.

The ISO 22196 represents a "best-case" scenario for antimicrobial surface testing for material developers since a small amount of dilute liquid microbial inoculum is spread over a large surface area in a thin layer, incubated at body temperature and $\geq 90\%$ RH for a period of 24 h. If strictly followed, this allows to compare materials and active ingredients against each other in a highly reproducible manner but is not relevant in most end-use scenarios (Campos et al., 2016; Ojeil et al., 2013). ISO 22196 test results have also been demonstrated to be heavily influenced by the often-modified factors *e.g.*, selection of microbial species, initial inoculum density, using exponential or stationary phase cultures, dilution factor of medium used, incubation time and temperature resulting in poor interlaboratory reproducibility especially in case of moderately effective surfaces (Campos et al., 2016; Wiegand et al., 2018).

Microbial contaminants in real life, as opposed to the aforementioned ISO method, tend to dry quickly onto surfaces under ambient conditions or are already carried over in relatively dry form not in droplets or aerosols. This limits the time that a liquid medium is available to mediate interaction between the antimicrobial surface and microorganisms. Also, much shorter exposure times than 24h would be needed to effectively avoid pathogen carryover by fomites. Instead of relatively simple "best case" scenarios of currently available standard tests, "worst-case" scenarios accounting for real-life like use conditions, drying, soiling, cleaning regimen, wearing *etc.* should be used for antimicrobial efficacy assessment of treated articles. Modifications to the ISO protocol that interfere with test validity conditions, *e.g.*, less than required viability on control surfaces due to drying, might cause challenges in cooperation with large international accredited testing service providers.

1.2.3.2 Towards application-appropriate tailored protocols

Silver is a good example to illustrate the importance of application-appropriate testing of antimicrobial materials. Silver, as an active ingredient, can achieve antibacterial activity towards the same strain of bacteria in up to a 1000 times different concentrations based on MBC values, depending on the liquid test environment and its organic content and the concentration of respective ions (Suppi et al., 2015). Therefore, its efficacy as an active ingredient and in respective treated articles can be, both substantially overestimated or underestimated depending on test media used or organic soiling applied to a surface. And even if silver salt or Ag NPs are efficient against bacteria in liquid suspensions, silver might still utterly fail as an antimicrobial surface when tested in application-appropriate dry conditions as opposed to more efficient copper based surface (Knobloch et al., 2017; Michels et al., 2009; Villapún et al., 2018). Interestingly, copper salt and Cu NPs were less potent than silver in liquid suspensions (Suppi et al., 2015).

Active ingredients in antimicrobial surface applications therefore do not possess a constant value of antimicrobial activity. On the opposite, antimicrobial properties of different treated articles with the same active ingredient can have very different antimicrobial efficacy depending on their field use conditions and microbial species encountered. These conditions must be critically evaluated and simulated in efficacy testing to really measure antimicrobial efficacy of the surface in a proposed application and not the testing system itself.

Tests, more tailored to touch surface specific conditions are available. For example the U.S. Environmental Protection Agency (EPA) has issued methods for testing copper touch surfaces (EPA, 2020a) and lately widened the scope to other hard non-porous surfaces (EPA, 2020b) allowing for shorter exposure times, drying, organic soiling, simulated wear, repeated inoculation *etc.* A 3-log reduction in bacterial viability during 1-2h is required to apply for public health claims (EPA, 2021). Other approaches can be found in the literature. For example, semi-dry aerosolization of the initial inoculum might be considered (McDonald et al., 2020; Ojeil et al., 2013). Such methods, while closer to end use scenarios are still heavily dependent on ambient conditions. For example, although it is generally recognized that drying of the inoculum has an effect on microbial viability (Lin & Marr, 2020) and it is an important part of simulated touch-surface test methods, the actual drying of an inoculum droplet is more complicated and dependent on RH. Differences in RH affect efficacy of some surface types more than others. For example, Michels *et al.* have demonstrated that copper alloys retained their antimicrobial activity towards methicillin-resistant *S. aureus* at >90%, 35% and 20% RH while silver surfaces that were highly efficient at >90% RH completely lost antimicrobial activity at the lower RH values (Michels et al., 2009). It is not only indoor ambient RH that varies in wide range, but it can also be complicated to control RH using conventional approaches such as deploying humidity chambers with saturated salts, especially in case of short sequential time points (Redfern et al., 2018). Furthermore, residual microscopic surface wetness may affect bacterial viability on surfaces (Grinberg et al., 2019) and different soiling agents, for example heavily glycosylated mucins in respiratory droplets may offer protection against reduction in infectivity due to drying (Yang et al., 2012).

Organic soiling is an important variable in testing protocols ranging from 500x diluted nutrient broth in ISO 22196, elaborate formulation of mucin, bovine serum albumin (BSA) and yeast extract in EPA methods to only BSA or fetal bovine serum (FBS) mimicking 'dirty' conditions in various standardized and literature sources. While analogously to growth medium presenting protective effect towards bacterial viability *versus* water in case of silver toxicity (Suppi et al., 2015), organic soiling is generally expected to reduce antimicrobial activity of surfaces. However, there are surprising deviations from this generalization. For example, copper surfaces have been shown to present faster antimicrobial activity when exposed to aerosols containing microbes and BSA (Ojeil et al., 2013). This either hints at different mechanisms of action of silver and copper or different toxicity-modifying effect of growth medium and BSA.

Antimicrobial activity is also heavily dependent on the selection of microbial species and strain even if the same testing protocol is used (Campos et al., 2016; Koseoglu Eser et al., 2015). In standardized protocols at least one Gram-negative and a Gram-positive species are used to substantiate antimicrobial claims, sometimes with an addition of a yeast, usually *C. albicans*. In the ISO standards *E. coli*, *K. pneumoniae* and *S. aureus* are indicated while US protocols tend to prefer *P. aeruginosa* and *S. aureus*.

With a few rare exceptions (Dauvergne et al., 2020; Knobloch et al., 2017; Róžańska et al., 2017) complex approaches considering multiple test variables are not routinely used, especially on publications describing novel materials and applications.

All the above suggests that comparison against reference surfaces with relatively well-described efficacy or the ones widely used in the field of application might produce more comparable results than individual antimicrobial activity values for different materials from different laboratories even if modifications of the same method are used to tailor the approach to any given application. Considering that here is a conflict of interest built in the “worst case” application-appropriate lab simulations as they are generally expected to result in lower antimicrobial efficacy than the “best case” scenario of ISO 22196, this clearly puts the focus on enforcing end-use simulations prior to allowing products to the market by the legislative systems.

1.2.3.3 Biofilm viability assessment and surface testing

Different antimicrobial approaches can be applied to eradicate existing biofilms but as the biofilms are less susceptible to antimicrobials than their planktonic counterparts inhibition of surface colonisation could be considered even more important than inactivating planktonic microbes by surface materials in various applications including high touch surfaces.

The extracellular matrix, not viable cells, can make up most of the volume of a mature biofilm (Flemming & Wingender, 2010). The amount of biofilm biomass, if sufficiently present, can be easily evaluated by the crystal violet assay (Christensen et al., 1985; Merritt et al., 2005) and can be used to evaluate biomass buildup. However, during initial attachment of microbes to the surfaces not much biomass is present and viable microbes are needed for both further biofilm formation and/or carryover of potential pathogens by the colonized surfaces. That is the reason why the few standardized biofilm methods that have been developed relevant to the context of antibiofilm surfaces efficacy assessment disregard biomass and biovolume and rely on plated viable counts. Viable counts, the gold standard of microbiology, depend on viable cell harvesting efficiency and dispersion of harvested aggregates prior to cultivation (Kobayashi et al., 2009; Mandakhalikar et al., 2018) and cultivability of the microbes (Chavez de Paz et al., 2008; Li et al., 2014). Despite the limitation, it has been lately demonstrated that CFU counts offer better reproducibility and responsiveness to different levels of efficacy of antibiofilm treatment than crystal violet or resazurin in microtiter plate format (Allkja et al., 2021). qPCR (Álvarez et al., 2013; Nocker & Camper, 2009) or flow cytometry combined with fluorescent stains (Cerca et al., 2011) could be considered to complement for some of the limitations of cultivation.

Confocal laser scanning microscopy (CLSM) has made it possible to directly observe the distinct biofilm architecture (Lawrence et al., 1991). Different staining methods have been applied to visualize structurally or functionally important components of biofilms as well as to evaluate metabolic activity or proportion of viable and dead cells and their localization in an undisturbed biofilm (Azeredo et al., 2017). One of the newest and promising addition to the CLSM toolbox are non-toxic fluorescent tracer molecules (*e.g.*, the ones developed by Ebba Biotech AB (Butina et al., 2020; Choong et al., 2016)). Viability staining with intact membrane-impermeable DNA-binding stains (*e.g.*, propidium iodide) and spectrally suitable membrane permeable counter-stains (Boulos et al., 1999) has been the most exploited for *in situ* viability assessment of biofilms via microscopy.

2 AIMS OF THE STUDY

Although ZnO and Ag NPs have shown great potential in antimicrobial applications, less is known about nano-enabled surfaces and combined antimicrobial effects of multimodal surfaces. Methods for studying antimicrobial surfaces in general largely rely on planktonic cultures and/or effects of released active agent and less on direct microbe-surface interactions. To address both challenges, main aims of the current thesis were twofold.

Firstly, we aimed to suggest methodological improvements to the current best-practice analysis methodologies by:

- adapting luminescent biosensor bacteria to measure microbe-surface interaction *in situ*.
- critically evaluating the appropriateness of selected bacterial viability assays to study microbe-surface interactions and biofilms.

Secondly, our goal was to improve the currently developed antimicrobial surface coatings by:

- characterizing microbe-surface interactions in response to multimodal metal-based antimicrobial surface coatings beyond the ISO test format and use that knowledge to improve the antimicrobial surface design.
- assessing antimicrobial and antibiofilm properties of novel proof-of-concept nano-ZnO and nano-ZnO/Ag enabled solid surfaces based on metal toxicity and photocatalytic activity.

3 MATERIALS AND METHODS

I used the following experimental methods that are described in detail in the indicated publications.

- Luminescence measurement from copper-exposed bacteria in microplate format or from copper and copper-alloy surfaces using *E. coli* transgenic Cu-biosensor strain in multiplate format and *in situ*, respectively for bioavailable copper content estimation in direct surface contact (I).
- *In situ* and on-filter epifluorescence microscopy of mono- or double-stained early-stage biofilms (II, IV).
- Viability staining of planktonic and/or sessile microbial cells based on membrane integrity (propidium iodide, Syto9) or enzymatic activity (fluorescein diacetate) (II, IV).
- Harvesting microbial biofilms via ultrasonication, optimization of the method (II, IV).
- Microbial attachment and biofilm formation monitoring in oligotrophic conditions and growth medium using viable counts of harvested biofilm bacteria (II, IV).
- Flow cytometry of harvested and fluorescently stained microbial cells (II).
- DNase I treatment of bacterial biofilms for degradation of extracellular DNA (II).
- Confocal laser scanning microscopy of fluorescently stained biofilms (II, IV).
- Evaluation of antibacterial activity of photocatalytic surfaces in multiple time points using in-house modification of combined ISO22196/ISO27447 standard protocols for solid surface testing with thin layer of microbial suspension (III).
- Evaluating ionic Zn toxicity in surface test conditions based on the above protocol (III).
- Cultivation of microbes for viability estimation (I-IV).
- Statistical analysis, including correlation, two-tailed Student's *t*-test, one-way and two-way ANOVA analysis with appropriate *post-hoc* tests at $\alpha=0.05$ performed in either R or GraphPad Prism (I-IV).

4 RESULTS AND DISCUSSION

To provide a methodological overview of the publications used in the current thesis, combinations of the main methods contributed by the author, surface types and test organisms used in the publications are summarized in Table 2.

Table 2. Overview of the surfaces, target organisms, test environment used, and main methods contributed by the author in publications I-IV.

Paper	Anti-microbial ingredient	Main method	Viability endpoint	Test medium	Test organism
I	Copper and copper alloy coupon surfaces	Planktonic: surface incubation with bioluminescent bacterial biosensors	Bioluminescence measurement in plate format; CFU counts	LB	<i>E. coli</i> MC1061 (pSLcueR/pDNPcopAlux) <i>E. coli</i> MC1061 (pDNIux)
II	None, uncoated glass substrate	Biofilm formation in static system; viability staining, epifluorescent microscopy, flow cytometry	Fluorescent signal count; CFU count	PBS	<i>E. coli</i> MG1655 <i>Staphylococcus epidermidis</i> DSM 20044
III	Nano-ZnO or nano-ZnO/Ag on glass substrate	Planktonic: modified ISO22196/ISO27447 (antibacterial activity of photocatalytic materials)	CFU count	500x diluted nutrient broth in deionized water	<i>E. coli</i> MG1655 <i>S. aureus</i> ATCC25923 <i>C. albicans</i> CA14
IV	Nano-ZnO/Ag on glass substrate	Biofilm formation in static system; epifluorescent microscopy	CFU count	Oligotrophic: 500x diluted nutrient broth in synthetic tap water; Growth media: LB, YPD	<i>E. coli</i> MG1655 <i>S. aureus</i> ATCC25923 <i>C. albicans</i> CA14

4.1 Bacterial biosensors in rapid *in situ* screening of copper-based antibacterial surfaces (Publication I).

Recombinant bioluminescent viability indicator and metal-induced sensor strains of *E. coli* have been successfully used for rapid evaluation of bacterial viability and metal bioavailability of soluble metal salts and NP suspensions (Bondarenko et al., 2013; Ivask et al., 2009). In case of solutions or suspensions usually homogenous distribution of metal ions and/or NPs is expected or achieved by *e.g.*, ultrasonication, and analysis is easily carried out in multiwell plate format. In the current study we aimed to adapt the bioluminescence assay for *in situ* surface screening to measure not only antibacterial effect of released metal ions but also microbe-surface interactions.

Main results:

- Recombinant bioluminescent *E. coli* copper biosensor system was successfully optimized to be used for rapid *in situ* antimicrobial surface screening.
- Decrease in bioluminescence of constitutively expressing *E. coli* strain on copper-based surfaces showed a good correlation with viable counts.
- Bioluminescence intensity of inducible copper biosensor was in correlation with copper content in copper alloy surfaces and not with amount of copper released from the material indicating a major role of direct microbe-surface interactions on antimicrobial copper-based surfaces in addition to release of copper ions.
- Biosensor performance was dependent on medium of choice and amount of inoculum.

Discussion

In this publication we present a quick and robust method for measuring both antimicrobial properties (“lights off”; Fig. 5, left) of solid surfaces as well as sub-lethal interactions (“lights on”, Fig. 5, right) of copper-based materials and biosensor *E. coli* cells. The method deploys a non-disruptive real-time *in situ* luminescence read-out at room temperature that can measure both a decrease in bioluminescence of the “lights off” strain due to bactericidal effects of the tested surfaces and an increase in bioluminescence of the “lights on” strain due to release or direct contact and bioavailability of active antimicrobial ingredient. The test format could be coupled to more time-consuming traditional plate counts and released active ingredient quantification as a reference. This enables the method to be used as a robust and easily up-scaled screening tool in material development phase. Here we used an *E. coli* strain sensing copper ions, but biosensor strains for other metal ions (Ivask et al., 2009) or intracellular stress conditions (Bondarenko et al., 2012) providing mechanistic information on microbe-surface interactions *etc.* can be adapted to specific needs.

Although it is a planktonic test using short incubation with liquid culture, we were able to demonstrate surface effect as copper biosensor signal intensity was correlated with material copper content and not the amount of copper released from the surfaces. Similar correlation with material copper content has been observed also by Róžańska *et al.* (Róžańska et al., 2017). This effect is possibly caused by direct microbe-surface interactions and variable local Cu ion concentration in bacterial microenvironments as opposed to instrumentally measured released copper concentration providing a mean value in the test system. Thus, these direct interactions can only be registered *in situ* and

not using *e.g.*, surface eluates that only represent released ion proportion of the antibacterial properties of copper surfaces.

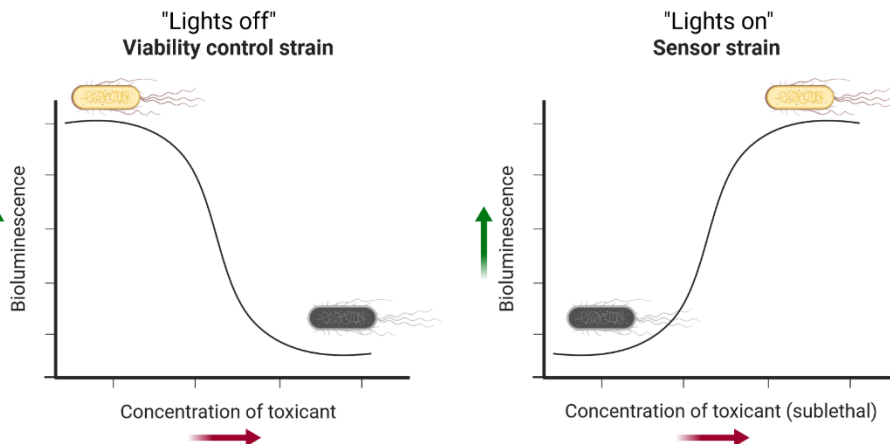


Figure 5. Working principle of bacterial viability control strain and inducible sensor strain in the bioluminescence assay. Viability control strain (left) constitutively expresses *luxCDABE* resulting in luminescence (yellow cell) and loses luminescence intensity with increase of toxicant (*e.g.*, metal ions) and decrease in bacterial viability (“lights off”). Inducible sensor strain (right) does not initially express luminescence (grey cell) and demonstrates concentration-dependent increases in luminescence intensity at sublethal metal concentrations (“lights on”). Combining the two *E. coli* strains relative bioavailable metal concentrations can be assessed against solutions with known concentrations of soluble metal salts in otherwise identical conditions. In this publication copper biosensor *E. coli* [pSLcueR/pDNPcopAlux] and constitutively expressing *E. coli* [pDNlux] were used.

Although the test format presents an easy and fast method for the characterization of metal-based antimicrobial surfaces, limitations of the method should be taken into account *e.g.*, that it is metal-dependent promotor activity of the *E. coli* biosensor strain that causes bioluminescence read-out and not directly extracellular total or intracellular bioavailable copper concentration. The set-up also requires the use of a reference assay based on known concentrations of soluble metal ions for calibration to measure relative bioavailability in otherwise identical setup. Another limitation of the method is its usability in different media. Bioluminescence signal production is an energy-extensive process, needs liquid environment and is not supported in nutrient-poor test environments such as water or extremely diluted nutrient broths used in ISO methods such as ISO 22196. Minimally complexing media can be used to increase sensitivity of the method and metal-complexing organic-rich culture media, such as LB in this publication, can be used to analyse metal surfaces that have too high antibacterial activity to measure sub-toxic effects in non-complexing media. One has to also consider that different media not only differ in their metal complexing properties and thus affect metal toxicity but also affect metal release from the surface materials as demonstrated by us in this study and others (Hans et al., 2013; Käkinen et al., 2011; Molteni et al., 2010).

Main conclusion:

Recombinant bacterial biosensors can be used for rapid screening of antimicrobial surface materials and *in situ* measurement of luminescence reveals sub-lethal surface contact effects that could not be observed using surface eluates.











4.2 *In situ* biofilm viability staining with propidium iodide (Publication II)

Membrane integrity based *in situ* fluorescent viability staining is widely used for biofilm visualization in microscopy as well as for quantitative viability evaluation and assessment of antibiofilm intervention efficacy as it allows for studying undisturbed biofilms (Azeredo et al., 2017). Working principle of Syto9 and propidium iodide (PI) or similar combinations of membrane-permeable and impermeable DNA stains, respectively, is based on the assumption that nucleic acids in a viable cell are surrounded by intact membrane impermeable to stains such as PI (Boulos et al., 1999). While this largely applies to planktonic cultures, extracellular DNA (eDNA) is a well-known phenomenon in biofilms since Whitchurch *et al.* (Whitchurch, 2002) and is in many cases critically needed for biofilm formation (Okshevsky & Meyer, 2015) or even actively secreted resulting in enhanced biofilm formation (Zweig et al., 2014). We aimed to investigate if PI can stain viable adherent bacterial cells and therefore cause underestimation of biofilm viability using double-staining with PI and Syto9.

Main results:

- *In situ* double-staining with PI and Syto9 dramatically underestimated *E. coli* and *S. epidermidis* initial biofilm vitality and viability compared to fluorescein diacetate (FDA) staining and CFU counts, respectively. Quantitative results are summarized in Table 3.
- Red (PI) to green (Syto9) staining ratio was reversed after harvesting biofilm cells by ultrasonication suggesting that the component staining red *in situ* was in the ECM of the biofilms and was removed during harvesting of biofilm cells.
- CLSM revealed double-staining of individual adherent cells with green (Syto9) interiors and diffuse extracellular red corona (PI).
- Double-staining with DNA-binding Syto9 and amyloid stain Congo red resulted in similar staining pattern illustrating possible spatial energy transfer from intracellular green signal to extracellular red signal masking the former.

Table 3. Viability estimates of identical 24 h biofilms acquired with different methods. Each coloured cell denotes 5% of total cellular signal count (red – dead; green – viable; grey - leftover proportion of estimated total cell count in a sample).

	<i>In situ</i> staining with PI+Syto9	<i>In situ</i> FDA vs PI+Syto9 total count	Harvested, PI+Syto9, on filter	Harvested, PI+Syto9, flow cytometry	Harvested, plate count vs PI+Syto9 total count on filter
<i>E. coli</i>					
<i>S. epidermidis</i>					

Discussion

The presented results not only demonstrate that PI-staining can underestimate biofilm viability but also give a quantitative assessment of the potentially dramatic effect. The presence of extracellular nucleic acids and eDNA in particular, although speculated to interfere with PI-staining before (Gião & Keevil, 2014; Vilain et al., 2009), is still largely overlooked in publications using viability staining of biofilms. Since our study of biofilms formed in extremely oligotrophic conditions (in PBS), underestimation of viability using PI has also been demonstrated in rich growth medium (Kragh et al., 2019) which suggests a more universal critical flaw in viability staining with DNA-binding dyes on biofilms.

Our CLSM results demonstrating green fluorescing cell interiors (Syto9) surrounded by diffuse red PI corona look similar to what has been found but not quantified in previous publications (Gallo et al., 2015; Vilain et al., 2009). This double-staining pattern is visualized in the middle scenario on Fig. 6 above as opposed to cells with damaged membranes (left) and intact ones (right). The inset illustrating excitation/emission spectra of PI and Syto9 offers insight to why the double-stained cells look red in epifluorescence microscopy while revealing green interiors in CLSM. It might be due to the fact that Syto9 emission largely overlaps with PI excitation wavelengths thereby enabling spatial energy transfer.

Interestingly, similar staining pattern in epifluorescence microscopy was detected for combining Syto9 with Congo red (Supplementary Fig. 12 in Paper IV). Congo red is an amyloid stain binding to surface-associated amyloid fibres with similar excitation/emission characteristics to PI but not competing for nucleic acid binding.

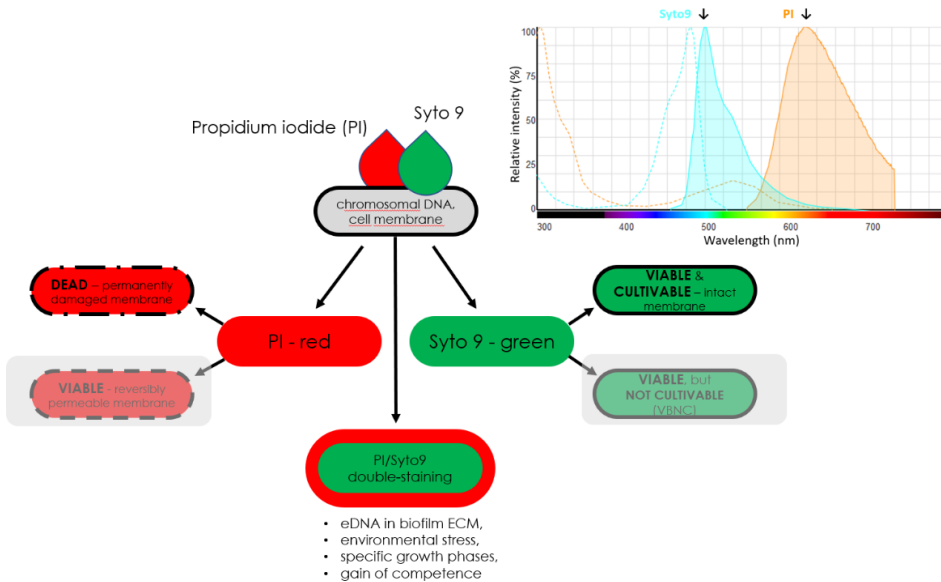


Figure 6. Working principle of viability staining with intact membrane impermeable propidium iodide (PI) and membrane-permeable Syto9 and proposed mechanism for PI/Syto9 double-staining. Excitation (dotted lines) and emission (filled areas) spectra of both stains generated by Thermo Fisher Fluorescence SpectraViewer demonstrating overlap of Syto9 emission (blue fill) and PI excitation (orange dotted line) is shown in the top right corner.

On one hand it confirms the energy transfer hypothesis with extracellular Congo red signal masking the intracellular Syto9 signal similarly to PI but without competition to bind DNA. On the other hand, it suggests that there might be a shared cause for similar staining patterns. Indeed, it has been shown that SAFs can bind eDNA and eDNA can enhance SAF formation (Fernández-Tresguerres et al., 2010; Gallo et al., 2015; Nicastro et al., 2019; Schwartz et al., 2016). Thereby, SAF could mediate eDNA binding to bacterial cell walls. Amyloid proteins are known to be associated with DNA conformational change from right-handed B-DNA to left-handed Z-DNA (Hegde et al., 2004; Suram et al., 2002; Yu et al., 2007). It has been recently confirmed that B-DNA to Z-DNA conversion of eDNA is also occurring during biofilm maturation of several bacterial species (Buzzo et al., 2021) and could thereby also negatively affect PI-staining of eDNA in mature biofilms based on PI similarity to ethidium bromide (Walker et al., 1985). The latter indicates that discrepancies in viability staining with DNA-binding stains could be dependent not only on the presence of eDNA, but also the stage of biofilm development.

Main conclusion:

Membrane integrity based viability staining using nucleic acid stains such as PI, although widely used on biofilms, can dramatically underestimate viability of adherent bacterial cells. If used, caution should be taken in result interpretation and proper viability controls should be used.

4.3 Antimicrobial and antibiofilm properties of solid surfaces coated with nano-ZnO or nano-ZnO/Ag (Publications III, IV)

Antimicrobial properties of ionic silver and zinc as well as Ag and ZnO NPs are well known and widely published but generally tested as respective salt solutions or NP suspensions with uniform ion/particle distribution in the test system. Our aim was to characterise antimicrobial and antibiofilm properties of nano-ZnO and nano-ZnO/Ag covered solid surfaces as a proof-of-concept for further antimicrobial high-touch surface development and to assess optimal coating densities of such surfaces.

Main results:

1. The nano-ZnO and nano-ZnO/Ag covered surfaces showed antimicrobial activity in both dark and UVA-exposed conditions using 500x diluted nutrient broth and thin layer planktonic method (modified ISO 27447, illustrated on Fig. 7).
 - Antibacterial dose effect was demonstrated in dark and UVA-exposed lighting conditions for both NP surface coverage densities and Ag content.
 - Photocatalysis and higher Zn dissolution contributed to antibacterial action during UVA-exposure.
 - Due to the lack of photocatalysis and lower Zn dissolution antibacterial efficacy in dark conditions was generally lower than with UVA exposure. Higher Ag dissolution contributed to antibacterial action in dark conditions.
 - *S. aureus* was more sensitive to surface-bound ZnO and *E. coli* to Ag in dark conditions, although *E. coli* appeared more sensitive to ionic Zn in respective salt exposure.
 - Antifungal activity against *C. albicans* was negligible with < 1 log maximal reduction in viable count after 1 hour, regardless of lighting condition.
 - Dense coverage nano-ZnO and sparse coverage nano-ZnO/Ag (2.7 mol% Ag) surfaces were the most effective.
2. The nano-ZnO and nano-ZnO/Ag covered surfaces demonstrated selective medium-dependent antibiofilm properties in static system under dark ambient conditions.
 - Surfaces inhibited *E. coli* and *S. aureus* biofilm formation in oligotrophic conditions (500x diluted nutrient broth in synthetic tap water, nor supporting exponential growth).
 - Nano-ZnO surfaces enhanced *C. albicans* biofilm formation in oligotrophic conditions. Such enhancement was eliminated by Ag.
 - Antibiofilm properties were accompanied by antibacterial properties towards planktonic bacteria and could be attributed to general metal toxicity.
 - Antibiofilm effects were minor to non-existent in growth medium (organics rich, supporting exponential growth).

- Liquid manipulation steps during sample preparation reduced biofilm biomass and may potentially introduce bias to comparison of biofilms formed in different conditions (e.g., treatment vs control).

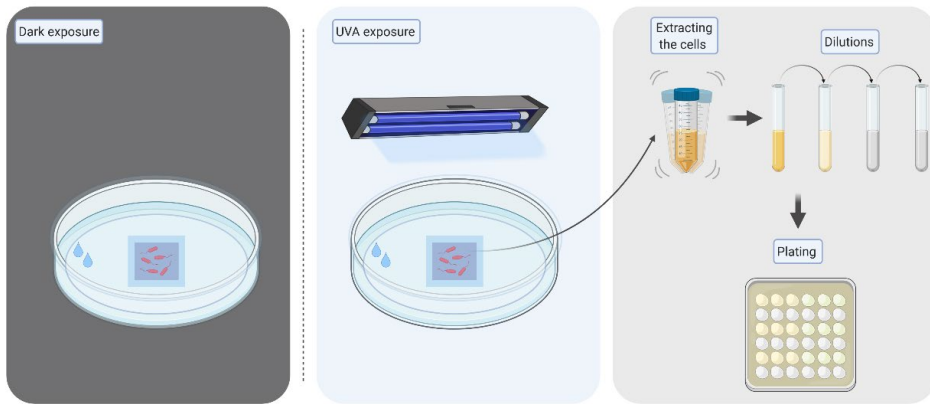


Figure 7. Scheme of modified ISO 27447 method. Surfaces are suspended above wet filter paper (by a glass U rod) and the Petri dishes are covered by lids in dark conditions (left panel) or by UVA-transmissive borosilicate glass exposed to UVA light (middle panel). Bacterial suspension is evenly distributed across the surfaces of interest by UVA-transmissive polyethylene cover film. Cells are extracted from the exposed surfaces using a toxicity neutralizing medium, serially diluted in PBS and drop-plated for counting (right panel).

Discussion

It is generally regarded, that silver tends to be more toxic to Gram-negative bacteria than Gram-positive bacteria. Our results follow the same trend in both thin layer exposure (Publication III) and static biofilm test (Publication IV) with *E. coli* being more susceptible to Ag than *S. aureus*. This could be explained by differences in the cell wall and Gram-positive bacteria having less exposed membrane and more of the negatively charged silver ion trapping peptidoglycan and teichoic acids on the cell surface.

There also seems to be a consistent trend of *S. aureus* being more susceptible to zinc-based surfaces in dark exposure than *E. coli* although ionic zinc was more toxic to *E. coli* in thin layer mock exposure (Publication III, Supplementary Fig. S5). Free ZnO NPs have also been demonstrated to be more toxic to *S. aureus* than *E. coli* (Wahab et al., 2012). We cannot yet offer an experimental explanation to this phenomenon and it needs to be studied further, but we propose that there is a combined effect of two mechanisms of action to account for. Firstly, surface-specific antimicrobial activity arising from direct microbe-surface interaction that could be suspected from the fact that nano-ZnO surfaces were more toxic to *S. aureus* and *C. albicans* than the corresponding released Zn concentration (Publication III, Fig. 5). Secondly, it is possible that ZnO NPs produce ROS without photoactivation (Lipovsky et al., 2009; Sun et al., 2019) resulting in respective antimicrobial activity (Hirota et al., 2010; Lipovsky et al., 2011). Hydrogen peroxide that has antibacterial activity due to the formation of ROS is generally more toxic to Gram-positive than Gram-negative bacteria (McDonnell & Russell, 1999). Hence, ROS formation on nano-ZnO surfaces without photoactivation would explain lower viability of *S. aureus* on nano-ZnO surfaces than in the corresponding released Zn

concentration (Publication III, Fig. 5). Availability of both Mn and Zn are limited in host organisms resulting in nutritional immunity and impaired defensive response against host immune system, especially ROS-response of *S. aureus* (Gaupp et al., 2012). On the other hand, also Zn excess has been described to interfere with manganese transport resulting in Mn starvation that can lead to impaired ROS response, a system well described for *Streptococcus pneumoniae* (Eijkelkamp et al., 2014; McDevitt et al., 2011; Morey et al., 2015). No change in ROS response (Raghupathi et al., 2011) or even down-regulation of ROS response (Pati et al., 2014) upon ZnO NP exposure has also been described for *S. aureus* suggesting possible presence of similar metal binding competition.

Combining ZnO, silver and UVA exposure could therefore target a wider range of microbial species in close contact wet conditions (Publication III), lead to biofilm formation inhibition and control of planktonic viability (Publication IV).

Main conclusion

Nano-ZnO and nano-ZnO/Ag covered surfaces offer rapid dual-action antibacterial activity with >2 logs decrease in viability of *E. coli* and *S. aureus* by combining metal ion toxicity with photocatalysis. Combination of ZnO and Ag grants a more uniform activity against Gram- positive and Gram-negative species with differing metal ion sensitivity. Antimicrobial and antibiofilm properties of the surfaces depend on both, surface coating composition and test media while ZnO potentially enhances biofilm formation by *C. albicans* in oligotrophic medium. The latter effect is counteracted with the addition of Ag.

5. CONCLUSIONS

The principal findings of the present thesis are:

1. *In situ* application of bioluminescent sensor bacteria offers better insight into sublethal contact-driven effects of antibacterial release-based copper surfaces than measuring the amount of copper released from the surfaces during exposure (I).
2. Antimicrobial activity of release-based solid surfaces cannot be predicted solely from the amount of released agents due to direct contact effects (I, III)
3. Methods developed for studying planktonic bacteria can in some cases be successfully applied to microbe-surface interactions (I) but special consideration has to be given to adapt planktonic methods to study biofilms as they can produce false results (II).
4. Membrane-integrity based viability staining of biofilms with DNA-binding dyes can dramatically underestimate biofilm viability, possibly due to extracellular nucleic acids (II).
5. Combining release-based and photocatalytic agents on solid surfaces improves overall antimicrobial activity of nano-coated surfaces (III). Combination of ZnO and Ag acting via release of ionic Zn and Ag as well as photocatalytic properties of ZnO presented highest efficacy.
6. Biofilm formation depends on liquid environment used and can be enhanced or decreased by surface coating depending on the type of microorganism used for testing (IV).
7. Antimicrobial and anti-biofilm efficiency is very different towards bacteria and fungi; therefore, different and fit for purpose organisms should be used for antimicrobial testing of the surfaces (III, IV).

References

- Adlhart, C., Verran, J., Azevedo, N. F., Olmez, H., Keinänen-Toivola, M. M., Gouveia, I., Melo, L. F., & Crijns, F. (2018). Surface modifications for antimicrobial effects in the healthcare setting: A critical overview. *Journal of Hospital Infection*, *99*(3), 239–249. <https://doi.org/10.1016/j.jhin.2018.01.018>
- Alhede, M., Kragh, K. N., Qvortrup, K., Allesen-Holm, M., van Gennip, M., Christensen, L. D., Jensen, P. Ø., Nielsen, A. K., Parsek, M., Wozniak, D., Molin, S., Tolker-Nielsen, T., Høiby, N., Givskov, M., & Bjarnsholt, T. (2011). Phenotypes of Non-Attached *Pseudomonas aeruginosa* Aggregates Resemble Surface Attached Biofilm. *PLoS ONE*, *6*(11), e27943. <https://doi.org/10.1371/journal.pone.0027943>
- Allkja, J., van Charante, F., Aizawa, J., Reigada, I., Guarch-Pérez, C., Vazquez-Rodriguez, J. A., Cos, P., Coenye, T., Fallarero, A., Zaat, S. A. J., Felici, A., Ferrari, L., Azevedo, N. F., Parker, A. E., & Goeres, D. M. (2021). Interlaboratory study for the evaluation of three microtiter plate-based biofilm quantification methods. *Scientific Reports*, *11*(1), 13779. <https://doi.org/10.1038/s41598-021-93115-w>
- Al-Shabib, N. A., Husain, F. M., Ahmed, F., Khan, R. A., Ahmad, I., Alsharaeh, E., Khan, M. S., Hussain, A., Rehman, M. T., Yusuf, M., Hassan, I., Khan, J. M., Ashraf, G. M., Alsalmeh, A., Al-Ajmi, M. F., Tarasov, V. V., & Aliev, G. (2016). Biogenic synthesis of Zinc oxide nanostructures from *Nigella sativa* seed: Prospective role as food packaging material inhibiting broad-spectrum quorum sensing and biofilm. *Scientific Reports*, *6*(1), 36761. <https://doi.org/10.1038/srep36761>
- Álvarez, G., González, M., Isabal, S., Blanc, V., & León, R. (2013). Method to quantify live and dead cells in multi-species oral biofilm by real-time PCR with propidium monoazide. *AMB Express*, *3*(1), 1. <https://doi.org/10.1186/2191-0855-3-1>
- Andreini, C., Bertini, I., Cavallaro, G., Holliday, G. L., & Thornton, J. M. (2008). Metal ions in biological catalysis: From enzyme databases to general principles. *JBIC Journal of Biological Inorganic Chemistry*, *13*(8), 1205–1218. <https://doi.org/10.1007/s00775-008-0404-5>
- Azeredo, J., Azevedo, N. F., Briandet, R., Cerca, N., Coenye, T., Costa, A. R., Desvaux, M., Di Bonaventura, G., Hébraud, M., Jaglic, Z., Kačániová, M., Knøchel, S., Lourenço, A., Mergulhão, F., Meyer, R. L., Nychas, G., Simões, M., Tresse, O., & Sternberg, C. (2017). Critical review on biofilm methods. *Critical Reviews in Microbiology*, *43*(3), 313–351. <https://doi.org/10.1080/1040841X.2016.1208146>
- Baker-Austin, C., Wright, M. S., Stepanauskas, R., & McArthur, J. V. (2006). Co-selection of antibiotic and metal resistance. *Trends in Microbiology*, *14*(4), 176–182. <https://doi.org/10.1016/j.tim.2006.02.006>
- Barillo, D. J., & Marx, D. E. (2014). Silver in medicine: A brief history BC 335 to present. *Burns*, *40*, S3–S8. <https://doi.org/10.1016/j.burns.2014.09.009>
- Bazzi, W., Abou Fayad, A. G., Nasser, A., Haraoui, L.-P., Dewachi, O., Abou-Sitta, G., Nguyen, V.-K., Abara, A., Karah, N., Landecker, H., Knapp, C., McEvoy, M. M., Zaman, M. H., Higgins, P. G., & Matar, G. M. (2020). Heavy Metal Toxicity in Armed Conflicts Potentiates AMR in *A. baumannii* by Selecting for Antibiotic and Heavy Metal Co-resistance Mechanisms. *Frontiers in Microbiology*, *11*, 68. <https://doi.org/10.3389/fmicb.2020.00068>

- Bednarska, N. G., van Eldere, J., Gallardo, R., Ganesan, A., Ramakers, M., Vogel, I., Baatsen, P., Staes, A., Goethals, M., Hammarström, P., Nilsson, K. P. R., Gevaert, K., Schymkowitz, J., & Rousseau, F. (2016). Protein aggregation as an antibiotic design strategy: Aggregating Antimicrobial Peptides. *Molecular Microbiology*, *99*(5), 849–865. <https://doi.org/10.1111/mmi.13269>
- Behra, R., Sigg, L., Clift, M. J. D., Herzog, F., Minghetti, M., Johnston, B., Petri-Fink, A., & Rothen-Rutishauser, B. (2013). Bioavailability of silver nanoparticles and ions: From a chemical and biochemical perspective. *Journal of the Royal Society, Interface*, *10*(87), 20130396. <https://doi.org/10.1098/rsif.2013.0396>
- Bjarnsholt, T., Alhede, M., Alhede, M., Eickhardt-Sørensen, S. R., Moser, C., Kühn, M., Jensen, P. Ø., & Høiby, N. (2013). The in vivo biofilm. *Trends in Microbiology*, *21*(9), 466–474. <https://doi.org/10.1016/j.tim.2013.06.002>
- Bondarenko, O., Ivask, A., Käkänen, A., & Kahru, A. (2012). Sub-toxic effects of CuO nanoparticles on bacteria: Kinetics, role of Cu ions and possible mechanisms of action. *Environmental Pollution*, *169*, 81–89. <https://doi.org/10.1016/j.envpol.2012.05.009>
- Bondarenko, O., Ivask, A., Käkänen, A., Kurvet, I., & Kahru, A. (2013). Particle-Cell Contact Enhances Antibacterial Activity of Silver Nanoparticles. *PLoS ONE*, *8*(5), e64060. <https://doi.org/10.1371/journal.pone.0064060>
- Borkow, G. (2012). Using Copper to Fight Microorganisms. *Current Chemical Biology*, *6*(2), 93–103. <https://doi.org/10.2174/187231312801254723>
- Boulos, L., Prévost, M., Barbeau, B., Coallier, J., & Desjardins, R. (1999). LIVE/DEAD® BacLight™: Application of a new rapid staining method for direct enumeration of viable and total bacteria in drinking water. *Journal of Microbiological Methods*, *37*(1), 77–86. [https://doi.org/10.1016/S0167-7012\(99\)00048-2](https://doi.org/10.1016/S0167-7012(99)00048-2)
- Boyce, J. M. (2007). Environmental contamination makes an important contribution to hospital infection. *Journal of Hospital Infection*, *65*, 50–54. [https://doi.org/10.1016/S0195-6701\(07\)60015-2](https://doi.org/10.1016/S0195-6701(07)60015-2)
- Bragg, P. D., & Rainnie, D. J. (1974). The effect of silver ions on the respiratory chain of *Escherichia coli*. *Canadian Journal of Microbiology*, *20*(6), 883–889. <https://doi.org/10.1139/m74-135>
- Brayner, R., Ferrari-Iliou, R., Brivois, N., Djediat, S., Benedetti, M. F., & Fiévet, F. (2006). Toxicological Impact Studies Based on *Escherichia coli* Bacteria in Ultrafine ZnO Nanoparticles Colloidal Medium. *Nano Letters*, *6*(4), 866–870. <https://doi.org/10.1021/nl052326h>
- Butina, K., Tomac, A., Choong, F. X., Shirani, H., Nilsson, K. P. R., Löffler, S., & Richter-Dahlfors, A. (2020). Optotracing for selective fluorescence-based detection, visualization and quantification of live *S. aureus* in real-time. *Npj Biofilms and Microbiomes*, *6*(1), 35. <https://doi.org/10.1038/s41522-020-00150-y>
- Buzzo, J. R., Devaraj, A., Gloag, E. S., Jurgisek, J. A., Robledo-Avila, F., Kesler, T., Wilbanks, K., Mashburn-Warren, L., Balu, S., Wickham, J., Novotny, L. A., Stoodley, P., Bakaletz, L. O., & Goodman, S. D. (2021). Z-form extracellular DNA is a structural component of the bacterial biofilm matrix. *Cell*, *S0092867421012204*. <https://doi.org/10.1016/j.cell.2021.10.010>
- Campos, M. D., Zucchi, P. C., Phung, A., Leonard, S. N., & Hirsch, E. B. (2016). The Activity of Antimicrobial Surfaces Varies by Testing Protocol Utilized. *PLoS ONE*, *11*(8), e0160728. <https://doi.org/10.1371/journal.pone.0160728>

- Cerca, F., Trigo, G., Correia, A., Cerca, N., Azeredo, J., & Vilanova, M. (2011). SYBR green as a fluorescent probe to evaluate the biofilm physiological state of *Staphylococcus epidermidis*, using flow cytometry. *Canadian Journal of Microbiology*, *57*(10), 850–856. <https://doi.org/10.1139/w11-078>
- Ceri, H., Olson, M. E., Stremick, C., Read, R. R., Morck, D., & Buret, A. (1999). The Calgary Biofilm Device: New technology for rapid determination of antibiotic susceptibilities of bacterial biofilms. *Journal of Clinical Microbiology*, *37*(6), 1771–1776.
- Chavez de Paz, L. E., Hamilton, I. R., & Svensater, G. (2008). Oral bacteria in biofilms exhibit slow reactivation from nutrient deprivation. *Microbiology*, *154*(7), 1927–1938. <https://doi.org/10.1099/mic.0.2008/016576-0>
- Chen, D., Li, J., Pan, T., Wu, R., Tao, Y., & Lin, H. (2020). The broad-spectrum antibiofilm activity of amyloid-forming hexapeptides. *Microbial Biotechnology*, *14*(2), 656–667. <https://doi.org/10.1111/1751-7915.13721>
- Choong, F. X., Bäck, M., Fahlén, S., Johansson, L. B., Melican, K., Rhen, M., Nilsson, K. P. R., & Richter-Dahlfors, A. (2016). Real-time optotracing of curli and cellulose in live *Salmonella* biofilms using luminescent oligothiophenes. *Npj Biofilms and Microbiomes*, *2*(1), 16024. <https://doi.org/10.1038/npjbiofilms.2016.24>
- Christensen, G. D., Simpson, W. A., Younger, J. J., Baddour, L. M., Barrett, F. F., Melton, D. M., & Beachey, E. H. (1985). Adherence of coagulase-negative staphylococci to plastic tissue culture plates: A quantitative model for the adherence of staphylococci to medical devices. *Journal of Clinical Microbiology*, *22*(6), 996. <http://jcm.asm.org/content/22/6/996.abstract>
- Costerton, J. W., Geesey, G. G., & Cheng, K.-J. (1978). How Bacteria Stick. *Scientific American*, *238*(1), 86–95. <https://doi.org/10.1038/scientificamerican0178-86>
- Costerton, J. W., Lewandowski, Z., Caldwell, D. E., Korber, D. R., & Lappin-Scott, H. M. (1995). Microbial Biofilms. *Annual Review of Microbiology*, *49*(1), 711–745. <https://doi.org/10.1146/annurev.mi.49.100195.003431>
- Couñago, R. M., Ween, M. P., Begg, S. L., Bajaj, M., Zuegg, J., O'Mara, M. L., Cooper, M. A., McEwan, A. G., Paton, J. C., Kobe, B., & McDevitt, C. A. (2014). Imperfect coordination chemistry facilitates metal ion release in the Psa permease. *Nature Chemical Biology*, *10*(1), 35–41. <https://doi.org/10.1038/nchembio.1382>
- Dauvergne, E., Lacquemant, C., Adjidé, C., & Mullié, C. (2020). Validation of a Worst-Case Scenario Method Adapted to the Healthcare Environment for Testing the Antibacterial Effect of Brass Surfaces and Implementation on Hospital Antibiotic-Resistant Strains. *Antibiotics*, *9*(5), 245. <https://doi.org/10.3390/antibiotics9050245>
- Dibrov, P., Dzioba, J., Gosink, K. K., & Häse, C. C. (2002). Chemiosmotic Mechanism of Antimicrobial Activity of Ag⁺ in *Vibrio cholerae*. *Antimicrobial Agents and Chemotherapy*, *46*(8), 2668–2670. <https://doi.org/10.1128/AAC.46.8.2668-2670.2002>
- Dutta, R. K., Nenavathu, B. P., Gangishetty, M. K., & Reddy, A. V. R. (2012). Studies on antibacterial activity of ZnO nanoparticles by ROS induced lipid peroxidation. *Colloids and Surfaces B: Biointerfaces*, *94*, 143–150. <https://doi.org/10.1016/j.colsurfb.2012.01.046>
- ECHA. (2018). *Guidance on the Biocidal Products Regulation. Volume II Efficacy—Assessment and Evaluation (Parts B+C)*. Publications Office. <https://data.europa.eu/doi/10.2823/95242>

- Eijkelkamp, B. A., Morey, J. R., Ween, M. P., Ong, C. Y., McEwan, A. G., Paton, J. C., & McDevitt, C. A. (2014). Extracellular Zinc Competitively Inhibits Manganese Uptake and Compromises Oxidative Stress Management in *Streptococcus pneumoniae*. *PLoS ONE*, *9*(2), e89427. <https://doi.org/10.1371/journal.pone.0089427>
- EPA. (2020a). *Interim Method for the Evaluation of Bactericidal Activity of Hard, Non-porous Copper-Containing Surface Products*. <https://www.epa.gov/pesticide-analytical-methods/antimicrobial-testing-methods-procedures-interim-method-evaluation>
- EPA. (2020b). *Interim Method for Evaluating the Efficacy of Antimicrobial Surface Coatings*. <https://www.epa.gov/pesticide-analytical-methods/antimicrobial-testing-methods-procedures-interim-method-evaluating>
- EPA. (2021). *Interim Guidance—Review for Products Adding Residual Efficacy Claims*. <https://www.epa.gov/pesticide-registration/interim-guidance-review-products-adding-residual-efficacy-claims>
- Feng, Q. L., Wu, J., Chen, G. Q., Cui, F. Z., Kim, T. N., & Kim, J. O. (2000). A mechanistic study of the antibacterial effect of silver ions on *Escherichia coli* and *Staphylococcus aureus*. *Journal of Biomedical Materials Research*, *52*(4), 662–668. [https://doi.org/10.1002/1097-4636\(20001215\)52:4<662::aid-jbm10>3.0.co;2-3](https://doi.org/10.1002/1097-4636(20001215)52:4<662::aid-jbm10>3.0.co;2-3)
- Fernández-Tresguerres, M. E., Moreno-Díaz de la Espina, S., Gasset-Rosa, F., & Giraldo, R. (2010). A DNA-promoted amyloid proteinopathy in *Escherichia coli*: Synthetic bacterial amyloidosis. *Molecular Microbiology*, *77*(6), 1456–1469. <https://doi.org/10.1111/j.1365-2958.2010.07299.x>
- Flemming, H.-C., Baveye, P., Neu, T. R., Stoodley, P., Szewzyk, U., Wingender, J., & Wuertz, S. (2021). Who put the film in biofilm? The migration of a term from wastewater engineering to medicine and beyond. *Npj Biofilms and Microbiomes*, *7*(1), 10. <https://doi.org/10.1038/s41522-020-00183-3>
- Flemming, H.-C., & Wingender, J. (2010). The biofilm matrix. *Nature Reviews Microbiology*. <https://doi.org/10.1038/nrmicro2415>
- Flemming, H.-C., & Wuertz, S. (2019). Bacteria and archaea on Earth and their abundance in biofilms. *Nature Reviews Microbiology*, *17*(4), 247–260. <https://doi.org/10.1038/s41579-019-0158-9>
- France, M. T., Cornea, A., Kehlet-Delgado, H., & Forney, L. J. (2019). Spatial structure facilitates the accumulation and persistence of antibiotic-resistant mutants in biofilms. *Evolutionary Applications*, *12*(3), 498–507. <https://doi.org/10.1111/eva.12728>
- Friehs, E., AlSalka, Y., Jonczyk, R., Lavrentieva, A., Jochums, A., Walter, J.-G., Stahl, F., Scheper, T., & Bahnemann, D. (2016). Toxicity, phototoxicity and biocidal activity of nanoparticles employed in photocatalysis. *Journal of Photochemistry and Photobiology C: Photochemistry Reviews*, *29*, 1–28. <https://doi.org/10.1016/j.jphotochemrev.2016.09.001>
- Gallo, P. M., Rapsinski, G. J., Wilson, R. P., Oppong, G. O., Sriram, U., Goulian, M., Buttaro, B., Caricchio, R., Gallucci, S., & Tükel, Ç. (2015). Amyloid-DNA Composites of Bacterial Biofilms Stimulate Autoimmunity. *Immunity*, *42*(6), 1171–1184. <https://doi.org/10.1016/j.immuni.2015.06.002>
- García-Lara, B., Saucedo-Mora, M. Á., Roldán-Sánchez, J. A., Pérez-Eretza, B., Ramasamy, M., Lee, J., Coria-Jimenez, R., Tapia, M., Varela-Guerrero, V., & García-Contreras, R. (2015). Inhibition of quorum-sensing-dependent virulence factors and biofilm formation of clinical and environmental *Pseudomonas aeruginosa* strains by ZnO nanoparticles. *Letters in Applied Microbiology*, *61*(3), 299–305. <https://doi.org/10.1111/lam.12456>

- Gaupp, R., Ledala, N., & Somerville, G. A. (2012). Staphylococcal response to oxidative stress. *Frontiers in Cellular and Infection Microbiology*, 2. <https://doi.org/10.3389/fcimb.2012.00033>
- Ghandour, W., Hubbard, Julia A., Deistung, J., Hughes, Martin N., & Poole, Robert K. (1988). The uptake of silver ions by *Escherichia coli* K12: Toxic effects and interaction with copper ions. *Applied Microbiology and Biotechnology*, 28(6). <https://doi.org/10.1007/BF00250412>
- Gião, M. S., & Keevil, C. W. (2014). *Listeria monocytogenes* Can Form Biofilms in Tap Water and Enter Into the Viable but Non-Cultivable State. *Microbial Ecology*, 67(3), 603–611. <https://doi.org/10.1007/s00248-013-0364-3>
- Gogoi, S. K., Gopinath, P., Paul, A., Ramesh, A., Ghosh, S. S., & Chattopadhyay, A. (2006). Green Fluorescent Protein-Expressing *Escherichia coli* as a Model System for Investigating the Antimicrobial Activities of Silver Nanoparticles. *Langmuir*, 22(22), 9322–9328. <https://doi.org/10.1021/la060661v>
- Gómez-Gómez, B., Arregui, L., Serrano, S., Santos, A., Pérez-Corona, T., & Madrid, Y. (2019). Unravelling mechanisms of bacterial quorum sensing disruption by metal-based nanoparticles. *Science of The Total Environment*, 696, 133869. <https://doi.org/10.1016/j.scitotenv.2019.133869>
- Grass, G., Rensing, C., & Solioz, M. (2011). Metallic Copper as an Antimicrobial Surface. *Applied and Environmental Microbiology*, 77(5), 1541–1547. <https://doi.org/10.1128/AEM.02766-10>
- Grinberg, M., Orevi, T., Steinberg, S., & Kashtan, N. (2019). Bacterial survival in microscopic surface wetness. *ELife*, 8, e48508. <https://doi.org/10.7554/eLife.48508>
- Habash, M. B., Goodyear, M. C., Park, A. J., Surette, M. D., Vis, E. C., Harris, R. J., & Khursigara, C. M. (2017). Potentiation of Tobramycin by Silver Nanoparticles against *Pseudomonas aeruginosa* Biofilms. *Antimicrobial Agents and Chemotherapy*, 61(11), e00415-17, e00415-17. <https://doi.org/10.1128/AAC.00415-17>
- Haferburg, G., & Kothe, E. (2010). Metallomics: Lessons for metalliferous soil remediation. *Applied Microbiology and Biotechnology*, 87(4), 1271–1280. <https://doi.org/10.1007/s00253-010-2695-z>
- Hans, M., Erbe, A., Mathews, S., Chen, Y., Solioz, M., & Mücklich, F. (2013). Role of Copper Oxides in Contact Killing of Bacteria. *Langmuir*, 29(52), 16160–16166. <https://doi.org/10.1021/la404091z>
- Harrison, J. J., Ceri, H., Stremick, C. A., & Turner, R. J. (2004). Biofilm susceptibility to metal toxicity. *Environmental Microbiology*, 6(12), 1220–1227. <https://doi.org/10.1111/j.1462-2920.2004.00656.x>
- Harrison, J. J., Tremaroli, V., Stan, M. A., Chan, C. S., Vacchi-Suzzi, C., Heyne, B. J., Parsek, M. R., Ceri, H., & Turner, R. J. (2009). Chromosomal antioxidant genes have metal ion-specific roles as determinants of bacterial metal tolerance. *Environmental Microbiology*, 11(10), 2491–2509. <https://doi.org/10.1111/j.1462-2920.2009.01973.x>
- Hegde, M. L., Anitha, S., Latha, K. S., Mustak, M. S., Stein, R., Ravid, R., & Rao, K. S. J. (2004). First Evidence for Helical Transitions in Supercoiled DNA by Amyloid β Peptide (1-42) and Aluminum: A New Insight in Understanding Alzheimer's Disease. *Journal of Molecular Neuroscience*, 22(1–2), 19–32. <https://doi.org/10.1385/JMN:22:1-2:19>

- Hengge, R. (2009). Principles of c-di-GMP signalling in bacteria. *Nature Reviews Microbiology*, 7(4), 263–273. <https://doi.org/10.1038/nrmicro2109>
- Hirota, K., Sugimoto, M., Kato, M., Tsukagoshi, K., Tanigawa, T., & Sugimoto, H. (2010). Preparation of zinc oxide ceramics with a sustainable antibacterial activity under dark conditions. *Ceramics International*, 36(2), 497–506. <https://doi.org/10.1016/j.ceramint.2009.09.026>
- Hobman, J. L., & Crossman, L. C. (2015). Bacterial antimicrobial metal ion resistance. *Journal of Medical Microbiology*, 64(5), 471–497. <https://doi.org/10.1099/jmm.0.023036-0>
- Hodgson, E. (2010). Metals. In *A textbook of modern toxicology* (4th ed., pp. 49–54). John Wiley & Sons.
- Holt, K. B., & Bard, A. J. (2005). Interaction of Silver(I) Ions with the Respiratory Chain of *Escherichia coli*: An Electrochemical and Scanning Electrochemical Microscopy Study of the Antimicrobial Mechanism of Micromolar Ag⁺. *Biochemistry*, 44(39), 13214–13223. <https://doi.org/10.1021/bi0508542>
- Hosler, J. P., Ferguson-Miller, S., & Mills, D. A. (2006). Energy Transduction: Proton Transfer Through the Respiratory Complexes. *Annual Review of Biochemistry*, 75(1), 165–187. <https://doi.org/10.1146/annurev.biochem.75.062003.101730>
- Huma, Z., Javed, I., Zhang, Z., Bilal, H., Sun, Y., Hussain, S. Z., Davis, T. P., Otzen, D. E., Landersdorfer, C. B., Ding, F., Hussain, I., & Ke, P. C. (2020). Nanosilver Mitigates Biofilm Formation via FapC Amyloidosis Inhibition. *Small*, 1906674. <https://doi.org/10.1002/smll.201906674>
- ISO. (2011). *ISO 22196:2011 Measurement of antibacterial activity on plastics and other non-porous surfaces*.
- ISO. (2013). *ISO 20743:2013 Textiles—Determination of antibacterial activity of textile products*.
- ISO. (2015). *ISO 13697:2015 Chemical disinfectants and antiseptics—Quantitative non-porous surface test for the evaluation of bactericidal and/or fungicidal activity of chemical disinfectants used in food, industrial, domestic and institutional areas—Test method and requirements without mechanical action (phase 2, step 2)*.
- ISO. (2019a). *ISO 18184:2019 Textiles—Determination of antiviral activity of textile products*.
- ISO. (2019b). *ISO 27447:2019 Fine ceramics (advanced ceramics, advanced technical ceramics)—Test method for antibacterial activity of semiconducting photocatalytic materials*.
- Ivask, A., Rõlova, T., & Kahru, A. (2009). A suite of recombinant luminescent bacterial strains for the quantification of bioavailable heavy metals and toxicity testing. *BMC Biotechnology*, 9(1), 41. <https://doi.org/10.1186/1472-6750-9-41>
- Jenal, U., Reinders, A., & Lori, C. (2017). Cyclic di-GMP: Second messenger extraordinaire. *Nature Reviews Microbiology*, 15(5), 271–284. <https://doi.org/10.1038/nrmicro.2016.190>
- Jennings, L. K., Storek, K. M., Ledvina, H. E., Coulon, C., Marmont, L. S., Sadovskaya, I., Secor, P. R., Tseng, B. S., Scian, M., Filloux, A., Wozniak, D. J., Howell, P. L., & Parsek, M. R. (2015). Pel is a cationic exopolysaccharide that cross-links extracellular DNA in the *Pseudomonas aeruginosa* biofilm matrix. *Proceedings of the National Academy of Sciences*, 112(36), 11353–11358. <https://doi.org/10.1073/pnas.1503058112>

- Jensen, L. K., Koch, J., Aalbaek, B., Moodley, A., Bjarnsholt, T., Kragh, K. N., Petersen, A., & Jensen, H. E. (2017). Early implant-associated osteomyelitis results in a peri-implanted bacterial reservoir. *APMIS: Acta Pathologica, Microbiologica, et Immunologica Scandinavica*, *125*(1), 38–45. <https://doi.org/10.1111/apm.12597>
- Jin, S.-E., & Jin, H.-E. (2021). Antimicrobial Activity of Zinc Oxide Nano/Microparticles and Their Combinations against Pathogenic Microorganisms for Biomedical Applications: From Physicochemical Characteristics to Pharmacological Aspects. *Nanomaterials*, *11*(2), 263. <https://doi.org/10.3390/nano11020263>
- Joost, U., Juganson, K., Visnapuu, M., Mortimer, M., Kahru, A., Nõmmiste, E., Joost, U., Kisand, V., & Ivask, A. (2015). Photocatalytic antibacterial activity of nano-TiO₂ (anatase)-based thin films: Effects on *Escherichia coli* cells and fatty acids. *Journal of Photochemistry and Photobiology B: Biology*, *142*, 178–185. <https://doi.org/10.1016/j.jphotobiol.2014.12.010>
- Käkinen, A., Bondarenko, O., Ivask, A., & Kahru, A. (2011). The Effect of Composition of Different Ecotoxicological Test Media on Free and Bioavailable Copper from CuSO₄ and CuO Nanoparticles: Comparative Evidence from a Cu-Selective Electrode and a Cu-Biosensor. *Sensors*, *11*(11), 10502–10521. <https://doi.org/10.3390/s111110502>
- Karlin, K. (1993). Metalloenzymes, structural motifs, and inorganic models. *Science*, *261*(5122), 701–708. <https://doi.org/10.1126/science.7688141>
- Kim, J. S., Kuk, E., Yu, K. N., Kim, J.-H., Park, S. J., Lee, H. J., Kim, S. H., Park, Y. K., Park, Y. H., Hwang, C.-Y., Kim, Y.-K., Lee, Y.-S., Jeong, D. H., & Cho, M.-H. (2007). Antimicrobial effects of silver nanoparticles. *Nanomedicine: Nanotechnology, Biology and Medicine*, *3*(1), 95–101. <https://doi.org/10.1016/j.nano.2006.12.001>
- Knobloch, J. K.-M., Tofern, S., Kunz, W., Schütze, S., Riecke, M., Solbach, W., & Wuske, T. (2017). “Life-like” assessment of antimicrobial surfaces by a new touch transfer assay displays strong superiority of a copper alloy compared to silver containing surfaces. *PLOS ONE*, *12*(11), e0187442. <https://doi.org/10.1371/journal.pone.0187442>
- Kobayashi, H., Oethinger, M., Tuohy, M. J., Procop, G. W., & Bauer, T. W. (2009). Improved detection of biofilm-formative bacteria by vortexing and sonication: A pilot study. *Clinical Orthopaedics and Related Research*, *467*(5), 1360–1364. <https://doi.org/10.1007/s11999-008-0609-5>
- Koseoglu Eser, O., Ergin, A., & Hascelik, G. (2015). Antimicrobial Activity of Copper Alloys Against Invasive Multidrug-Resistant Nosocomial Pathogens. *Current Microbiology*, *71*(2), 291–295. <https://doi.org/10.1007/s00284-015-0840-8>
- Kragh, K. N., Alhede, M., Kvich, L., & Bjarnsholt, T. (2019). Into the well—A close look at the complex structures of a microtiter biofilm and the crystal violet assay. *Biofilm*, 100006. <https://doi.org/10.1016/j.biofilm.2019.100006>
- Kramer, A., Schwebke, I., & Kampf, G. (2006). How long do nosocomial pathogens persist on inanimate surfaces? A systematic review. *BMC Infectious Diseases*, *6*(1), 130. <https://doi.org/10.1186/1471-2334-6-130>
- Lakshmi Prasanna, V., & Vijayaraghavan, R. (2015). Insight into the Mechanism of Antibacterial Activity of ZnO: Surface Defects Mediated Reactive Oxygen Species Even in the Dark. *Langmuir*, *31*(33), 9155–9162. <https://doi.org/10.1021/acs.langmuir.5b02266>
- Laland, K., Matthews, B., & Feldman, M. W. (2016). An introduction to niche construction theory. *Evolutionary Ecology*, *30*(2), 191–202. <https://doi.org/10.1007/s10682-016-9821-z>

- Lawrence, J. R., Korber, D. R., Hoyle, B. D., Costerton, J. W., & Caldwell, D. E. (1991). Optical sectioning of microbial biofilms. *Journal of Bacteriology*, *173*(20), 6558–6567. <https://doi.org/10.1128/JB.173.20.6558-6567.1991>
- Lee, J.-H., Kim, Y.-G., Cho, M. H., & Lee, J. (2014). ZnO nanoparticles inhibit *Pseudomonas aeruginosa* biofilm formation and virulence factor production. *Microbiological Research*, *169*(12), 888–896. <https://doi.org/10.1016/j.micres.2014.05.005>
- Lee, L. J., Barrett, J. A., & Poole, R. K. (2005). Genome-wide transcriptional response of chemostat-cultured *Escherichia coli* to zinc. *Journal of Bacteriology*, *187*(3), 1124–1134. <https://doi.org/10.1128/JB.187.3.1124-1134.2005>
- Lemire, J. A., Harrison, J. J., & Turner, R. J. (2013). Antimicrobial activity of metals: Mechanisms, molecular targets and applications. *Nature Reviews Microbiology*, *11*(6), 371–384. <https://doi.org/10.1038/nrmicro3028>
- Li, L., Mendis, N., Trigui, H., Oliver, J. D., & Faucher, S. P. (2014). The importance of the viable but non-culturable state in human bacterial pathogens. *Frontiers in Microbiology*, *5*. <https://doi.org/10.3389/fmicb.2014.00258>
- Limoli, D. H., Jones, C. J., & Wozniak, D. J. (2015). Bacterial Extracellular Polysaccharides in Biofilm Formation and Function. *Microbiology Spectrum*, *3*(3). <https://doi.org/10.1128/microbiolspec.MB-0011-2014>
- Lin, K., & Marr, L. C. (2020). Humidity-Dependent Decay of Viruses, but Not Bacteria, in Aerosols and Droplets Follows Disinfection Kinetics. *Environmental Science & Technology*, *54*(2), 1024–1032. <https://doi.org/10.1021/acs.est.9b04959>
- Linares, J. F., Gustafsson, I., Baquero, F., & Martinez, J. L. (2006). Antibiotics as intermicrobial signaling agents instead of weapons. *Proceedings of the National Academy of Sciences*, *103*(51), 19484–19489. <https://doi.org/10.1073/pnas.0608949103>
- Linic, S., Christopher, P., & Ingram, D. B. (2011). Plasmonic-metal nanostructures for efficient conversion of solar to chemical energy. *Nature Materials*, *10*(12), 911–921. <https://doi.org/10.1038/nmat3151>
- Linklater, D. P., Baulin, V. A., Juodkazis, S., Crawford, R. J., Stoodley, P., & Ivanova, E. P. (2021). Mechano-bactericidal actions of nanostructured surfaces. *Nature Reviews Microbiology*, *19*(1), 8–22. <https://doi.org/10.1038/s41579-020-0414-z>
- Lipovsky, A., Nitzan, Y., Gedanken, A., & Lubart, R. (2011). Antifungal activity of ZnO nanoparticles—The role of ROS mediated cell injury. *Nanotechnology*, *22*(10), 105101. <https://doi.org/10.1088/0957-4484/22/10/105101>
- Lipovsky, A., Tzitrinovich, Z., Friedmann, H., Applerot, G., Gedanken, A., & Lubart, R. (2009). EPR Study of Visible Light-Induced ROS Generation by Nanoparticles of ZnO. *The Journal of Physical Chemistry C*, *113*(36), 15997–16001. <https://doi.org/10.1021/jp904864g>
- Macomber, L., & Imlay, J. A. (2009). The iron-sulfur clusters of dehydratases are primary intracellular targets of copper toxicity. *Proceedings of the National Academy of Sciences*, *106*(20), 8344–8349. <https://doi.org/10.1073/pnas.0812808106>
- Macomber, L., Rensing, C., & Imlay, J. A. (2007). Intracellular Copper Does Not Catalyze the Formation of Oxidative DNA Damage in *Escherichia coli*. *Journal of Bacteriology*, *189*(5), 1616–1626. <https://doi.org/10.1128/JB.01357-06>
- Mandakhlikar, K. D., Rahmat, J. N., Chiong, E., Neoh, K. G., Shen, L., & Tambyah, P. A. (2018). Extraction and quantification of biofilm bacteria: Method optimized for urinary catheters. *Scientific Reports*, *8*(1), 8069. <https://doi.org/10.1038/s41598-018-26342-3>

- McDevitt, C. A., Ogunniyi, A. D., Valkov, E., Lawrence, M. C., Kobe, B., McEwan, A. G., & Paton, J. C. (2011). A Molecular Mechanism for Bacterial Susceptibility to Zinc. *PLoS Pathogens*, 7(11), e1002357. <https://doi.org/10.1371/journal.ppat.1002357>
- McDonald, M., Wesgate, R., Rubiano, M., Holah, J., Denyer, S. P., Jermann, C., & Maillard, J.-Y. (2020). Impact of a dry inoculum deposition on the efficacy of copper-based antimicrobial surfaces. *Journal of Hospital Infection*, 106(3), 465–472. <https://doi.org/10.1016/j.jhin.2020.08.013>
- McDonnell, G., & Russell, A. D. (1999). Antiseptics and disinfectants: Activity, action, and resistance. *Clinical Microbiology Reviews*, 12(1), 147–179.
- Merritt, J. H., Kadouri, D. E., & O'Toole, G. A. (2005). Growing and Analyzing Static Biofilms. In R. Coico, T. Kowalik, J. Quarles, B. Stevenson, & R. Taylor (Eds.), *Current Protocols in Microbiology* (p. mc01b01s00). John Wiley & Sons, Inc. <https://doi.org/10.1002/9780471729259.mc01b01s00>
- Michels, H. T., Noyce, J. O., & Keevil, C. W. (2009). Effects of temperature and humidity on the efficacy of methicillin-resistant *Staphylococcus aureus* challenged antimicrobial materials containing silver and copper. *Letters in Applied Microbiology*, 49(2), 191–195. <https://doi.org/10.1111/j.1472-765X.2009.02637.x>
- Mills, D. A., Schmidt, B., Hiser, C., Westley, E., & Ferguson-Miller, S. (2002). Membrane Potential-controlled Inhibition of Cytochrome c Oxidase by Zinc. *Journal of Biological Chemistry*, 277(17), 14894–14901. <https://doi.org/10.1074/jbc.M111922200>
- Mitchell, P. (2016). *Anatomy and surgery in Europe and the Middle East during the Middle Ages*. Apollo - University of Cambridge Repository. <https://doi.org/10.17863/CAM.13163>
- Molteni, C., Abicht, H. K., & Solioz, M. (2010). Killing of Bacteria by Copper Surfaces Involves Dissolved Copper. *Applied and Environmental Microbiology*, 76(12), 4099–4101. <https://doi.org/10.1128/AEM.00424-10>
- Morey, J. R., McDevitt, C. A., & Kehl-Fie, T. E. (2015). Host-imposed manganese starvation of invading pathogens: Two routes to the same destination. *BioMetals*, 28(3), 509–519. <https://doi.org/10.1007/s10534-015-9850-z>
- Morones-Ramirez, J. R., Winkler, J. A., Spina, C. S., & Collins, J. J. (2013). Silver enhances antibiotic activity against gram-negative bacteria. *Science Translational Medicine*, 5(190), 190ra81. <https://doi.org/10.1126/scitranslmed.3006276>
- Nan, L., Liu, Y., Lü, M., & Yang, K. (2008). Study on antibacterial mechanism of copper-bearing austenitic antibacterial stainless steel by atomic force microscopy. *Journal of Materials Science: Materials in Medicine*, 19(9), 3057–3062. <https://doi.org/10.1007/s10856-008-3444-z>
- Nicastro, L. K., Tursi, S. A., Le, L. S., Miller, A. L., Efimov, A., Buttaro, B., Tam, V., & Tükel, Ç. (2019). Cytotoxic Curli Intermediates Form during *Salmonella* Biofilm Development. *Journal of Bacteriology*, 201(18), e00095-19, /j.b/201/18/JB.00095-19.atom. <https://doi.org/10.1128/JB.00095-19>
- NIH. (2002). *Research on microbial biofilms: PA Number: PA-03-047*. National Institute of Health. <http://grants.nih.gov/grants/guide/pa-files/PA-03-047.html>
- Nocker, A., & Camper, A. K. (2009). Novel approaches toward preferential detection of viable cells using nucleic acid amplification techniques. *FEMS Microbiology Letters*, 291(2), 137–142. <https://doi.org/10.1111/j.1574-6968.2008.01429.x>
- Novotny, L. A., Chiang, T., Goodman, S. D., Elmaraghy, C. A., & Bakaletz, L. O. (2021). Humanized ANTI-DNABII Fab Fragments Plus Ofloxacin Eradicated Biofilms in Experimental Otitis Media. *The Laryngoscope*, lary.29497. <https://doi.org/10.1002/lary.29497>

- Odermatt, A., Krapf, R., & Solioz, M. (1994). Induction of the Putative Copper ATPases, CopA and CopB, of *Enterococcus hirae* by Ag⁺ and Cu²⁺, and Ag⁺ Extrusion by CopB. *Biochemical and Biophysical Research Communications*, 202(1), 44–48. <https://doi.org/10.1006/bbrc.1994.1891>
- O’Gorman, J., & Humphreys, H. (2012). Application of copper to prevent and control infection. Where are we now? *Journal of Hospital Infection*, 81(4), 217–223. <https://doi.org/10.1016/j.jhin.2012.05.009>
- Ojeil, M., Jermann, C., Holah, J., Denyer, S. P., & Maillard, J.-Y. (2013). Evaluation of new in vitro efficacy test for antimicrobial surface activity reflecting UK hospital conditions. *Journal of Hospital Infection*, 85(4), 274–281. <https://doi.org/10.1016/j.jhin.2013.08.007>
- Okshevsky, M., & Meyer, R. L. (2015). The role of extracellular DNA in the establishment, maintenance and perpetuation of bacterial biofilms. *Critical Reviews in Microbiology*, 41(3), 341–352. <https://doi.org/10.3109/1040841X.2013.841639>
- Oli, M. W., Otoo, H. N., Crowley, P. J., Heim, K. P., Nascimento, M. M., Ramsook, C. B., Lipke, P. N., & Brady, L. J. (2012). Functional amyloid formation by *Streptococcus mutans*. *Microbiology (Reading, England)*, 158(Pt 12), 2903–2916. <https://doi.org/10.1099/mic.0.060855-0>
- Olsen, I. (2015). Biofilm-specific antibiotic tolerance and resistance. *European Journal of Clinical Microbiology & Infectious Diseases*, 34(5), 877–886. <https://doi.org/10.1007/s10096-015-2323-z>
- Olson, M. E., Ceri, H., Morck, D. W., Buret, A. G., & Read, R. R. (2002). Biofilm bacteria: Formation and comparative susceptibility to antibiotics. *Canadian Journal of Veterinary Research = Revue Canadienne De Recherche Veterinaire*, 66(2), 86–92.
- Ong, C. Y., Walker, M. J., & McEwan, A. G. (2015). Zinc disrupts central carbon metabolism and capsule biosynthesis in *Streptococcus pyogenes*. *Scientific Reports*, 5(1), 10799. <https://doi.org/10.1038/srep10799>
- Otter, J. A., Vickery, K., Walker, J. T., deLancey Pulcini, E., Stoodley, P., Goldenberg, S. D., Salkeld, J. A. G., Chewins, J., Yezli, S., & Edgeworth, J. D. (2015). Surface-attached cells, biofilms and biocide susceptibility: Implications for hospital cleaning and disinfection. *Journal of Hospital Infection*, 89(1), 16–27. <https://doi.org/10.1016/j.jhin.2014.09.008>
- Otter, J. A., Yezli, S., & French, G. L. (2011). The Role Played by Contaminated Surfaces in the Transmission of Nosocomial Pathogens. *Infection Control & Hospital Epidemiology*, 32(7), 687–699. <https://doi.org/10.1086/660363>
- Pal, C., Asiani, K., Arya, S., Rensing, C., Stekel, D. J., Larsson, D. G. J., & Hobman, J. L. (2017). Metal Resistance and Its Association With Antibiotic Resistance. In *Advances in Microbial Physiology* (Vol. 70, pp. 261–313). Elsevier. <https://doi.org/10.1016/bs.ampbs.2017.02.001>
- Pasquet, J., Chevalier, Y., Pelletier, J., Couval, E., Bouvier, D., & Bolzinger, M.-A. (2014). The contribution of zinc ions to the antimicrobial activity of zinc oxide. *Colloids and Surfaces A: Physicochemical and Engineering Aspects*, 457, 263–274. <https://doi.org/10.1016/j.colsurfa.2014.05.057>
- Pati, R., Mehta, R. K., Mohanty, S., Padhi, A., Sengupta, M., Vaseeharan, B., Goswami, C., & Sonawane, A. (2014). Topical application of zinc oxide nanoparticles reduces bacterial skin infection in mice and exhibits antibacterial activity by inducing oxidative stress response and cell membrane disintegration in macrophages. *Nanomedicine: Nanotechnology, Biology and Medicine*, 10(6), 1195–1208. <https://doi.org/10.1016/j.nano.2014.02.012>

- Paula, A. J., Hwang, G., & Koo, H. (2020). Dynamics of bacterial population growth in biofilms resemble spatial and structural aspects of urbanization. *Nature Communications*, *11*(1), 1354. <https://doi.org/10.1038/s41467-020-15165-4>
- Pendleton, J. N., Gorman, S. P., & Gilmore, B. F. (2013). Clinical relevance of the ESKAPE pathogens. *Expert Review of Anti-Infective Therapy*, *11*(3), 297–308. <https://doi.org/10.1586/eri.13.12>
- Penesyan, A., Paulsen, I. T., Gillings, M. R., Kjelleberg, S., & Manefield, M. J. (2020). Secondary Effects of Antibiotics on Microbial Biofilms. *Frontiers in Microbiology*, *11*, 2109. <https://doi.org/10.3389/fmicb.2020.02109>
- Perez-Gavilan, A., de Castro, J. V., Arana, A., Merino, S., Retolaza, A., Alves, S. A., Francone, A., Kehagias, N., Sotomayor-Torres, C. M., Cocina, D., Mortera, R., Crapanzano, S., Pelegrín, C. J., Garrigos, M. C., Jiménez, A., Galindo, B., Araque, M. C., Dykeman, D., Neves, N. M., & Marimón, J. M. (2021). Antibacterial activity testing methods for hydrophobic patterned surfaces. *Scientific Reports*, *11*(1), 6675. <https://doi.org/10.1038/s41598-021-85995-9>
- Pietsch, F., Heidrich, G., Nordholt, N., & Schreiber, F. (2021). Prevalent Synergy and Antagonism Among Antibiotics and Biocides in *Pseudomonas aeruginosa*. *Frontiers in Microbiology*, *11*, 615618. <https://doi.org/10.3389/fmicb.2020.615618>
- Raghupathi, K. R., Koodali, R. T., & Manna, A. C. (2011). Size-Dependent Bacterial Growth Inhibition and Mechanism of Antibacterial Activity of Zinc Oxide Nanoparticles. *Langmuir*, *27*(7), 4020–4028. <https://doi.org/10.1021/la104825u>
- Redfern, J., Tucker, J., Simmons, L., Askew, P., Stephan, I., & Verran, J. (2018). Environmental and Experimental Factors Affecting Efficacy Testing of Nonporous Plastic Antimicrobial Surfaces. *Methods and Protocols*, *1*(4), 36. <https://doi.org/10.3390/mps1040036>
- Røder, H. L., Trivedi, U., Russel, J., Kragh, K. N., Herschend, J., Thalsø-Madsen, I., Tolker-Nielsen, T., Bjarnsholt, T., Burmølle, M., & Madsen, J. S. (2021). Biofilms can act as plasmid reserves in the absence of plasmid specific selection. *Npj Biofilms and Microbiomes*, *7*(1), 78. <https://doi.org/10.1038/s41522-021-00249-w>
- Romero, D., Aguilar, C., Losick, R., & Kolter, R. (2010). Amyloid fibers provide structural integrity to *Bacillus subtilis* biofilms. *Proceedings of the National Academy of Sciences*, *107*(5), 2230–2234. <https://doi.org/10.1073/pnas.0910560107>
- Römling, U., & Balsalobre, C. (2012). Biofilm infections, their resilience to therapy and innovative treatment strategies. *Journal of Internal Medicine*, *272*(6), 541–561. <https://doi.org/10.1111/joim.12004>
- Rosenberg, M., Ilić, K., Juganson, K., Ivask, A., Ahonen, M., Vinković Vrček, I., & Kahru, A. (2019). Potential ecotoxicological effects of antimicrobial surface coatings: A literature survey backed up by analysis of market reports. *PeerJ*, *7*, e6315. <https://doi.org/10.7717/peerj.6315>
- Róžańska, A., Chmielarczyk, A., Romaniszyn, D., Sroka-Oleksiak, A., Bulanda, M., Walkowicz, M., Osuch, P., & Knych, T. (2017). Antimicrobial Properties of Selected Copper Alloys on *Staphylococcus aureus* and *Escherichia coli* in Different Simulations of Environmental Conditions: With vs. without Organic Contamination. *International Journal of Environmental Research and Public Health*, *14*(7), 813. <https://doi.org/10.3390/ijerph14070813>
- Rumbaugh, K. P., & Sauer, K. (2020). Biofilm dispersion. *Nature Reviews Microbiology*, *18*(10), 571–586. <https://doi.org/10.1038/s41579-020-0385-0>

- Salgado, C. D., Sepkowitz, K. A., John, J. F., Cantey, J. R., Attaway, H. H., Freeman, K. D., Sharpe, P. A., Michels, H. T., & Schmidt, M. G. (2013). Copper Surfaces Reduce the Rate of Healthcare-Acquired Infections in the Intensive Care Unit. *Infection Control & Hospital Epidemiology*, *34*(5), 479–486. <https://doi.org/10.1086/670207>
- Santo, C. E., Lam, E. W., Elowsky, C. G., Quaranta, D., Domaille, D. W., Chang, C. J., & Grass, G. (2011). Bacterial Killing by Dry Metallic Copper Surfaces. *Applied and Environmental Microbiology*, *77*(3), 794–802. <https://doi.org/10.1128/AEM.01599-10>
- Santo, C. E., Taudte, N., Nies, D. H., & Grass, G. (2008). Contribution of Copper Ion Resistance to Survival of Escherichia coli on Metallic Copper Surfaces. *Applied and Environmental Microbiology*, *74*(4), 977–986. <https://doi.org/10.1128/AEM.01938-07>
- Santos-Lopez, A., Marshall, C. W., Scribner, M. R., Snyder, D. J., & Cooper, V. S. (2019). Evolutionary pathways to antibiotic resistance are dependent upon environmental structure and bacterial lifestyle. *ELife*, *8*. <https://doi.org/10.7554/eLife.47612>
- Schwartz, K., Ganesan, M., Payne, D. E., Solomon, M. J., & Boles, B. R. (2016). Extracellular DNA facilitates the formation of functional amyloids in *S taphylococcus aureus* biofilms: EDNA promotes functional amyloid formation. *Molecular Microbiology*, *99*(1), 123–134. <https://doi.org/10.1111/mmi.13219>
- Schwartz, K., Syed, A. K., Stephenson, R. E., Rickard, A. H., & Boles, B. R. (2012). Functional amyloids composed of phenol soluble modulins stabilize Staphylococcus aureus biofilms. *PLoS Pathogens*, *8*(6), e1002744. <https://doi.org/10.1371/journal.ppat.1002744>
- Seil, J. T., & Webster, T. J. (2011). Reduced Staphylococcus aureus proliferation and biofilm formation on zinc oxide nanoparticle PVC composite surfaces. *Acta Biomaterialia*, *7*(6), 2579–2584. <https://doi.org/10.1016/j.actbio.2011.03.018>
- Seviour, T., Derlon, N., Dueholm, M. S., Flemming, H.-C., Girbal-Neuhauser, E., Horn, H., Kjelleberg, S., van Loosdrecht, M. C. M., Lotti, T., Malpei, M. F., Nerenberg, R., Neu, T. R., Paul, E., Yu, H., & Lin, Y. (2019). Extracellular polymeric substances of biofilms: Suffering from an identity crisis. *Water Research*, *151*, 1–7. <https://doi.org/10.1016/j.watres.2018.11.020>
- Seviour, T., Winnerdy, F. R., Wong, L. L., Shi, X., Mugunthan, S., Foo, Y. H., Castaing, R., Adav, S. S., Subramoni, S., Kohli, G. S., Shewan, H. M., Stokes, J. R., Rice, S. A., Phan, A. T., & Kjelleberg, S. (2021). The biofilm matrix scaffold of Pseudomonas aeruginosa contains G-quadruplex extracellular DNA structures. *Npj Biofilms and Microbiomes*, *7*(1), 27. <https://doi.org/10.1038/s41522-021-00197-5>
- Sifri, C. D., Burke, G. H., & Enfield, K. B. (2016). Reduced health care-associated infections in an acute care community hospital using a combination of self-disinfecting copper-impregnated composite hard surfaces and linens. *American Journal of Infection Control*, *44*(12), 1565–1571. <https://doi.org/10.1016/j.ajic.2016.07.007>
- Silver, S., & Phung, L. T. (1996). BACTERIAL HEAVY METAL RESISTANCE: New Surprises. *Annual Review of Microbiology*, *50*(1), 753–789. <https://doi.org/10.1146/annurev.micro.50.1.753>
- Silver, S., & Phung, L. T. (2005). A bacterial view of the periodic table: Genes and proteins for toxic inorganic ions. *Journal of Industrial Microbiology & Biotechnology*, *32*(11–12), 587–605. <https://doi.org/10.1007/s10295-005-0019-6>

- Sirelkhatim, A., Mahmud, S., Seeni, A., Kaus, N. H. M., Ann, L. C., Bakhori, S. K. M., Hasan, H., & Mohamad, D. (2015). Review on Zinc Oxide Nanoparticles: Antibacterial Activity and Toxicity Mechanism. *Nano-Micro Letters*, 7(3), 219–242. <https://doi.org/10.1007/s40820-015-0040-x>
- Slavin, Y. N., Asnis, J., Häfeli, U. O., & Bach, H. (2017). Metal nanoparticles: Understanding the mechanisms behind antibacterial activity. *Journal of Nanobiotechnology*, 15(1), 65. <https://doi.org/10.1186/s12951-017-0308-z>
- Solioz, M., & Odermatt, A. (1995). Copper and Silver Transport by CopB-ATPase in Membrane Vesicles of *Enterococcus hirae*. *Journal of Biological Chemistry*, 270(16), 9217–9221. <https://doi.org/10.1074/jbc.270.16.9217>
- Stabryla, L. M., Johnston, K. A., Diemler, N. A., Cooper, V. S., Millstone, J. E., Haig, S.-J., & Gilbertson, L. M. (2021). Role of bacterial motility in differential resistance mechanisms of silver nanoparticles and silver ions. *Nature Nanotechnology*, 16(9), 996–1003. <https://doi.org/10.1038/s41565-021-00929-w>
- Stewart, P. S., & Franklin, M. J. (2008). Physiological heterogeneity in biofilms. *Nature Reviews Microbiology*, 6(3), 199–210. <https://doi.org/10.1038/nrmicro1838>
- Stoodley, P., Sauer, K., Davies, D. G., & Costerton, J. W. (2002). Biofilms as Complex Differentiated Communities. *Annual Review of Microbiology*, 56(1), 187–209. <https://doi.org/10.1146/annurev.micro.56.012302.160705>
- Stout, J. E., & Yu, V. L. (2003). Experiences of the First 16 Hospitals Using Copper-Silver Ionization for *Legionella* Control: Implications for the Evaluation of Other Disinfection Modalities. *Infection Control & Hospital Epidemiology*, 24(8), 563–568. <https://doi.org/10.1086/502251>
- Su, H.-L., Chou, C.-C., Hung, D.-J., Lin, S.-H., Pao, I.-C., Lin, J.-H., Huang, F.-L., Dong, R.-X., & Lin, J.-J. (2009). The disruption of bacterial membrane integrity through ROS generation induced by nanohybrids of silver and clay. *Biomaterials*, 30(30), 5979–5987. <https://doi.org/10.1016/j.biomaterials.2009.07.030>
- Sun, H., Yang, Z., Pu, Y., Dou, W., Wang, C., Wang, W., Hao, X., Chen, S., Shao, Q., Dong, M., Wu, S., Ding, T., & Guo, Z. (2019). Zinc oxide/vanadium pentoxide heterostructures with enhanced day-night antibacterial activities. *Journal of Colloid and Interface Science*, 547, 40–49. <https://doi.org/10.1016/j.jcis.2019.03.061>
- Suppi, S., Kasemets, K., Ivask, A., Künnis-Beres, K., Sihtmäe, M., Kurvet, I., Aruoja, V., & Kahru, A. (2015). A novel method for comparison of biocidal properties of nanomaterials to bacteria, yeasts and algae. *Journal of Hazardous Materials*, 286, 75–84. <https://doi.org/10.1016/j.jhazmat.2014.12.027>
- Suram, A., Rao, J. K. S., S., L. K., & A., V. M. (2002). First Evidence to Show the Topological Change of DNA from B-DNA to Z-DNA Conformation in the Hippocampus of Alzheimer's Brain. *NeuroMolecular Medicine*, 2(3), 289–298. <https://doi.org/10.1385/NMM:2:3:289>
- Swartjes, J. J. T. M., Das, T., Sharifi, S., Subbiahdoss, G., Sharma, P. K., Krom, B. P., Busscher, H. J., & van der Mei, H. C. (2013). A Functional DNase I Coating to Prevent Adhesion of Bacteria and the Formation of Biofilm. *Advanced Functional Materials*, 23(22), 2843–2849. <https://doi.org/10.1002/adfm.201202927>
- Taglialegna, A., Lasa, I., & Valle, J. (2016). Amyloid Structures as Biofilm Matrix Scaffolds. *Journal of Bacteriology*, 198(19), 2579–2588. <https://doi.org/10.1128/JB.00122-16>
- Taglialegna, A., Navarro, S., Ventura, S., Garnett, J. A., Matthews, S., Penades, J. R., Lasa, I., & Valle, J. (2016). Staphylococcal Bap Proteins Build Amyloid Scaffold Biofilm Matrices in Response to Environmental Signals. *PLoS Pathogens*, 12(6), e1005711. <https://doi.org/10.1371/journal.ppat.1005711>

- Turner, J. S. (2000). *The extended organism: The physiology of animal-built structures*. Harvard University Press.
- Turner, R. J., Huang, L.-N., Viti, C., & Mengoni, A. (2020). Metal-Resistance in Bacteria: Why Care? *Genes*, *11*(12), 1470. <https://doi.org/10.3390/genes11121470>
- Van Gerven, N., Van der Verren, S. E., Reiter, D. M., & Remaut, H. (2018). The Role of Functional Amyloids in Bacterial Virulence. *Journal of Molecular Biology*, *430*(20), 3657–3684. <https://doi.org/10.1016/j.jmb.2018.07.010>
- Vieira, E. F. S., de A. Simoni, J., & Airoidi, C. (1997). Interaction of cations with SH-modified silica gel: Thermochemical study through calorimetric titration and direct extent of reaction determination. *Journal of Materials Chemistry*, *7*(11), 2249–2252. <https://doi.org/10.1039/a704286h>
- Vilain, S., Pretorius, J. M., Theron, J., & Brozel, V. S. (2009). DNA as an Adhesin: *Bacillus cereus* Requires Extracellular DNA To Form Biofilms. *Applied and Environmental Microbiology*, *75*(9), 2861–2868. <https://doi.org/10.1128/AEM.01317-08>
- Villapún, V. M., Lukose, C. C., Birkett, M., Dover, L. G., & González, S. (2018). Tuning the antimicrobial behaviour of Cu₈₅Zr₁₅ thin films in “wet” and “dry” conditions through structural modifications. *Surface and Coatings Technology*, *350*, 334–345. <https://doi.org/10.1016/j.surfcoat.2018.06.094>
- von Dessauer, B., Navarrete, M. S., Benadof, D., Benavente, C., & Schmidt, M. G. (2016). Potential effectiveness of copper surfaces in reducing health care–associated infection rates in a pediatric intensive and intermediate care unit: A nonrandomized controlled trial. *American Journal of Infection Control*, *44*(8), e133–e139. <https://doi.org/10.1016/j.ajic.2016.03.053>
- Wahab, R., Mishra, A., Yun, S.-I., Hwang, I. H., Mussarat, J., Al-Khedhairy, A. A., Kim, Y.-S., & Shin, H.-S. (2012). Fabrication, growth mechanism and antibacterial activity of ZnO micro-spheres prepared via solution process. *Biomass and Bioenergy*, *39*, 227–236. <https://doi.org/10.1016/j.biombioe.2012.01.005>
- Walker, G. T., Stone, M. P., & Krugh, T. R. (1985). Ethidium binding to left-handed (Z) DNAs results in regions of right-handed DNA at the intercalation site. *Biochemistry*, *24*(25), 7462–7471. <https://doi.org/10.1021/bi00346a065>
- Wang, H., Yan, A., Liu, Z., Yang, X., Xu, Z., Wang, Y., Wang, R., Koohi-Moghadam, M., Hu, L., Xia, W., Tang, H., Wang, Y., Li, H., & Sun, H. (2019). Deciphering molecular mechanism of silver by integrated omic approaches enables enhancing its antimicrobial efficacy in *E. coli*. *PLOS Biology*, *17*(6), e3000292. <https://doi.org/10.1371/journal.pbio.3000292>
- Warnes, S. L., Green, S. M., Michels, H. T., & Keevil, C. W. (2010). Biocidal Efficacy of Copper Alloys against Pathogenic Enterococci Involves Degradation of Genomic and Plasmid DNAs. *Applied and Environmental Microbiology*, *76*(16), 5390–5401. <https://doi.org/10.1128/AEM.03050-09>
- Watnick, P., & Kolter, R. (2000). Biofilm, City of Microbes. *Journal of Bacteriology*, *182*(10), 2675–2679. <https://doi.org/10.1128/JB.182.10.2675-2679.2000>
- Weber, D. J., Rutala, W. A., Miller, M. B., Huslage, K., & Sickbert-Bennett, E. (2010). Role of hospital surfaces in the transmission of emerging health care-associated pathogens: Norovirus, *Clostridium difficile*, and *Acinetobacter* species. *American Journal of Infection Control*, *38*(5), S25–S33. <https://doi.org/10.1016/j.ajic.2010.04.196>
- West, S. A., Griffin, A. S., Gardner, A., & Diggle, S. P. (2006). Social evolution theory for microorganisms. *Nature Reviews Microbiology*, *4*(8), 597–607. <https://doi.org/10.1038/nrmicro1461>

- Whitchurch, C. B. (2002). Extracellular DNA Required for Bacterial Biofilm Formation. *Science*, 295(5559), 1487–1487. <https://doi.org/10.1126/science.295.5559.1487>
- Wiegand, C., Völpel, A., Ewald, A., Remesch, M., Kuever, J., Bauer, J., Griesheim, S., Hauser, C., Thielmann, J., Tonndorf-Martini, S., Sigusch, B. W., Weisser, J., Wyrwa, R., Elsner, P., Hipler, U.-C., Roth, M., Dewald, C., Lüdecke-Beyer, C., & Bossert, J. (2018). Critical physiological factors influencing the outcome of antimicrobial testing according to ISO 22196 / JIS Z 2801. *PLOS ONE*, 13(3), e0194339. <https://doi.org/10.1371/journal.pone.0194339>
- Xiu, Z.-M., Ma, J., & Alvarez, P. J. J. (2011). Differential effect of common ligands and molecular oxygen on antimicrobial activity of silver nanoparticles versus silver ions. *Environmental Science & Technology*, 45(20), 9003–9008. <https://doi.org/10.1021/es201918f>
- Yang, W., Elankumaran, S., & Marr, L. C. (2012). Relationship between humidity and influenza A viability in droplets and implications for influenza's seasonality. *PLoS One*, 7(10), e46789. <https://doi.org/10.1371/journal.pone.0046789>
- Yarawsky, A. E., Johns, S. L., Schuck, P., & Herr, A. B. (2020). The biofilm adhesion protein Aap from *Staphylococcus epidermidis* forms zinc-dependent amyloid fibers. *Journal of Biological Chemistry*, 295(14), 4411–4427. <https://doi.org/10.1074/jbc.RA119.010874>
- Yoshida, Y., Furuta, S., & Niki, E. (1993). Effects of metal chelating agents on the oxidation of lipids induced by copper and iron. *Biochimica et Biophysica Acta (BBA) - Lipids and Lipid Metabolism*, 1210(1), 81–88. [https://doi.org/10.1016/0005-2760\(93\)90052-B](https://doi.org/10.1016/0005-2760(93)90052-B)
- Yu, H., Ren, J., & Qu, X. (2007). Time-Dependent DNA Condensation Induced by Amyloid β -Peptide. *Biophysical Journal*, 92(1), 185–191. <https://doi.org/10.1529/biophysj.106.093559>
- Zähringer, F., Lacanna, E., Jenal, U., Schirmer, T., & Boehm, A. (2013). Structure and Signaling Mechanism of a Zinc-Sensory Diguanylate Cyclase. *Structure*, 21(7), 1149–1157. <https://doi.org/10.1016/j.str.2013.04.026>
- Zaleska-Medynska, A., Marchelek, M., Diak, M., & Grabowska, E. (2016). Noble metal-based bimetallic nanoparticles: The effect of the structure on the optical, catalytic and photocatalytic properties. *Advances in Colloid and Interface Science*, 229, 80–107. <https://doi.org/10.1016/j.cis.2015.12.008>
- Zerbib, S., Vallet, L., Muggeo, A., de Champs, C., Lefebvre, A., Jolly, D., & Kanagaratnam, L. (2020). Copper for the Prevention of Outbreaks of Health Care–Associated Infections in a Long-term Care Facility for Older Adults. *Journal of the American Medical Directors Association*, 21(1), 68–71.e1. <https://doi.org/10.1016/j.jamda.2019.02.003>
- Zweig, M., Schork, S., Koerdt, A., Siewering, K., Sternberg, C., Thormann, K., Albers, S.-V., Molin, S., & van der Does, C. (2014). Secreted single-stranded DNA is involved in the initial phase of biofilm formation by *N. eisseria gonorrhoeae*: Biofilm formation by *Neisseria gonorrhoeae*. *Environmental Microbiology*, 16(4), 1040–1052. <https://doi.org/10.1111/1462-2920.12291>

Acknowledgements

I would like to dedicate this thesis to my late grandfather, who always encouraged my “whys” and “hows” and tried his best to explain what energy and matter, sound, light and color are on our long car-rides way before I learnt about them at school. He taught me to be curious, to ask questions regardless of whether these could be answered and to find the answers.

Secondly, I thank my family. This work would not have been possible without the infinite support from my husband and oftentimes fragile patience of my daughters.

I also wish to thank my form master and biology teacher, Mrs. Riina Otsus, who made biology interesting for me. It has remained so ever since and has greatly influenced my subsequent choices.

I greatly acknowledge all my thesis advisors Prof Angela Ivask, Dr Vambola Kisand, Dr Kaja Kasemets and lab members for their support and guidance throughout the PhD journey. I am especially thankful to Prof Angela Ivask for her patience, for believing in me and enabling me the freedom to follow my own scientific pursuits deviating from the labs main focus and I thank the head and neck of the laboratory, academician Anne Kahru for providing the means to do so. I am also thankful to great coincidences, the COST AMiCI network and Dr Nuno Azevedo for introducing me to the beautifully interesting field of biofilms. I would like to thank Dr Heiti Paves for invaluable help with confocal microscopy, Heiki Vija for assistance with elemental analysis, Imbi Kurvet for being the lab angel that she is and Dr Vambola Kisand and Dr Meeri Visnapuu for assisting me with everything beyond biology. I appreciate the chaotic presence of Dr Villem Aruoja that kept the mood up and pressure down for anyone working in the same room.

I sincerely thank Katre, Meeri, Liina, Sandra and Eliise for sharing this journey with me and supporting each other in and out of lab when needed the most.

The work presented in this thesis was carried out mainly in the Laboratory of Environmental Toxicology at the National Institute of Chemical Physics and Biophysics (photoactive surfaces and biofilm work) and partly in the University of Southampton (copper surfaces) and University of Porto (biofilms on glass). Funding was provided by Estonian Research Council (PUT748, IUT23-5, EAG20, PRG749, TT13), University of Tartu (PLTFYARENG53), European Regional Development Fund (including: Dora Plus; Graduate School of Functional materials and technologies, 2014-2020.4.01.16-0027; CER TK134 EQUITANT, 2014-2020.4.01.15-0005; NAMUR+, 2014-2020.4.01.16-0123) and EU COST Action CA15114 AMiCI.

Figures 3, 4, 5, 7 and images in Table 1 and 3 were created with Biorender.com

Abstract

Microbial interactions with inanimate solid surfaces: a methodological approach

In the face of rapid spread of antimicrobial resistance and potential pathogen carryover by contaminated surfaces in health care settings, food industry, public spaces *etc.*, passive antimicrobial strategies, such as antimicrobial surface coatings, are often seen as an additional tool to reduce bioburden in critical applications and mitigate spread of the aforementioned threats. However, while antimicrobial materials are incorporated to and successfully marketed as consumer products, their use in critical applications in health care and industry has been more cautious. This is largely due to the challenges of translating laboratory results to real-life benefits of the costly materials as well as gaps in standardization and legislation. Methods for studying antimicrobial surfaces in general historically largely rely on planktonic cultures and/or effects of released active agent not the actual surface in more application-appropriate conditions.

More specifically, while various metal-based nanoparticles have shown great potential in antimicrobial applications under standard laboratory conditions, less is known about nano-enabled surfaces and combined effects of multimodal surfaces. The main aims of the current thesis were twofold. We aimed to critically evaluate the widely used methods measuring viability of surface-associated microbes and adapting metal-sensing bacterial biosensors to *in situ* surface analysis to enable a more mechanistic approach to studying antimicrobial surfaces. Additionally, we aimed to characterize antimicrobial properties of novel proof-of concept nano-ZnO and nano-ZnO/Ag based surfaces in a biologically meaningful way.

In the current thesis two methods were assessed to study microbe-surface interactions. Firstly, recombinant luminescent bacterial biosensor strains were adopted to quantitatively evaluate sublethal effects of copper on copper and copper-alloy surfaces *in situ*. It was demonstrated that the copper biosensor signal intensity was correlated with material copper content and not the copper concentration in the test medium caused by copper ions released from the surfaces. This clearly indicates the importance of direct contacts between the cells and the surface in antimicrobial applications and respective testing protocols.

Secondly, bacterial viability staining with nucleic acid stains propidium iodide and Syto9 was assessed for predicting viability of initial biofilms of *Escherichia coli* and *Staphylococcus epidermidis* in oligotrophic conditions. A critical limitation of the widely used method was revealed as the viability staining method dramatically underestimated both enzymatic activity as well as cultivability of the biofilm cells. We propose that this caveat could be caused by extracellular nucleic acids in biofilms. The finding illustrates the need for thorough validation of methodology when applying methods designed for planktonic cultures to biofilms.

To further assess the antimicrobial efficacy of novel proof-of concept nano-ZnO and nano-ZnO/Ag based surfaces we deployed a widely used industrial standard approach based on ISO 22196/ISO 27447 followed by characterization of antibiofilm properties in high nutrient and oligotrophic conditions. It was demonstrated that the nano-ZnO and nano-ZnO/Ag covered surfaces offered rapid multimodal antibacterial activity against *E. coli* and *Staphylococcus aureus* by combining metal ion toxicity and photocatalysis. Antimicrobial and antibiofilm properties of the surfaces depended on both, surface

coating composition and test media with better biofilm inhibition in oligotrophic conditions compared to growth medium with high organic content. While the surfaces were clearly antibacterial, they had negligible effect on the potentially pathogenic yeast *Candida albicans* viability and nano-ZnO even enhanced biofilm formation by *C. albicans* in oligotrophic environment. The latter highlights the need to not only choose application-appropriate test methods but also the test species beyond the usual Gram-negative and Gram-positive bacteria.

In conclusion the current thesis highlights the need to find ways for better efficacy assessment of antimicrobial surfaces in more application-relevant conditions taking into account also direct cell-surface interactions and test organism specificity and to validate planktonic methods use on biofilms more thoroughly to avoid false viability estimates and overestimations of efficacy.

Lühikokkuvõte

Mikroobide interaktsioonid tahkete eluta pindadega: meetodiline käsitlus

Arvestades antibiootikumiresistentsuse kiiret levikut ja võimalike haigustekitajate ülekandumist saastunud pindade kaudu tervishoiuasutustes, toiduainetööstuses, avalikus ruumis jne, käsitletakse passiivseid mikroobivastaseid strateegiaid, näiteks mikroobivastaseid pinnamaterjale, sageli täiendava vahendina haigustekitajate leviku piiramiseks kriitilise tähtsusega rakendustes. Kuigi selliseid materjale kasutatakse ja turundatakse edukalt laiatarbekaupades, on nende kasutuselevõtt tervishoiuvaldkonnas ja tööstuses olnud tagasihoidlikum. Kasin huvi on suuresti tingitud lisakulust tootjale ja tarbijale, raskustest laboratoorsete testide tulemuste tõlgendamisel saadavasse kasusse lõppkasutuses ja puudustest meetodite standardiseerimises ning meetodika kasutamist reguleerivates õigusaktides. Mikroobivastaste pindade efektiivsuse hindamise meetodid põhinevad ajalooliselt suuresti mikroobide vedelkultuuridel ja/või vabanenud toimeaine mõju kaudsel hindamisel, mitte pinna mõju hindamisel rakendusspetsiifilistes, toote lõppkasutust imiteerivates tingimustes. Puutepindadel nagu uksenupud, tööpinnad, käsipuud, klaviatuurid jne on keskkond võrreldes enamkasutatud meetoditega kuivem, jahedam ja toitainevaesem. Enim toodetakse hõbedal ja vasel põhinevaid mikroobivastaseid materjale, sh nanotehnoloogilisi. Kuigi metallipõhised nanoosakesed on näidanud suurt potentsiaali mikroobivastastes rakendustes laboritingimustes, on neil põhinevate nanotehnoloogiliste ja multimodaalsete pindade toimet vähem uuritud.

Käesoleva töö eesmärgid võib tinglikult jagada meetodilisteks ja praktilisteks. Esiteks, soovisime hinnata laialdaselt kasutatavate meetodite kohasust pinnale kinnitunud mikroobide elumuse mõõtmisel ja kohandada pinnaefektide uurimiseks rekombinantsete metallitundlike bakteriaalsete biosensorite testformaati. Teiseks, soovisime iseloomustada uudsete multimodaalsete ZnO ja ZnO/Ag nanoosakestega kaetud pindade mikroobivastaseid omadusi.

Meetodilises osas kohandati rekombinantsete luminescentseeruvate *Escherichia coli* biosensorite katseskeem signaali kiireks mõõtmiseks söötmetilgas otse testitava materjali pinnalt. See võimaldas hinnata kvantitatiivselt vase ja vasesulamite subletaalseid mõjusid bakteritele pinnaformaadis. Vase biosensori signaali intensiivsus korreleerus pinnamaterjali vasesisaldusega, mitte pinnalt vabanenud vaseioonide kontsentratsiooniga katsekeskkonnas. Sellest järeldub bakterirakkude ja pinna vaheliste otsekontaktide olulisus mikroobivastastes rakendustes ja vastavates testprotokollides.

Samuti kasutati kahel erineva membraaniläbivusega fluorestseerival nukleiinhapetele seonduval värvil propiidiidijodiidil ja Syto9-l põhinevat meetodit, et hinnata tahkele pinnale kinnitunud *E. coli* ja *Staphylococcus epidermidise* biokilerakkude elujõulisust ja elumust toitainevaestes tingimustes fluorestsentsmikroskoopia abil. Laialdaselt kasutatava elumuse mõõtmise meetodi puhul ilmnes kriitiline puudus, sest meetod alahindas oluliselt nii rakkude ensümaatilist aktiivsust kui ka pinnalt eraldatud rakkude paljunemisevõimet ja ei sobi seetõttu kasutatud tingimustel elumuse ega elujõulisuse hindamiseks. Kuna peale rakkude pinnalt eraldamist sonikeerimise teel andis värvimine kõrgema elumushinnangu kui pinnal värvides, järeldasime, et nähtust võib põhjustada propiidiidijodiidiga värvuv komponent biokile rakuvälises maatriksis. Erinevalt vedelkultuuridest, on rakuvälised nukleiinhapped hästi teadaolev biokile rakuvälise maatriksi komponent, mis asub rakkude vahetus läheduses. See võib biokilerakkude

propiidiumjodiidiga värvimise korral põhjustada elusate rakkude punast fluorestsentsi sarnaselt kahjustunud membraaniga surnud rakkudele vedelkultuuris. Leid illustreerib vajadust meetodika põhjalikuma valideerimise järele, kui biokilede uurimisel rakendatakse vedelkultuuridele optimeeritud meetodeid.

Praktilise väljundina valiti ZnO ja ZnO/Ag nanoosakestega kaetud uudsete multimodaalsete pindade mikroobivastase efektiivsuse hindamiseks esmaseks meetodiks tööstuses laialdaselt kasutatav ja mikroobivastase tootega turule tulemisel nõutav standardmeetod. Meetod põhineb bakterisuspensiooni tilga eksponeerimises pinnale kattekile all õhukese kihina toitainevaeses keskkonnas. Nii tagatakse suurem testitava pinna ja bakterisuspensiooni mahu suhe, mis võimaldas näha ka otsekontaktist tulenevaid bakterivastaseid efekte, mis ei olnud seletatavad vabanenud metalli kontsentratsiooni toksilisusega testkeskkonnas. Sellele järgnes pindade biofilmivastase mõju iseloomustamine toitaainerikastes ja toitainevaestes staatilistes tingimustes. ZnO ja ZnO/Ag nanoosakestega kaetud pinnad omasid kiiret bakterivastast toimet *E. coli* ja *Staphylococcus aureuse* vastu, mis tulenes metalliioonide toksilisuse ja fotokatalüütilise aktiivsuse kombinatsioonist. Tulenevalt bakterite erinevast tundlikkusest metallide toksilisele toimele avaldas tsinkoksiidi kombineerimine hõbedaga laiemat bakterivastast toimet. Pindade mikroobivastased ja biofilmi teket pärssivad omadused sõltusid nii pinnakatte koostisest kui ka katsekeskkonnast. Mõlemad omadused ilmsid paremini toitainevaeses keskkonnas. Kuigi pinnad käitusid bakterivastaselt, ei mõjutanud need oluliselt pärmseene *Candida albicans* elumust. ZnO nanoosakestega kaetud pinnad, vastupidi, isegi suurendasid *C. albicansi* biokile moodustumist toitainevaeses keskkonnas. Viimane vastuolu toob esile vajaduse mitte ainult valida lõpprakendust arvestades sobivad testmeetodid, vaid ka kasutatavad organismid.

Kokkuvõttes toob käesolev töö välja vajaduse mikroobivastaste pindade efektiivsuse hindamiseks kasutatava meetodika kitsaskohti paremini kaardistada, rakendada meetodeid, mis võimaldavad hinnata pinna ja mikroobide otsekontakti ning kohandada meetodikat pindade lõppkasutuse tingimustele nii testkeskkonna kui sihtmärkorganismide osas.

Appendix

Publication I

Rosenberg, M.; Vija, H.; Kahru, A.; Keevil, C. W.; Ivask, A. (2018). Rapid *in situ* assessment of Cu-ion mediated effects and antibacterial efficacy of copper surfaces. *Scientific Reports*, 8 (8172). DOI: 10.1038/s41598-018-26391-8

© The Author(s) 2018. This article is licensed under a Creative Commons Attribution 4.0 International License, which permits use, sharing, adaptation, distribution and reproduction in any medium or format, as long as you give appropriate credit to the original author(s) and the source, provide a link to the Creative Commons license, and indicate if changes were made. The images or other third party material in this article are included in the article's Creative Commons license, unless indicated otherwise in a credit line to the material. <https://creativecommons.org/licenses/by/4.0/>

SCIENTIFIC REPORTS

OPEN

Rapid *in situ* assessment of Cu-ion mediated effects and antibacterial efficacy of copper surfaces

Merilin Rosenberg^{1,2}, Heiki Vija¹, Anne Kahru^{1,3}, C. William Keevil⁴ & Angela Ivask¹

Release of metal ions from metal-based surfaces has been considered one of the main drivers of their antimicrobial activity. Here we describe a method that enables parallel assessment of metal ion release from solid metallic surfaces and antimicrobial efficacy of these surfaces in a short time period. The protocol involves placement of a small volume of bioluminescent bacteria onto the tested surface and direct measurement of bioluminescence at various time points. In this study, two recombinant *Escherichia coli* strains, one expressing bioluminescence constitutively and applicable for general antimicrobial testing, and the other induced by Cu ions, were selected. Decrease in bioluminescence of constitutive *E. coli* on the surfaces showed a good correlation with the decrease in bacterial viability. Response of Cu-inducible *E. coli* showed a correlation with Cu content in the tested surfaces but not with Cu dissolution suggesting the role of direct bacteria-surface contact in Cu ion-driven antibacterial effects. In summary, the presented protocol enables the analysis of microbial toxicity and bioavailability of surface-released metal ions directly on solid surfaces within 30–60 min. Although optimized for copper and copper alloy surfaces and *E. coli*, the method can be extended to other types of metallic surfaces and bacterial strains.

Metal-, metal alloy or metal nanoparticle-based surfaces have been used extensively as antimicrobial surfaces in water treatment (filters, water pipes), in ventilation and air-conditioning systems, general high touch surfaces such as door handles and knobs, and more importantly in healthcare settings^{1–4}. Copper-based surfaces were the first registered solid antimicrobial surfaces by US EPA in 2008, after being supported by extensive antimicrobial efficacy testing. According to those studies, copper and copper alloys such as brass and bronze were able to decrease the counts of bacteria, including pathogens such as methicillin resistant *Staphylococcus aureus*, by 7 to 8 logs within hours⁵. Remarkably, such a decrease has not only been reported in laboratory conditions but also in hospitals, in field conditions⁶. On the other hand, some studies have shown that the antimicrobial efficacy of copper-based surfaces is modest and statistically not sound in preventing healthcare associated infections and spreading of antibiotic resistant organisms⁷. It is likely that these discrepancies between the different test results are mainly due to different testing conditions. Indeed, antimicrobial activity of copper surfaces has been shown to be affected by test conditions such as temperature and relative humidity^{4,7–10} as well as by the presence of any residues, or for example an oxide layer on the surfaces¹¹. Thus, one step closer to obtaining relevant correct and sound information on antimicrobial efficacy of copper (and other solid) surfaces is the use of standardized and appropriate test methods. Currently, a variety of test methods and testing suggestions that differ in their requirements for inoculum volume to surface area ratio, microbial culture density, relative humidity conditions, and that require testing in wet or dry conditions, are available for solid surfaces. The standard test methods generally approved and frequently used for antimicrobial efficacy assessment in Europe, US and Japan^{12–15} usually require the placement of a small volume of microbial suspension onto the tested surface, incubation in wet or dry conditions during a pre-determined time, and subsequent assessment of microbial viability, 24–48 h after agar plating. Although testing in “dry” conditions may be closer to real environmental conditions^{5,16} several studies have shown that this test format is more prone to errors due to experimental variations e.g., in humidity and temperature⁹ which suggests that testing in “wet” conditions may be more reliable and needs less optimization for screening purposes.

¹Laboratory of Environmental Toxicology, National Institute of Chemical Physics and Biophysics, Tallinn, Estonia.

²Department of Natural Sciences, Tallinn University of Technology, Tallinn, Estonia. ³Estonian Academy of Sciences, Kohtu 6, Tallinn, Estonia. ⁴Faculty of Natural and Environmental Sciences, Centre for Biological Sciences, University of Southampton, Southampton, UK. Correspondence and requests for materials should be addressed to C.W.K. (email: C.W.Keevil@soton.ac.uk) or A.I. (email: angela.ivask@kbfi.ee)

In this study, we introduce a new robust “wet” test format that can be used for the testing of solid metal-based antimicrobial surfaces and optimized this method for copper and copper alloy surfaces. The test is based on bioluminescent microbial cells, recombinant bioluminescent *Escherichia coli* cells used in this study. Due to the fact that release of copper ions is generally considered as the key mechanism of antimicrobial activity of copper surfaces^{4,17} a recombinant bioluminescent *E. coli* strain that enables the quantitative assessment of bioavailable Cu ions release is used in the same test format in parallel to the constitutively bioluminescent *E. coli*. The combination of those two bacterial strains allows the assessment released bioavailable copper from the surface and its bactericidal effect. The measurement of bioluminescence is carried out directly on surfaces and the duration of the new test format can be varied but we propose test times from 15 to 60 minutes. Although the method was optimized for copper surfaces in this study, it could be easily adapted for the assessment of metal ion release and antibacterial properties of other metal-based solid surfaces. Additionally, a constitutively bioluminescent *E. coli* strain can be individually used as a rapid first tool to evaluate the antibacterial effect of other (non-metallic) solid surfaces.

Results

Optimization of the measurement set-up. *Microplate configuration.* The novel set-up of our measurement system involving direct measurement of bacterial bioluminescence on solid surfaces was optimized to provide a reproducible test protocol. Due to the size of copper coupons (1 × 1 cm), 12-well plates were selected as a testing platform in this study. However, other plate types accommodating the surfaces of interest can also be selected. Due to the leakage of luminescence between wells in transparent plates and high background luminescence of white plates, we selected black plates from Cellvis (P12–1.5H–N). Because of the sensitivity limits of the luminometers and the fact that the bioluminescence intensity of bacteria on copper surfaces may be relatively low, we introduced adapters that increased the height of metal coupons by 5, 12 and 15 mm, respectively, to be closer to the photomultipliers collecting and amplifying the luminescence signal (Fig. 1a,b). To demonstrate the effect of adapters in obtained readings, we placed 1 × 1 cm polyethylene (PE) surfaces onto the adapters, added 75 µL suspension of bioluminescent *E. coli* (copper-induced strain of *E. coli* (pSLcueR/pDNPcopAlux) was used) and registered the baseline bioluminescence of the Cu-inducible *E. coli* strain. The measured values were clearly dependent on the position of the surface on the microplate wells and the highest bioluminescence reading was measured when the surfaces were lifted by 15 mm (4 mm from the surface of the microplate top) (Fig. 1b). Thus, this configuration was used in all further experiments.

In order to validate the measurement of bacterial bioluminescence on surfaces in a 12-well microplate set-up, we compared the bioluminescence values measured with the new 12-well set-up with those from an already established 96-well set-up. For that, *E. coli* (pSLcueR/pDNPcopAlux) was mixed with known concentrations of Cu ions which enabled us to obtain bioluminescence values at different intensities due to the fact that the bioluminescence in the copper sensor strain is induced concentration-dependently by bioavailable Cu²⁺ ions. *E. coli* (pSLcueR/pDNPcopAlux) mixed with various ionic copper concentrations were placed either onto PE control surfaces fitted into 12-well plate or into the wells of a 96-well plate. As seen from Fig. 2, the results obtained on 12- and 96-well microplates were in good correlation ($r = 0.98$; CI 95% 0.97–0.99; $p < 0.0001$) indicating that measurement of bioluminescence directly on solid surfaces is a viable analysis strategy.

Test medium. Based on information from our previous studies¹⁸ and the studies of other authors^{19,20} we assumed that the response of bioluminescent copper sensor *E. coli* (pSLcueR/pDNPcopAlux) and constitutively bioluminescent *E. coli* (pDNlux) is significantly affected by the test medium in which the bacteria are applied to the surfaces. As an example, Molteni *et al.*²⁰ indicated that Tris-buffer dramatically enhances contact killing of bacteria on copper surfaces, due to increasing release of Cu ions in this environment compared with water or phosphate buffer. On the other hand, our previous study by Käkinen *et al.*¹⁸ showed that increasing organic matter decreases the toxicity of Cu formulations. Here we tested the effect of four different exposure media on bioluminescence of *E. coli* copper sensor bacteria on C11000 copper surfaces. We chose 1:500 diluted nutrient broth (NB) medium which is a suggested medium in the ISO 22196 standard test protocol for solid surfaces¹⁴; heavy metal MOPS medium (HMM) that due to its non-complexing nature²¹ has been used in a series of studies focusing on metal testing (the medium was supplemented with either 0.5 or 0.01% cas-aminoacids as in¹⁸); and nutrient rich media LB and TSB, the first being a standard microbiological medium and the second being widely used in standard protocols, e.g., US EPA surface testing guidelines^{12,13}. As seen from Fig. 2a, when applied onto C11000 surfaces, Cu biosensor bacteria *E. coli* (pSLcueR/pDNPcopAlux) were only induced in LB and TSB media whereas in all other tested media the bacterial bioluminescence decreased below baseline luminescence indicating the antibacterial effect of copper surfaces in these conditions. The latter was also confirmed by counting surviving bacterial cells after their 60 min exposure on copper surfaces: around 3-log reduction of Cu biosensor bacteria was observed in HMM medium supplemented with 0.5% cas-aminoacids and no viable bacteria were registered when they were exposed to copper surfaces in 0.01% cas-aminoacid supplemented HMM or in 1:500 diluted NB medium (Fig. 2b). As the release of Cu ions from copper surfaces has been considered the main reason for the toxicity of those surfaces, we assumed that the differential response of *E. coli* copper sensor to C11000 surfaces in the selected test media was likely due to different susceptibility of the bacteria to Cu²⁺ in those media. Therefore, we next studied the response of *E. coli* (pSLcueR/pDNPcopAlux) to a range of concentrations of ionic Cu which covered those released from C11000 surfaces during the testing (Fig. 2c). It was evident that HMM supplemented with 0.01% amino acids and 1:500 NB media did not support the induction of bacterial bioluminescence during 60 min exposure, likely due to relatively high toxicity of Cu ions in those media as shown by us earlier¹⁸ but also due to shortage of nutrients to support bacterial bioluminescence production. The best bioluminescence induction and lowest Cu ions toxicity was observed in LB and TSB where the bioluminescence inhibition of *E. coli* (pSLcueR/pDNPcopAlux) was measured only at ~500 µg ionic Cu/L. Comparison of the induction profiles of the *E. coli* Cu sensor (Fig. 2c) with the release of Cu ions from C11000 surfaces in the different media (9.8 µg

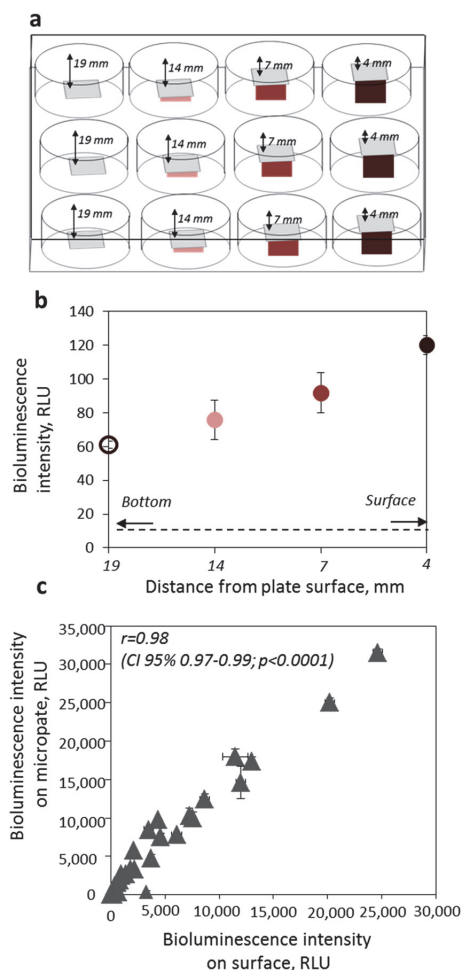


Figure 1. Set-up of 12-well microplate for optimal signal collection from bioluminescent bacteria that were placed onto a 1×1 cm copper coupon. **(a)** Is a schematic representation of 12-well microplate in which column 1 represents coupons on the plate bottom, column 2 coupons raised using 5 mm adapters, column 3 coupons raised using 12 mm and column 4 coupons raised using 15 mm adapters; **(b)** shows the measured baseline bioluminescence values of Cu biosensor *E. coli* (pSLcueR/pDNpCopAlux) on coupons on the plate bottom, 14, 7 and 4 mm from the plate surface. **(c)** Shows the linear correlation between bioluminescence of the Cu biosensor bacteria that had been previously exposed to known concentrations of Cu ions (0.1–100 $\mu\text{g Cu/mL}$; to cover different bioluminescence intensities) and either placed onto solid polyethylene surfaces in 12-well plates or onto the wells or 96-well microplates. Mean and standard deviation of three experiments are shown.

Cu ions was released from one C11000 coupon in LB medium, 53 μg in HMM medium supplemented with 0.5% cas-aminoacids, 13 μg in HMM medium with 0.01% cas-aminoacids, 7 μg in TSB medium and 0.7 μg in 1:500 diluted NB medium; these concentrations in $\mu\text{g/mL}$ are indicated with arrows in Fig. 2c) showed that in HMM media and in 1:500 diluted NB medium the released amount of ionic Cu was already toxic to bacteria and inhibited their bioluminescence even after 15 min exposure (Fig. 2d). However, the amount of Cu ions released from C11000 coupon in LB and TSB media was still within the measurable range in these specific media (Fig. 2c,d). Based on these results and keeping in mind the fact that one of the goals was to observe and quantitatively measure the bioluminescence induction of Cu biosensors, we selected LB medium for further testing. Although poorer media with less organic constituents would be certainly more relevant in mimicking actual exposure scenarios, Cu biosensor bacteria would not survive in these conditions with no results obtained.

Volume of biosensor bacteria on the surfaces. Due to the different requirements for bacterial volume on solid surfaces in different standard test methods (1.5×10^4 cells/cm² applied in 25 $\mu\text{L/cm}^2$ under film in ISO 22196¹⁴;

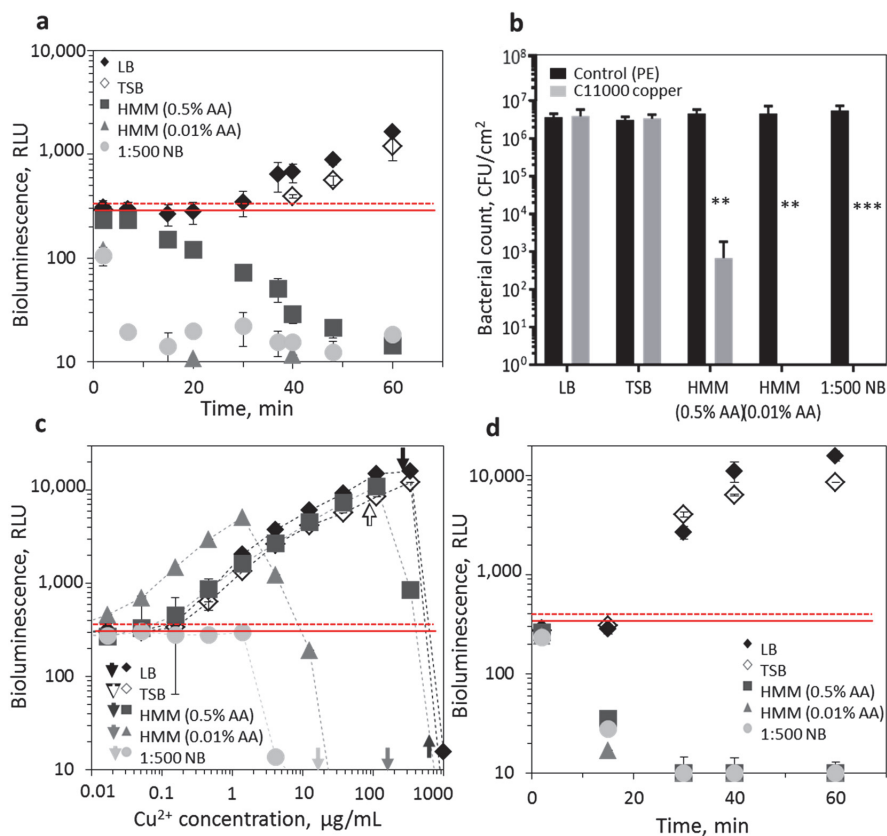


Figure 2. Induction of bioluminescence in *E. coli* (pSLcueR/pDNPcopAlux) Cu biosensor in different test media. (a) Bioluminescence of the Cu biosensor on C11000 copper surfaces in Heavy Metal MOPS Medium (HMM) with 0.01 and 0.5% casein acid hydrolysate (HMM 0.5% AA and 0.01% AA, respectively), 1:500 diluted Nutrient Broth (NB) medium, Luria Bertani (LB) medium and Tryptone Soy Broth (TSB) medium. (b) Bacterial counts after 60 min exposure in the specified media on control or C11000 surface. Significant differences in viable counts from control value based on two-way analysis of variance (ANOVA) and Bonferroni's multiple comparisons test are marked $p < 0.1$ (.); $p < 0.05$ (*); $p < 0.01$ (**); $p < 0.001$ (***) ; $p < 0.0001$ (****); (c) bioluminescence of the Cu biosensor in different media in CuSO_4 standard solutions (0.01–1000 mg/L Cu^{2+}) after 60 min exposure. Solid red line indicates background, i.e., non-induced bioluminescence of *E. coli* (pSLcueR/pDNPcopAlux) and dotted red line indicates the limit for significantly increase bioluminescence. Arrows indicate concentrations of Cu ions that according to TR-XRF were released from C11000 surfaces within 60 min in each medium. (d) time-dependent induction of bioluminescence in *E. coli* (pSLcueR/pDNPcopAlux) copper sensor in the presence of Cu concentrations indicated with arrows on (c). Mean and standard deviation of three replicates are shown.

1.6×10^6 cells/cm² applied in 16 $\mu\text{L}/\text{cm}^2$ and dried in CSN EN 13697¹⁵; 1.4–5.8 $\mu\text{L}/\text{cm}^2$ with at least 3.1×10^3 recoverable CFU/cm² in US EPA standards for copper surfaces^{12,13}) we optimized the volume and number of bacteria on copper surfaces. It must be noted that the use of bioluminescent bacteria sets certain requirements for the assay. Specifically, the test needs to be conducted in wet conditions (i.e., measurable bioluminescence is not induced under dry conditions) and in case of copper induced bacteria, exposure times longer than 20 min are required (for bioluminescence to be induced, see Fig. 2d). Our results showed that volumes smaller than 25 μL spread on 1 cm² (1 × 1 cm) solid coupons tended to significantly dry during 20–60 min exposure and thus, 25 μL was used as smallest volume of bacterial suspension in our optimization study. 50 $\mu\text{L}/\text{cm}^2$ and 75 $\mu\text{L}/\text{cm}^2$ of bacterial suspension were tested as larger volumes and, in all tested volumes, the bacterial number per surface area was kept constant ($2\text{--}3 \times 10^6$ cells/cm²). As seen from Fig. 3, when 25 μL of *E. coli* (pSLcueR/pDNPcopAlux) copper sensor bacteria was applied to and spread on a C11000 copper coupon, the bioluminescence decreased after 10 min (Fig. 3a). A similar time-dependent decrease in bioluminescence was observed in case of constitutively bioluminescent *E. coli* (pDNLux) (Fig. 3b). This decrease in bioluminescence was likely due the release of high concentrations of Cu ions from the surfaces in the 25 μL volume (30 μg Cu released per 1 cm² Cu surface,

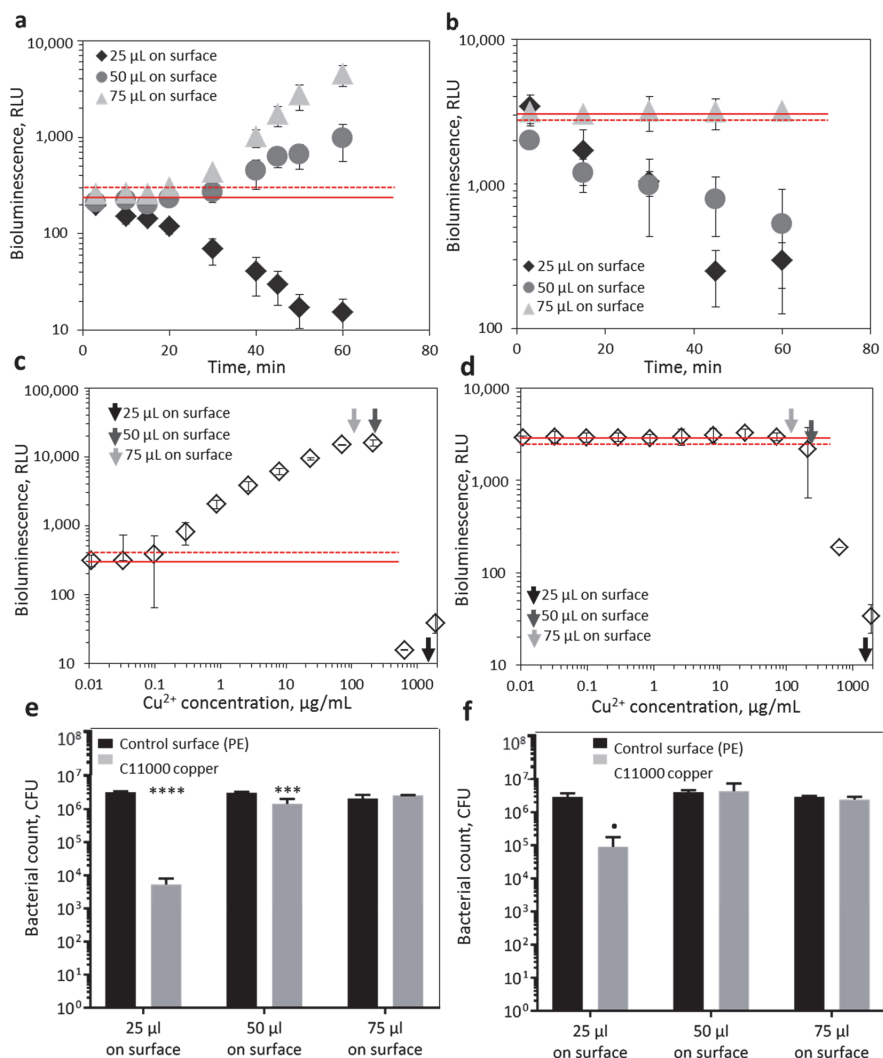


Figure 3. Optimization of bacterial test volume on copper surfaces. $\sim 1 \times 10^7$ cells of *E. coli* Cu biosensor (a,c,e) or constitutively bioluminescent *E. coli* (b,d,f) in 25, 50 or 75 μL was placed onto 1×1 cm C11000 surfaces. Bacterial bioluminescence was registered during 60 min (a,b). The concentration of released copper from C11000 surfaces during 60 min in 25, 50 or 75 μL (indicated with arrows) was compared with standard response curve of the Cu sensor strain and constitutively bioluminescent strain (c,d). The number of viable cells in 25, 50 or 75 μL Cu biosensor or constitutively bioluminescent *E. coli* strain on C11000 surfaces after 60 min (e and f). Significant differences in viable counts from control value based on two-way analysis of variance (ANOVA) and Bonferroni's multiple comparisons test are marked $p < 0.1$ (.); $p < 0.05$ (*); $p < 0.01$ (**); $p < 0.001$ (***) and $p < 0.0001$ (****). Solid red dotted line designates the background luminescence of *E. coli* Cu biosensor or constitutively bioluminescent *E. coli*; dotted red line designates significant increase (*E. coli* Cu biosensor) or decrease (constitutively bioluminescent *E. coli*) of bioluminescence. Mean and standard deviation of three replicates are shown.

i.e., bacteria on the coupon surface were exposed to $1200 \mu\text{g Cu/mL}$). Indeed, when the released concentration of Cu was compared with the response of bioluminescent bacteria to copper standard solutions, it was obvious that it was already toxic, both to *E. coli* copper sensor as well as to constitutively bioluminescent *E. coli* (see black arrows in Fig. 3c,d). However, drying of 25 μL bacterial suspension on copper surfaces could have also contributed to bioluminescence inhibition. Toxicity of copper surfaces to 25 μL bacterial suspension is further evident from the approximately 2-log decrease in viable bacterial count after 60 min exposure (Fig. 3e,f). When 50 μL of

UNS code	Trade name	Cu, %	Zn, %	Ni, %	Fe, %	Sn, %	Pb, %	Mn, %
C11000	Electrolytic Tough Pitch Copper	99.9	—	—	—	—	—	—
C51000	Phosphor Bronze, 5%	94.2	0.3	—	0.1	5.8	0.005	—
C70600	Copper-Nickel, 10%	89	—	10	1	—	—	—
n.a.	Nordic gold	89	5	—	—	1	—	—
C26000	Cartridge Brass, 70%	69–72	28–31	—	0.05	—	0.07	—
C71500	Copper-Nickel, 30%	64–69	1	29–33	0.4–1	—	0.05	1
C75200	Nickel Silver, 65–18	63–67	13–20	17–20	0.25	—	0.05	0.5
C28000	Muntz Metal, 60%	59–63	37–41	—	0.07	—	0.09	—

Table 1. Copper and copper alloy surfaces used. Specification of the alloys is per their Unified Numbering System (UNS) and according to Copper Development Association Inc. “n.a.” – not available; “—” – not stated by manufacturer.

Cu biosensor bacteria was added to copper coupons, Cu-dependent induction of bioluminescence was observed (Fig. 3a). However, the bioluminescence of constitutively bioluminescent *E. coli* strain in 50 μ L decreased (Fig. 3b) which allowed us to conclude that the concentration of Cu ions released from copper coupons in this volume also exhibited a toxic effect which in Cu biosensor was masked by Cu-driven bioluminescence induction. Indeed, when the released concentration of Cu (11 μ g per surface or 215 μ g Cu/mL bacterial suspension) was compared with the copper standard curve, it was very close to toxic Cu concentrations (grey arrows in Fig. 3c,d). Differently from the 50 μ L volume, no decrease in bioluminescence of the constitutively bioluminescent *E. coli* was observed when bacteria were applied to C11000 surfaces in 75 μ L and also the bioluminescence induction of copper sensor strain in 75 μ L was higher than in 50 μ L volume. Additionally, the released concentration of copper ions in 75 μ L (10 μ g per surface or 130 μ g/mL bacterial suspension) was lower than in 50 μ L (Fig. 3c,d). Considering these results 75 μ L volume was considered optimal for further analyses. Volumes larger than 75 μ L/cm² were not considered due to their instability on the surface.

Optimized protocol for the analysis of copper and copper alloy surfaces with bioluminescent bacteria. The optimized surface analysis protocol was tested on 1 \times 1 cm coupons of a variety of copper and copper alloy surfaces (Table 1). The protocol included the placement of 1 \times 1 cm coupons into 12-well microplates on 15 mm plastic adapters (Fig. 1a and Supplementary Figure S1), addition of 75 μ L bacteria in LB medium at OD₆₀₀ 0.15 (approximately 1 \times 10⁷ cells/cm²) and direct measurement of bioluminescence during 60 min exposure at room temperature.

Constitutively bioluminescent E. coli for general toxicity assessment of surfaces. One of the main advantages of the analysis protocol presented in this study is its rapidity: bioluminescent bacteria are applied onto the surfaces, and bioluminescence readings can be measured at any desired timepoint, starting from 20 min after exposure. The bioluminescence of constitutively bioluminescent *E. coli* (pDNlux) on copper and copper alloy surfaces shown in Fig. 4b demonstrates that the bacterial bioluminescence decreased on the tested surfaces to different extents indicating different toxicity of the studied surfaces. To verify that the decrease in bioluminescence was also correlated with decrease in viable bacterial count in the assay, we analyzed *E. coli* viability after 60 min exposure (Fig. 4f) and observed that the C70600 surface that caused a significant substantial decrease in bioluminescence caused also a significant decrease in viable bacterial counts. To further correlate bacterial bioluminescence and viability in our novel test system, we exposed the constitutively bioluminescent bacteria to different copper solutions, placed them onto control PE surfaces and measured both bioluminescence as well as registered viable counts. As shown on Supplementary Fig. S2, there was a clear correlation between bioluminescence and bacterial viability ($r = 0.95$, CI 95% 0.9–0.98; $p < 0.0001$), evaluated on the basis of traditional cultured plate counts. Based on linear regression between decrease of bioluminescence and viable counts ($R^2 = 0.91$; $y = 117620 \cdot x + 906854$; Supplementary Fig. S2) we were able to calculate that e.g., 10% decrease in bioluminescence translated to the death of 2.1 \times 10⁶ CFUs and 90% decrease in bioluminescence to the death of 1.1 \times 10⁷ CFUs. Based on those data we suggest that screening of bacterial bioluminescence on solid surfaces could indeed be used as a rapid (60-min) tool for the evaluation of their antibacterial activity.

Analysis of copper ion release with the bioluminescent copper sensor. As already mentioned, surface released Cu ions have been considered as the main reason for antibacterial activity of copper-based surfaces and, therefore, addition of bioluminescent Cu sensor bacteria to the analysis with constitutively bioluminescent strains was considered relevant in evaluating the mechanism of antibacterial activity of copper-based surfaces. Results obtained with Cu biosensor *E. coli* (pSLcueR/pDNPcopAlux) on different copper and copper alloy surfaces are shown on Fig. 4. From eight tested surfaces, six induced the bioluminescence of the biosensor strain (Fig. 4a,c). Two surfaces that did not induce the biosensor, contained either the lowest amount of Cu (C28000, 63% Cu, Table 1) or were toxic and inhibited also the bioluminescence of the constitutively bioluminescent strain (C70600; see also decreased viable counts on that surface in Fig. 4e,f). In order to account for this toxicity-driven decrease of bacterial bioluminescence, the results of the constitutively bioluminescent *E. coli* strain were used to correct the bioluminescence induction of the Cu biosensor strain (see red symbols in Fig. 5). The corrected bioluminescence induction values of the Cu sensor strain correlated with Cu content of the surfaces ($r = 0.8$; CI 95% 0.21–0.96; $p = 0.018$, Fig. 5a) whereas there was no significant correlation between Cu content and raw bioluminescence

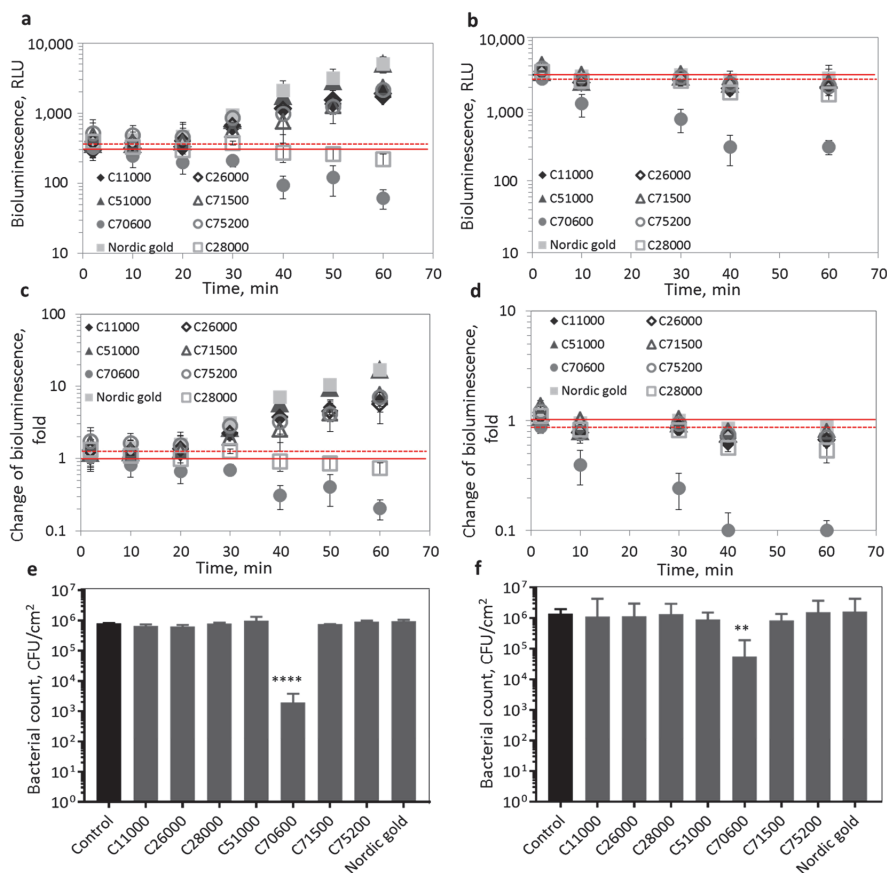


Figure 4. Changes of bacterial bioluminescence on copper and copper alloy surfaces. Results on Cu-induced *E. coli* (pSLcueR/pDNPcopAlux) (a,c,e) and on constitutively bioluminescent *E. coli* (b,d,f). Bioluminescence in relative light units (a,b) and fold change (c,d) when exposed to copper surfaces: C11000 (99.9% Cu), C51000 (94.2% Cu, 5.8% Sn), C70600 (89% Cu, 10% Zn), C26000 (69–72% Cu, 28–31% Zn), C71500 (64–69% Cu, 29–33% Ni), C75200 (63–67% Cu, 13–20% Zn, 17–20% Ni), C28000 (59–63% Cu, 37–41% Zn) during 60 min in LB medium. Solid red line indicates background (non-exposed) bioluminescence and dotted red line significantly increased (Cu biosensor) or decreased (constitutively bioluminescent *E. coli*). (e,f) Viable bacterial counts on copper surfaces after 60 min exposure compared to control (PE) surface. Significant differences in viable counts from control value based one-way analysis of variance (ANOVA) and Dunnett's multiple comparisons test are marked $p < 0.1$ (.); $p < 0.05$ (*); $p < 0.01$ (**); $p < 0.001$ (***) ; $p < 0.0001$ (****).

data ($r = 0.54$; CI 95% $-0.27-0.9$; $p > 0.05$; Fig. 5a). However, there was also no significant correlation between Cu biosensor bioluminescence and Cu ion release from the surfaces during 60 min of biosensor assay ($r = -0.49$; CI 95% $-0.89-0.33$; $p > 0.05$ for raw values and $r = -0.085$; CI 95% $-0.75-0.66$; $p > 0.05$ for corrected values; Fig. 5b). Indeed, the TR-XRF measured dissolution of copper from different surfaces were not in line with surface Cu content (Fig. 5c) and, based on an earlier study by Suarez *et al.*²², we propose that in addition to surface chemical composition also certain physical properties of the surfaces such as roughness affect the release of metals from solid surfaces. We suggest that bioavailability of Cu on copper-based surfaces to bacteria was affected by direct contact between bacterial cells and the surfaces followed by local release of copper in the bacterial microenvironment. A similar observation has been reported by us in earlier papers for soil samples^{23,24}. In this respect, bacterial biosensors can be used as unique tools to analyze surface-released bioavailable metal ions directly on solid samples.

Discussion

Here we present a novel, robust and rapid test method that can be applied for the analysis of solid surfaces which in this study was optimized for copper and copper alloy-based surfaces. The method allows direct analysis of the surfaces and does not require an additional cultivation step for colony counting or other indirect measurement.

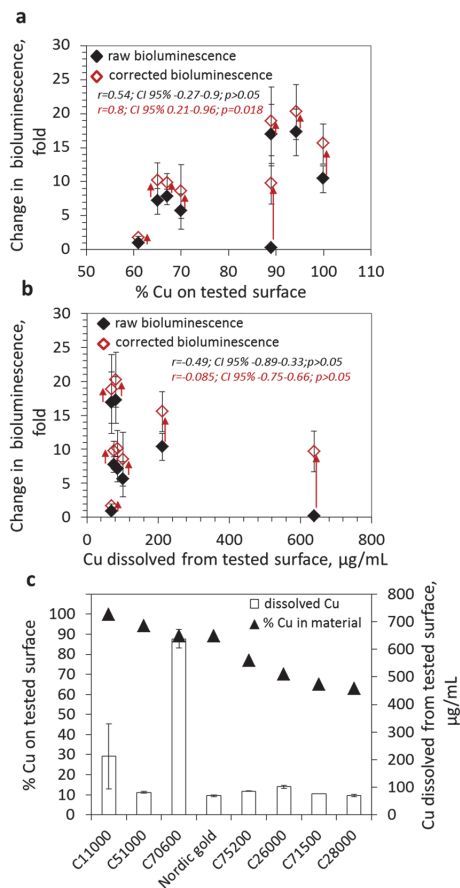


Figure 5. Correlation between Cu biosensor induction by copper surfaces and Cu content or dissolution of the surface material. Linear correlation between raw and corrected bioluminescence induction of the Cu biosensor on copper and copper alloy surfaces and Cu content of those surfaces (a) or copper release from these surfaces (b) after 60 min. Arrows indicate the difference between raw and corrected bioluminescence induction. All experiments were performed in LB medium in three replicates. (c) Copper content and release of Cu from the different copper surfaces in LB medium. Mean and standard deviation of three replicates are shown.

The test protocol requires the use of bioluminescent bacteria that are applied to the surface in liquid form, exposure for a specified period at room temperature and real-time measurement of bioluminescence. Although a variety of natural as well as recombinant bioluminescent bacteria can be obtained through commercial suppliers or from research laboratories are available, we here used two *E. coli* strains because this bacterium is a medically relevant test organism and because we have constructed a series of *E. coli*-based bioluminescent sensor strains that enable detection of metal ions²⁵ as well as other intracellular stress conditions²⁶. A liquid test method was chosen for several reasons, the most important being the fact that bacterial bioluminescence is not produced in dry conditions but also because the results of dry tests have shown to greatly depend on different testing conditions, e.g., temperature and relative humidity. Here we identified that inoculum volume on copper coupons as well as the exposure medium had a significant effect on antibacterial efficacy of the surfaces. Our results showed that a poor medium, e.g., 1:500 diluted NB medium which is a suggested medium in ISO 22196 standard test protocol for solid surfaces, is not suitable when bioluminescent bacteria are used as the nutrient supply in poor media is too low to support the energy-expensive bioluminescence reaction. The latter can be only supported by organic-rich media, e.g., LB medium which is a standard microbiological growth medium, or TSB medium which is a suggested medium in US EPA standards for the testing of copper surfaces^{12,13}. Similar exposure medium-dependent antibacterial effects of copper surfaces have been observed earlier e.g., by Molteni *et al.*²⁰ who demonstrated that exposure to medium containing Tris buffer showed lower antibacterial effect than for example phosphate buffer and Hans *et al.*¹⁹ who showed 10–50-fold faster copper ion release in Tris-HCl buffer compared to phosphate buffered saline (PBS). Indeed, as also demonstrated by us, the amount of released Cu ions in the different exposure

media differed around 50-fold, being the lowest in 1:500 diluted NB medium (0.7 µg Cu per cm² surface; Fig. 2c) and the highest in Heavy Metal MOPS medium supplemented with 0.5% cas-aminoacids (53 µg Cu per cm² surface; Fig. 2c). At the same time, in the same volume of MilliQ water the released Cu concentration was 0.3 µg Cu per cm² surface. Therefore, certain media components, most notably organics, significantly enhanced the release of Cu ions from copper surfaces. As a compromise between supporting bacterial bioluminescence production and release of Cu ions from the surfaces in the range that is capable of inducing the bioluminescence of Cu-sensing bacteria, LB was selected as an optimal medium for further testing. Yet as our test optimization indicated, the volume of bacterial suspension in LB medium also affected the release of ionic copper from the tested surfaces. A smaller volume (25 µL) of bacterial suspension on surfaces released significantly more copper from the surface than a larger volume (75 µL), thus inhibiting bacterial bioluminescence and interfering with Cu biosensor measurement. This finding suggested that a larger volume, in our case 75 µL bacterial suspension on the surface, supports bacterial bioluminescence production and is favorable.

One of the novelties of our test system is the possibility to use bacteria that report on the mechanisms of anti-bacterial actions of the surfaces. In our previous studies we have constructed a range of bioluminescent bacteria that not only are able to report on the presence of bioavailable metal ions in their environment²⁵ but also bacteria whose bioluminescence is induced by e.g., the presence of reactive oxygen species and DNA damage²⁶. As it is generally suggested that the key mechanism through which copper surfaces exhibit their antimicrobial activity is the release of copper ions^{1,17,20,27}, in this study we applied the copper sensing bioluminescent *E. coli* strain to analyze and quantify the release of bioavailable ionic copper from the studied surfaces. However, as also other toxicity pathways, e.g., oxidative damage in the form of lipid peroxidation and oxidation of proteins due to superoxide and hydroxyl radicals, and DNA degradation have been proposed for copper surfaces^{3,5,28–31}, other previously mentioned mechanism-based sensor bacteria could be used in this test format. Our results with bioluminescent copper sensors showed that significant amounts of Cu ions were released and entered bacterial cells from copper and copper alloy-based surfaces and that this released and bacteria-bioavailable fraction showed a positive correlation with copper content on the surfaces. Interestingly, there was no significant correlation between surface released Cu and response of the copper biosensor: on six surfaces that released 69 to 85 µg Cu / mL, the induction of the copper biosensor varied from 1 to about 20-fold. The fact that Cu biosensor induction correlated better with material properties (i.e., Cu content) than with material-released Cu suggests that bacteria-bioavailable Cu is rather a function of direct interactions between microbes and surfaces than of simple Cu dissolution. These direct interactions could lead to variable local Cu ion concentrations in bacterial microenvironments. Similar observations have been reported previously by us for soil samples where bioavailability of Cu and also other bivalent metals (e.g., Cd and Pb) had relatively poor correlation with water-extracted metal ions^{23,24}. In the case of surfaces, similar direct contact-driven bacterial effects have been observed by Zeiger *et al.*²⁷ who demonstrated that the physical nature of copper surfaces affected their antibacterial activity. These direct interactions between microbes and solid surfaces can be only elucidated using real-time biological analysis methods, as the one described here. Considering this unique capability of our test system and the rapidity and simplicity of the analysis procedure we propose that direct analysis of bacterial bioluminescence from solid surfaces could be used as an efficient screening tool to evaluate the bioavailability of Cu (and in case of other types of metal surfaces, other metals, e.g., release of Ag ions from antibacterial silver nanoparticles³²) from antibacterial copper-based surfaces, and their toxicity. As with any (anti)bacterial assay, our protocol involves pre-cultivation of bacteria, but lacks the need for cell removal (and associated issues regarding removal efficiency versus survivor viability) as well as post-cultivation for viable cell count determination or microscopy based counting steps. Results are collected in real-time and in digital form that is easy to automate. Given the good correlation between the survival of bacteria on copper-based surfaces and the bioluminescence of constitutively bioluminescent bacteria on the surfaces, our suggestion for the use of the presented direct surface measurement set-up is justified.

In conclusion, in this study we have presented a protocol for the direct analysis of Cu surfaces for i) their bioavailable copper release and ii) antibacterial efficacy using a Cu ion inducible bioluminescent *E. coli* strain and a constitutively bioluminescent *E. coli* strain. The main advantages of our test protocol are: i) rapidity (an indication on antimicrobial effects can be obtained within 30–60 min), ii) cost efficiency (due to saving of laboratory consumables needed for traditional colony counting), and iii) possibility to in addition to antimicrobial efficacy evaluate its cause. Although our methodology was optimized for copper-based surfaces and *E. coli* bacteria in this study, its use can certainly be extended to other metallic surfaces, including but not limited to, silver and zinc-based surfaces and other types of bioluminescent bacteria.

Methods

Surfaces and their preparation for test. The copper-based surfaces tested here (Table 1) originated from Copper Development Association Inc. and were cut to 1 × 1 cm coupons. Prior to experiments, all copper alloy coupons were treated by washing with acetone and ethanol using glass beads. Each coupon was individually flamed for sterilization purposes prior to inoculation. As control surfaces, 1 × 1 cm squares were cut from polyethylene (PE) plastic, sterilized with ethanol, and allowed to dry.

Preparation of bacteria for the test. Recombinant bioluminescent strains of *E. coli*, a constitutively bioluminescent strain *E. coli* (pDNlux)²⁵, and a Cu-induced bioluminescent strain *E. coli* (pSLcueR/pDNPcopAlux)²⁵ were used. The bacteria were routinely maintained on LB agar (LB medium (Supplementary Table 1) with 15 g agar/L) supplemented with 10 µg/mL tetracycline (*E. coli* (pDNlux)) or 10 µg/mL tetracycline and 100 µg/mL ampicillin (*E. coli* (pSLcueR/pDNPcopAlux)). In preparation for the test, the bacteria were grown in the appropriate medium overnight, diluted 1:50 with fresh medium and grown until OD₆₀₀ 0.6. Then the cells were diluted either with LB medium until OD₆₀₀ 0.15 or washed and diluted in a different test medium (see below).

Optimization of the test set-up. Testing of surfaces with recombinant bioluminescent bacteria was optimized for the black 12-well microplate configuration and room temperature (20–22 °C). This plate type was selected to accommodate 1 × 1 cm sized coupons and respective control surfaces inside the wells. However, depending on the size of specific surfaces, microplates with less (e.g., 6-well plate) or more (e.g., 24-well plate) wells can be selected. For test optimization, the 1 × 1 cm PE plastic surfaces on black 12-well microplates (Cellvis, CA, US) were placed onto the well bottoms or raised by using 5, 12 and 15 mm high plastic adaptors (Fig. 1), to bring the surfaces closer to photomultiplier tube and increase the bioluminescence signal intensity. A 75 µL drop of *E. coli* (pSLcueR/pDNpcopAlux) culture (OD₆₀₀ 0.15) in LB medium containing ~1 × 10⁷ cells was placed onto the surfaces on 12-well microplates and spread so that the coupon surface was covered. The relative luminescence (RLU) was measured from the middle of each well using a Promega Glowmax plate luminometer or Fluoroskan Ascent plate luminometer. For setting the background value, the luminescence signals of empty wells were measured; in bacterial experiments only signals that exceeded this background at least 3-fold were counted. Using 15 mm high adaptors on 12-well plates was considered as the most suitable test format for further experiments.

To validate the performance of bacterial bioluminescence measurement on surfaces and in 12-well plates, bioluminescence of *E. coli* (pSLcueR/pDNpcopAlux) in 12- and 96-well plates was compared; 96-well plates were used for comparison as an already established method used by our and other research groups in a variety of reports^{25,33,34}. To compare exactly the same conditions in 12- and 96-well plates, 150 µL of *E. coli* (pSLcueR/pDNpcopAlux) bacteria (OD₆₀₀ 0.15 in LB medium) were mixed with variable (0.1–100 µg Cu/mL) concentrations of CuSO₄ × 5H₂O (Sigma-Aldrich) (0.002 to 2000 µg/mL Cu); 75 µL of the mixture was added to PE control surface on 15 mm adaptor in a 12-well plate and 75 µL of the mixture was pipetted to a well of a black 96-well microplate. The bioluminescence of both plates was measured after 60 min incubation at room temperature and the readings from 96 and 12-well plates were correlated. Three independent experiments were performed.

To optimize the test medium, *E. coli* (pSLcueR/pDNpcopAlux) and *E. coli* (pDNlux) were suspended in LB which is a traditional bacterial growth medium, TSB (tryptic soy broth) that is one of the suggested media in US EPA suggested surface testing methods^{12,13}, HMM (heavy metal MOPS medium) that was suggested for transition metal testing by LaRossa *et al.*²¹ and has been used earlier to study metal bioavailability to bacteria^{18,25,35} (in our experiments, HMM medium was supplemented with different amounts, 0.01 and 0.5% of casein amino acids), and 1:500 diluted NB (nutrient broth) that is suggested as an exposure medium in ISO 22196¹⁴ (for the composition of test media, see Supplementary Table 1). Prior to the test, bacteria pre-grown in LB until OD₆₀₀ 0.6 were double washed (centrifugation at 5000 g for 5 min and resuspension in specific test medium) and diluted to OD₆₀₀ of 0.15 using specific test medium. 75 µL of bacteria was spread onto C11000 surfaces on 15 mm high adaptors in 12-well plates, incubated for 60 min and bioluminescence was measured. Bacteria in each test medium were analyzed thrice. According to the results, LB and TSB were considered as most optimal and LB was used in all further experiments. In order to check for culture viability in different media after 60 min incubation on C11000 surfaces, the exposed bacteria were collected, serially diluted and plated onto NB (15 g agar/L) plates. Colonies were counted after 24–36 h incubation at 30 °C. To quantify release (dissolution) of copper from C11000, bacterial suspensions exposed to the surfaces in different media were collected, 1 mg/L Ga (internal standard) was added and Cu content was quantified using total reflection X-ray fluorescence (TR-XRF; S2 Picofox, Bruker).

Due to different volume requirements for the bacterial inoculum in different surface testing standards (5–20 µL on 2.5 × 2.5 cm surfaces followed by drying in US EPA^{12,13}, 50 µL on 2 cm diameter surfaces followed by drying in EN13697¹⁵, 100 µL on 4 × 4 cm surfaces in ISO 22196 standard¹⁴), we here optimized the volume of bioluminescent bacteria on 1 × 1 cm surfaces. For that, 25, 50 and 75 µL of *E. coli* (pSLcueR/pDNpcopAlux) and *E. coli* (pDNlux) suspension in LB (25 µL being the smallest volume that was possible to be spread on the surface without visible drying during 60 min exposure and 75 µL being close to the maximum volume of droplet that remained stable on the surfaces while handling) was applied onto the 1 × 1 cm surfaces. In each exposure, the bacterial number was kept similar (~1 × 10⁷ cells per surface) and thus, 75 µL of bacteria was added at OD₆₀₀ 0.15, 50 µL at OD₆₀₀ 0.22 and 25 µL at OD₆₀₀ 0.45. Bacteria were spread on C11000 coupons and bioluminescence was registered over 60 minutes. The experiment was performed in triplicate. In order to check for bacterial viability in different volumes after 60 min exposure on copper surfaces, the exposed bacteria were collected, diluted and plated onto NB agar plates. Colonies were counted after 24–36 h incubation at 30 °C and surface released (dissolved) copper was quantified using TR-XRF, as described above. According to the results, 75 µL was selected as optimal volume of bacteria on the surfaces.

Analysis of copper and copper alloy surfaces for bacterial toxicity and bioavailable Cu. After optimization, copper and copper alloy coupons (Table 1) along with similar sized (1 × 1 cm) control surfaces (PE) were analyzed with constitutively bioluminescent *E. coli* (pDNlux) and Cu-induced *E. coli* (pSLcueR/pDNpcopAlux) bacteria (75 µL of bacterial suspension at OD₆₀₀ 0.15 in LB medium spread on a surface) and bioluminescence of the bacteria was registered during 60 min. The results for copper surfaces (i.e., test surfaces) were expressed both in relative bioluminescence units (RLU) as well as in fold change in bioluminescence. Fold induction of the Cu sensor or constitutively bioluminescent *E. coli* was calculated as follows:

$$\text{Fold change in bioluminescence} = \frac{\text{RLU}_{\text{test surface}}}{\text{RLU}_{\text{control surface}}} \quad (1)$$

In order to account for potential toxicity and unspecific effects of the tested surfaces, bioluminescence of the Cu biosensor strain prior to calculating the fold change (eq. 1) was corrected using *E. coli* (pDNlux):

$$\text{Corrected RLU Cu sensor}_{\text{test surface}} = \text{RLU Cu sensor}_{\text{test surface}} \times \frac{\text{RLU constitutive strain}_{\text{control surface}}}{\text{RLU constitutive strain}_{\text{test surface}}} \quad (2)$$

To check for bacterial viability of Cu biosensor and constitutively bioluminescent bacteria on the different copper surfaces after 60 min exposure, the exposed bacteria were collected, diluted and plated onto NB agar plates. Colonies were counted after 24–36 h incubation at 30 °C and surface-released (dissolved) copper was quantified using TR-XRF as described above. Additionally, to correlate the decrease of bioluminescence and colonies of the constitutively bioluminescent *E. coli* on surfaces, *E. coli* (pDNlux) was exposed to CuSO₄ solutions (100–1000 µg Cu²⁺/mL) for 60 min after which bioluminescence and CFU count on nutrient agar plates was registered.

Statistical analysis. Mean values, standard deviations and correlation plots were produced by Microsoft Excel standard functions. Correlation statistics, linear regression and analysis of variance (ANOVA) followed by Dunnett's or Bonferroni's multiple comparisons test were executed in GraphPad Prism 7.04. Alpha value 0.05 and two-tailed calculations were used where applicable.

Data availability. The datasets generated during and/or analysed during the current study are available from the corresponding author on reasonable request.

References

- Molling, J. W., Seezink, J. W., Teunissen, B. E. J., Muijters-Chen, I. & Borm, P. J. A. Comparative performance of a panel of commercially available antimicrobial nanocoatings in Europe. *Nanotechnol Sci Appl* **7**, 97–104 (2014).
- Muller, M. P. *et al.* Antimicrobial surfaces to prevent healthcare-associated infections: a systematic review. *J Hosp Infect* **92**, 7–13 (2009).
- Villapún, M. V., Dover, G. L., Cross, A. & González, S. Antibacterial Metallic Touch Surfaces. *Materials* **9** (2016)
- Vincent, M., Hartemann, P. & Engels-Deutsch, M. Antimicrobial applications of copper. *Int J Hyg Environ Health* **219**, 585–591 (2016).
- Grass, G., Rensing, C. & Solioz, M. Metallic Copper as an Antimicrobial Surface. *Appl Environ Microbiol* **77**, 1541–1547 (2011).
- Michels, H. T., Keevil, C. W., Salgado, C. D. & Schmidt, M. G. From Laboratory Research to a Clinical Trial: Copper Alloy Surfaces Kill Bacteria and Reduce Hospital-Acquired Infections. *Herd* **9**, 64–79 (2015).
- Elguindi, J., Wagner, J. & Rensing, C. Genes involved in copper resistance influence survival of *Pseudomonas aeruginosa* on copper surfaces. *J Appl Microbiol* **106**, 1448–1455 (2009).
- Michels, H. T., Noyce, J. O. & Keevil, C. W. Effects of temperature and humidity on the efficacy of methicillin-resistant *Staphylococcus aureus* challenged antimicrobial materials containing silver and copper. *Lett Appl Microbiol* **49**, 191–195 (2009).
- Ojeil, M., Jermann, C., Holah, J., Denyer, S. P. & Maillard, J. Y. Evaluation of new *in vitro* efficacy test for antimicrobial surface activity reflecting UK hospital conditions. *J Hosp Infect* **85**, 274–281 (2013).
- Wilks, S. A., Michels, H. & Keevil, C. W. The survival of *Escherichia coli* O157 on a range of metal surfaces. *Int J Food Microbiol* **105**, 445–454 (2005).
- Elguindi, J. *et al.* Metallic copper corrosion rates, moisture content, and growth medium influence survival of copper-ion resistant bacteria. *Appl Microbiol Biotechnol* **89**, 1963–1970 (2011).
- US Environmental Protection Agency. Test Method for the Continuous Reduction of Bacterial Contamination on Copper Alloy Surfaces (2009).
- US Environmental Protection Agency. Test Method for Efficacy of Copper Alloy Surfaces as a Sanitizer (2009).
- International Organization for Standardization. ISO 22196:2011. Measurement of antibacterial activity on plastics and other non-porous surfaces (2011).
- European Committee for Standardization. CSN EN 13697. Chemical disinfectants and antiseptics - Quantitative non-porous surface test for the evaluation of bactericidal and/or fungicidal activity of chemical disinfectants used in food, industrial, domestic and institutional areas - Test method and requirements without mechanical action (2015).
- Warnes, S. L. & Keevil, C. W. Mechanism of copper surface toxicity in vancomycin-resistant enterococci following 'wet' or 'dry' contact. *Appl Environ Microbiol* (2011).
- Michels, H. T. & Anderson, D. Antimicrobial regulatory efficacy testing of solid copper alloy surfaces in the USA. In: *Metal Ions in Biology and Medicine: Vol. 10* (eds Collery, Ph., Maynard, I., Theophanides, T., Khassanova, L., Collery, T.) 185–190 (John Libbey Eurotext, Paris 2008).
- Käkinen, A., Bondarenko, O., Ivask, A. & Kahru, A. The Effect of Composition of Different Ecotoxicological Test Media on Free and Bioavailable Copper from CuSO₄ and CuO Nanoparticles: Comparative Evidence from a Cu-Selective Electrode and a Cu-Biosensor. *Sensors* **11**, 10502 (2011).
- Hans, M. *et al.* Role of Copper Oxides in Contact Killing of Bacteria. *Langmuir* **29**, 16160–16166 (2013).
- Molteni, C., Abicht, H. K. & Solioz, M. Killing of Bacteria by Copper Surfaces Involves Dissolved Copper. *Appl Environ Microbiol* **76**, 4099–4101 (2010).
- LaRossa, R. A., Smulski, D. R. & Van Dyk, T. K. Interaction of lead nitrate and cadmium chloride with *Escherichia coli* K-12 and *Salmonella typhimurium* global regulatory mutants. *J Ind Microbiol* **14**, 252–258 (1995).
- Suárez, C., Vilar, T., Gil, J. & Sevilla, P. *In vitro* evaluation of surface topographic changes and nickel release of lingual orthodontic archwires. *J Mater Sci Mater Med* **21**, 675–683 (2010).
- Ivask, A. *et al.* Recombinant luminescent bacterial sensors for the measurement of bioavailability of cadmium and lead in soils polluted by metal smelters. *Chemosphere* **55**, 147–156 (2004).
- Peltola, P., Ivask, A., Åström, M. & Virta, M. Lead and Cu in contaminated urban soils: Extraction with chemical reagents and bioluminescent bacteria and yeast. *Sci Tot Environ* **350**, 194–203 (2005).
- Ivask, A., Rölöva, T. & Kahru, A. A suite of recombinant luminescent bacterial strains for the quantification of bioavailable heavy metals and toxicity testing. *BMC Biotechnol* **9**, 41 (2009).
- Bondarenko, O., Ivask, A., Käkinen, A. & Kahru, A. Sub-toxic effects of CuO nanoparticles on bacteria: Kinetics, role of Cu ions and possible mechanisms of action. *Environmental Pollution* **169**, 81–89 (2012).
- Zeiger, M., Solioz, M., Edongué, H., Arzt, E. & Schneider, A. S. Surface structure influences contact killing of bacteria by copper. *MicrobiologyOpen* **3**, 327–332 (2014).
- Helbig, K., Bleuel, C., Krauss, G. J. & Nies, D. H. Glutathione and Transition-Metal Homeostasis in *Escherichia coli*. *J Bacteriol* **190**, 5431–5438 (2008).
- Tkeshelashvili, L. K., McBride, T., Spence, K. & Loeb, L. A. Mutation spectrum of copper-induced DNA damage. *J Biol Chem* **266**, 6401–6406 (1991).

30. Warnes, S. L., Caves, V. & Keevil, C. W. Mechanism of copper surface toxicity in *Escherichia coli* O157:H7 and *Salmonella* involves immediate membrane depolarization followed by slower rate of DNA destruction which differs from that observed for Gram-positive bacteria. *Environ Microbiol* **14**, 1730–1743 (2012).
31. Warnes, S. L. & Keevil, C. W. Lack of Involvement of Fenton Chemistry in Death of Methicillin-Resistant and Methicillin-Sensitive Strains of *Staphylococcus aureus* and Destruction of Their Genomes on Wet or Dry Copper Alloy Surfaces. *Appl Environ Microbiol* **82**, 2132–2136 (2016).
32. Visnapuu, M. *et al.* Dissolution of Silver Nanowires and Nanospheres Dictates Their Toxicity to *Escherichia coli*. *Biomed Res Int*. **2013**, 9 (2013).
33. Mortimer, M., Kasemets, K., Heinlaan, M., Kurvet, I. & Kahru, A. High throughput kinetic *Vibrio fischeri* bioluminescence inhibition assay for study of toxic effects of nanoparticles. *Toxicol in Vitro* **22**, 1412–1417 (2008).
34. Tauriainen, S., Karp, M., Chang, W. & Virta, M. Luminescent bacterial sensor for cadmium and lead. *Biosens Bioelectron* **13**, 931–938 (1998).
35. Leedjärv, A., Ivask, A. & Virta, M. Interplay of Different Transporters in the Mediation of Divalent Heavy Metal Resistance in *Pseudomonas putida* KT2440. *J Bacteriol* **190**, 2680–2689 (2008).

Acknowledgements

We are thankful to EU COST Action CA15114, Estonian Research Council grants IUT 23-5 and PUT748, European Regional Development Fund project TK134 and 2014-2020.4.01.16-0041 for financial support.

Author Contributions

M.R. participated in planning, performed experimental work and participated in writing, H.V. participated in experimental work and writing of the manuscript, A.K. was involved in planning and writing of the manuscript, W.K. was active in initiating and planning as well as in writing, A.I. was active in planning, performed experimental work and participated in writing.

Additional Information

Supplementary information accompanies this paper at <https://doi.org/10.1038/s41598-018-26391-8>.

Competing Interests: The authors declare no competing interests.

Publisher's note: Springer Nature remains neutral with regard to jurisdictional claims in published maps and institutional affiliations.



Open Access This article is licensed under a Creative Commons Attribution 4.0 International License, which permits use, sharing, adaptation, distribution and reproduction in any medium or format, as long as you give appropriate credit to the original author(s) and the source, provide a link to the Creative Commons license, and indicate if changes were made. The images or other third party material in this article are included in the article's Creative Commons license, unless indicated otherwise in a credit line to the material. If material is not included in the article's Creative Commons license and your intended use is not permitted by statutory regulation or exceeds the permitted use, you will need to obtain permission directly from the copyright holder. To view a copy of this license, visit <http://creativecommons.org/licenses/by/4.0/>.

© The Author(s) 2018

Supplementary Material for

Rapid *in situ* assessment of Cu-ion mediated effects and antibacterial efficacy of copper surfaces

Merilin Rosenberg^{1,2}, Heiki Vija¹, Anne Kahru^{1,3}, C. William Keevil^{4*}, Angela Ivask^{1*}

¹ Laboratory of Environmental Toxicology, National Institute of Chemical Physics and Biophysics, Tallinn, Estonia

² Department of Natural Sciences, Tallinn University of Technology, Tallinn, Estonia

³ Estonian Academy of Sciences, Kohtu 6, Tallinn, Estonia

⁴ Faculty of Natural and Environmental Sciences, Centre for Biological Sciences, University of Southampton, Southampton, UK

* Corresponding authors: C.W.Keevil@soton.ac.uk, angela.ivask@kbfi.ee

Table S1. Composition of bacterial test media

Test medium		Composition	pH	Characteristics	Reference
LB	Luria-Bertani	<i>per L:</i> 10g tryptone 5 g yeast extract 5 g NaCl	7.2	Traditional bacterial growth medium	Sigma-Aldrich
TSB	Tryptic Soy Broth	<i>per L:</i> 17 g casein peptone 3 g soy peptone 5 g NaCl 2.5 g K ₂ HPO ₄ 2.5 g glucose	7.3	Suggested medium in US EPA standards ^{1, 2}	Sigma-Aldrich
HMM (0.5% AA)	Heavy Metal MOPS Medium, supplemented with 0.5% aminoacids	<i>per L:</i> 0.63 g MOPS 0.28 g KCl 0.04 g NH ₄ Cl 0.009 g MgSO ₄ 0.4 g glucose 0.002 g glycerol-2-phosphate 0.005 mg FeCl ₃ 5 g casein aminoacids	7.2	Used for metal testing in earlier studies ³⁻⁵	LaRossa <i>et al.</i> ⁶
HMM (0.01% AA)	Heavy Metal MOPS Medium, supplemented with 0.5% aminoacids	<i>per L:</i> 0.63 g MOPS 0.28 g KCl 0.04 g NH ₄ Cl 0.009 g MgSO ₄ 0.4 g glucose 0.002 g glycerol-2-phosphate 0.005 mg FeCl ₃ 0.1 g casein aminoacids	7.2	Used for metal testing in earlier studies ³⁻⁵	LaRossa <i>et al.</i> ⁶
NB	Nutrient Broth	<i>per L:</i> 10 g peptone 3 g meat extract 5 g NaCl	6.8-7.2	500-fold dilution in water suggested as an exposure medium in ISO 22196 ⁷	ISO 22196:2011 ⁷



Figure S1. Set-up of 12-well microplate for optimal signal collection from bioluminescent bacteria on 1×1 cm copper surfaces. Photograph of a 12-well microplate in which the left column represents copper coupons on the plate bottom; left and right middle columns show coupons raised using 5 and 12 mm adapters, respectively; and the right column shows adapters raised using 15 mm plastic adapters; 75 μ L bacterial suspension was applied to each copper coupon.

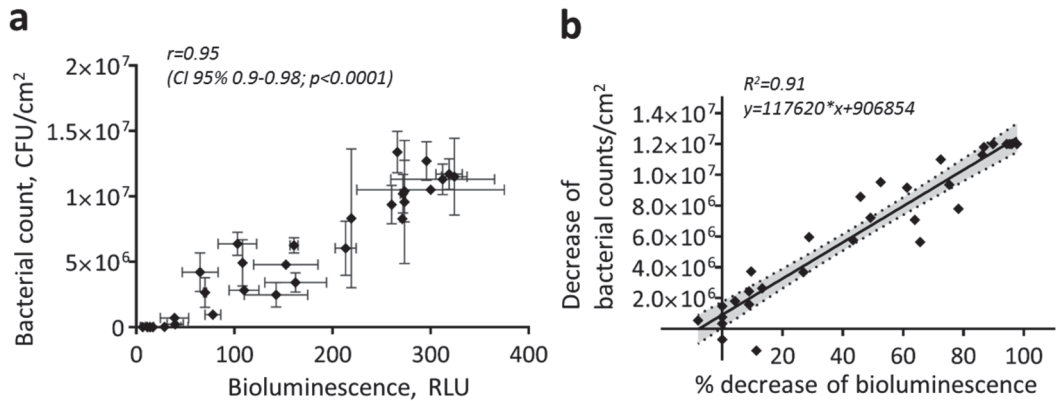


Figure S2. Correlation between bioluminescence and viable counts of the constitutively bioluminescent *E. coli* strain on solid surfaces. Correlation between bioluminescence and viable count of *E. coli* (pDNlux) that was exposed to CuSO₄ solutions (100-1000 µg Cu²⁺/mL) of different toxicities on PE control surfaces for 30-60 min. (a) linear correlation between bioluminescence and colony counting method; every data point is a mean of two parallel experiments with standard deviation. (b) decrease of bacterial counts at different levels of bioluminescence inhibition; coefficient of determination, equation for linear regression and 95% confidence intervals (grey area) are shown. The linear regression equation enables calculation of the amount of colony forming units that are affected when certain decrease in bioluminescence is measured.

References

1. US Environmental Protection Agency. Test Method for the Continuous Reduction of Bacterial Contamination on Copper Alloy Surfaces. (2009)
2. US Environmental Protection Agency. Test Method for Efficacy of Copper Alloy Surfaces as a Sanitizer. (2009)
3. Ivask, A., Rõlova, T. & Kahru, A. A suite of recombinant luminescent bacterial strains for the quantification of bioavailable heavy metals and toxicity testing. *BMC Biotechnol* **9**, 41 (2009)
4. Käkinen, A., Bondarenko, O., Ivask, A. & Kahru, A. The Effect of Composition of Different Ecotoxicological Test Media on Free and Bioavailable Copper from CuSO₄ and CuO Nanoparticles: Comparative Evidence from a Cu-Selective Electrode and a Cu-Biosensor. *Sensors* **11**, 10502 (2011)
5. Leedjärv, A., Ivask, A. & Virta, M. Interplay of Different Transporters in the Mediation of Divalent Heavy Metal Resistance in *Pseudomonas putida* KT2440. *J Bacteriol* **190**, 2680-2689 (2008)
6. LaRossa, R. A., Smulski, D. R. & Van Dyk, T. K. Interaction of lead nitrate and cadmium chloride with *Escherichia coli* K-12 and *Salmonella typhimurium* global regulatory mutants. *J Ind Microbiol* **14**, 252-258 (1995)
7. International Organization for Standardization. ISO 22196:2011. Measurement of antibacterial activity on plastics and other non-porous surfaces. (2011)

Publication II

Rosenberg, M.; Azevedo, N.F.; Ivask, A. (2019). Propidium iodide staining underestimates viability of adherent bacterial cells. *Scientific Reports*, 9(1). DOI: 1038/s41598-019-42906-3.

© The Author(s) 2019. This article is licensed under a Creative Commons Attribution 4.0 International License, which permits use, sharing, adaptation, distribution and reproduction in any medium or format, as long as you give appropriate credit to the original author(s) and the source, provide a link to the Creative Commons license, and indicate if changes were made. The images or other third party material in this article are included in the article's Creative Commons license, unless indicated otherwise in a credit line to the material. <https://creativecommons.org/licenses/by/4.0/>

SCIENTIFIC REPORTS

OPEN

Propidium iodide staining underestimates viability of adherent bacterial cells

Merilin Rosenberg^{1,2}, Nuno F. Azevedo³ & Angela Ivask¹

Combining membrane impermeable DNA-binding stain propidium iodide (PI) with membrane-permeable DNA-binding counterstains is a widely used approach for bacterial viability staining. In this paper we show that PI staining of adherent cells in biofilms may significantly underestimate bacterial viability due to the presence of extracellular nucleic acids (eNA). We demonstrate that gram-positive *Staphylococcus epidermidis* and gram-negative *Escherichia coli* 24-hour initial biofilms on glass consist of 76 and 96% PI-positive red cells *in situ*, respectively, even though 68% the cells of either species in these aggregates are metabolically active. Furthermore, 82% of *E. coli* and 89% *S. epidermidis* are cultivable after harvesting. Confocal laser scanning microscopy (CLSM) revealed that this false dead layer of red cells is due to a subpopulation of double-stained cells that have green interiors under red coating layer which hints at eNA being stained outside intact membranes. Therefore, viability staining results of adherent cells should always be validated by an alternative method for estimating viability, preferably by cultivation.

Propidium iodide (PI) is widely used for bacterial viability staining, especially since Boulos *et al.* (1999) published the method¹. PI can only cross compromised bacterial membranes and is therefore considered to be an indicator of membrane integrity. It stains DNA and RNA inside of dead cells or the ones with reversibly damaged membranes. For viability staining PI is usually coupled with a universal stain that crosses intact membranes and stains nucleic acids (NA) of all cells, thereby enabling to obtain total cell counts. One of the most common examples of such co-stain is SYTO 9. During co-staining with PI and SYTO 9, SYTO 9 can enter all cells regardless of their membrane integrity, bind to DNA and RNA and emit green fluorescence while PI can only enter cells with compromised membranes, bind to DNA and RNA and emit a red fluorescent signal. With higher affinity to bind DNA and in sufficient excess to SYTO 9, PI replaces SYTO 9, when both stains are exposed to the same DNA resulting in red fluorescent signal. As a result of coupling of those two DNA-binding and membrane permeability dependent stains red signals from cells are considered as “dead” and green signals as “alive”^{2–3}. Although this principle is widely applied and proven to work well for an array of planktonic cultures, it has its limitations i.e. unequal SYTO 9 staining of viable and dead cells, incomplete replacement of SYTO 9 by PI or energy transfer during co-staining^{2,4}. It has also been demonstrated that PI might in some cases provide false dead signals that could be associated with high membrane potential⁵, and that the staining result might be dependent on physiological processes other than membrane damage⁶. PI-based viability staining results do not always correlate with cultivability also due to the viable but not cultivable (VBNC) state of bacterial cells⁷ or cell clumping⁸. Despite its above-mentioned draw-backs, PI and SYTO 9 co-staining is also a widely used and suggested method in biofilm research^{8–17}.

Another factor to consider when staining cells with NA-binding fluorophores is that NAs are not always only localized inside bacterial cells and surrounded by a membrane. For example, extracellular DNA (eDNA) can be present in planktonic cultures in specific growth phases¹⁸. During biofilm formation, eDNA mediates bacterial attachment to surfaces¹⁹, and it also plays a major role in mature biofilms. The importance of eDNA in biofilm formation has been proven by the fact that DNase I inhibits biofilm formation or detaches existing biofilm of

¹Laboratory of Environmental Toxicology, National Institute of Chemical Physics and Biophysics, Akadeemia tee 23, 12618, Tallinn, Estonia. ²Department of Chemistry and Biotechnology, Tallinn University of Technology, Akadeemia tee 15, 12618, Tallinn, Estonia. ³LEPABE - Laboratory for Process Engineering, Environment, Biotechnology and Energy; Department of Chemical Engineering; Faculty of Engineering, University of Porto, Rua Dr. Roberto Frias, 4200-465, Porto, Portugal. Correspondence and requests for materials should be addressed to M.R. (email: rosenbergmerilin@gmail.com)

several gram-positive and gram-negative bacterial species²⁰. For the same reason, DNase is also proposed to be used as an anti-biofilm agent^{21,22}. The presence of DNA from non-viable sources (eDNA and DNA from dead cells) has also introduced the need to use ethidium monoazide (EMA), propidium monoazide (PMA) or endonuclease (DNase I) treatment prior to viability assessment by quantitative polymerase chain reaction (qPCR)^{23–25}. All the above-mentioned treatment agents, EMA, PMA as well as DNase I are intact membrane impermeable DNA-targeting compounds spatially targeting the same DNA as PI, depending on membrane integrity.

To get an overview whether the presence of eDNA in biofilms has been considered as a factor that may interfere with PI-based fluorescent staining, we performed a search in Scopus database for “biofilm” and “propidium iodide” and received 683 results while adding “extracellular DNA” or “eDNA” to the search decreased the number of results to 43 indicating that while PI is used for staining biofilms, possible presence of eDNA is generally not taken into account in this context. In the literature we can find that PI is also used for staining of eDNA^{26,27}, but no clear quantitative proof about PI not being suitable for biofilm viability staining because of the presence of NA in biofilm extracellular matrix (ECM). More surprisingly, viability staining based on intact membrane impermeable DNA-binding stains like PI are occasionally used even while specifically studying eDNA²⁸. Nonetheless, from some of the articles, hints of such threat can be found. For example, Gião and Keevil observed that some of *Listeria monocytogenes* biofilms in tap water and most of the old biofilms grown in rich media stained red with PI and SYTO 9 co-staining, but were cultivable and suspected red staining not to be indicative of dead cells but to be caused by eDNA²⁹. From these sources it could be suspected that PI-based viability staining of biofilms, although commonly used, could be critically affected by eDNA and cause underestimation of biofilm viability. To address this possibility, we performed quantitative viability assessment of adherent cells using various staining and culture-based methods.

Results

A combination of epifluorescence microscopy (EM), flow cytometry (FCM) and confocal laser scanning microscopy (CLSM) performed on propidium iodide (PI) and SYTO 9 stained adherent and harvested bacterial cells in parallel with culture-based methods was used to reveal whether staining of adherent bacteria with PI may underestimate their viability. Initial (24 h) biofilms of gram-negative *E. coli* K-12 wild-type substrain MG1655 and a gram-positive *S. epidermidis* type strain DSM-20044 were used for the experiments. *E. coli* MG1655 is widely used in molecular biology and capable of forming biofilm under both aerobic and anaerobic conditions^{30–34}. *S. epidermidis* strains have well established biofilm forming properties similarly to *Staphylococcus aureus* and have been shown to produce eDNA^{13,35}. The biofilms of these two bacterial strains on glass surfaces were formed in phosphate buffered saline (PBS) to rule out potential effect of osmotic stress on bacterial membranes and possibly consequently on viability staining outcome.

Viability staining *in situ*. As can be seen on representative images (Fig. 1) and from quantitative data (Fig. 2), after PI + SYTO 9 co-staining, most adherent cells ($96.35 \pm 5.30\%$ of *E. coli* and $75.69 \pm 18.44\%$ of *S. epidermidis* cells) in 24 h biofilm in PBS stained red with PI *in situ* (Figs 1a,b and 2a,b) while most (about 99%) planktonic cells from suspension above the respective biofilms stained green with SYTO 9 on a filter (Supplementary Fig. 1). This could normally be interpreted as simply showing the differences in the physiology of adherent and planktonic cells and different proportion of dead and alive cells indicating better viability of planktonic cells. However, decreased viability of adherent cells was not an expected result. Adherent cells presented biofilm-specific aggregation into microcolonies which is characteristic of viable initial biofilms. No toxic agent was used, and samples were rinsed before staining to ensure removal of loose dead planktonic cells. Also, the proportion of red-stained cells in the initial biofilms was surprisingly high. For example, using the same staining method, Wang *et al.* noted only a few dead cells among viable cells on a 24 h *E. coli* biofilm on silicone in PBS³⁶. Starved biofilms incubated in PBS are more commonly used in oral health studies where most of the cells in biofilm tend to stain green similar to Zhu *et al.* reporting 76.7% viability of 24 h *Streptococcus mutans* biofilm on glass in phosphate buffer⁹. To exclude single stain effects, viable and ethanol-fixed biofilms were stained with PI, SYTO 9 and PI + SYTO 9 (Supplementary Figs 2 and 3). Single staining resulted in only red signals for PI and green signals for SYTO 9. Fixed samples stained with PI or PI + SYTO 9 showed only red cells. However, it could be observed that while single-stained fixed samples comprised of cells with similar PI or SYTO 9 intensity, variable signal intensities were observed for viable biofilms. Different binding affinity of SYTO 9 to viable and dead gram-negative bacteria is a known limitation of the method⁴. With adherent cells, we observed the same phenomenon also for gram-positive *S. epidermidis*.

As PI uptake by viable planktonic bacteria with increased membrane potential has been suggested by Kirchhoff and Cypionka⁵ and biofilms have been shown to demonstrate membrane potential fluctuations³⁷ a control experiment deploying 3,3'-diethylloxycarbocyanine iodide (DiOC₂(3)) and membrane potential eliminating carbonyl cyanide m-chlorophenylhydrazone (CCCP) pre-treatment was executed. No increased membrane potential signals described by Kirchhoff and Cypionka were observed for *in situ* DiOC₂(3) staining and CCCP pre-treatment did not affect overall PI + SYTO 9 double-staining pattern of the biofilms (Supplementary Fig. 4), excluding the possibility of PI signals being caused by increased membrane potential.

To reveal the metabolic activity of *E. coli* and *S. epidermidis* in biofilms, we also stained the adherent cells with fluorescein diacetate (FDA), not a DNA-binding, but enzymatic activity indicative stain that emits green fluorescence after intracellular enzymatic cleavage³⁸. It was observed that 67.91% *E. coli* and 68.30% *S. epidermidis* cells were metabolically active compared to *in situ* PI + SYTO 9 total counts (Figs 1c,d, 2a,b). Comparison of the results from staining the cells with FDA and PI + SYTO 9 showed that for both species of bacteria, there is a statistically significant difference in FDA and SYTO 9 signal counts (Fig. 2a,b) but there is no significant difference between FDA and PI or total (PI + SYTO 9) signal counts. On the assumption that dead cells are not metabolically active, and starvation may even cause underestimation of viable cell count based on FDA staining, this result

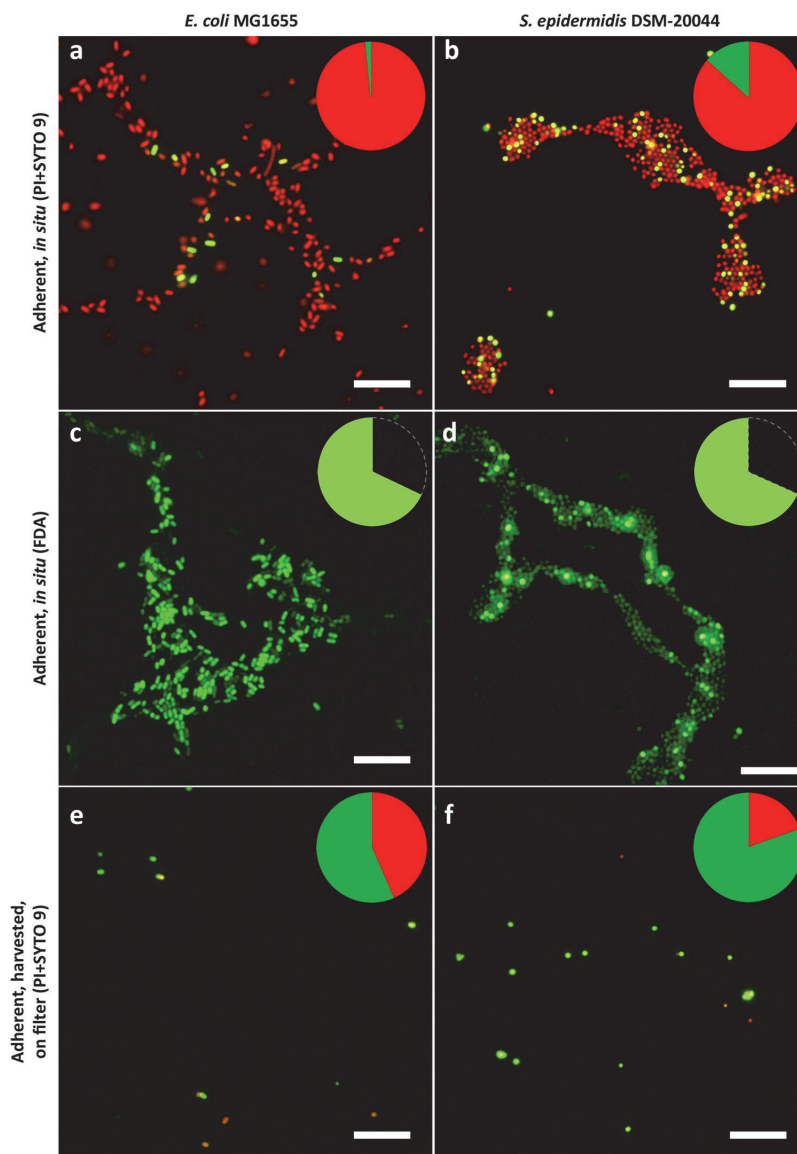


Figure 1. Epifluorescence microscopy images of adherent *E. coli* (a,c,e) and *S. epidermidis* (b,d,f) viability staining. 24 h initial monolayer biofilm formed on glass in PBS stained *in situ* with propidium iodide (PI) and SYTO 9 (a,b), with fluorescein diacetate (FDA) (c,d) or harvested via sonication, stained with PI and SYTO 9 and collected on filter (e,f). Pie diagrams represent total cell count on surfaces with PI, SYTO 9 and FDA stained signal proportions marked in red, dark green and light green respectively. Scale bars correspond to 10 μ m.

sharply contradicts PI + SYTO 9 viability staining results. From these results demonstrating that most of the cells on glass surfaces are metabolically active and stain with PI while a minority of presumably viable cells stain with SYTO 9 only it can be concluded that SYTO 9 signal count significantly underestimates viability and PI signal count significantly overestimates dead cell count as a result of PI + SYTO 9 co-staining *in situ*. Counting possible weak background FDA signals from dead cells was ruled out as FDA-staining of ethanol-fixed biofilms did not produce observable signals (Supplementary Fig. 5). However, neither membrane integrity nor enzymatic activity, especially when incubated in a nutrient-poor environment, can truly indicate the reproduction capability of the cells. This can only be measured by cultivation-based methods.

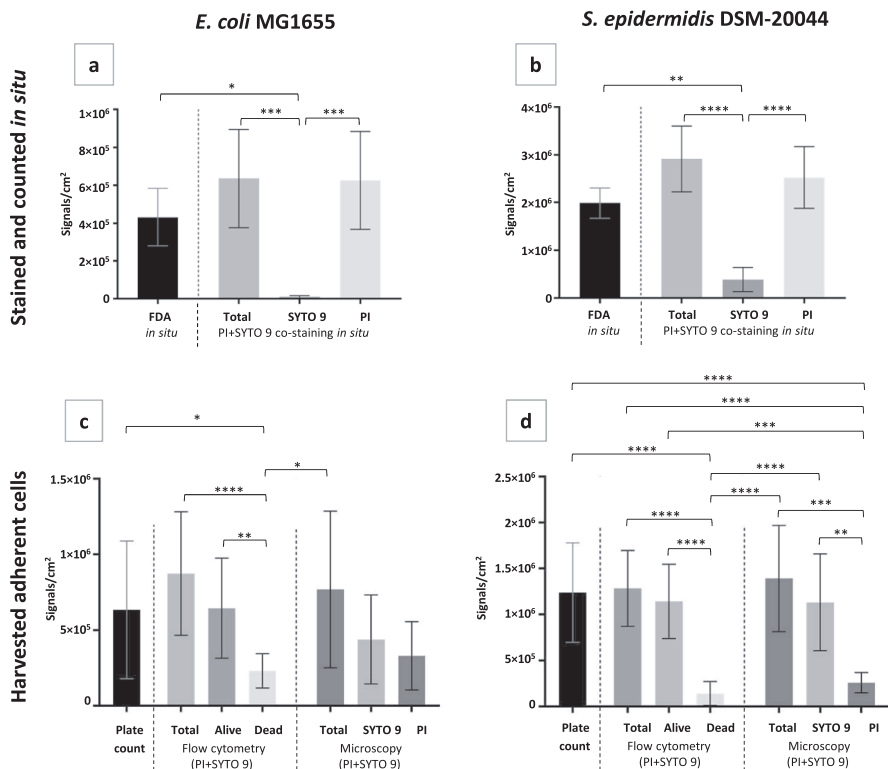


Figure 2. Comparison of multiple approaches to evaluate adherent cell viability in *E. coli* (a,c) and *S. epidermidis* (b,d) biofilms on surface *in situ* (a,b) or after harvesting via ultrasonication (c,d). 24 h initial monolayer biofilm formed on glass in PBS stained *in situ* (a,b) with propidium iodide (PI) and SYTO 9 or FDA followed by epifluorescence microscopy (EM) and signal counting or harvested (c,d) and cultivated for plate counts, co-stained with PI and SYTO 9 and analyzed by flow cytometry (FCM) or collected on filter followed by EM and signal counting. Cell counting results are presented as signals/cm² where one signal counted corresponds to a single fluorescent cell or compact diplococcus (microscopy), a CFU (cultured plate count) or an FCM event. Live/dead gating of FCM signal populations was based on known proportions of viable and ethanol-killed planktonic bacteria. Mean and standard deviation of 4–6 independent values for *in situ* staining and filtering and 10–16 independent values for plate counts and FCM are shown and only statistically significant differences ($p < 0.05$) marked on graphs (“ $>$ ” > 0.05 ; * < 0.05 ; ** < 0.01 ; *** < 0.001 ; **** < 0.0001).

Viability staining and cultivability of harvested cells. Adherent bacteria were harvested from the surfaces via ultrasonication optimized to acquire the maximum number of viable cells (Supplementary Fig. 6) and plated or stained with PI and SYTO 9 and analyzed by flow cytometry (FCM) or collected on filter followed by epifluorescence microscopy (Figs 1e,f, 2c,d). Of the $96.35 \pm 5.30\%$ *in situ* PI-positive *E. coli* cells, only $43.50 \pm 5.30\%$ were PI-positive after harvesting, subsequent staining and collection on filter, and only $27.76 \pm 9.61\%$ of those cells could be assigned to the “dead” gate in FCM, based on ethanol-killed planktonic cells. Similarly, of the $75.69 \pm 18.44\%$ *in situ* PI-positive *S. epidermidis* cells, only $19.56 \pm 8.93\%$ were PI-positive after harvesting, staining and collection on filter, and only 11.07 ± 10.70 those cells could be assigned to the “dead” gate in FCM. This result showing increased fraction of SYTO 9 stained cells after harvesting of adherent cells via ultrasonication compared with adherent cells *in situ* (Fig. 1a vs 1e; 1b vs 1f) was rather surprising. One would expect that ultrasonication does not increase but rather decreases cellular viability due to physical damage as longer ultrasonication durations resulted in decreased planktonic cell viability as well as decreased viable yield of adherent cells (Supplementary Fig. 6). However, due to the seemingly reversed red to green ratio after ultrasonication we hypothesized that this treatment affects the staining of viable cells with PI. One of the possible explanations for that was partial removal of eNA containing ECM from adherent cells. Indeed, ultrasonication is a technique that is commonly used for ECM extraction^{39,40}. Removal of eNA and false dead signals along with ECM was further confirmed by cultivating the harvested bacteria. Following the PI + SYTO 9 staining principle, plate counts could be expected to be smaller than the number of SYTO 9 signals from *in situ* staining due to possible cell aggregates forming only one colony but yielding several signals counted. On the contrary, compared to total signal counts

Species	<i>In situ</i> PI + SYTO 9	<i>In situ</i> FDA vs PI + SYTO 9 total count	Harvested, PI + SYTO 9, on filter	Harvested, PI + SYTO 9, flow cytometry	Harvested, plate count vs PI + SYTO 9 total count on filter
<i>E. coli</i>	3.65 ± 5.30	67.91	56.50 ± 5.30	77.20 ± 9.60	82.43
<i>S. epidermidis</i>	24.31 ± 18.44	68.30	80.44 ± 8.93	88.90 ± 10.70	89.02

Table 1. Viability estimates (%)* of 24 h biofilms acquired with different methods. *Mean and standard deviation of 4–6 independent values for *in situ* staining and filtering and 10–16 independent values for plate counts and FCM are shown. Percentages calculated as ratios of mean values are presented without standard deviations.

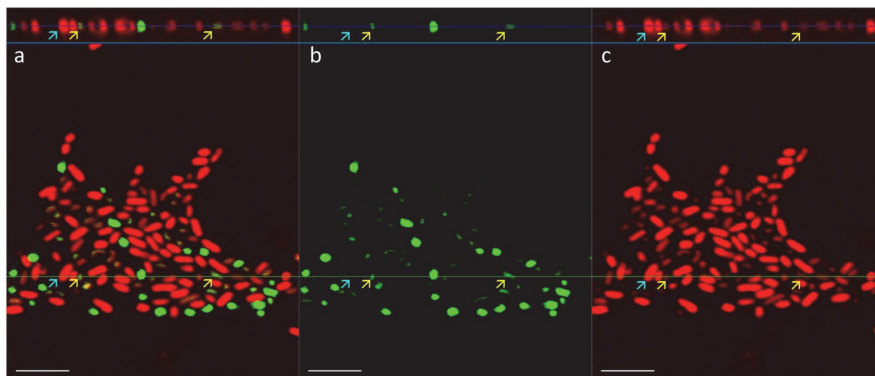


Figure 3. Confocal laser scanning microscopy (CLSM) images of 24 h *E. coli* biofilm co-stained with propidium iodide (PI) and SYTO 9: vertical and horizontal cross-sections in multichannel (a), green channel (b) and red channel (c) view. Dead cells stained with PI are indicated with cyan and viable cells double-stained with PI and SYTO 9 with yellow arrows. Scale bars correspond to 5 μm. Single images of the Z-stack are available in Supplementary Album 1.

from harvested and PI + SYTO 9 stained samples at least 82.43% of *E. coli* and 89.02% of *S. epidermidis* cells were cultivable and formed colonies on nutrient agar.

There was no statistically significant difference in plate counts of biofilm harvested cells, FCM total event counts FCM “alive” event counts, and SYTO 9 counts of harvested, PI + SYTO 9 stained and filtered samples for neither species, indicating that the majority of the harvested cells are truly viable (Figs 2c,d) and the fact that they stained red with PI in *in situ* biofilms was indeed an artifact, most likely due to the presence of eNA in the biofilm matrix.

Of the approaches used for harvested cell viability assessment, FCM proved to be a quicker and less elaborate method than filtering stained samples and counting fluorescent signals from microscopy images but gating harvested sample signals in FCM proved to be problematic. FCM alive and dead gates were based on viable and ethanol-killed planktonic cultures but unlike planktonic samples from the same test system, ultrasonicated biofilm samples had much higher noise level and less defined and/or shifted “alive” signal populations (Supplementary Fig. 7) easily explained by partial ECM removal during harvesting and resulting double-staining of viable bacteria to various degrees in contrast to more strictly PI-defined “dead gate”.

The fact that viability estimate based on *in situ* PI-staining was significantly lower than the ones based on *in situ* FDA staining or harvested cell plate count (Table 1) suggested that eNAs could indeed play a major role in false “dead” PI-staining of biofilm bacteria *in situ*. To further confirm the hypothesis, confocal microscopy was used to better visualize the PI and SYTO 9 co-stained bacterial biofilms.

Confocal laser scanning microscopy (CLSM) of PI + SYTO 9 stained biofilms. CLSM cross-sections of monolayer biofilms revealed overlapping PI and SYTO 9 signals of *E. coli* (Fig. 3) and *S. epidermidis* (Fig. 4) creating a wider diffuse red PI corona around SYTO 9 signals except for the most intensely red cells that lacked green signal and could presumably be true dead signals. It must be noted that the result was seriously affected by vertical resolution limit of CLSM due to bacterial cell size, especially for *E. coli*. However, it was still possible to bring light to the fact that a large proportion of the cells of both species demonstrated double-staining with green interiors under red PI-stained exteriors. This double-staining was only characteristic of viable biofilms and also not a single stain effect, as co-stained ethanol-fixed biofilms lacked green signals with the same CLSM setup and biofilms monostained with PI or SYTO 9 only produced signal in their respective emission channels (Supplementary Figs 8 and 9). Full width at half maximum (FWHM) measurements of CLSM cross-sections of non-saturated cellular signals confirm that red signals from double-stained cells of both species are significantly wider than green signals (Supplementary Fig. 10).

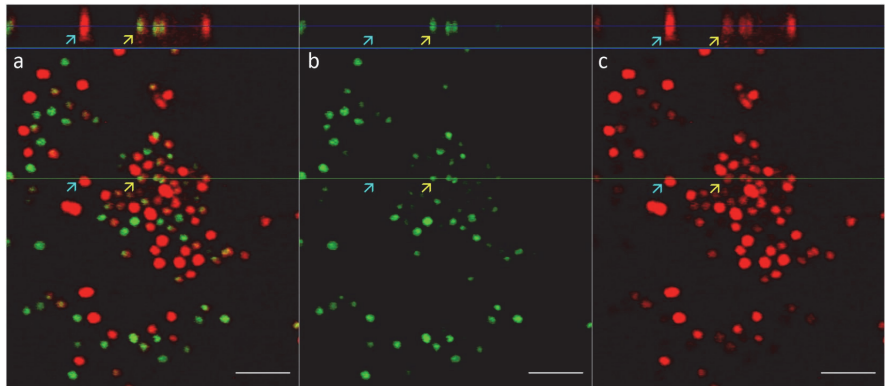


Figure 4. Confocal laser scanning microscopy (CLSM) images of 24 h *S. epidermidis* biofilm co-stained with propidium iodide (PI) and SYTO 9: vertical and horizontal cross-sections in multichannel (a), green channel (b) and red channel (c) view. Dead cells stained with PI are indicated with cyan and viable cells double-stained with PI and SYTO 9 with yellow arrows. Scale bars correspond to 5 μm . Single images of the Z-stack are available in Supplementary Album 1.

As suspected from the comparison of staining of cells with PI + SYTO 9 *in situ* and after ultrasonication, CLSM confirms that PI really does stain cells externally and is therefore not indicative of viability but produces false dead signals under these experimental conditions. Unfortunately, the CLSM resolution limit does not allow to confirm PI exclusion from cell interiors. To compare the staining pattern of PI + SYTO 9 to SYTO 9 co-staining with membrane or membrane-associated ECM components, we combined SYTO 9 with CellMask Orange (CMO), Nile red (NR) and Congo red (CR). NR + SYTO 9 staining resulted in the strongest signals of both NR and SYTO 9 (Supplementary Fig. 11) with a similar red corona around green cell interiors apparent in CLSM as was observed for PI + SYTO 9 staining (Fig. 4). CMO staining resulted in weaker signals for *S. epidermidis* (Supplementary Fig. 11) and was not usable for *E. coli* but demonstrated a similar red corona around green *S. epidermidis* cells as PI + SYTO 9 and NR + SYTO 9. Due to imaging at the CLSM resolution limit, membrane signals (NR, CMO) can also be seen inside the cells similarly to PI signals on Figs 3 and 4. Expected extracellular DNA signal (SYTO 9) outside the membranes similar to extracellular PI signal in case of PI + SYTO 9 co-staining is lost in these images (Supplementary Fig. 11) possibly due to limited dynamic range and loss of weaker signals in single channel SYTO 9 acquisition as opposed to individually adjustable separate channels for intracellular SYTO 9 and extracellular PI signal acquisition (Figs 3 and 4).

CR is an amyloid stain fluorescing red when bound to bacterial surface-associated amyloid fibrils (SAFs)⁴¹. CR signals appeared too weak and quickly bleaching to use in CLSM, but images could be attained in epifluorescence microscopy using long exposures. Interestingly CR + SYTO 9 staining pattern in epifluorescence microscopy (Supplementary Fig. 12) appears similar to that of PI + SYTO 9 (Fig. 1a,b) with some cells lacking red signals and staining green with SYTO 9 while most present red CR signals of variable intensities. It is also evident that SYTO 9 signal is completely masked by more intense CR signals, similarly to PI + SYTO 9 with the significant difference that CR + SYTO 9 eliminates competing for DNA binding.

To further prove the role of eDNA in PI-staining, we also attempted to treat biofilms and similar amount of planktonic cells with DNase I, remove the cells from the surfaces by scraping, concentrate by centrifugation and demonstrate larger amount of DNase degradable DNA signal on adherent cells than on planktonic cells. Unfortunately, the number of adherent cells optimized for *in situ* counting was too low to provide a signal in ethidium bromide agarose gel electrophoresis. Also, ECM removed from scraped cells by suspending them in 1.5 M sodium chloride⁴² did not produce DNA signal on gel likely due to too low amount of DNA. PI + SYTO 9 staining and epifluorescence microscopy of 1.5 M NaCl-treated cells confirmed that most of the cells indeed stained green suggesting successful removal of ECM, including eDNA, from the cells. It was also empirically observed that physical manipulations of adherent cells from scraping to centrifugation, vortexing and ultrasonication all shifted the red to green staining ratio to more green, indicating (partial) ECM removal in various steps of the process which makes cell number normalization between planktonic and low numbers of adherent cells prior to analysis difficult to achieve without losing significant amounts of eDNA.

Discussion

The need to study possible false dead results of PI-based viability staining arose from our previous experiments carried out with bacterial biofilms in water and PBS, where we have similarly to this study, observed a large fraction of red PI-stained cells in biofilms on untreated glass but significantly smaller fraction of red-stained cells on glass surfaces with antibacterial treatment, although total cell counts on treated surfaces tended to be much lower than on untreated controls (unpublished data; Supplementary Fig. 13; surfaces described in⁴³). Yet the morphology of biofilms on untreated glass appeared normal while on antibacterial glass surfaces the biofilm structure as

well as *S. epidermidis* characteristic diplococcal aggregation was disturbed. This result suggested almost reverse staining of alive and dead bacterial cells with PI and SYTO 9 in biofilms. In this study we show that in similar conditions on untreated glass membrane integrity based viability staining with NA-binding PI can and will significantly overestimate the dead cell count in 24 h gram-positive and gram-negative monospecies biofilms in PBS. $96.35 \pm 5.30\%$ of *E. coli* and $75.69 \pm 18.44\%$ of *S. epidermidis* cells stained red and according to general viability staining principles could be considered “dead” when co-staining with PI and SYTO 9 *in situ* compared to 67.91% *E. coli* and 68.30% *S. epidermidis* staining FDA-positive – metabolically active *in situ*, and at least 82.43% of *E. coli* and 89.02% of *S. epidermidis* cells being cultivable after harvesting from biofilms via ultrasonication. It was also evident that the red (PI) to green (SYTO 9) signal ratio was reversed after ultrasonication which indicates PI signal localization in the ECM and (partial) ECM removal during physical manipulation of the cells. To our knowledge, non-specific fluorescence of PI in biofilm ECM has not been described as a factor possibly influencing viability staining results. PI does also bind RNA, not only DNA. However, while the presence of eDNA in ECM is well described, not much is known about extracellular RNA (eRNA) in biofilms. It has been shown that bacteria can secrete RNA in outer membrane vesicles (OMVs). For example, Ghosal *et al.* have demonstrated eRNA outside planktonic *E. coli* MG1655⁴⁴, the very same strain that was used in our experiments. Whether eRNA has a role in biofilm formation is yet scarcely studied, but it cannot be ruled out. For example, eRNA has been demonstrated to be important in *Haemophilus influenzae* *in vitro* biofilm formation⁴⁵.

Compared to harvested cell plate count, FDA staining results *in situ* seem to underestimate viability (Table 1). This could be due to a few reasons. Firstly, the FDA method is challenging to work with due to weak fluorescent signals that require long exposures leading to photobleaching, high background fluorescence and varying signal intensities between individual cells (especially in the case of *S. epidermidis*). Secondly, FDA is indicative of metabolic activity, but biofilms were formed in a very nutrient-poor environment in which metabolic activity is expected to be slowed and as shown by Chavez de Paz *et al.* for oral bacteria, can reversibly affect FDA staining outcome⁴⁶.

Confocal laser scanning microscopy revealed double-stained cells with green fluorescing interiors under red stained exteriors of individual cells and confirmed PI staining not only being indicative of membrane integrity but rather staining of eDNA which is one of the components of bacterial ECM. This double-staining was only characteristic of viable biofilms as ethanol-fixed biofilms consistently produced only red signals in both EM (Supplementary Figs 2 and 3) and CLSM (Supplementary Figs 8 and 9). Due to CLSM resolution limit, super-resolution microscopy allowing for nanoscale discrimination between membrane and chromosomal DNA signals⁴⁷ would be needed to confidently confirm PI exclusion from cell interiors.

CLSM results look similar to what has been previously demonstrated, but not quantified in terms of falsely assigned dead signal counts for viability staining. For example, Vilain *et al.* demonstrated similar PI corona around adherent *Bacillus cereus* cells on glass wool⁴⁸, although in their study, the biofilm was formed in rich medium. Gallo *et al.*⁴¹ also noted a similar picture using membrane-anchored surface amyloid fibril (SAF) producing and GFP-expressing *Salmonella typhimurium* biofilm cells surrounded by a “corona” of PI-stained eDNA and SAF complexes concluding that PI stains the cells externally. SAF and eDNA interactions have also been demonstrated for other species. For example, eDNA has been shown to facilitate the polymerization of SAF monomers in *Staphylococcus aureus* biofilms⁴⁹ and *E. coli* SAF monomer has been shown to bind to DNA, promoting SAF assembly⁵⁰. SAF and eDNA have been shown to facilitate bacterial attachment to surfaces and cell-cell aggregation⁵¹. SAF and eDNA interactions in the context of biofilm formation and mechanical resistance need to be studied further to bring light to underlying mechanisms. We also demonstrated that amyloid stain Congo red stained both *E. coli* and *S. epidermidis* (Supplementary Fig. 12). CR combined with SYTO 9 presented similar staining pattern in epifluorescence microscopy as PI + SYTO 9 leading to hypothesis that eDNA-SAF complexes could bind PI, mask intracellular SYTO 9 signals and lead to false dead signals in epifluorescence microscopy. In mammalian amyloid diseases research, it has been observed that amyloids not only bind DNA, but also mediate its configurational changes between B and Z form^{52–54}. If it similarly applies to bacterial amyloids, then that might explain why this caveat in viability staining has not been shown to be a critical problem for older biofilms that quickly become insensitive to DNase during maturation²⁰ and generally stain green with PI + SYTO 9. This could be due to Z-DNA not being efficiently degraded by DNase I⁵⁵ nor detected by ethidium bromide (EB)⁵⁶, latter of which is structurally very similar to PI.

SAF-bound eDNA could also explain why PI stains biofilms on untreated glass and not on nano-ZnO coated surfaces (Supplementary Fig. 13) that release ionic Zn(II). Zn(II) is known to modulate amyloid formation. Exact mechanisms and related interactions are not well known, but Zn(II) has been demonstrated to inhibit fibrillar growth or cause destabilization of amyloid fibrils^{57–61}. If Zn(II) prevents functional SAF formation or disrupts existing amyloids, then it could also prevent SAF-bound eDNA in close proximity to the cells. More specifically, Tougu *et al.*⁵⁷ demonstrated dose-dependent inhibition of amyloid β fibril formation with strong effect at $5\text{--}10\ \mu\text{M}$ Zn(II) in physiological conditions while Zn concentration in our biofilm experiment with nano-ZnO coated surfaces facilitating SYTO9-positive *S. epidermidis* biofilms in PBS reached about $15\ \mu\text{M}$ with potentially higher local concentrations near the treated surface. The mechanisms behind DNA, amyloid and Zn or other metal ion interactions need further investigation and may reveal novel strategies to prevent biofilm formation.

Moreover, the role of eDNA in PI-staining of adherent bacterial cells may not be constant in different biofilms but significantly affected by biofilm growth conditions. In our study we used biofilms grown in nutrient-poor PBS at ambient temperature and no other conditions that could negatively affect adherent cultures were applied. However, in a more usual experimental setup, different treatments causing physical, toxic, starvation *etc.* stress to the biofilms, especially in antimicrobial or anti-biofilm research together with a negative no-stress control are used. In the light of eDNA interfering with viability staining results, these stress factors could not only affect cell viability but also adherence efficiency and with that the amount of ECM and eDNA thereby potentially falsely exaggerating mortality of stress-treated samples compared to no-stress controls. For example, metabolic stress

due to sub-lethal concentrations of antibiotics or other toxic compounds has been shown to enhance biofilm formation and/or result in higher eDNA content of the biofilms^{62–65}. Growth conditions, such as temperature, aerobic and starvation stress were reported to affect surface attachment and eDNA-mediated mechanism of biofilm formation of *Campylobacter jejuni*⁶⁶. DNase-sensitive eDNA dependent biofilm formation of *Streptococcus mutans* was observed in low pH stress and not in neutral pH⁶⁷. Higher eDNA content of biofilms subjected to physico-chemical stress was recently also observed for *S. epidermidis*⁶⁸. Not only severe stress, but also growth media selection can be of importance. Kadam *et al.* observed highest biofilm formation in nutrient-poor mediums and noticed that DNase-sensitive *Listeria monocytogenes* biofilms grown in nutrient broth consisted of clearly higher proportion of PI-positive cells during PI + SYTO 9 co-staining than DNase-insensitive biofilms of the same strains grown in a more nutrient rich brain heart infusion⁶⁹. Also SAF biogenesis, discussed above, is stimulated by temperature below 30 °C and lack of nutrients⁷⁰.

Together, this hints that the external staining phenomenon of PI might not only be dependent on the species used or starvation conditions but is also attachment-specific and dependent on conditions affecting matrix eDNA content, including different stress-responses.

Conclusion

Viability estimation is of critical importance in evaluating antimicrobial/anti-biofilm surfaces and substances efficiency. Although the presence of extracellular nucleic acids in bacterial biofilm matrixes is well established in the literature, PI-based viability staining has remained a widely used tool for *in situ* viability estimate of adherent cells not taking into account possible eDNA interference in the viability staining results. From this study it can be concluded that membrane integrity based viability staining with DNA-binding dyes, including, but presumably not limited by PI, can significantly overestimate dead cell counts in the presence of eNA in biofilms. To overcome this, the possible effect of eNA should be controlled for by either: (1) using culture-based methods as a reference; (2) assess metabolic activity (e.g. staining for enzyme activity, respiration etc.) in parallel to NA-staining and/or (3) minimizing ECM co-harvesting if harvested cell viability is to be assessed by staining. None of the aforementioned approaches are perfect for biofilms, but combination of methods rather than one approach is expected to result in more accurate estimations of viability.

Methods

Preparation of glass surfaces for bacterial attachment. 18 mm × 18 mm soda-lime glass microscopy cover glasses (Corning, 2855-18) were used as biofilm carriers. Before inoculation carriers were rinsed with 70 vol% ethanol in deionized water and dried in biosafety cabinet with ultraviolet light irradiation for at least 20 minutes on both sides.

Bacterial strains and biofilm cultivation. *S. epidermidis* DSM-20044 and *E. coli* MG1655 were grown overnight in Luria-Bertani broth (LB: 10 g/L tryptone, 5 g/L yeast extract in deionized water) at 30 °C. Sterilized 18 × 18 mm glass cover slips were placed into wells of 6-well polycarbonate non-tissue culture coated plates (Corning, 351146). Bacterial cells were washed twice with PBS (180 mM sodium chloride, 3 mM potassium chloride, 9 mM dibasic sodium phosphate, 1.5 mM potassium hydrogen phosphate in deionized water, pH~7) using centrifugation at 7000 g for 10 min. Cell suspensions were immediately diluted to OD₆₀₀ 0.01 in PBS and 5 ml of inoculum was pipetted onto glass surfaces in each well of the 6-well plates. Serial dilutions of remaining inoculum were made and drop-plated on nutrient agar (NA: 5 g/L meat extract, 10 g/L peptone, 5 g/L sodium chloride, 15 g/L agar powder in deionized water) to confirm inoculum cell count. Plates with inoculated surfaces were covered with lids and incubated at room temperature and ambient indoor lighting for 24 h to acquire biofilm density suitable for consecutive counting.

Ethanol-fixation was used to kill and permeate biofilm samples used as controls. 24 h biofilms were dip-rinsed twice in PBS and drained. Biofilms were submerged in 70 vol% ethanol in deionized water, incubated 1 h at room temperature, liquid aspirated, and samples dried in 60 °C incubator for 5 min.

Staining. Staining with PI (81845, Sigma) 20 mM and SYTO 9 (S-34854, Invitrogen™ Thermo Fisher Scientific) 3.34 mM stock solutions in DMSO was carried out according to BacLight™ Bacterial Viability Kit manual. Final concentrations of stains in 1:1 stain mixture in PBS was 30 μM PI and 5 μM SYTO 9. Stain mixture was either added to surfaces with biofilms (15 μl PBS-diluted stain mix pipetted straight onto surfaces and covered by cover slip), to cells harvested from surfaces by ultrasonication or to planktonic bacteria collected from above the bacterial biofilms. The stained samples were incubated for 15 minutes in the dark (foil covered box) at room temperature.

FDA (201642, Sigma) stock solution used was 5 mg/ml in acetone, diluted 200-fold in PBS and kept on ice during the experiment. 15 μl of the stain solution was pipetted directly onto surfaces, covered by coverslip and incubated in the dark for 10 min before microscopy. Longer incubation periods yielded in high background fluorescence and not significantly stronger signals from cells and therefore longer incubation was not used to obtain stronger signals.

Final concentrations for other stains combined with 5 μM SYTO 9: 20 μg/ml Congo red (Merck), 1 μg/ml Nile red (Thermo Fisher Scientific), 5 μg/ml (1 ×) CellMask Orange (Thermo Fisher Scientific). Same staining conditions were applied as for PI + SYTO 9, described above.

For membrane potential evaluation, 15 μl 30 μM 3,3'-diethyloxycarbocyanine iodide (DiOC₂(3); 320684, Sigma) in PBS was used *in situ* followed by 5 min incubation in the dark and epifluorescence microscopy with or without 5 min pre-treatment submerged in 5 μM carbonyl cyanide m-chlorophenylhydrazone (CCCP; C2759, Sigma) in PBS. DiOC₂(3) used by Kirchhoff and Cypionka⁵ was chosen over Thioflavin T used by Humphries *et*

al.³⁷ for membrane potential staining due to Thioflavin T being a widely used amyloid dye and potentially staining also amyloid fibrils⁵⁷ present in biofilm matrix.

Ultrasonication. Branson Digital Sonifier model 450 (max power 400 W) equipped with horn model 101-135-066 R was used to harvest adherent cells from glass surfaces. The protocol was optimized to achieve maximal viable cell yield for ultrasonication of glass surfaces in 50 ml glass beaker filled with 10 ml PBS at 25% sonication amplitude. For optimization, planktonic culture was used in parallel to biofilm and viability of both planktonic and harvested cells was evaluated during up to 30 sec sonication (Supplementary Fig. 6). Optimal time for sonication to achieve maximal viable cell yield was found to be 15 seconds for both bacterial species. Ultrasonicated surfaces were stained with PI and SYTO 9 and microscopied to confirm removal of biofilm. Harvested biofilm samples were either stained as described above and analyzed by flow cytometry or filtered through 0.2 µm pore size filters (Whatman Nuclepore Polycarbonate Black Membrane Filter) prior to microscopy and counting or drop-plated for CFU counts on nutrient agar. For more reproducible result presentation, CFU and cell counts are given per cm².

Microscopy. Epifluorescence microscopy (EM) was carried out using Olympus CX41 microscope equipped with 100x oil immersion objective. Excitation filter cube DMB-2 (exciter filter BP475, dichroic mirror DM500, barrier filter O515IF) was used to filter mercury lamp emission allowing detection of both FDA as well as simultaneous detection of PI and SYTO 9 fluorescent signals with 515 nm longpass filter. Images were captured with Olympus DP71 camera and Cell[^]B software.

Signals were manually counted in ImageJ software using “point” tool thereby acquiring cell counts for *E. coli* and diplococcal counts for *S. epidermidis*. Compact diplococci with one green and one red cell were counted as separate signals. For counting purposes at least 10 images were taken per sample at random locations. “Subtract background” (rolling = 50) function of ImageJ was used on FDA-stained images prior to counting signals with recognizable cell morphology. For more reproducible result presentation, cell/diplococcal counts are given per cm².

Confocal laser scanning microscopy (CLSM) was carried out using Zeiss LSM 510 META equipped with 100x oil immersion objective and acquired images analyzed in Zeiss LSM Image Browser. For acquiring SYTO 9 signals, 488 nm laser and 505–550 nm emission filter was used. For PI, NL and CMO, 561 nm laser in combination with 575 nm longpass emission filter was used. Separate tracks were employed for both excitation/emission paths to avoid signal bleed-through between emission channels. To obtain more precise Z-stack imaging interval, motorized piezo stage was used to image at 0.1 µm interval (PI + SYTO9 samples) or at 0.15 µm (SYTO 9 + NL/CMO). Full Z-stacks for cross-sections on Figs 3 and 4 can be found in Supplementary Album 1.

Full width at half maximum (FWHM) was measured from non-saturated double-stained cells separately from green and red channels from the same line selection in ImageJ using Gaussian fit function.

Flow cytometry. FCM analysis of PI and SYTO 9 co-stained bacteria was carried out using BD Accuri™ C6 device (BD Biosciences). Primary forward scatter (FCS-H) and secondary fluorescence signal (FL1-H) thresholds were used to filter out noise with minimal loss in bacterial cell signals and live-dead gating was done for *E. coli* and *S. epidermidis* using different proportions of viable overnight culture and ethanol-killed overnight culture (1 h incubation in 70% ethanol) confirmed by plate counts. Gating of dead and alive signal populations was executed on SYTO 9 (FL1-A; 533/30 nm)/Propidium iodide (FL3-A; 670 nm LP) scatter plot as illustrated on Supplementary Fig. 7. For more reproducible result presentation, event counts are given per cm².

DNase treatment. 15 surfaces per condition were prepared and rinsed as described and incubated with 500 µl 1x DNase I buffer (10x buffer: 100 mM Tris-HCl (pH 7.5), 25 mM MgCl₂, 1 mM CaCl₂) with or without DNase I (final concentration 100 U/ml, EN0523, Thermo Fisher Scientific). As a planktonic control, 3 ml of *E. coli* and 20 ml of *S. epidermidis* planktonic fraction, with estimated cell count similar to adherent cells on 15 surfaces were pelleted at 7000 g for 10 minutes, supernatant discarded and pellet suspended in DNase buffer with or without DNase I. Both, surfaces with biofilm and tubes with planktonic bacteria were incubated at 37 °C for 4 hours. Adherent cells were harvested by scraping with cell scraper in the same buffer and pelleted by centrifugation at 7000 g for 10 min, suspended in 300 µl 1.5 M NaCl to remove ECM as described in⁴², thoroughly vortexed and pelleted again to remove cells from ECM fraction. 30 µl of ECM fraction in the supernatant was run on agarose gel electrophoresis (0.8% agarose in Tris-acetate-EDTA (TAE) buffer, stained with 0.5 µg/ml ethidium bromide; 60 V, 60 min, visualized on UV-transilluminator). Pelleted cells were resuspended in PI and SYTO 9 co-stain solution in final concentrations as described above and either analyzed by FCM or 5 µl pipetted onto microscopy slide, covered by cover slip, incubated in dark for 15 min and visualized with epifluorescence microscope.

Statistical analysis. Mean values and standard deviations were calculated by Microsoft Excel standard functions. P-values used in Fig. 2 were acquired using analysis of variance (ANOVA) followed by Tukey’s multiple comparisons test at $\alpha = 0.05$ in GraphPadPrism 7.04 where analysis was executed individually for data presented on each graph (Fig. 2a–d). P-values used in Supplementary Fig. 10 were calculated in Microsoft Excel using two-tailed T-test.

Data Availability

The data generated in the current study is available from the corresponding author on reasonable request.

References

- Boulos, L., Prévost, M., Barbeau, B., Coallier, J. & Desjardins, R. LIVE/DEAD[®] BacLight[™]: application of a new rapid staining method for direct enumeration of viable and total bacteria in drinking water. *J. Microbiol. Methods* **37**, 77–86 (1999).
- Stocks, S. M. Mechanism and use of the commercially available viability stain, BacLight. *Cytometry* **61A**, 189–195 (2004).
- User Manual: LIVE/DEAD BacLight Bacterial Viability Kits. (2004).
- Stiefel, P., Schmidt-Emrich, S., Maniura-Weber, K. & Ren, Q. Critical aspects of using bacterial cell viability assays with the fluorophores SYTO9 and propidium iodide. *BMC Microbiol.* **15**, 36 (2015).
- Kirchhoff, C. & Cypionka, H. Propidium ion enters viable cells with high membrane potential during live-dead staining. *J. Microbiol. Methods* **142**, 79–82 (2017).
- Yang, Y., Xiang, Y. & Xu, M. From red to green: the propidium iodide-permeable membrane of *Shewanella decolorationis* S12 is repairable. *Sci. Rep.* **5** (2016).
- Gião, M. S., Wilks, S. A., Azevedo, N. F., Vieira, M. J. & Keevil, C. W. Validation of SYTO 9/Propidium Iodide Uptake for Rapid Detection of Viable but Noncultivable *Legionella pneumophila*. *Microb. Ecol.* **58**, 56–62 (2009).
- Auty, M. A. E. *et al.* Direct *In Situ* Viability Assessment of Bacteria in Probiotic Dairy Products Using Viability Staining in Conjunction with Confocal Scanning Laser Microscopy. *Appl. Environ. Microbiol.* **67**, 420–425 (2001).
- Zhu, M., Takenaka, S., Sato, M. & Hoshino, E. Influence of starvation and biofilm formation on acid resistance of *Streptococcus mutans*. *Oral Microbiol. Immunol.* **16**, 24–27 (2001).
- Guggenheim, B., Giertsen, E., Schüpbach, P. & Shapiro, S. Validation of an *in vitro* Biofilm Model of Supragingival Plaque. *J. Dent. Res.* **80**, 363–370 (2001).
- Azeredo, J. *et al.* Critical review on biofilm methods. *Crit. Rev. Microbiol.* **43**, 313–351 (2017).
- Magana, M. *et al.* Options and Limitations in Clinical Investigation of Bacterial Biofilms. *Clin. Microbiol. Rev.* **31**, e00084–16 (2018).
- Rice, K. C. *et al.* The cida murein hydrolase regulator contributes to DNA release and biofilm development in *Staphylococcus aureus*. *Proc. Natl. Acad. Sci.* **104**, 8113–8118 (2007).
- Haagensen, J. A. J. *et al.* Differentiation and Distribution of Colistin- and Sodium Dodecyl Sulfate-Tolerant Cells in *Pseudomonas aeruginosa* Biofilms. *J. Bacteriol.* **189**, 28–37 (2007).
- Hope, C. K., Clements, D. & Wilson, M. Determining the spatial distribution of viable and nonviable bacteria in hydrated microcosm dental plaques by viability profiling. *J. Appl. Microbiol.* **93**, 448–455 (2002).
- Webb, J. S. *et al.* Cell Death in *Pseudomonas aeruginosa* Biofilm Development. *J. Bacteriol.* **185**, 4585–4592 (2003).
- Guilbaud, M., Piveteau, P., Desvaux, M., Brisse, S. & Briandet, R. Exploring the Diversity of *Listeria monocytogenes* Biofilm Architecture by High-Throughput Confocal Laser Scanning Microscopy and the Predominance of the Honeycomb-Like Morphotype. *Appl. Environ. Microbiol.* **81**, 1813–1819 (2015).
- Shi, L. *et al.* Limits of propidium iodide as a cell viability indicator for environmental bacteria. *Cytometry A* **71A**, 592–598 (2007).
- Whitchurch, C. B. Extracellular DNA Required for Bacterial Biofilm Formation. *Science* **295**, 1487–1487 (2002).
- Okshevsky, M. & Meyer, R. L. The role of extracellular DNA in the establishment, maintenance and perpetuation of bacterial biofilms. *Crit. Rev. Microbiol.* **41**, 341–352 (2015).
- Hymes, S. R., Randis, T. M., Sun, T. Y. & Ratner, A. J. DNase Inhibits *Gardnerella vaginalis* Biofilms *In Vitro* and *In Vivo*. *J. Infect. Dis.* **207**, 1491–1497 (2013).
- Okshevsky, M., Regina, V. R. & Meyer, R. L. Extracellular DNA as a target for biofilm control. *Curr. Opin. Biotechnol.* **33**, 73–80 (2015).
- Álvarez, G., González, M., Isabal, S., Blanc, V. & León, R. Method to quantify live and dead cells in multi-species oral biofilm by real-time PCR with propidium monoazide. *AMB Express* **3**, 1 (2013).
- Nocker, A. & Camper, A. K. Novel approaches toward preferential detection of viable cells using nucleic acid amplification techniques. *FEMS Microbiol. Lett.* **291**, 137–142 (2009).
- Reyneke, B., Ndlovu, T., Khan, S. & Khan, W. Comparison of EMA-, PMA- and DNase qPCR for the determination of microbial cell viability. *Appl. Microbiol. Biotechnol.* **101**, 7371–7383 (2017).
- Okshevsky, M. & Meyer, R. L. Evaluation of fluorescent stains for visualizing extracellular DNA in biofilms. *J. Microbiol. Methods* **105**, 102–104 (2014).
- Allesen-Holm, M. *et al.* A characterization of DNA release in *Pseudomonas aeruginosa* cultures and biofilms. *Mol. Microbiol.* **59**, 1114–1128 (2006).
- Mann, E. E. *et al.* Modulation of eDNA Release and Degradation Affects *Staphylococcus aureus* Biofilm Maturation. *PLoS ONE* **4**, e5822 (2009).
- Gião, M. S. & Keevil, C. W. *Listeria monocytogenes* Can Form Biofilms in Tap Water and Enter Into the Viable but Non-Cultivable State. *Microb. Ecol.* **67**, 603–611 (2014).
- Ito, A., May, T., Kawata, K. & Okabe, S. Significance of *rpoS* during maturation of *Escherichia coli* biofilms. *Biotechnol. Bioeng.* **99**, 1462–1471 (2008).
- Wood, T. K., González Barrios, A. F., Herzberg, M. & Lee, J. Motility influences biofilm architecture in *Escherichia coli*. *Appl. Microbiol. Biotechnol.* **72**, 361–367 (2006).
- Gonzalez Barrios, A. F. *et al.* Autoinducer 2 Controls Biofilm Formation in *Escherichia coli* through a Novel Motility Quorum-Sensing Regulator (MqsR, B3022). *J. Bacteriol.* **188**, 305–316 (2006).
- Bayramoglu, B., Toubiana, D. & Gillor, O. Genome-wide transcription profiling of aerobic and anaerobic *Escherichia coli* biofilm and planktonic cultures. *FEMS Microbiol. Lett.* fnx006, <https://doi.org/10.1093/femsle/fnx006> (2017).
- Lacqua, A., Wanner, O., Colangelo, T., Martinotti, M. G. & Landini, P. Emergence of Biofilm-Forming Subpopulations upon Exposure of *Escherichia coli* to Environmental Bacteriophages. *Appl. Environ. Microbiol.* **72**, 956–959 (2006).
- Qin, Z. *et al.* Role of autolysin-mediated DNA release in biofilm formation of *Staphylococcus epidermidis*. *Microbiology* **153**, 2083–2092 (2007).
- Wang, R. *et al.* Inhibition of *Escherichia coli* and *Proteus mirabilis* adhesion and biofilm formation on medical grade silicone surface. *Biotechnol. Bioeng.* **109**, 336–345 (2012).
- Humphries, J. *et al.* Species-Independent Attraction to Biofilms through Electrical Signaling. *Cell* **168**, 200–209.e12 (2017).
- Lundgren, B. Fluorescein Diacetate as a Stain of Metabolically Active Bacteria in Soil. *Oikos* **36**, 17 (1981).
- Comte, S., Guilbaud, G. & Baudu, M. Relations between extraction protocols for activated sludge extracellular polymeric substances (EPS) and EPS complexation properties. *Enzyme Microb. Technol.* **38**, 237–245 (2006).
- Pan, X. *et al.* A comparison of five extraction methods for extracellular polymeric substances (EPS) from biofilm by using three-dimensional excitation-emission matrix (3DEEM) fluorescence spectroscopy. *Water SA* **36** (2010).
- Gallo, P. M. *et al.* Amyloid-DNA Composites of Bacterial Biofilms Stimulate Autoimmunity. *Immunity* **42**, 1171–1184 (2015).
- Chiba, A., Sugimoto, S., Sato, F., Hori, S. & Mizunoe, Y. A refined technique for extraction of extracellular matrices from bacterial biofilms and its applicability: Extraction of ECM from bacterial biofilms. *Microb. Biotechnol.* **8**, 392–403 (2015).
- Visnapu, M. *et al.* UVA-induced antimicrobial activity of ZnO/Ag nanocomposite covered surfaces. *Colloids Surf. B Biointerfaces* **169**, 222–232 (2018).
- Ghosal, A. *et al.* The extracellular RNA complement of *Escherichia coli*. *MicrobiologyOpen* **4**, 252–266 (2015).
- Domenech, M., Pedrero-Vega, E., Prieto, A. & García, E. Evidence of the presence of nucleic acids and β -glucan in the matrix of non-typeable *Haemophilus influenzae* *in vitro* biofilms. *Sci. Rep.* **6** (2016).

46. Chavez de Paz, L. E., Hamilton, I. R. & Svensater, G. Oral bacteria in biofilms exhibit slow reactivation from nutrient deprivation. *Microbiology* **154**, 1927–1938 (2008).
47. Spahn, C. K. *et al.* A toolbox for multiplexed super-resolution imaging of the *E. coli* nucleoid and membrane using novel PAINT labels. *Sci. Rep.* **8** (2018).
48. Vilain, S., Pretorius, J. M., Theron, J. & Brozel, V. S. DNA as an Adhesin: *Bacillus cereus* Requires Extracellular DNA To Form Biofilms. *Appl. Environ. Microbiol.* **75**, 2861–2868 (2009).
49. Schwartz, K., Ganesan, M., Payne, D. E., Solomon, M. J. & Boles, B. R. Extracellular DNA facilitates the formation of functional amyloids in *Staphylococcus aureus* biofilms: eDNA promotes functional amyloid formation. *Mol. Microbiol.* **99**, 123–134 (2016).
50. Fernández-Tresguerres, M. E., Moreno-Díaz de la Espina, S., Gasset-Rosa, F. & Giraldo, R. A. DNA-promoted amyloid proteinopathy in *Escherichia coli*: Synthetic bacterial amyloidosis. *Mol. Microbiol.* **77**, 1456–1469 (2010).
51. Van Gerven, N., Van der Verren, S. E., Reiter, D. M. & Remaut, H. The Role of Functional Amyloids in Bacterial Virulence. *J. Mol. Biol.* **430**, 3657–3684 (2018).
52. Suram, A., Rao, J. K. S., Latha, K. S. & Viswamitra, M. A. First Evidence to Show the Topological Change of DNA from B-DNA to Z-DNA Conformation in the Hippocampus of Alzheimer's Brain. *NeuroMolecular Med.* **2**, 289–298 (2002).
53. Yu, H., Ren, J. & Qu, X. Time-Dependent DNA Condensation Induced by Amyloid β -Peptide. *Biophys. J.* **92**, 185–191 (2007).
54. Hegde, M. L. *et al.* First Evidence for Helical Transitions in Supercoiled DNA by Amyloid β Peptide (1–42) and Aluminum: A New Insight in Understanding Alzheimer's Disease. *J. Mol. Neurosci.* **22**, 19–32 (2004).
55. Suck, D. & Oefner, C. Structure of DNase I at 2.0 Å resolution suggests a mechanism for binding to and cutting DNA. *Nature* **321**, 620–625 (1986).
56. Walker, G. T., Stone, M. P. & Krugh, T. R. Ethidium binding to left-handed (Z) DNAs results in regions of right-handed DNA at the intercalation site. *Biochemistry* **24**, 7462–7471 (1985).
57. Töugu, V. *et al.* Zn(II)- and Cu(II)-induced non-fibrillar aggregates of amyloid- β (1–42) peptide are transformed to amyloid fibrils, both spontaneously and under the influence of metal chelators. *J. Neurochem.* **110**, 1784–1795 (2009).
58. Sarell, C. J., Wilkinson, S. R. & Viles, J. H. Substoichiometric Levels of Cu²⁺ Ions Accelerate the Kinetics of Fiber Formation and Promote Cell Toxicity of Amyloid- β from Alzheimer Disease. *J. Biol. Chem.* **285**, 41533–41540 (2010).
59. Abelein, A., Gräslund, A. & Danielsson, J. Zinc as chaperone-mimicking agent for retardation of amyloid β peptide fibril formation. *Proc. Natl. Acad. Sci.* **112**, 5407–5412 (2015).
60. Ma, B., Zhang, F., Wang, X. & Zhu, X. Investigating the inhibitory effects of zinc ions on amyloid fibril formation of hen egg-white lysozyme. *Int. J. Biol. Macromol.* **98**, 717–722 (2017).
61. Ban, D. K. & Paul, S. Nano Zinc Oxide Inhibits Fibrillar Growth and Suppresses Cellular Toxicity of Lysozyme Amyloid. *ACS Appl. Mater. Interfaces* **8**, 31587–31601 (2016).
62. Chang, W. *et al.* Methicillin-Resistant *Staphylococcus aureus* Grown on Vancomycin-Supplemented Screening Agar Displays Enhanced Biofilm Formation. *Antimicrob. Agents Chemother.* **59**, 7906–7910 (2015).
63. Marchal, M. *et al.* Subinhibitory Arsenite Concentrations Lead to Population Dispersal in *Thiomonas* sp. *PLoS ONE* **6**, e23181 (2011).
64. Doroshenko, N. *et al.* Extracellular DNA Impedes the Transport of Vancomycin in *Staphylococcus epidermidis* Biofilms Preexposed to Subinhibitory Concentrations of Vancomycin. *Antimicrob. Agents Chemother.* **58**, 7273–7282 (2014).
65. Schilcher, K. *et al.* Modulation of *Staphylococcus aureus* Biofilm Matrix by Subinhibitory Concentrations of Clindamycin. *Antimicrob. Agents Chemother.* **60**, 5957–5967 (2016).
66. Feng, J., Ma, L., Nie, J., Konkel, M. E. & Lu, X. Environmental Stress-Induced Bacterial Lysis and Extracellular DNA Release Contribute to *Campylobacter jejuni* Biofilm Formation. *Appl. Environ. Microbiol.* **84** (2017).
67. Kawarai, T., Narisawa, N., Suzuki, Y., Nagasawa, R. & Senpuku, H. *Streptococcus mutans* biofilm formation is dependent on extracellular DNA in primary low pH conditions. *J. Oral Biosci.* **58**, 55–61 (2016).
68. Olwal, C. O., Ang'ienda, P. O., Onyango, D. M. & Ochiel, D. O. Susceptibility patterns and the role of extracellular DNA in *Staphylococcus epidermidis* biofilm resistance to physico-chemical stress exposure. *BMC Microbiol.* **18** (2018).
69. Kadam, S. R. *et al.* Diversity assessment of *Listeria monocytogenes* biofilm formation: Impact of growth condition, serotype and strain origin. *Int. J. Food Microbiol.* **165**, 259–264 (2013).
70. Barnhart, M. M. & Chapman, M. R. Curli Biogenesis and Function. *Annu. Rev. Microbiol.* **60**, 131–147 (2006).

Acknowledgements

We would like to thank Dr. Heiti Paves for consulting on CLSM imaging. This work was supported by the Estonian Research Council grants IUT 23-5, PUT 748, European Regional Development Fund project TK134 and ERDF project Centre of Technologies and Investigations of Nanomaterials (NAMUR+, project number 2014-2020.4.01.16-0123) and EU COST Action CA15114 “Anti-Microbial Coating Innovations to prevent infectious diseases” (AMICI). N.F.A. also acknowledges project POCI-01-0145-FEDER-006939 (Laboratory for Process Engineering, Environment, Biotechnology and Energy – UID/EQU/00511/2019), funded by the European Regional Development Fund (ERDF) through COMPETE2020 – Programa Operacional Competitividade e Internacionalização (POCI), and by national funds (PIDDAC) through FCT – Fundação para a Ciência e a Tecnologia/MCTES; project “LEPABE-2-ECO-INNOVATION” – NORTE-01-0145-FEDER-000005, funded by Norte Portugal Regional Operational Programme (NORTE 2020), under PORTUGAL 2020 Partnership Agreement, through the European Regional Development Fund (ERDF).

Author Contributions

M.R. executed the experiments, participated in planning of the experiments and writing the paper. A.I. and N.F.A. participated in planning of the experiments, writing the paper and providing background information on the subject.

Additional Information

Supplementary information accompanies this paper at <https://doi.org/10.1038/s41598-019-42906-3>.

Competing Interests: The authors declare no competing interests.

Publisher's note: Springer Nature remains neutral with regard to jurisdictional claims in published maps and institutional affiliations.



Open Access This article is licensed under a Creative Commons Attribution 4.0 International License, which permits use, sharing, adaptation, distribution and reproduction in any medium or format, as long as you give appropriate credit to the original author(s) and the source, provide a link to the Creative Commons license, and indicate if changes were made. The images or other third party material in this article are included in the article's Creative Commons license, unless indicated otherwise in a credit line to the material. If material is not included in the article's Creative Commons license and your intended use is not permitted by statutory regulation or exceeds the permitted use, you will need to obtain permission directly from the copyright holder. To view a copy of this license, visit <http://creativecommons.org/licenses/by/4.0/>.

© The Author(s) 2019

Propidium iodide staining underestimates viability of adherent bacterial cells

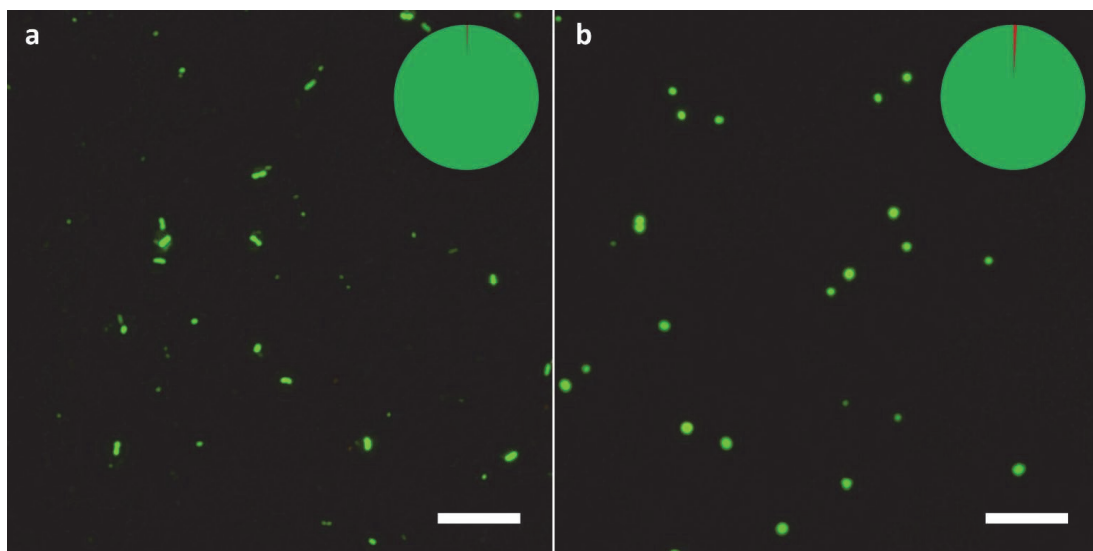
Merilin Rosenberg* ^{1,2}, Nuno F. Azevedo³, Angela Ivask¹

¹ Laboratory of Environmental Toxicology; National Institute of Chemical Physics and Biophysics; Akadeemia tee 23, 12618 Tallinn, Estonia

² Department of Chemistry and Biotechnology; Tallinn University of Technology; Akadeemia tee 15, 12618 Tallinn, Estonia

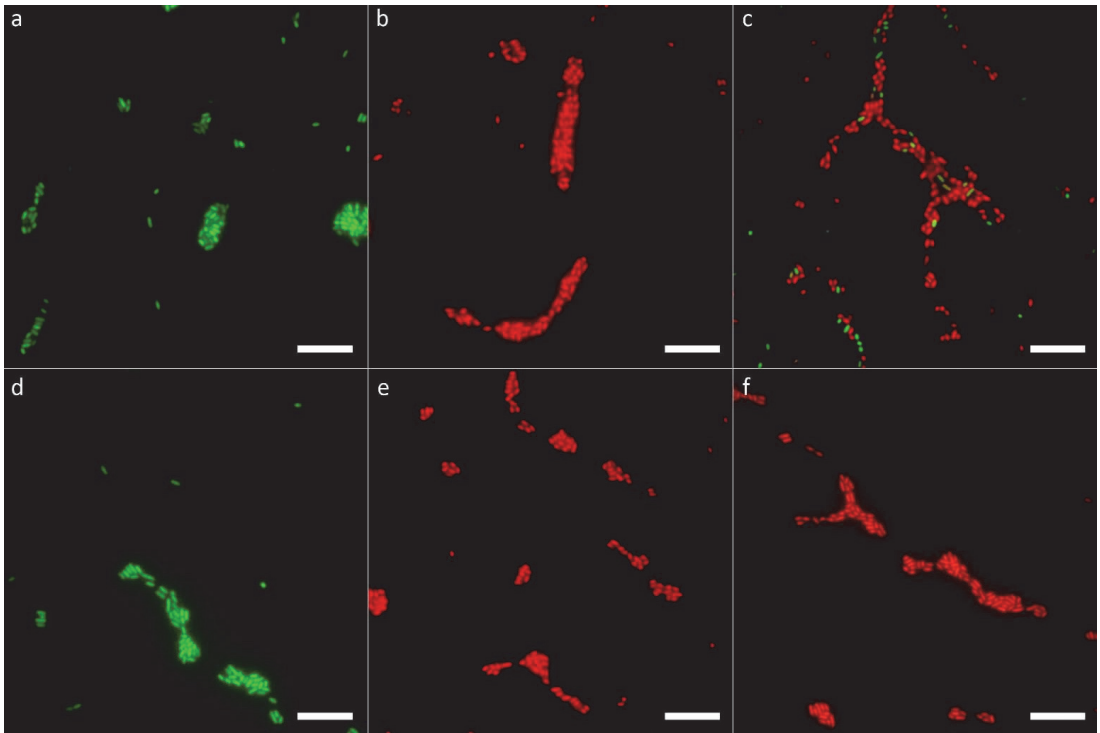
³ LEPABE - Laboratory for Process Engineering, Environment, Biotechnology and Energy; Department of Chemical Engineering; Faculty of Engineering; University of Porto; Rua Dr. Roberto Frias, 4200-465 Porto, Portugal

* rosenbergmerilin@gmail.com; (+372) 5268 384



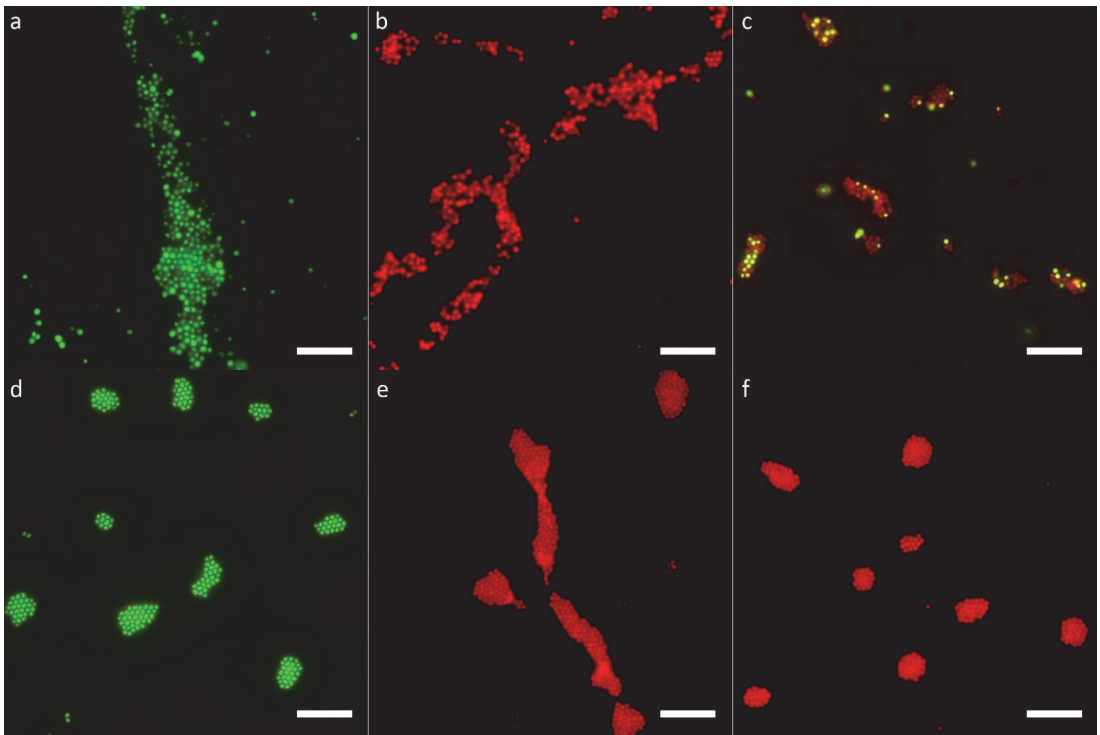
Supplementary Figure 1

Epifluorescence microscopy images of planktonic *E. coli* (a) and *S. epidermidis* (b) viability staining: planktonic cells from the biofilm experiment after 24 h incubation in phosphate buffered saline (PBS), stained with PI and SYTO 9 and collected on filter. Pie diagrams represent total cell count with PI, and SYTO 9 stained signal proportions marked in red and dark green respectively. Scale bars correspond to 10 μm .



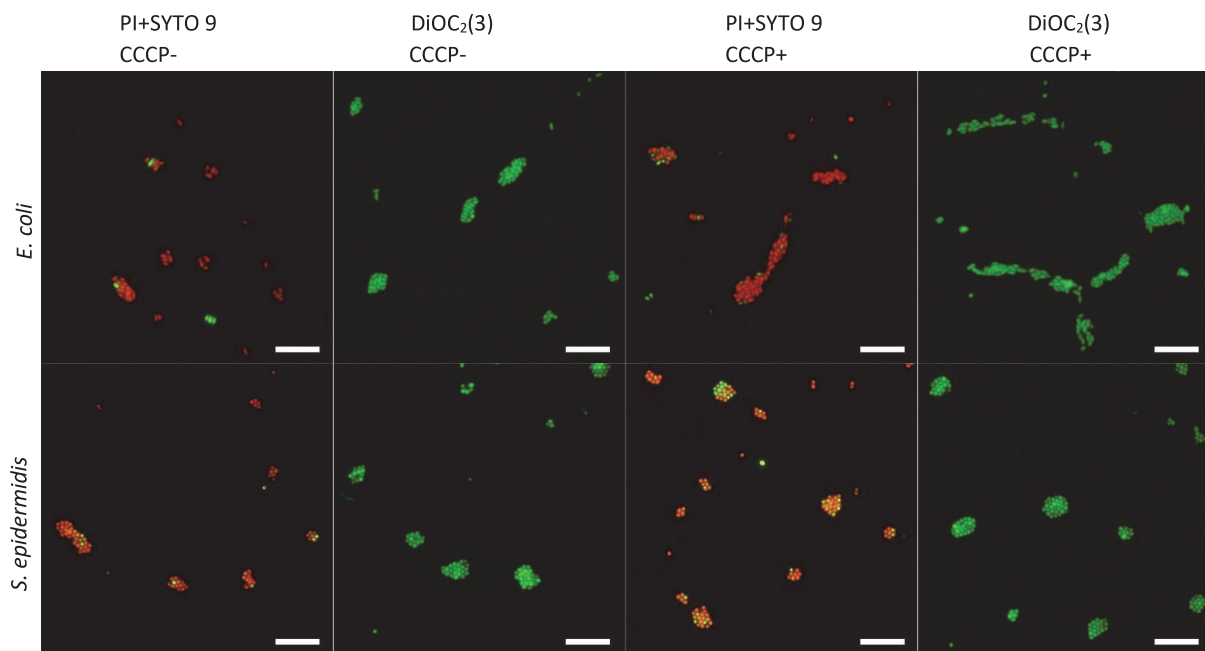
Supplementary Figure 2

Epifluorescence microscopy images of viable (a-c) and ethanol-fixed (d-e) 24 h *E. coli* biofilms stained with SYTO 9 (a, d), PI (b, e) or PI + SYTO 9 (c, f). Scale bars correspond to 10 μ m.



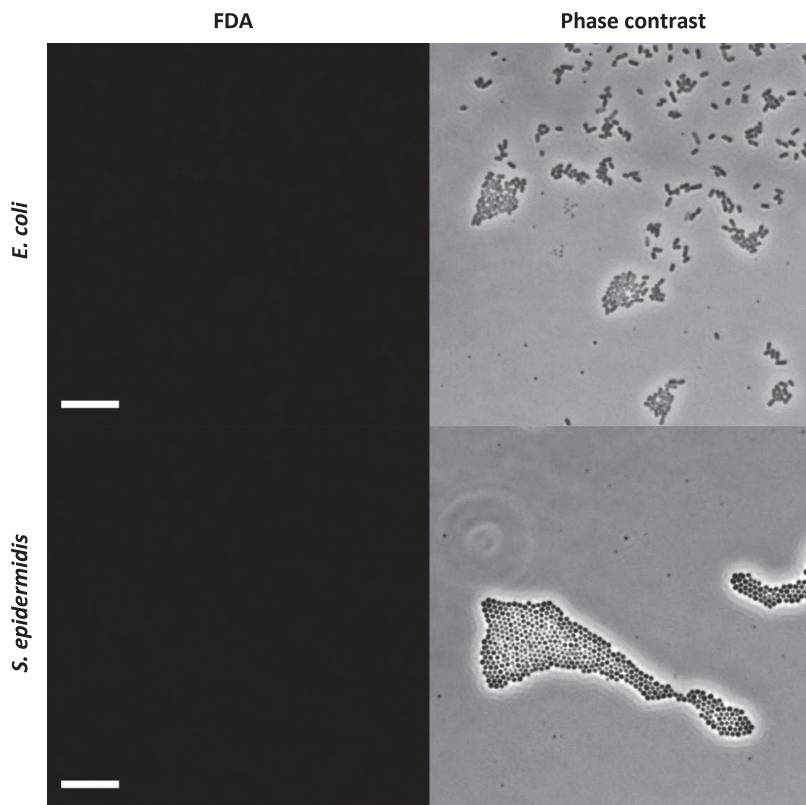
Supplementary Figure 3

Epifluorescence microscopy images of viable (a-c) and ethanol-fixed (d-e) 24 h *S. epidermidis* biofilms stained with SYTO 9 (a, d), PI (b, e) or PI + SYTO 9 (c, f). Scale bars correspond to 10 μm .

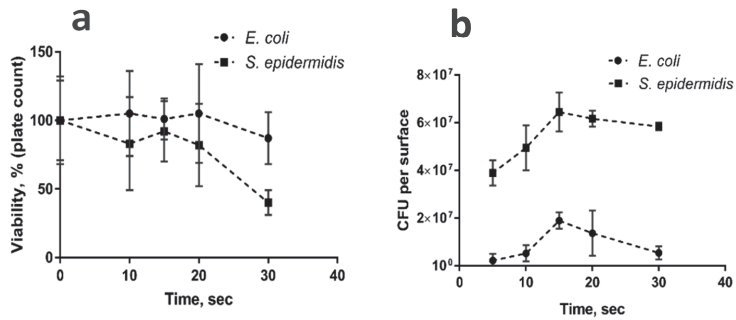


Supplementary Figure 4

Representative epifluorescence microscopy images of 24 h biofilms of *E. coli* and *S. epidermidis* stained in situ with PI + SYTO 9 or with DiOC₂(3) with or without membrane potential relieving CCCP pre-treatment. No increased membrane potential signals were observed without CCCP pretreatment (CCCP-) and CCCP pretreatment (CCCP+) did not change overall PI + SYTO 9 staining pattern. Therefore, PI + SYTO 9 staining pattern is not caused by increased membrane potential of adherent cells. Scale bars correspond to 10 μm.

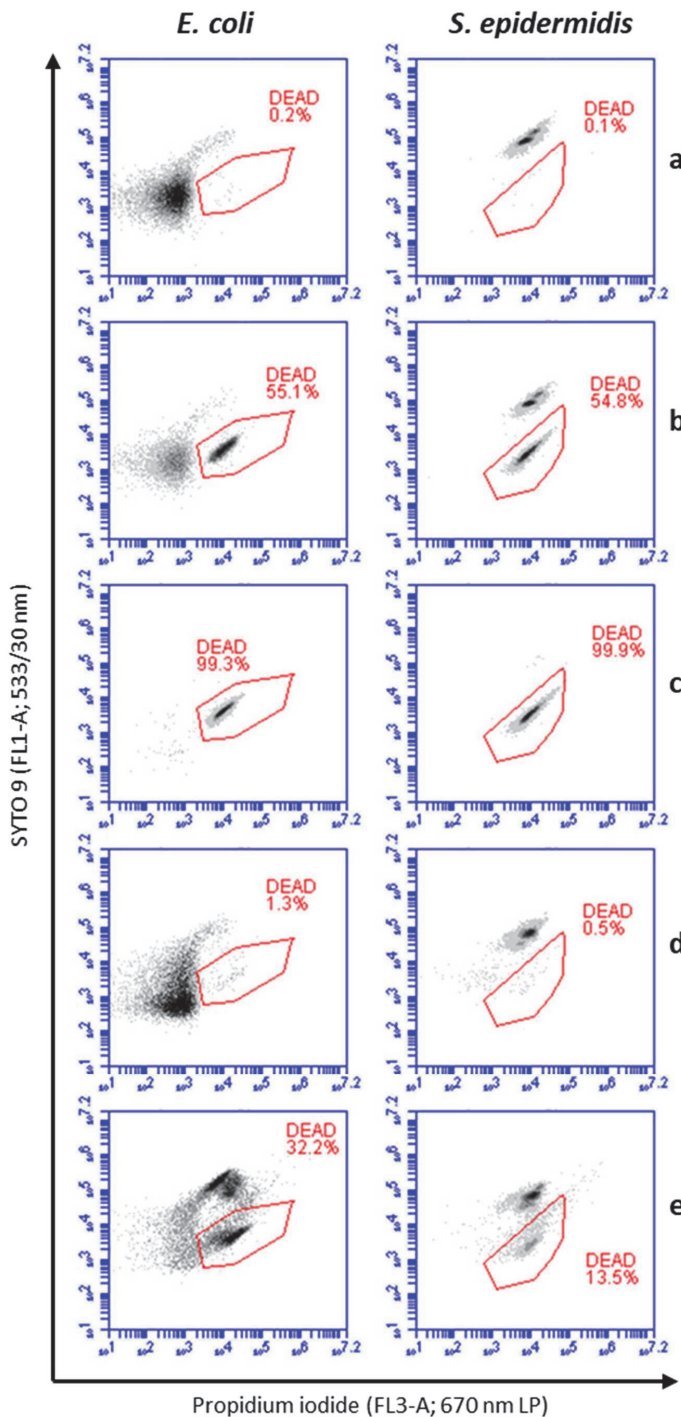


Supplementary Figure 5
Epifluorescence and phase
contrast images of ethanol-fixed
E. coli* and *S. epidermidis
stained with fluorescein diacetate (FDA). Fluorescence and phase contrast image are captured from the same view field. No background FDA signals from killed cells are captured. Scale bars correspond to 10 μm .



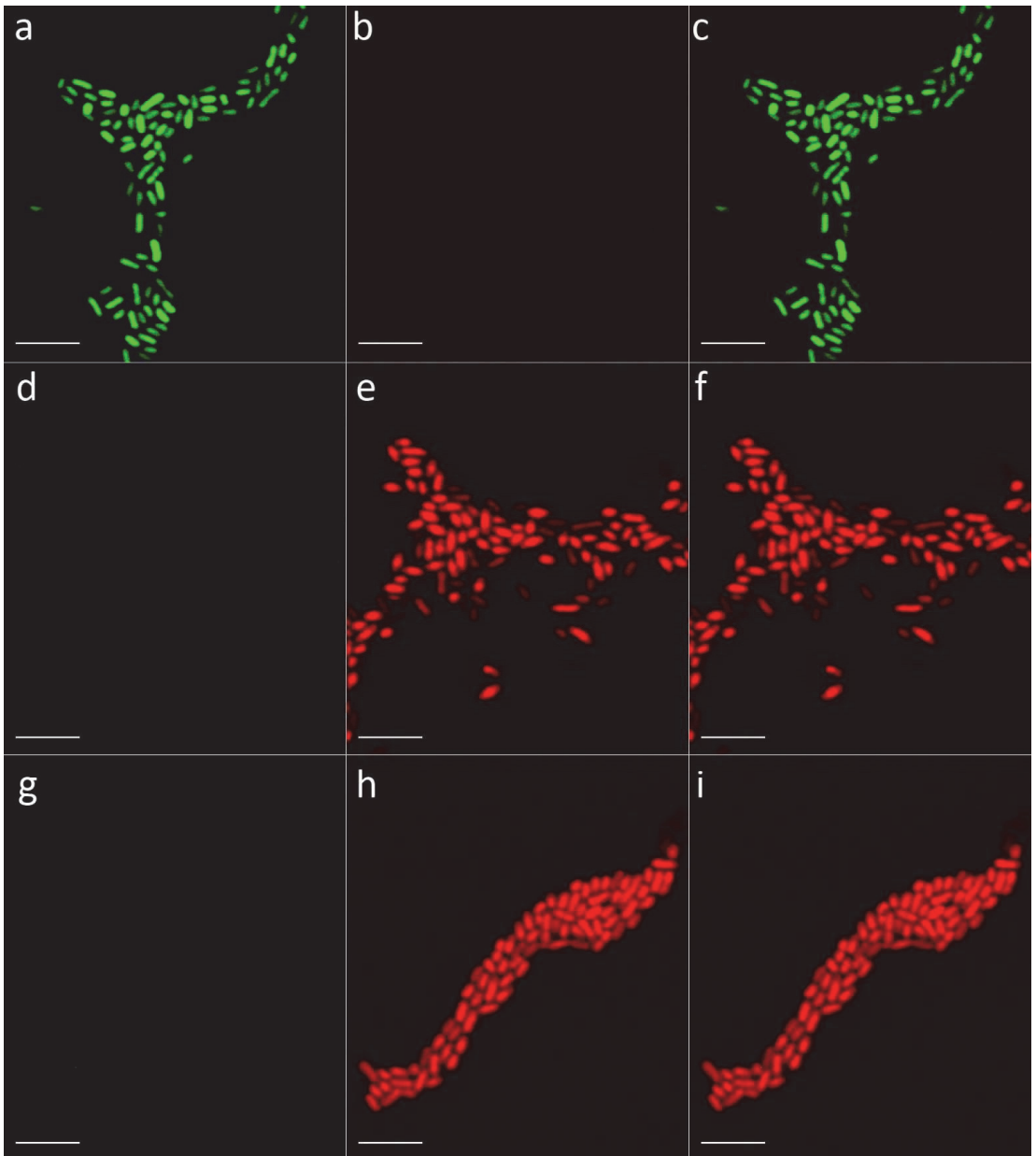
Supplementary Figure 6

Optimization of protocol for ultrasonication of adherent bacteria from biofilms on glass surfaces. Viability of planktonic bacteria ($OD_{600}=0.05$ in 10 ml PBS) during 0, 10, 15, 20 and 30 seconds sonication at 25% amplitude (a) and release of viable cells/aggregates from 24 h biofilm ($OD_{600}=0.05$ inoculum) in 10 ml PBS under the same conditions (b). Although planktonic culture endures longer treatment without decreasing viability, 15 seconds ultrasonication resulted in highest CFU per surface yield for biofilm cells. Glass surfaces were stained with propidium iodide and SYTO 9 after ultrasonication to confirm removal of biofilm.



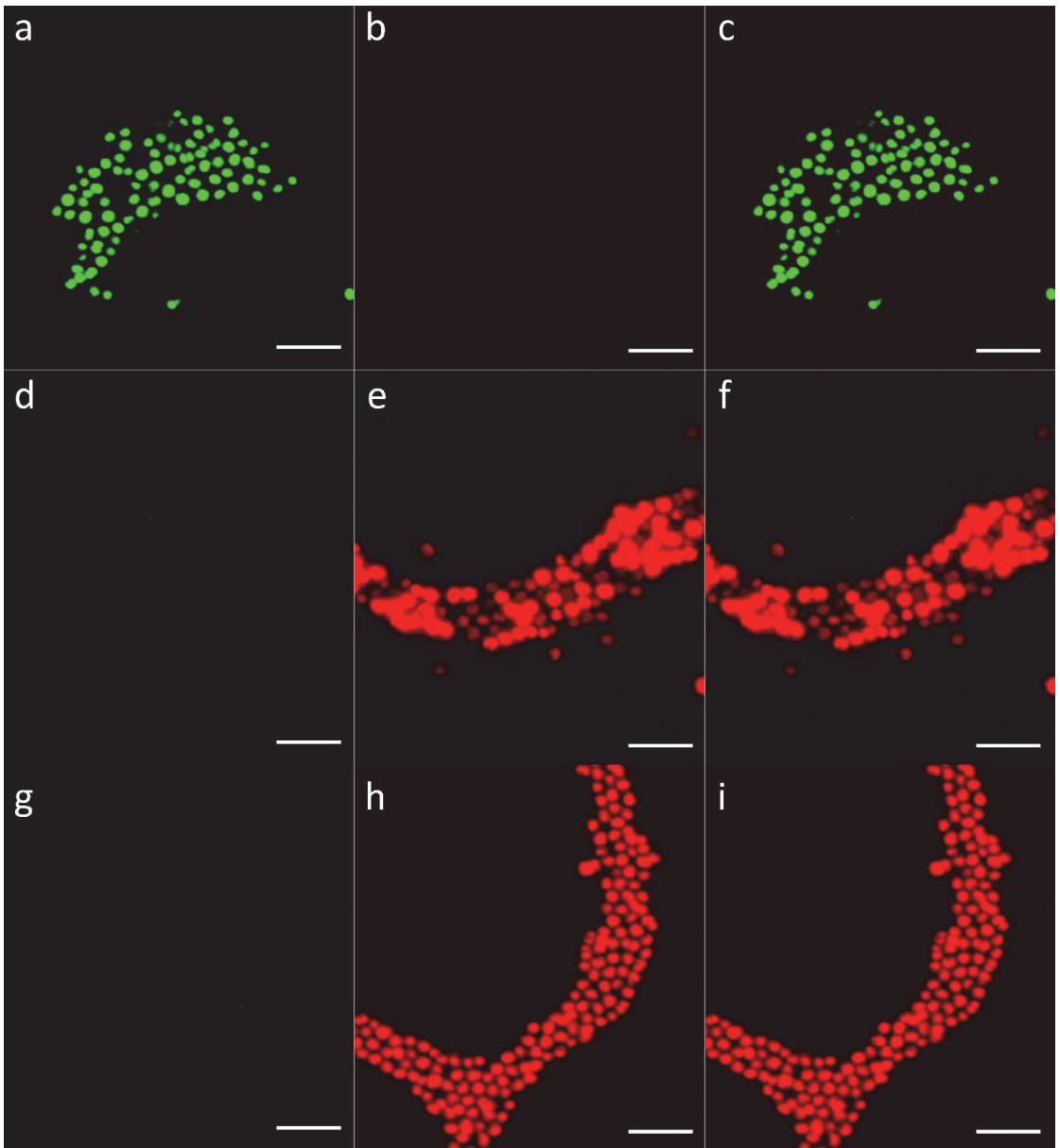
Supplementary Figure 7
Flow cytometry (FCM) density plots of propidium iodide (PI) and SYTO 9 co-stained *E. coli* MG1655 and *S. epidermidis* DSM20044:

PBS washed overnight planktonic culture (a); 1:1 mix of viable and ethanol-killed overnight cultures (b); PBS washed and ethanol-killed overnight culture (c); pooled and ultrasonicated planktonic cells from biofilm experiment (d); ultrasonicated and pooled sessile cells from biofilm (e). Live/dead gating based on known proportions of viable and ethanol-killed planktonic bacteria was used to evaluate viability of bacteria harvested from 24 h biofilms. It is evident that gating strategy used is applicable for planktonic bacteria from the biofilm experiment even after incubating in PBS and sonication (d) while FCM populations of harvested *E. coli* biofilm cells have shifted and plots are much noisier. For adherent cells, dead gate seems to be better defined by PI staining than shifting populations of viable cells with presumably variable degrees of extracellular PI staining.



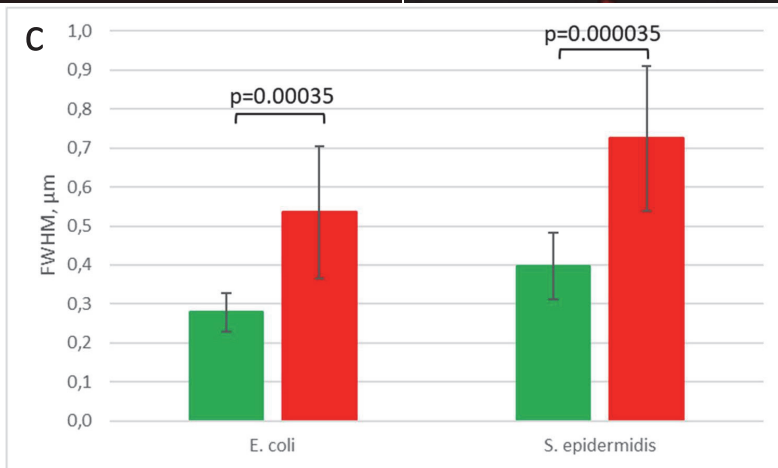
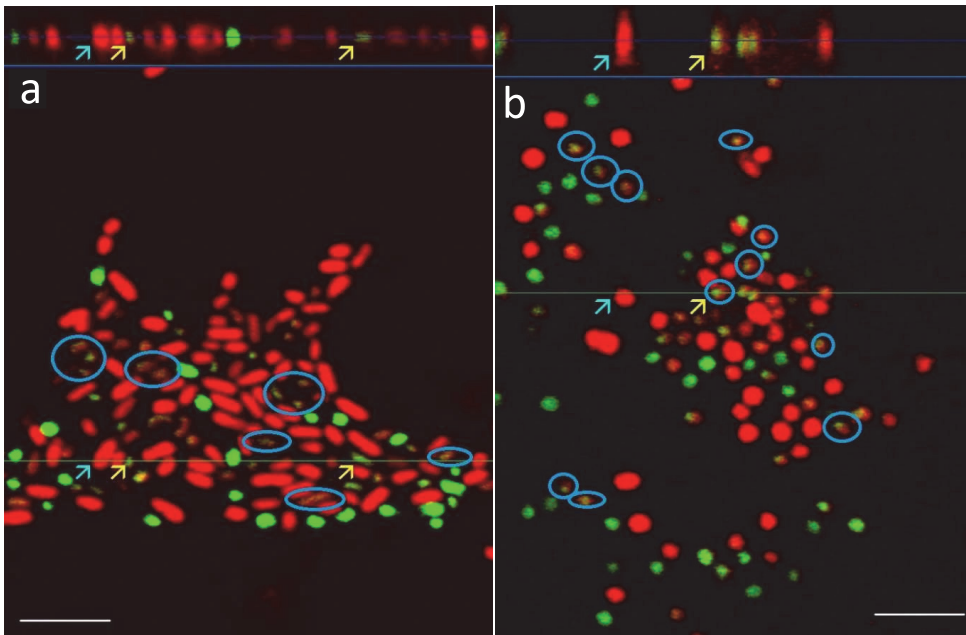
Supplementary Figure 8

Maximum projections of CLSM Z-stacks of viable *E. coli* biofilm stained with SYTO 9 (a-c) or PI (d-f) and ethanol-fixed biofilm stained with PI + SYTO 9 (g-i). Green channel (a, d, g), red channel, (b, e, h) and multichannel (c, f, i) projections are presented. The same acquisition and linear post-adjustment settings were applied to all images. Scale bars correspond to 5 μm .



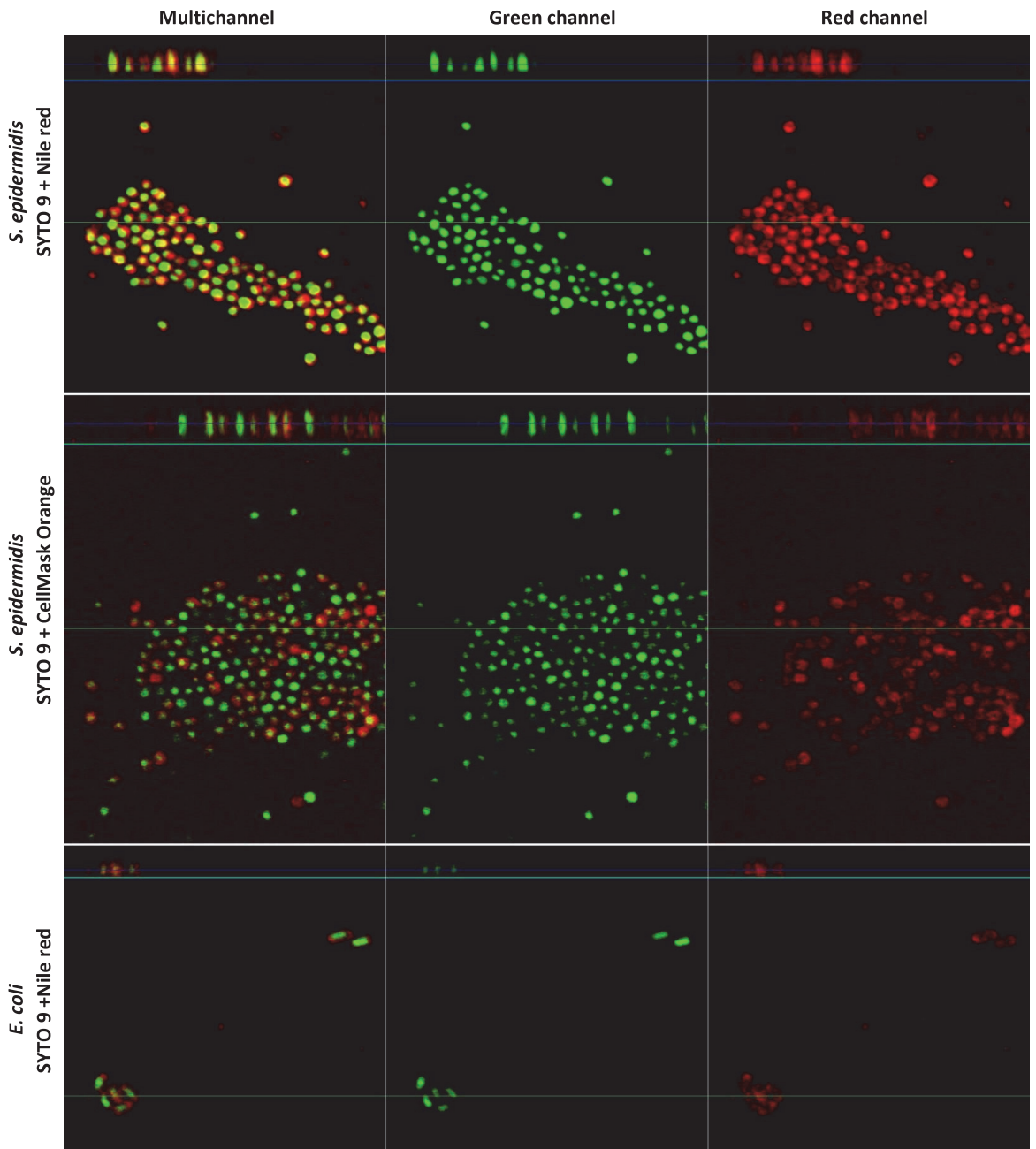
Supplementary Figure 9

Maximum projections of CLSM Z-stacks of viable *S. epidermidis* biofilm stained with SYTO 9 (a-c) or PI (d-f) and **ethanol-fixed biofilm** stained with PI + SYTO 9 (g-i). Green channel (a, d, g), red channel, (b, e, h) and multichannel (c, f, i) projections are presented. The same acquisition and linear post-adjustment settings were applied to all images. Scale bars correspond to 5 μm .



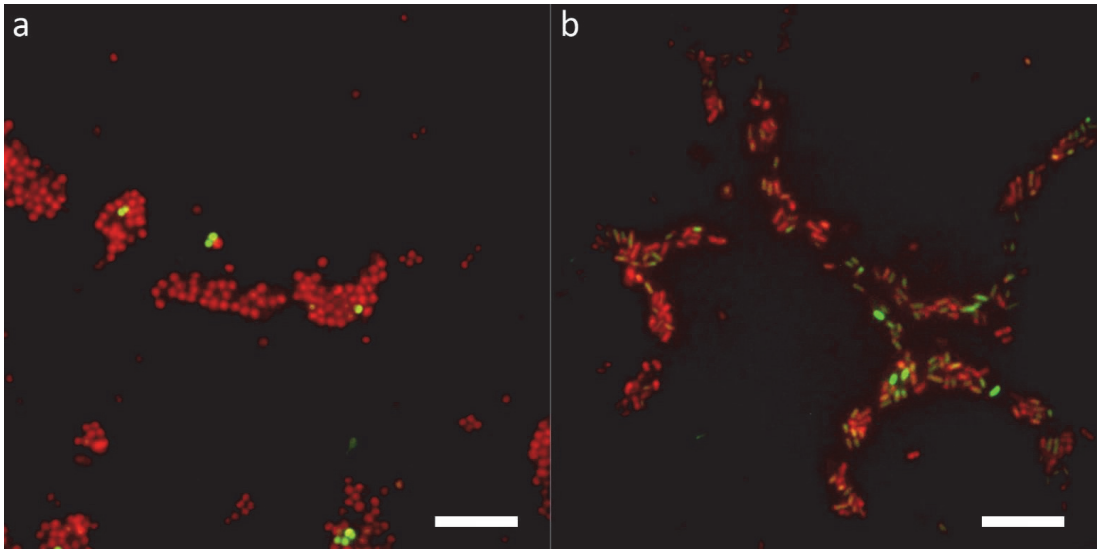
Supplementary Figure 10

Full width at half maximum (FWHM) measurement of non-saturated green SYTO 9 and red PI signals from CLSM cross-sections of *E. coli* (a) and *S. epidermidis* (b) biofilms. Mean and standard deviation of 11 values measured for signals indicated with blue circles on panels a and b are presented (c). Scale bars correspond to 5 μm.



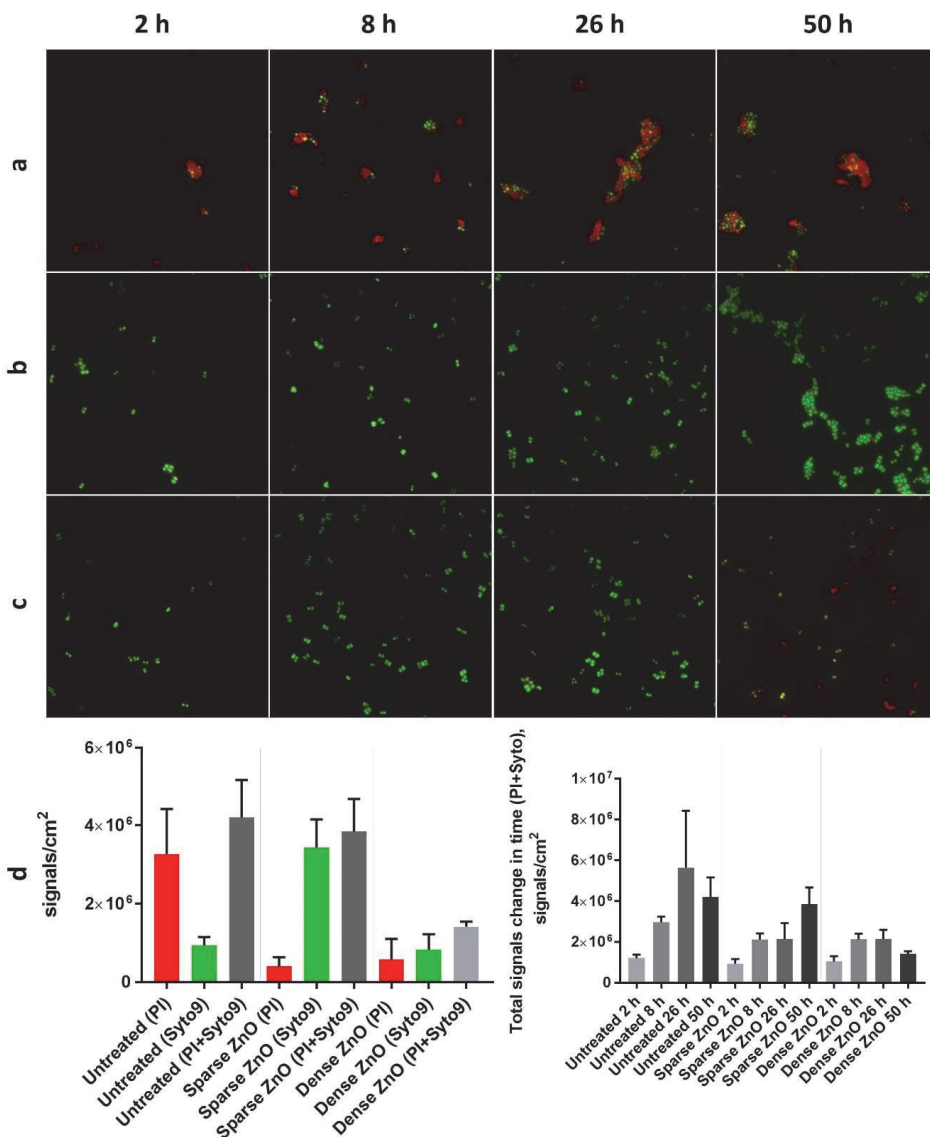
Supplementary Figure 11

Vertical and horizontal CLSM cross-sections of 24 h *S. epidermidis* and *E. coli* biofilms stained with Nile red and CellMask Orange to visualize cell membranes. Scale bars correspond to 5 μm .



Supplementary Figure 12

Epifluorescence microscopy images 24 h *S. epidermidis* (a) and *E. coli* (b) biofilms co-stained with SYTO 9 and Congo red (CR). Scale bars correspond to 10 μm .

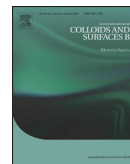


Supplementary Figure 13

Staining of *S. epidermidis* biofilms on glass with propidium iodide (PI) and SYTO 9. *S. epidermidis* DSM20044 biofilm on untreated glass (row a) and on antimicrobial nano-ZnO covered surface described in [51] (row b shows glasses with lower nano-ZnO content and row c shows glasses with higher ZnO content) in PBS stained *in situ* with PI and SYTO 9 and signal counts (row d) of 50 h biofilm (d, left) or total signal count change in time (d, right). Red staining is predominantly observed on non-toxic untreated glass with biofilm specific aggregates formed by tightly bound diplococci while on nano-ZnO antibacterial surfaces biofilm-specific aggregates appear later (b), but stain predominantly green and comprise of loosely bound diplococci and tetrads. Same staining pattern and forming loose diplococci and tetrads is true even in the case on surfaces with even higher nano-ZnO content where biofilm-specific aggregation is not observed during 50 h.

Publication III

Visnapuu, M.; **Rosenberg, M.**; Truska, E.; Nõmmiste, E.; Šutka, A.; Kahru, A.; Rähn, M.; Vija, H.; Orupõld, K.; Kisand, V.; Ivask, A. (2018). UVA-induced antimicrobial activity of ZnO/Ag nanocomposite covered surfaces. *Colloids and Surfaces B: Biointerfaces*, 169, 222–232. DOI: 10.1016/j.colsurfb.2018.05.009.



UVA-induced antimicrobial activity of ZnO/Ag nanocomposite covered surfaces

Meeri Visnapuu^{a,b}, Merilin Rosenberg^{b,c}, Egle Truska^{b,c}, Ergo Nõmmiste^{a,d},
Andris Šutka^{a,e}, Anne Kahru^{b,d}, Mihkel Rähn^a, Heiki Vija^b, Kaja Orupõld^f,
Vambola Kisand^{a,*}, Angela Ivask^{b,*}

^a Institute of Physics, University of Tartu, W. Ostwaldi Str 1, 50411, Tartu, Estonia

^b National Institute of Chemical Physics and Biophysics, Akadeemia tee 23, 12618, Tallinn, Estonia

^c Tallinn University of Technology, Ehitajate tee 5, 19086, Tallinn, Estonia

^d Estonian Academy of Sciences, Kohtu 6, Tallinn, Estonia

^e Research Laboratory of Functional Materials Technologies, P. Valdena 3/7, LV-1048, Riga, Latvia

^f Estonian University of Life Sciences, Fr. R. Kreutzwaldi 1, 51014, Tartu, Estonia

ARTICLE INFO

Article history:

Received 10 January 2018

Received in revised form 16 April 2018

Accepted 4 May 2018

Available online 4 May 2018

Keywords:

Nanoparticles

Silver

Zinc

Photocatalytic activity

Antimicrobial surface

Reusability

ABSTRACT

Application of efficient antimicrobial surfaces has been estimated to decrease both, the healthcare-associated infections and the spread of antibiotic-resistant bacteria. In this paper, we prepared ZnO and ZnO/Ag nanoparticle covered surfaces and evaluated their antimicrobial efficacy towards a Gram-negative bacterial model (*Escherichia coli*), a Gram-positive bacterial model (*Staphylococcus aureus*) and a fungal model (*Candida albicans*) in the dark and under UVA illumination. The surfaces were prepared by spin coating aliquots of ZnO and ZnO/Ag nanoparticle suspensions onto glass substrates. Surfaces contained 2 or 20 $\mu\text{g Zn/cm}^2$ and 0–0.02 $\mu\text{g Ag/cm}^2$. No significant antimicrobial activity of the surfaces, except of those with the highest Ag or Zn content was observed in the dark. On the other hand, UVA illuminated surfaces containing 20 $\mu\text{g Zn/cm}^2$ and 2 $\mu\text{g Zn}$ plus 0.02 $\mu\text{g Ag/cm}^2$ caused >3 log decrease in the viable counts of *E. coli* and *S. aureus* in 30 min. As proven by brilliant blue FCF dye degradation and elemental analysis of the surfaces, this remarkable antimicrobial activity was a combined result of photocatalytic effect and release of Zn and Ag ions from surfaces. Surfaces retained significant antibacterial and photocatalytic properties after several usage cycles. Compared to bacteria, yeast *C. albicans* was significantly less sensitive to the prepared surfaces and only about 1 log reduction of viable count was observed after 60 min UVA illumination. In conclusion, the developed ZnO/Ag surfaces exhibit not only high antibacterial activity but also some antifungal activity.

© 2018 Elsevier B.V. All rights reserved.

1. Introduction

Antimicrobial surfaces are particularly important in hospitals, food preparation and kitchens, sanitary facilities, air conditioning and ventilation systems. It has been estimated that in hospitals in the US around 700,000 additional infections (contributing to 75,000 annual deaths) occur due to inappropriate hygiene and resulting spreading of microbes in hospital settings [1]. In Europe, between 2011 and 2012, 3.2 million cases of hospital acquired infections

were registered in acute care hospitals by European Centre for Disease Prevention and Control [2]. The use of appropriate antimicrobial surfaces can be expected to decrease this high number of healthcare related infections and, consequently, the spread of antibiotic resistant microorganisms.

Most widespread is the use of antimicrobial agent based coatings to kill microbes on contact. Other strategies include the use of physical surface structure e.g. nanopatterned surfaces [3] to kill bacteria on contact or surface modifications inhibiting initial microbial adhesion [4], however that doesn't necessarily prevent bacterial growth and biofilm formation [5].

There are available classic metal-based microbe inhibiting surfaces, used already for centuries – objects made from or coated with copper and its alloys or silver [6]. Such surfaces acting mainly

* Corresponding authors.

E-mail addresses: vambola.kisand@ut.ee (V. Kisand), angela.ivask@kbi.fi (A. Ivask).

via metal ion release [7] are not perfect as there is high possibility that the remains of dead bacteria retain on the surface, that the appearance of metal details will change e.g., due to oxidation, and these materials are usually costly [8]. Therefore, research to explore more efficient and cost effective tailored antimicrobial surfaces is needed. One promising method is the development of antimicrobial surfaces containing photocatalysts that induce microbial killing and degradation of organic matter under specific illumination conditions. The most popular photocatalyst is TiO₂ [9,10] but also ZnO [11] is widely used. Photocatalytic materials need excitation with photons which energy exceeds band gap energy (E_g , for ZnO 3.37 eV) to create electron-hole pairs. Produced photoelectrons can be easily trapped at electronic acceptors like adsorbed O₂ and produce a superoxide anion radical $\cdot\text{O}_2^-$. The photoinduced holes can be easily trapped by OH⁻ to further produce hydroxyl radical ($\cdot\text{OH}$), which is an extremely strong oxidant for the partial or complete mineralization of organic chemicals [12]. Unfortunate challenges with the use of photocatalytic materials exist. Most importantly only a small fraction of photons in the solar spectrum exceed the band gap energy and rapid recombination of photoinduced charge carriers can occur [13]. To overcome this limitation, one efficient way is to deposit noble metals on photocatalytic semiconductors such as TiO₂ or ZnO. In this case the photogenerated electrons in the conduction band can be transferred to metal deposits due to the Schottky barrier formed at the metal–semiconductor interface, while the holes can remain on the semiconductor surfaces [14]. Thus, noble metal deposits on semiconductor particle surface can act as electron sinks, facilitating charge separation and improving photocatalytic efficiency. Several studies have attempted to determine the optimal concentration of deposited noble metals. Lu et al. reported that optimal Ag content (on the nanoparticle surfaces) to improve photocatalytic properties of ZnO was approximately 1.20 atom% [13]. Georgekutty et al. reported 3 mol% Ag material relative to ZnO as optimal for improved photocatalytic effect [15] and Sun et al. demonstrated the efficacy of 1.12 atom% Ag content in Ag/ZnO nanomaterial [16]. An alternative possibility to improve photocatalytic properties of a material is band gap narrowing by incorporating metal atoms into crystal lattice [17]. Also, visible light plasmonic absorption on metal deposits with following energy transfer to semiconductor may improve photocatalytic properties [18]. Beside photocatalytic materials an alternative approach on the way to more effective and cost effective tailored antimicrobial surfaces are composites, which include different antimicrobial agents and mechanisms acting simultaneously. Creation of composites of semiconductor materials, such as ZnO with silver, is a promising approach to create antimicrobial materials [19] in which silver in addition to improving the photocatalytic activity of the semiconductor material, is expected to inhibit microbial cells due to the release of ionic silver [20,21]. The effect of such composites rises from a combined and complex influence of Zn²⁺ ions, Ag⁺ ions, and nano-ZnO and nano-ZnO/Ag as UV-induced photocatalysts. Assuming, the different processes influence microbes at different extent.

The advantages of ZnO/Ag nanocomposites as antimicrobials were utilized in this study. Here, we created ZnO/Ag nanocomposite particles by depositing Ag on ZnO nanorods at different ZnO:Ag ratios and applied the resulting nanocomposites to glass substrates to create antimicrobial surfaces. Antimicrobial efficacy of the prepared coatings was evaluated against *Escherichia coli*, *Staphylococcus aureus* and *Candida albicans* using an in-house test protocol modified from ISO 27447:2009 under UVA illumination and in the dark. In parallel, photocatalytic activity of the nanocomposites was analyzed using brilliant blue FCF degradation assay, and release of ionic zinc and silver was evaluated using atomic absorption spectroscopy (AAS) or total reflection X-ray spectroscopy (TXRF).

2. Materials and methods

2.1. Materials

Zinc acetate dihydrate ($\text{Zn}(\text{CH}_3\text{COO})_2 \times 2\text{H}_2\text{O}$; Sigma-Aldrich, puriss. p.a., ACS reagent), methanol (Sigma-Aldrich, puriss. p.a., ACS reagent), potassium hydroxide (Lach-Ner, reagent grade), acetylacetone (acac; Fluka Analytical, puriss. p.a. grade), *n*-butanol (Sigma-Aldrich, puriss. p.a., ACS reagent), silver nitrate (AgNO₃; Alfa Aesar, ACS reagent), sodium 2-ethylhexanoate (Sigma-Aldrich, purity 97%), erioglaucine (brilliant blue FCF; Sigma-Aldrich), hydrogen peroxide (Sigma-Aldrich, 30% in H₂O, reagent grade), ammonia solution (AppliChem, 25% in H₂O, reagent grade) were used. Water purified with MilliQ (Millipore, USA) equipment was used throughout the experiments, hereafter referred to as deionized water. For UVA exposures, a self-built fluorescent Hg lamp consisting of 4 fluorescent light bulbs (15 W iSOLde Cleo, $\lambda_{\text{max}} = 355$ nm) was used. The distance between light bulbs and test surfaces was 55 cm. Light intensity was further attenuated by placing two metal wire grids (0.7 mm wire, 3.3 mm square mesh) directly below light bulbs. Light intensity at test surface height was 2.7–3.2 W/m² at 315–400 nm spectral range (measured using Delta Ohm UVA probe).

2.2. Synthesis of ZnO particles

Hydrothermal synthesis based on Pacholski et al. [22] was used to prepare rod-like ZnO nanoparticles. Stock solution of $\text{Zn}(\text{CH}_3\text{COO})_2 \times 2\text{H}_2\text{O}$ in methanol (27 wt%) was prepared by stirring and heating under reflux. 37 mL of 22 wt% KOH in methanol was added to stock solution under continuous stirring and the mixture was heated under stirring in an 80 °C oil bath for 72 h. The suspension was allowed to cool to room temperature and the resulting white solid was washed with methanol. ZnO nanoparticles were stored as a methanol containing paste in the dark at room temperature. ZnO concentration in the paste was determined by thermogravimetric analysis.

2.3. Synthesis of silver 2-ethylhexanoate

Silver 2-ethylhexanoate was prepared based on Li and Hsu [23] by mixing together equal volumes of 0.1 M AgNO₃ and 0.1 M sodium 2-ethylhexanoate aqueous solutions. The resulting white precipitate was washed with deionized water and methanol and subsequently left to dry in the dark at room temperature for a week.

2.4. Preparation of ZnO/Ag composite nanoparticles

Either 0.6 wt% or 5 wt% ZnO nanoparticle suspension in butanol was prepared with the addition of acetylacetone as a stabilizing ligand (40 mol% of ZnO). Silver 2-ethylhexanoate was added as a slow releasing silver ion source. Ag content in the suspension was varied (0.6, 1.1 and 2.7 mol% of ZnO). The silver containing suspension as well as pure ZnO containing suspension was stirred under UVA irradiation (UVA diode; 120 W/m²) for 3 h and subsequently washed twice with butanol via centrifugation. The preparation method was based on Tzeng et al. [24] and slightly modified.

2.5. Preparation of ZnO/Ag covered surfaces

Surfaces were prepared by spin coating (3000 rpm, 30 s) 40 μL aliquots of 0.6 wt% ZnO with 0, 0.6, 1.1, 2.7 mol% Ag (sparse coverage) and 5 wt% ZnO (dense coverage) nanoparticle suspensions onto acetone washed 25 \times 25 mm glass substrates (Corning; No 2 cover glasses). The resulting surfaces were heated at 200 °C for 6 h to assure the removal of organic residues.

2.6. Characterization of ZnO/Ag composite particles and particle covered surfaces

The morphology and elemental content of ZnO and ZnO/Ag particles was investigated by FEI Titan Themis 200 Cs corrected transmission electron microscope (TEM) at 80 kV. Energy dispersive X-ray spectroscopy (EDX) signal of the particles was collected with SuperX silicon drift detector (Bruker) in STEM mode. For TEM analysis 200 $\mu\text{g}/\text{mL}$ particle suspension was deposited onto a 400 mesh holey carbon coated copper grid. High angle annular dark-field (HAADF)-STEM image was combined with EDX element mapping. Signal for silver L_{α} , zinc K_{α} and oxygen K_{α} was extracted to visualize their elemental distribution. UV–vis absorbance of ZnO and ZnO/Ag particle suspensions in butanol was measured from 100 $\mu\text{g}/\text{mL}$ particle suspensions in 1 cm path length quartz cuvettes using Cary 5000 UV–vis–NIR spectrophotometer. ZnO and ZnO/Ag covered surfaces were visualized using scanning electron microscope (FEI Helios NanoLab 600). The crystal phase composition of particles on covered surfaces was analysed by XRD. X-ray diffractograms were measured using Rigaku SmartLab instrument in Grazing Incidence X-ray Diffraction (GIXRD) regime. This regime allows to suppress signal from the substrate and get stronger signal from the coating itself. Elemental analysis of particle suspensions and prepared surface coatings were performed using total reflection X-ray fluorescence (TXRF; S2 Picofox, Bruker) or atom absorption spectrometer (AAS; SpectrAA 220Z, Varian). Prior to the analysis, nanoparticle suspensions were acidified with 1% HNO_3 , and for TXRF analysis also 1 $\mu\text{g}/\text{mL}$ Ga standard was added. Zn and Ag from surfaces were dissolved by treating the 2.5×2.5 cm coverslips in 1 mL concentrated HNO_3 for 1 h and further diluting the samples with water.

2.7. Evaluation of photocatalytic activity of ZnO and ZnO/Ag nanoparticles

65-fold diluted 0.6 wt% suspensions in butanol (0.09 mg/mL) containing model brilliant blue FCF dye (absorbance at 630 nm 0.85 a. u.) were tested on 96 well microplates (200 μL suspension per well) in three parallels. 650-fold dilution in butanol was used to compare 0.6 and 5 wt% ZnO suspensions (0.009 and 0.08 mg/mL, respectively). Microplate cover was replaced with UVA-transmissive borosilicate moisture preservation glass. Prior to testing, microplates containing suspensions were kept in the dark for 30 min to establish adsorption equilibrium of dye. After given irradiation times under UVA UV–vis absorption of samples in 615–640 nm spectral range was measured using microplate spectrophotometer (Multiskan Spectrum, Thermo Scientific). Nanoparticle solutions without dye and solutions containing only dye were used as controls. In parallel to UVA exposure also dark exposures were carried out. To evaluate photocatalytic degradation of model dye, UV–vis absorption of each sample at characteristic wavelength (630 nm) after given exposure times (C) was compared with initial absorption (C_0).

2.8. Evaluation of antimicrobial activity of surfaces

Antimicrobial testing was carried out towards model gram-negative bacterium *Escherichia coli* MG1655, gram-positive bacterium *Staphylococcus aureus* ATCC25923 and yeast *Candida albicans* CA14 using test protocol modified from ISO 27447:2009 [25] to allow higher throughput. Test organisms were grown on nutrient agar (NA) (5 g/L meat extract, 10 g/L peptone, 5 g/L sodium chloride, 15 g/L agar powder in deionized water). Suspension of test organisms at optical density (600 nm) of 0.01 for bacteria, 0.7 for *C. albicans* (corresponding to $\sim 3 \times 10^5$ CFU/surface for all organisms) was prepared in 500-fold diluted nutrient broth (1:500 NB)

(undiluted broth contained 3 g/L meat extract, 10 g/L peptone, 5 g/L sodium chloride in deionized water) and kept on ice between inoculations. To determine antimicrobial properties of test surfaces 25 μL of microbe suspension was applied to test surface and covered with $20 \times 20 \times 0.05$ mm polyethylene film in 6 parallels for each time point of which 3 were incubated in dark while 3 were exposed to UVA. Uncoated glass substrates were used as control surfaces. Polyethylene cover film was used to attain even thin coverage of microbial suspension with good contact between microbes and the surface and even UVA exposure as well as to ensure similar humidity conditions on predefined test area. Exposures were carried out in humid environment on a bent glass U-rod over sterile wet filter paper covered by Petri dish cover in dark conditions or 1.1 mm thick UVA-transmissive borosilicate moisture preservation glass under UVA illumination (Supplementary Fig. S1). Prior to test, polyethylene cover films and control surfaces were rinsed with 70% ethanol and air-dried under UVC. After exposure, each surface was washed with 2 mL of toxicity neutralizing soybean casein digest broth with lecithin and polysorbate (SCDLP: 17 g/L casein peptone, 3 g/L soybean peptone, 5 g/L sodium chloride, 2.5 g/L disodium hydrogen phosphate, 2.5 g/L glucose, 1 g/L lecithin and 7 g/L polysorbate 80 in deionized water) by pipetting, then 10-fold serially diluted in phosphate buffered physiological saline (PBS) and 3×20 μL of each dilution was drop-plated for counting. Colony forming units on NA were counted after 24 h incubation at 30 °C for bacteria or after 48 h incubation at 30 °C for *C. albicans*. The threshold for colony counting was set to >2 colonies per each drop which translates to practical limit of quantification at about 300 CFU/surface. Smaller counts were registered but not used for log reduction calculations.

2.9. Quantification of Zn and Ag release from the surfaces

Release of Zn and Ag from ZnO and ZnO/Ag surfaces was measured in conditions analogous to antimicrobial test. 25 μL 1:500 NB (or microbial suspension in this medium as in antimicrobial test above) was pipetted onto the surfaces and incubated under $20 \times 20 \times 0.05$ mm polyethylene film for specified duration. The liquid was then washed off with 2 mL deionized water. Zn content in this washoff was determined by TXRF and Ag content by AAS. To check for the possibility of release of nanoparticles during antimicrobial testing, washoffs from 60 min incubated ZnO surfaces were ultracentrifuged at 273,000g zero deceleration for 30 min at 15 °C (Beckman L8–55 M) and Zn content in the sample before and after centrifugation was analysed by TXRF.

2.10. Evaluation of antimicrobial activity of Zn²⁺ ions

To control for ionic component of toxicity, a mock test with untreated glass surfaces and all three test organisms was performed in the initial test format as described above but using ZnSO_4 at Zn concentrations in the range that dissolved from ZnO covered surfaces (5–40 mg/L). For this test $2 \times$ more concentrated salt solutions and $2 \times$ denser microbial suspensions were prepared in 1:500 NB and combined in equal volumes immediately before surface inoculation to achieve desired final concentration and density. Microbes were incubated in the dark or exposed to UVA for 60 min, washed off and drop-plated for counting as described above.

2.11. Reusability of surfaces

To evaluate surface properties after several usage cycles, 10 cycles of use and cleaning were applied to sparse coverage ZnO/2.7 mol% Ag surfaces. Surfaces were inoculated with *E. coli* as in initial test conditions, incubated under UVA illumination for 15 min, washed off with 2 mL of PBS, rinsed with deionized water and sterilized with UVC. Washoff was serially diluted and drop-

Table 1

Elemental analysis of ZnO and ZnO/Ag composite nanoparticle suspensions and respective nanoparticle covered surfaces. * TXRF analysis, ** AAS analysis, ND – not detected.

Nanoparticle suspension			Nanoparticle covered surface		
Sample designation	Zn ($\mu\text{g}/\text{mL}^*$)	Ag, $\mu\text{g}/\text{mL}^{**}$ (mol% ZnO)	Sample designation	Zn ($\mu\text{g}/\text{cm}^{2*}$)	Ag ($\mu\text{g}/\text{cm}^{2**}$)
0.6 wt% ZnO	5090	ND	sparse coverage ZnO	2.1	ND
0.6 wt% ZnO/0.6mol% Ag	5080	50 (0.6)	sparse coverage ZnO/0.6mol% Ag	2.1	0.005
0.6 wt% ZnO/1.1mol% Ag	5070	95 (1.1)	sparse coverage ZnO/1.1mol% Ag	2.1	0.014
0.6 wt% ZnO/2.7mol% Ag	5150	229 (2.7)	sparse coverage ZnO/2.7mol% Ag	2.2	0.022
5 wt% ZnO	50870	ND	dense coverage ZnO	19.5	ND

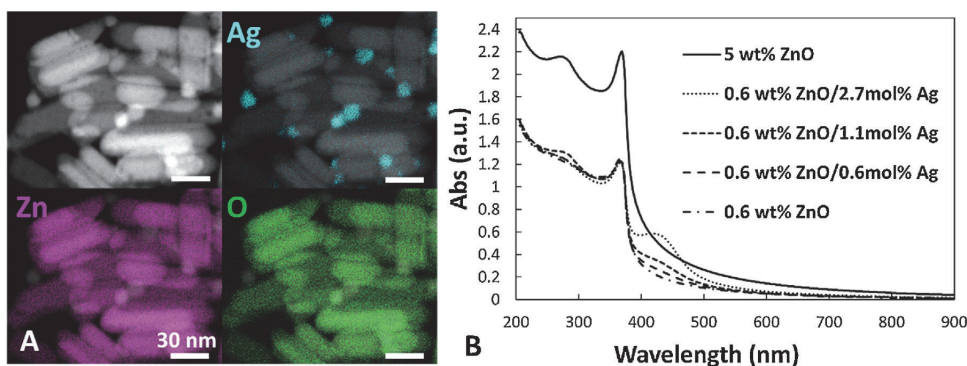


Fig. 1. Characterization of ZnO and ZnO/Ag nanoparticles in STEM, EDX and UV-vis. A: HAADF-STEM images and EDX mapping of ZnO/2.7 mol% Ag nanoparticles. HAADF-STEM images combined with EDX mapping results show silver (Ag) L_{α} in blue, zinc (Zn) K_{α} in violet and oxygen (O) K_{α} in green. Scale bars correspond to 30 nm. B: UV-vis absorbance spectra of ZnO and ZnO/Ag composite nanoparticle suspensions in butanol.

plated for counting after each cycle. Before use and after 3 and 10 usage cycles test samples were collected for SEM imaging, determining photocatalytic activity and for elemental analysis.

2.12. Statistical analysis

To detect statistically relevant differences in viable counts in antimicrobial testing of surfaces and Zn^{2+} ions one-way ANOVA followed by Tukey's HSD (Honestly Significant Difference) using R was performed. In case type II error was suspected, the most variable group was removed from the test, where mentioned. In the latter case pairwise two-tailed Student's t -test was applied in addition to one-way ANOVA as a comparison.

3. Results and discussion

3.1. Characterization of particles and particle covered surfaces

Imaging of ZnO nanoparticles with TEM proved the presence of well-defined and clearly separated $\sim 80 \times 30$ nm rod-like particles (Supplementary Fig. S2A). To create ZnO/Ag composite particles, ZnO particles were supplemented with silver (using UVA-induced photodeposition) at different ZnO/Ag ratios: Ag was added 0.6, 1.1 and 2.7 mol% of ZnO (Table 1). These concentrations of Ag were chosen on the basis of previous research on photocatalytic activity of ZnO/Ag composite particles. For example, [12,15,16,26] showed that the optimal Ag concentration for photocatalytic/antibacterial activity in ZnO/Ag material based on initial amounts of chemicals varied from 5 to 1 mol%. Assumingly one of the reasons for this variability in optimal Ag concentration is the fact that most of the studies have measured the concentrations based on added Ag and not the actual Ag content in the final product which may have differed. Indeed, only a few studies with particle suspensions have reported the actual Ag concentration in the end product [13,27–29]. In this respect our study is unique because reported Ag concen-

trations are based on actual measurements with AAS and TXRF. The other reason might be that ZnO particles with different sizes have been used in different studies and thus, similar Ag deposits on particle surface could have resulted in different ZnO/Ag mass ratios. In addition to ZnO/Ag composite particles, ZnO/Ag surfaces have been prepared and characterized in some earlier studies. ZnO nanoarrays on glass substrates supplemented with 0.37 atom% Ag were shown to exhibit increased photocatalytic activity compared to pure ZnO arrays [14]. Ag/ZnO coated cotton fabric (0.019 wt% Ag and 1.01 wt% ZnO) exhibited increased photocatalytic and antibacterial activity compared to pure ZnO coated fabric [30]. Behzadnia et al. also demonstrated increased photocatalytic effect and bactericidal/fungicidal activity of Ag doped ZnO covered wool compared to ZnO covered wool. However, the amount of ZnO and Ag loading on the substrate was not specified [31].

As seen from Supplementary Fig. S2B, the morphology of ZnO/Ag composite particles under TEM was similar to that of ZnO nanoparticles. STEM-EDX analysis of ZnO/Ag particles revealed silver depositions on ZnO particles indicating composite material (Fig. 1A). UV-vis measurements of ZnO/Ag composite particle suspensions in butanol demonstrated a localized surface plasmon resonance peak at ~ 425 nm which is particularly clear in case of ZnO with 2.7 mol% Ag and is characteristic to silver nanoparticles [32] (Fig. 1B). XRD analysis of ZnO/Ag composite particles showed the presence of crystalline ZnO [ICDD PDF2011, 01-070-8072] (Supplementary Fig. S3) while Ag structure with characteristic 2 θ peaks at 38° , 44° , 64° , 77° [ICDD PDF2011, 00-004-0783; [16]] was not detected. The latter can be attributed to low sensitivity of the XRD experiment (caused by the small amount of substances) or amorphous phase of Ag [33,34].

Two different surface coverage densities (sparse vs dense) and three different Ag concentrations were chosen to evaluate the influence of (i) the amount of ZnO on the surface and (ii) Ag on photocatalytic and antimicrobial effect. The surfaces prepared by spin coating particle suspensions onto glass carriers contained either

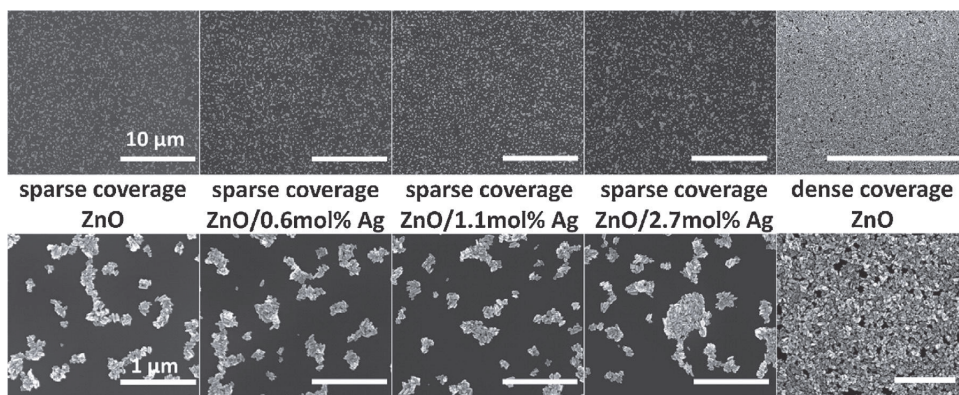


Fig. 2. SEM images of ZnO and ZnO/Ag composite nanoparticle covered surfaces. Scale bars correspond to 10 μm (upper panels) or 1 μm (lower panels).

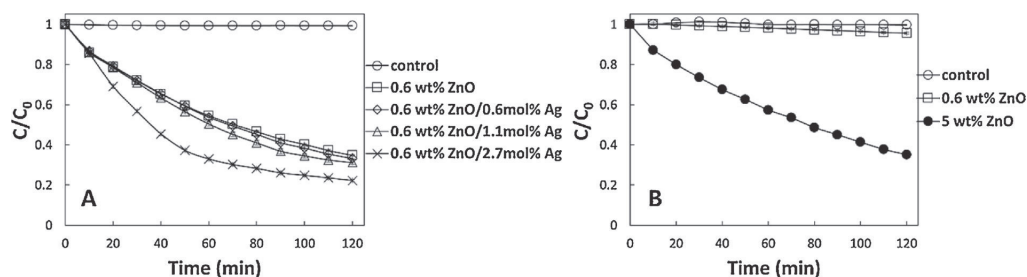


Fig. 3. Photocatalytic activity of ZnO and ZnO/Ag nanoparticles under UVA irradiation. A: 0.6 wt% ZnO and ZnO/Ag composite nanoparticle suspensions and B: $10 \times$ more diluted suspensions compared to A of 0.6 and 5 wt% ZnO nanoparticles in butanol. Control – model dye (brilliant blue FCF) solution. Graphs represent averages and standard deviations of three experiments. X-axis – UVA irradiation time (min). Y-axis – change in absorbance of model dye at characteristic wavelength (630 nm) (C/C_0).

2 μg Zn and 0, 0.005, 0.014 or 0.022 μg Ag (sparse coverage, prepared from 0.6 wt% ZnO suspension and ZnO/Ag suspensions) or 20 μg Zn/cm² (dense coverage, prepared from 5 wt% ZnO suspension) (Table 1).

Viewing of the prepared surfaces under SEM indicated even coverage of ZnO particles on all the prepared surfaces (Fig. 2). Although there was a clear difference between the coverage of surfaces prepared from 0.6 and 5 wt% ZnO suspensions, the even distribution of particles in both cases ensured the contact between microbial cells and nanoparticles in antimicrobial assay. In the first case, nanoparticles were placed on surfaces diffusely with 0.5–1 μm gaps between particle aggregates while in the second case, nanoparticles covered the surface almost entirely. Under SEM there was no visual difference between pure ZnO and Ag supplemented ZnO covered surfaces.

To support our hypothesis on improved photocatalytic activity of our ZnO/Ag composites compared to ZnO we characterized photodegradation of model dye by all nanoparticle suspensions. Clearly, addition of Ag showed increased efficacy compared to pure ZnO suspension (Fig. 3A), which proved our hypothesis on higher photocatalytic activity in the presence of transition metals. The most remarkable increase was seen with suspension with the highest Ag content (0.6 wt% ZnO/2.7 mol% Ag).

This increased photocatalytic activity has been claimed to be the result of added Ag acting as an electron sink and prolonging the lifetime of electron-hole pairs [12,26,35,36]. In addition to deposited Ag, the measured photodegradation of dye was dependent on the concentration of ZnO suspensions (Fig. 3B) and thus, eventually on the amount of ZnO on surfaces.

3.2. Antimicrobial efficacy of ZnO/Ag composite nanoparticle covered surfaces

Before discussing antimicrobial results in detail, we would like to emphasize that our in-house modification of ISO 27447 for the testing of non-porous photocatalytic surfaces enabled reliable quantitation of the decrease in viable microbial counts by about three logs (see Fig. 4). Thus, although it fulfills the requirement for 99.9% decrease of microbes on the surface as required by US standards [37–39] it does not allow the assessment of 4–5 logs decrease in microbial count as required by EN 13697 [40] and EN 13727 [41] for surfaces meant both for healthcare settings as well as for common use. Two bacterial strains, a Gram-negative bacterium *Escherichia coli*, a Gram-positive bacterium *Staphylococcus aureus*, and one yeast strain (*Candida albicans*) all of which are model organisms for potential pathogens were used for antimicrobial testing. Due to the photocatalytic activity of the prepared surfaces, the antimicrobial tests were conducted in parallel under UVA illumination and in the dark. In general, the antimicrobial effect of our ZnO and ZnO/Ag surfaces in dark conditions was relatively small as also shown by Thongsuriwong et al. [19]. Although being low, the toxic effect of surfaces in the dark was still statistically significant ($p < 0.001$) between control (uncoated glass) and ZnO covered surfaces after 60 min incubation (Fig. 5). The most significant antibacterial effect in the dark was observed for the highest Ag content sparse covered ZnO surface that killed *E. coli* (>3-log reduction) and caused 2.8-log reduction in viable counts of *S. aureus* after 1 h (Figs. 4 and S4).

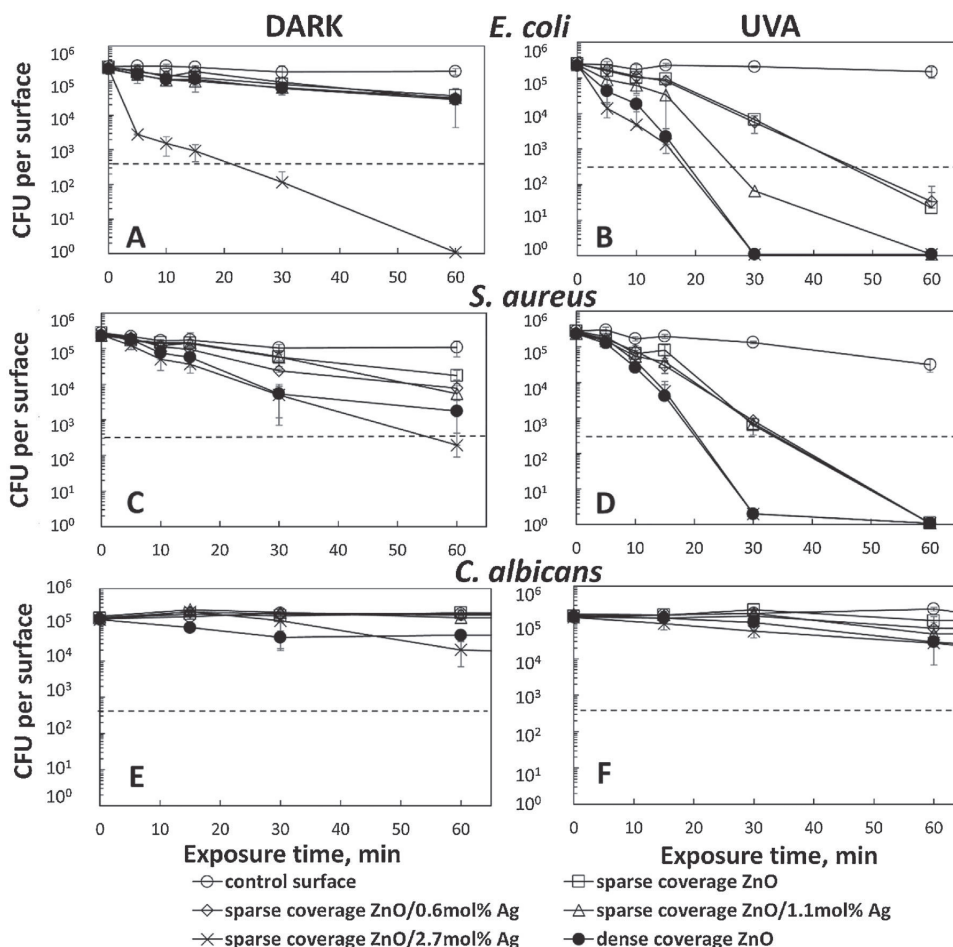


Fig. 4. Viability of microorganisms on ZnO and ZnO/Ag surfaces in the dark and under UVA illumination. Viability of *Escherichia coli* (A and B), *Staphylococcus aureus* (C and D), *Candida albicans* (E and F) exposed to ZnO and ZnO/Ag composite nanoparticle covered surfaces, expressed in colony forming units (CFU). Left – control surfaces kept in the dark. Right – UVA exposed surfaces. Graphs represent averages and standard deviations of three experiments. Dotted line: limit of quantification for CFUs.

In general, under the test conditions applied, *S. aureus* seemed to be more sensitive (0.8- and 1.8-log reduction on sparse and dense ZnO covered surfaces, respectively; $p < 0.001$) to surfaces compared to *E. coli* (0.7- and 0.8-log reduction, respectively; $p < 0.001$). *C. albicans* was the least sensitive species so that only dense coverage ZnO surface and sparse coverage ZnO surface with the highest Ag content demonstrated significant ($p < 0.01$) antimicrobial effect (0.6- and 1-log reduction in viable counts after 1 h; Fig. S4) compared to control.

We expected that the low but significant antimicrobial effects of ZnO and ZnO/Ag surfaces in dark exposure conditions were mainly caused by metal ions released from the surfaces. To control that, we quantified the Zn ion release from the surfaces (Fig. 6) and exposed microbial cells to the respective Zn^{2+} concentrations on uncoated glass. It could be expected that concentrations roughly corresponding to Zn^{2+} dissolution after 1 h are slightly more toxic in this experiment as on real surfaces the release of Zn^{2+} takes place over time and thus, microbial exposure is slower. Surprisingly the results (Fig. S5) showed no toxicity of Zn^{2+} ions to *S. aureus* or *C. albicans*, and significant toxicity was observed only to *E. coli* ($p < 0.001$)

(Fig. 5). However, for the latter similar toxicity was observed for all Zn^{2+} ion concentrations tested, and no concentration-dependence was seen (Fig. S5). The reason for higher sensitivity of *E. coli* toward Zn^{2+} ions could be related to its cell wall structure [42].

Comparison between surface and ionic toxicity (Fig. 5) shows expected results for *E. coli* and it could be plausible to explain surface toxicity in the dark with release of metal ions. For *E. coli* no significant difference in viability between sparse and dense ZnO coverage surfaces or respective Zn^{2+} ion concentrations was detected ($p > 0.9$). Interestingly, although Zn concentrations corresponding to dissolution from sparse or dense ZnO covered surfaces during 1 h were equally not toxic to *S. aureus* and *C. albicans*, corresponding surfaces themselves may demonstrate dose-dependent toxicity. Dense ZnO coverage surface demonstrated 1-log more reduction for *S. aureus* and 0.6-log more reduction in viable counts for *C. albicans* compared to sparse coverage ZnO surface. This difference is statistically significant for *C. albicans* ($p < 0.01$) and at first glance not significant for *S. aureus*. For the latter, type II error could be suspected as groups compared have notably unequal variance and this is known to reduce statistical power of one-way ANOVA

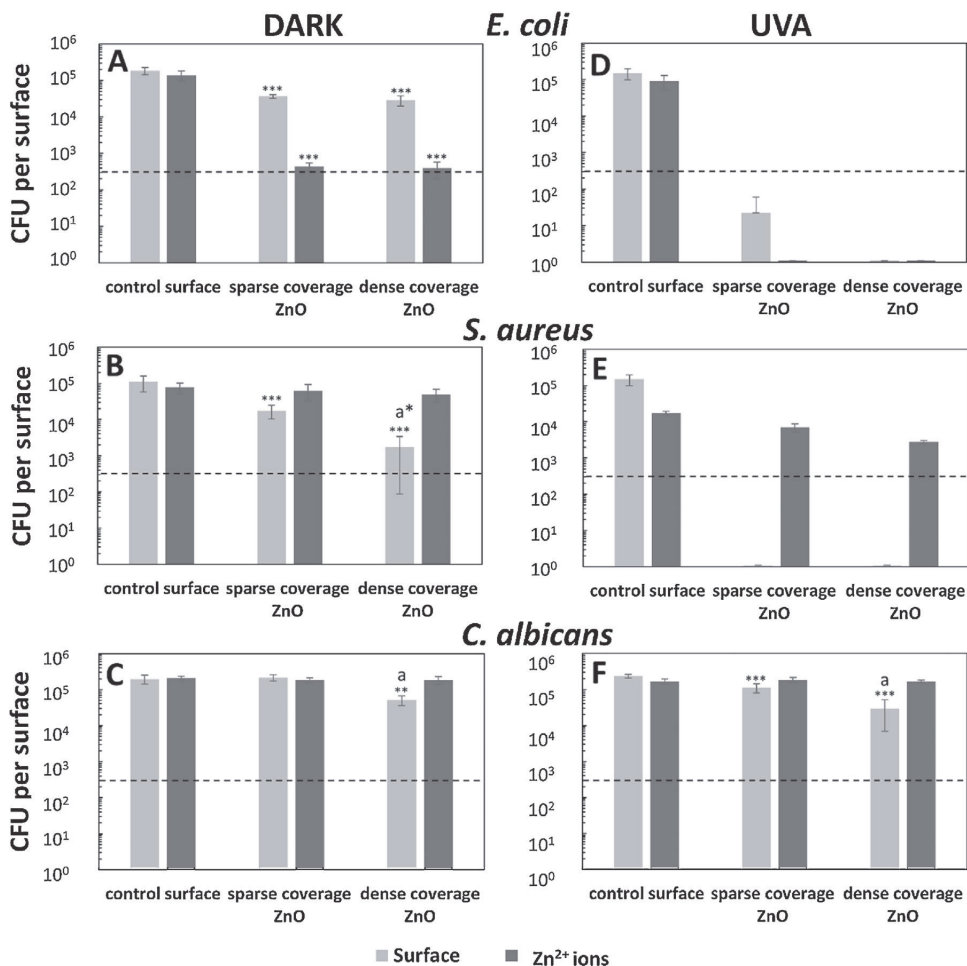


Fig. 5. Antimicrobial activity of ZnO and ZnO/Ag surfaces in comparison to the antimicrobial activity of Zn^{2+} ions in concentrations released from those surfaces. Decrease of CFUs of *E. coli* (A, D), *S. aureus* (B, E) and *C. albicans* (C, F) after 60 min incubation in no illumination conditions (A, B, C) or under UVA illumination (D, E, F) on ZnO or ZnO/Ag surfaces or with Zn^{2+} ions in concentrations released from those surfaces (Zn^{2+} ion concentration roughly corresponding to ZnO dissolution in 1:500 NB). *** $p < 0.001$, ** $p < 0.01$: statistically significant decrease in CFU count compared to control surface. a – decrease statistically significant compared to sparse coverage ZnO surface ($p < 0.05$). a* – statistically significant compared to sparse coverage ZnO surface ($p < 0.01$) according to two-tailed Student's *t*-test. Graphs represent averages and standard deviations of three experiments. Dotted line – limit of quantification for CFUs.

analysis combined with Tukey's HSD post hoc test. After the most variable group (non-treated control values) is removed from one-way ANOVA analysis the difference between sparse and dense ZnO covered surfaces becomes significant ($p = 0.00001$) and the same conclusion could be drawn from pairwise two-tailed Student's *t*-test ($p = 0.002$). Taking this into account, we can assume that metal ion release and resulting mean ion concentration does not explain surface toxicity in the dark for all tested organisms. This surface-specific phenomenon and underlying mechanisms of action should be further investigated.

Compared to antimicrobial activity in the dark, all the surfaces were notably more effective under UVA illumination (Figs. 4 and S4). This UVA-induced antimicrobial effect was lowest for *C. albicans* (the maximum decrease in fungal viable count was ~ 0.9 logarithms compared to control on sparse coverage ZnO/2.7mol% Ag surfaces and dense ZnO coverage surfaces after 60 min expo-

sure; Fig. 4F), likely due to higher resistance of fungal cells to ZnO surfaces compared to bacteria, as demonstrated for *S. aureus* and *C. albicans* by McCarthy et al. and Zeelie et al. [43,44]. In all cases, the UV-induced antimicrobial activity of the surfaces was dependent on their ZnO content: the densely covered surfaces were more effective than sparsely covered surfaces (Fig. 4). On dense coverage ZnO surfaces under UVA, 2.2 log reduction of *E. coli* and 1.7 log of *S. aureus* cells were observed within 15 min of exposure compared to control. After further incubation reduction in viable count exceeded our limit of quantification. This result indicated relatively fast antimicrobial activity of the surfaces upon illumination; indeed, as discussed by Villapun et al. [8], shorter killing times, even as short as 5 min, are preferred for practical applications and the current standards that foresee 24 h exposure times have been criticized due to their poor relevancy. Under UVA illumination, the addition of Ag to ZnO generally increased their antimicrobial

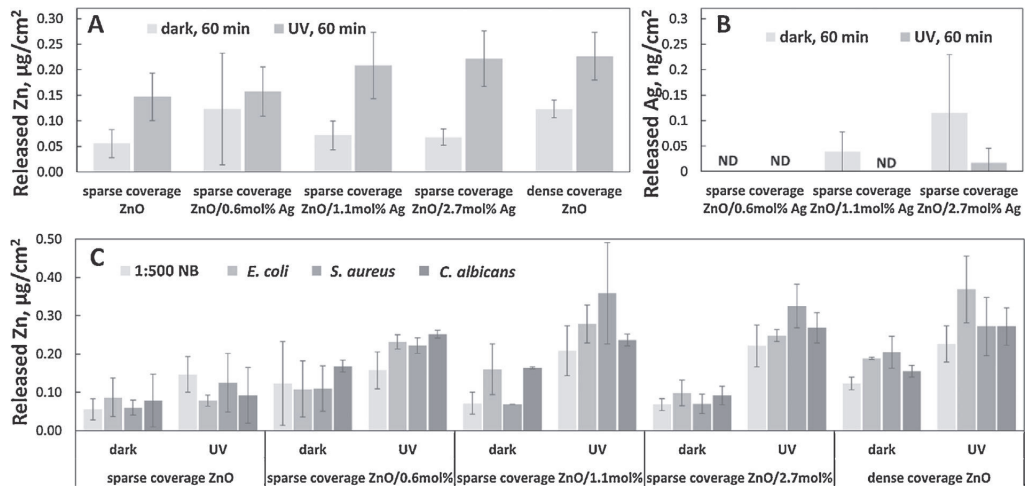


Fig. 6. Release of zinc and silver from ZnO and ZnO/Ag surfaces during testing. Zn (A) and Ag (B) dissolution during testing in 1:500 NB determined by TXRF and AAS analysis. C: comparison of Zn dissolution during testing in the presence of different microorganisms (*E. coli*, *S. aureus*, *C. albicans*). ND – not detected (<50 pg/cm²). Graphs represent averages and standard deviations of three experiments.

activity and the antibacterial effect of ZnO/Ag surfaces was significantly higher under UVA than in the dark. This was despite the fact that silver dissolution was decreased under UVA compared to dark conditions (Fig. 6B), probably due to photoreduction under UVA. When >3 logs reduction in *E. coli* viability on sparse coverage ZnO and sparse coverage ZnO/0.6mol% Ag surfaces was observed after 60 min UVA illumination, then on sparse coverage ZnO/1.1mol% Ag, and on sparse coverage ZnO/2.7mol% Ag surfaces already after 30 min UVA illumination (Fig. 4B) with the highest Ag content surface being most effective. Such dose effect for all three Ag-containing surfaces was not seen in case of dark exposure. In case of *S. aureus* neither lower Ag content (0.6 and 1.1 mol%) sparse coverage ZnO surface differed significantly from sparse ZnO coverage surface. However, sparse coverage ZnO/2.7mol% Ag surface had significantly higher UVA-induced activity than all the other sparse coverage ZnO surfaces (Fig. 4D) and demonstrated 1.2 log more reduction in viable count compared to sparse ZnO coverage surface already after 15 min. For *C. albicans* only the highest Ag content surface was significantly more effective than sparse ZnO covered surface after 1 h, but this difference was very small with only 0.6 logs reduction in viable count.

Similar to our results on high UVA-induced activity of ZnO/Ag surfaces Aladpoosh et al. showed good photocatalytic and antibacterial activity of Ag/ZnO particle covered cotton fabric under sunlight [45], however unmodified ZnO was not used as a reference in either case and therefore, the effect of Ag was not clear. Manna et al. showed 100% reduction of *S. aureus* and *P. aeruginosa* on Ag/ZnO covered cotton fabric after 4 h and 6 h incubation under visible light, respectively. At the same time, only 30% decrease in *S. aureus* and 50% decrease in *P. aeruginosa* cells was observed in similar conditions on non Ag-doped ZnO covered cotton. The authors also demonstrated increased zone-of-inhibition in case of Ag containing samples compared to ZnO only samples [30]. Although all the mentioned studies demonstrated increased antimicrobial activity of ZnO surfaces in the presence of Ag the results of these studies and many others are difficult to directly compare because of the differences in study set-ups [46], such as different relative humidity, aeration, culture density, medium, wet vs dry protocols etc.

3.3. Mechanisms of antimicrobial action of ZnO and ZnO/Ag surfaces

Taking into account the photocatalytic activity of ZnO and ZnO/Ag surfaces and the potential of those materials to release metal ions (Zn²⁺ and Ag⁺) (Fig. 6), we next evaluated the importance of those processes in UVA-induced antimicrobial effects of the surfaces. It is important to note that during the test no nanoparticles were released from the surfaces (Fig. S6) proving that the surfaces were rather stable and could only release ionic forms of Zn and Ag to exhibit antimicrobial effect.

As already discussed, photocatalysis-driven antimicrobial effect of the ZnO surfaces was clearly seen in our experiments: while only very low antimicrobial effect of sparse coverage ZnO surfaces was observed in the dark, under UVA three logarithm decrease in *S. aureus* and *E. coli* counts was observed within 30–60 min (Fig. 4). Theoretically for *E. coli*, this increased antibacterial activity of ZnO surfaces under UVA could be explained by greater Zn dissolution under UVA compared to the dark. However, the fact that ZnO surfaces were lacking dose effect in the dark but had very clear dose-dependent difference in activity under UVA confirms photocatalytic mechanism of toxicity. Also, the fact that for *S. aureus* both ZnO surfaces were drastically more effective under UVA than in the dark and that Zn at concentrations dissolved from surfaces was not toxic to this bacterium proves the contribution of photocatalytic effect. Indeed, the increased photocatalytic activity of more concentrated ZnO suspensions and consequently, more densely covered ZnO surfaces was shown by us in brilliant blue FCF degradation test. Our photodegradation assay indicated that similarly to increase in photocatalytic potential with increasing ZnO concentration, also addition of Ag to ZnO increased its photocatalytic activity (Fig. 3). Therefore, we suggest that increase in photocatalytic activity of ZnO/Ag surfaces could be behind the increased antimicrobial activity of Ag-doped ZnO surfaces under UVA illumination which was specifically evident for *E. coli* and *S. aureus* (Figs. 4 and S4).

Similar to our results also other previously published papers have shown that reactive oxygen species [35,47] and slow release of metal ions [30] are the main mechanisms driving the antimicrobial activity of ZnO/Ag containing material. We would like to emphasize that we observed the release of relatively low levels of Zn²⁺ ions

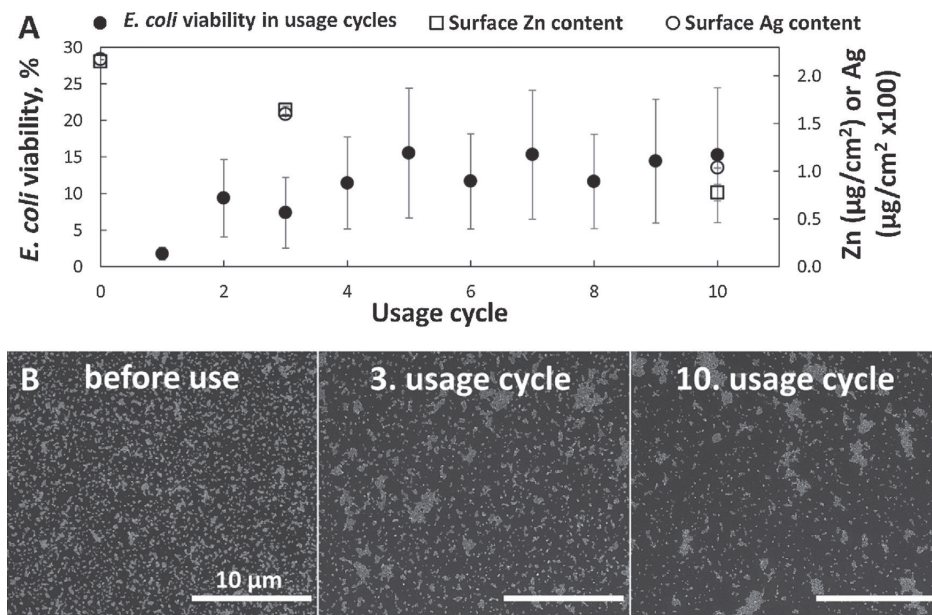


Fig. 7. Antimicrobial activity and appearance of sparse coverage ZnO/2.7mol% Ag surfaces during 10 usage cycles. A: *Escherichia coli* viability on the surfaces during 10 usage cycles, □ – Zn content on the surface ($\mu\text{g}/\text{cm}^2$), ○ – Ag content on the surface ($\mu\text{g}/\text{cm}^2 \times 100$). B: SEM images of surfaces before use and after 3 and 10 usage cycles. Scale bars correspond to 10 μm . Graph represents averages and standard deviations of three experiments.

from the surfaces in the dark and somewhat higher concentrations of Zn^{2+} under UVA illumination (Fig. 6A), likely due to photocorrosion [48]. For *S. aureus* and *C. albicans* this released amount of Zn was not enough to exert antimicrobial effect (Fig. S5). We suggest the possibility for additional release of Zn in near-surface microenvironment in the presence of different organisms. Similar process has been suggested by Joe et al. who claimed that local dissolution of ZnO near bacteria can cause antibacterial activity which can't be solely explained by overall ZnO dissolution [49]. It should be further investigated if some organisms are more exposed to near-surface microenvironment than others, for example because of their size and weight, tendency to cluster together rather than float free or differences in biofilm forming. The presumption of different levels of exposure to surface for different organisms due to their specific characteristics discussed above could explain our findings in dark exposure. It is not clear what could be the precise mechanism of toxicity in near surface microenvironment and if only higher local ion concentration near the source of ions could be the cause or are there additional mechanisms of action. For example, Prasanna and Vijayaraghavan have demonstrated the formation of reactive oxygen species (ROS) on the surface of ZnO particles in water environment in dark conditions [50]. In our study the production of ROS during testing was not evaluated and therefore further research is needed to conclusively distinguish between ionic effect and effect caused by active oxygen species as well as to confirm or reject possible ROS mediated mechanism for effects observed in dark exposure conditions as discussed above.

3.4. Reusability of ZnO/Ag surfaces

Reusability of nanoparticle covered antimicrobial surfaces is extremely important for practical applications. Thus, sparse coverage ZnO/2.7mol% Ag surfaces were tested for their antibacterial efficacy during ten cycles that consisted of inoculation of the surfaces with *E. coli*, 15-min UVA light exposure, rinsing and steril-

ization. As expected, the highest antibacterial efficacy was observed for unused surfaces, but significant antibacterial activity was still observed even after 10 use-rinse-sterilization cycles (Fig. 7A).

Antibacterial efficiency gradually decreased during first 4 usage cycles and remained quite unchanged from cycle 4–10. At the same time, Zn and Ag content on surfaces decreased (during 10 washing cycles from 2.2 μg Zn to 0.8 μg Zn/ cm^2 and from 0.02 μg Ag to 0.01 μg Ag/ cm^2) as proven by TXRF and AAS analysis (Fig. 7A). Likewise, the photodegradation capability of model dye by covered surfaces did not remarkably decrease even after 10 usage cycles (Fig. S7). SEM images of the unused and reused surfaces after 3 and 10 cycles of antibacterial testing, subsequent rinsing and sterilization indicated particle aggregation (Fig. 7B). Aggregation can be attributed to particle mobility which was possible while surfaces were drying after cleaning and we suggest that along with dissolution of Zn and Ag from the surfaces this aggregation of particles could be one of the reasons for the slight decrease of antibacterial and photodegradation activity of our surfaces during 10 usage cycles. According to our knowledge, our study is the first to demonstrate the reusability of ZnO/Ag surfaces for antimicrobial applications. In previous studies only the retainment of Raman scattering ability of ZnO/Ag nanoarray on Si after 3 usage cycles [51] and catalytic ability of Ag/ZnO impregnated cotton fabric after 5 usage cycles [30] has been shown. Manna et al. showed no Ag leaching from Ag/ZnO treated cotton fabric after 5 h incubation and hence considered the surfaces to be stable [30] and similarly, ZnO/Ag particles have been considered stable photocatalysts after several usage cycles [16,27,52,53].

4. Conclusions

ZnO/Ag surfaces designed in the current study exhibited significant antibacterial activity under UVA illumination killing $\geq 99.9\%$ *E. coli* and *S. aureus* bacteria within 30 min on most surfaces. The main mechanism behind the antimicrobial activity of ZnO/Ag surfaces was a combination of photocatalytic activity and release of

Zn²⁺ and Ag⁺ ions from the surfaces with minor surface-specific antimicrobial activity observed in dark conditions that could not be fully explained by ion release. Compared to bacterial cells, fungal cells (*Candida albicans*) were significantly more resistant towards the prepared surfaces and required longer exposure times to reduce viability. Prepared surfaces retained significant antimicrobial and photocatalytic properties even after repeated use. In further work, the designed ZnO/Ag composite particles will be incorporated into solid matrix for various practical applications.

Disclosure statement

The authors confirm that there is no conflict of interest.

Acknowledgements

Funding: This work was supported by the Estonian Ministry of Education and Research [PUT748, IUT2-25, PUT1096, IUT 23-5, IUT2-24]; the Estonian Centre of Excellence in Research Projects “Emerging orders in quantum and nanomaterials (TK134)” and “Advanced materials and high-technology devices for sustainable energetics, sensorics and nanoelectronics (TK141)”; Graduate School of Functional materials and technologies receiving funding from the European Regional Development Fund in University of Tartu, Estonia. The authors would like to thank Dr. Urmas Joost for consultations about nanoparticle synthesis, MSc Aivar Tarre for help with XRD measurements and MSc Rando Saar for SEM imaging.

Appendix A. Supplementary data

Supplementary data associated with this article can be found, in the online version, at <https://doi.org/10.1016/j.colsurfb.2018.05.009>.

References

- S.S. Magill, J.R. Edwards, W. Bamberg, Z.G. Beldavs, G. Dumyati, M.A. Kainer, R. Lynfield, M. Maloney, L. McAllister-Hollod, J. Nadle, S.M. Ray, D.L. Thompson, L.E. Wilson, S.K. Fridkin, Multistate point-prevalence survey of health care-associated infections, *N. Engl. J. Med.* 370 (2014) 1198–1208, <http://dx.doi.org/10.1056/NEJMoa1306801>.
- European Centre for Disease Prevention and Control, Point Prevalence Survey of Healthcare Associated Infections and Antimicrobial Use in European Acute Care Hospitals, ECDC, Stockholm, 2013.
- S. Pogodin, J. Hasan, V.A. Baulin, H.K. Webb, V.K. Truong, T.H. Phong Nguyen, V. Boshkovič, C.J. Fluke, G.S. Watson, J.A. Watson, R.J. Crawford, E.P. Ivanova, Biophysical model of bacterial cell interactions with nanopatterned cicada wing surfaces, *Biophys. J.* 105 (2013) 835–840, <http://dx.doi.org/10.1016/j.bpj.2012.12.046>.
- B. Gottenbos, D.W. Grijpma, H.C. Mei, J. Feijen, H.J. Busscher, Antimicrobial effects of positively charged surfaces on adhering gram-positive and gram-negative bacteria, *J. Antimicrob. Chemother.* 48 (2001) 7–13, <http://dx.doi.org/10.1093/jac/48.1.7>.
- N. Cerca, S. Martins, G.B. Pier, R. Oliveira, J. Azeredo, The relationship between inhibition of bacterial adhesion to a solid surface by sub-MICs of antibiotics and subsequent development of a biofilm, *Res. Microbiol.* 156 (2005) 650–655, <http://dx.doi.org/10.1016/j.resmic.2005.02.004>.
- G. Grass, C. Rensing, M. Solioz, Metallic copper as an antimicrobial surface, *Appl. Environ. Microb.* 77 (5) (2011) 1541–1547, <http://dx.doi.org/10.1128/AEM.02766-10>.
- J.A. Lemire, J.J. Harrison, R.J. Turner, Antimicrobial activity of metals: mechanisms, molecular targets and applications, *Nat. Rev. Microbiol.* 11 (2013) 371–384, <http://dx.doi.org/10.1038/nrmicro3028>.
- V.M. Villapun, L.G. Dover, A. Cross, S. Gonzales, Antibacterial metallic touch surfaces, *Materials* 9 (2016) 736, <http://dx.doi.org/10.3390/ma9090736>.
- H.A. Foster, I.B. Ditta, S. Varghese, A. Steele, Photocatalytic disinfection using titanium dioxide: spectrum and mechanism of antimicrobial activity, *Appl. Microbiol. Biotechnol.* 90 (2011) 1847–1868, <http://dx.doi.org/10.1007/s00253-011-3213-7>.
- A. Kubacka, M.S. Diez, D. Rojo, R. Bargiela, S. Ciordia, I. Zapico, J.A. Albar, C. Barbas, V.A.M.P. Santos, M. Fernandez-Garcia, M. Ferrer, Understanding the antimicrobial mechanism of TiO₂-based nanocomposite films in a pathogenic bacterium, *Sci. Rep.* 4 (2014) 4134, <http://dx.doi.org/10.1038/srep04134>.
- A. Sirelkhatim, S. Mahmud, A. Seeni, N.H.M. Kaus, L.C. Ann, S.K.M. Bakhori, H. Hasan, D. Mohamad, Review on zinc oxide nanoparticles: antibacterial activity and toxicity mechanism, *Nano-Micro Lett.* 7 (2015) 219–242, <http://dx.doi.org/10.1007/s40820-015-0040-x>.
- Y. Zheng, L. Zheng, Y. Zhan, X. Lin, Q. Zheng, K. Wei, Ag/ZnO heterostructure nanocrystals: synthesis, characterization, and photocatalysis, *Inorg. Chem.* 46 (2007) 6980–6986, <http://dx.doi.org/10.1021/jc700688f>.
- W. Lu, G. Liu, S. Gao, S. Xing, J. Wang, Tyrosine-assisted preparation of Ag/ZnO nanocomposites with enhanced photocatalytic performance and synergistic antibacterial activities, *Nanotechnology* 19 (2008) 445711, <http://dx.doi.org/10.1088/0957-4484/19/44/445711>.
- C. Ren, B. Yang, M. Wu, J. Xu, Z. Fu, Y. Lv, T. Guo, Y. Zhao, C. Zhu, Synthesis of Ag/ZnO nanorods array with enhanced photocatalytic performance, *J. Hazard. Mater.* 182 (2010) 123–129, <http://dx.doi.org/10.1016/j.jhazmat.2010.05.141>.
- R. Georgekutty, M.K. Seery, S.C. Pillai, A highly efficient Ag-ZnO photocatalyst: synthesis, properties, and mechanism, *J. Phys. Chem. C* 112 (2008) 13563–13570, <http://dx.doi.org/10.1021/jp802729a>.
- F. Sun, F. Tan, W. Wang, X. Qiao, X. Qiu, Facile synthesis of Ag/ZnO heterostructure nanocrystals with enhanced photocatalytic performance, *Mater. Res. Bull.* 47 (2012) 3357–3361, <http://dx.doi.org/10.1016/j.materresbull.2012.07.025>.
- M.A. Thomas, J.B. Cui, Electrochemical route to p-type doping of ZnO nanowires, *J. Phys. Chem. Lett.* 1 (2010) 1090–1094, <http://dx.doi.org/10.1021/jz100246e>.
- K. Awazu, M. Fujimaki, C. Rockstuhl, J. Tominaga, H. Murakami, Y. Ohki, N. Yoshida, T. Watanabe, A plasmonic photocatalyst consisting of silver nanoparticles embedded in titanium dioxide, *J. Am. Chem. Soc.* 130 (2008) 1676–1680, <http://dx.doi.org/10.1021/ja076503n>.
- K. Thongsuriwong, P. Amornpitoksuk, S. Suwanboon, Photocatalytic and antibacterial activities of Ag-doped ZnO thin films prepared by a sol-gel dip-coating method, *J. Sol-Gel Sci. Technol.* 62 (2012) 304–312, <http://dx.doi.org/10.1007/s10971-012-2725-7>.
- A. Ivask, I. Kurvet, K. Kasemets, I. Blinova, V. Aruoja, S. Suppi, H. Vija, A. Käkinen, T. Titma, M. Heinlaan, M. Visnapuu, D. Koller, V. Kisand, A. Kahru, Size-dependent toxicity of silver nanoparticles to bacteria, yeast, algae, crustaceans and mammalian cells in vitro, *PLoS One* 9 (7) (2014) e102108, <http://dx.doi.org/10.1371/journal.pone.0102108>.
- M. Visnapuu, U. Joost, K. Juganson, K. Künnis-Beres, A. Kahru, V. Kisand, A. Ivask, Dissolution of silver nanowires and nanospheres dictates their toxicity to *Escherichia coli*, *BioMed Res. Int.* 81925 (2013) 2, <http://dx.doi.org/10.1155/2013/819252>.
- C. Pacholski, A. Kornowski, H. Weller, Site-specific photodeposition of silver on ZnO nanorods, *Angew. Chem. Int. Ed.* 43 (2004) 4774–4777, <http://dx.doi.org/10.1002/anie.200453880>.
- T.-L. Li, S.L.-C. Hsu, Preparation and properties of conductive polyimide nanocomposites with assistance of a metallo-organic compound, *J. Mater. Chem.* 20 (2010) 1964–1969, <http://dx.doi.org/10.1039/b916101e>.
- S.-K. Tzeng, M.-H. Hon, I.-C. Leu, Improving the performance of a zinc oxide nanowire ultraviolet photodetector by adding silver nanoparticles, *J. Electrochem. Soc.* 159 (2012) H440–H443, <http://dx.doi.org/10.1149/2.088204jes>.
- International Standardization for Organization, ISO 27447:2009 Fine ceramics (advanced ceramics, advanced technical ceramics)—Test method for antibacterial activity of semiconductor photocatalytic materials, 2009.
- O. Bechambi, M. Chalbi, W. Najjar, S. Sayadi, Photocatalytic activity of ZnO doped with Ag on the degradation of endocrine disrupting under UV irradiation and the investigation of its antibacterial activity, *Appl. Surf. Sci.* 347 (2015) 414–420, <http://dx.doi.org/10.1016/j.apsusc.2015.03.049>.
- Q. Deng, X. Duan, D.H.L. Ng, H. Tang, Y. Yang, M. Kong, Z. Wu, W. Cai, G. Wang, Ag nanoparticle decorated nanoporous ZnO microrods and their enhanced photocatalytic activities, *ACS Appl. Mater. Interfaces* 4 (2012) 6030–6037, <http://dx.doi.org/10.1021/am301682g>.
- A. Meng, J. Xing, Z. Li, Q. Wei, Q. Li, Ag/AgCl/ZnO nano-networks: preparation, characterization, mechanism and photocatalytic activity, *J. Mol. Catal. A—Chem.* 411 (2016) 290–298, <http://dx.doi.org/10.1016/j.molcata.2015.10.037>.
- K. Saoud, R. Alsoubaihi, N. Bensalah, T. Bora, M. Bertino, J. Dutta, Synthesis of supported silver nano-spheres on zinc oxide nanorods for visible light photocatalytic applications, *Mater. Res. Bull.* 63 (2015) 134–140, <http://dx.doi.org/10.1016/j.materresbull.2014.12.001>.
- J. Manna, S. Goswami, N. Shilpa, N. Sahu, R.K. Rana, Biomimetic method to assemble nanostructured Ag@ZnO on cotton fabrics: application as self-cleaning flexible materials with visible-light photocatalysis and antibacterial activities, *ACS Appl. Mater. Interfaces* 7 (2015) 8076–8082, <http://dx.doi.org/10.1021/acsami.5b06633>.
- A. Behzadnia, M. Montazer, M.M. Rad, In situ photo-synthesis and characterize nonmetal/metal dual doped honeycomb-like ZnO nanocomposites on wool fabric, *Ultrason. Sonochem.* 27 (2015) 200–209, <http://dx.doi.org/10.1016/j.ultsonch.2015.05.021>.
- D.D. Evanoff, G. Chumanov, Synthesis and optical properties of silver nanoparticles and arrays, *ChemPhysChem* 6 (2005) 1221–1231, <http://dx.doi.org/10.1002/cphc.200500113>.
- Y. Liu, S. Wei, W. Gao, Ag/ZnO heterostructures and their photocatalytic activity under visible light: effect of reducing medium, *J. Hazard. Mater.* 287 (2015) 59–68, <http://dx.doi.org/10.1016/j.jhazmat.2014.12.045>.
- R.A. Salkar, P. Jeevanandam, S.T. Aruna, Y. Koltypin, A. Gedanken, The sonochemical preparation of amorphous silver nanoparticles, *J. Mater. Chem.* 9 (1999) 1333–1335, <http://dx.doi.org/10.1039/A900568D>.

- [35] X. Pan, L. Peng, Y. Liu, J. Wang, Highly antibacterial and toughened polystyrene composites with silver nanoparticles modified tetrapod-like zinc oxide whiskers, *J. Appl. Polym. Sci.* (2014) 40900, <http://dx.doi.org/10.1002/app.40900>.
- [36] S. Pyne, G.P. Sahoo, D.K. Bhui, H. Bar, P. Sarkar, S. Samanta, A. Maity, A. Misra, Enhanced photocatalytic activity of metal coated ZnO nanowires, *Spectrochim. Acta A* 93 (2012) 100–105, <http://dx.doi.org/10.1016/j.saa.2012.02.050>.
- [37] United States Environmental Protection Agency, Test Method for the Continuous Reduction of Bacterial Contamination on Copper Alloy Surfaces, 2009.
- [38] United States Environmental Protection Agency, Test Method for the Residual Self-Sanitizing Activity of Copper Alloy Surfaces.
- [39] United States Environmental Protection Agency, Test Method for Efficacy of Copper Alloy Surfaces as a Sanitizer.
- [40] European Standard, EN 13697:2015 Chemical disinfectants and antiseptics—Quantitative non-porous surface test for the evaluation of bactericidal and/or fungicidal activity of chemical disinfectants used in food, industrial, domestic and institutional areas—Test method and requirements without mechanical action (phase 2, step 2), 2015.
- [41] European Standard, EN 13727:2012 + A2:2015 Chemical disinfectants and antiseptics. Quantitative suspension test for the evaluation of bactericidal activity in the medical area. Test method and requirements (phase 2, step 1), 2015.
- [42] M.K. Rai, S.D. Deshmukh, A.P. Ingle, A.K. Gade, Silver nanoparticles: the powerful nanoweapon against multidrug-resistant bacteria, *J. Appl. Microbiol.* 112 (2012) 841–852, <http://dx.doi.org/10.1111/j.1365-2672.2012.05253.x>.
- [43] T.J. McCarthy, J.J. Zeelie, D.J. Krause, The antimicrobial action of zinc ion/antioxidant combinations, *J. Clin. Pharm. Ther.* 17 (1992) 51–54, <http://dx.doi.org/10.1111/j.1365-2710.1992.tb01265.x>.
- [44] J.J. Zeelie, T.J. McCarthy, Effects of copper and zinc ions on the germicidal properties of two popular pharmaceutical antiseptic agents cetylpyridinium chloride and povidone-iodine, *Analyst* 123 (1998) 503–507, <http://dx.doi.org/10.1039/a704895e>.
- [45] R. Aladpoosh, M. Montazer, Nano-photo active cellulosic fabric through in situ phytosynthesis of star-like Ag/ZnO nanocomposites: investigation and optimization of attributes associated with photocatalytic activity, *Carbohydr. Polym.* 141 (2016) 116–125, <http://dx.doi.org/10.1016/j.carbpol.2016.01.005>.
- [46] M.D. Campos, P.C. Zucchi, A. Phung, S.N. Leonard, E.B. Hirsch, The activity of antimicrobial surfaces varies by testing protocol utilized, *PLoS One* 11 (2016) 8, <http://dx.doi.org/10.1371/journal.pone.0160728>.
- [47] K. Hirota, M. Sugimoto, M. Kato, K. Tsukagoshi, T. Tanigawa, H. Sugimoto, Preparation of zinc oxide ceramics with a sustainable antibacterial activity under dark conditions, *Ceram. Int.* 36 (2) (2010) 497–506, <http://dx.doi.org/10.1016/j.ceramint.2009.09.026>.
- [48] Y.Q. Cao, J. Chen, H. Zhou, L. Zhu, X. Li, Z.Y. Cao, D. Wu, A.D. Li, Photocatalytic activity and photocorrosion of atomic layer deposited ZnO ultrathin films for the degradation of methylene blue, *Nanotechnology* 26 (2015) 024002, <http://dx.doi.org/10.1088/0957-4484/26/2/024002>.
- [49] A. Joe, S.-H. Park, K.-D. Shim, D.-J. Kim, K.-H. Jhee, H.-W. Lee, C.-H. Heo, H.-M. Kim, E.-S. Jang, Antibacterial mechanism of ZnO nanoparticles under dark conditions, *J. Ind. Eng. Chem.* 45 (2017) 430–439, <http://dx.doi.org/10.1016/j.jiec.2016.10.013>.
- [50] V.L. Prasanna, R. Vijayaraghavan, Insight into the mechanism of antibacterial activity of ZnO: surface defects mediated reactive oxygen species even in the dark, *Langmuir* 31 (2015) 9155–9162, <http://dx.doi.org/10.1021/acs.langmuir.5b02266>.
- [51] A.E. Kandjani, M. Mohammadtaheri, A. Thakkar, S.K. Bhargava, V. Bansal, Zinc oxide/silver nanoarrays as reusable SERS substrates with controllable 'hot-spots' for highly reproducible molecular sensing, *J. Colloid. Interf. Sci.* 436 (2014) 251–257, <http://dx.doi.org/10.1016/j.jcis.2014.09.017>.
- [52] M. Hosseini-Sarvari, T. Ataee-Kachouei, F. Moeini, Preparation, characterization, and catalytic application of nano Ag/ZnO in the oxidation of benzylic C–H bonds in sustainable media, *RSC Adv.* 5 (2015) 9050–9056, <http://dx.doi.org/10.1039/C4RA12396D>.
- [53] B. Krishnakumar, B. Subash, M. Swaminathan, AgBr-ZnO—an efficient nano-photocatalyst for the mineralization of Acid Black 1 with UV light, *Sep. Purif. Technol.* 85 (2012) 35–44, <http://dx.doi.org/10.1016/j.seppur.2011.09.037>.

Supplementary material for

UVA-induced antimicrobial activity of ZnO/Ag nano-composite covered surfaces

Meeri Visnapuu^{a,b}, Merilin Rosenberg^{b,c}, Egle Truska^{b,c}, Ergo Nõmmiste^{a,d}, Andris Šutka^{a,e}, Anne Kahru^{b,d}, Mihkel Rähn^a, Heiki Vija^b, Kaja Orupõld^f, Vambola Kisand^{a*}, Angela Ivask^{b*}

^a*Institute of Physics, University of Tartu, W. Ostwaldi Str 1, 50411, Tartu, Estonia*

^b*National Institute of Chemical Physics and Biophysics, Akadeemia tee 23, 12618, Tallinn, Estonia*

^c*Tallinn University of Technology, Ehitajate tee 5, 19086, Tallinn, Estonia*

^d*Estonian Academy of Sciences, Kohtu 6, Tallinn, Estonia*

^e*Research Laboratory of Functional Materials Technologies, P. Valdena 3/7, LV-1048, Riga, Latvia*

^f*Estonian University of Life Sciences, Fr. R. Kreutzwaldi 1, 51014, Tartu, Estonia*

* Corresponding authors: angela.ivask@kbfi.ee, vambola.kisand@ut.ee

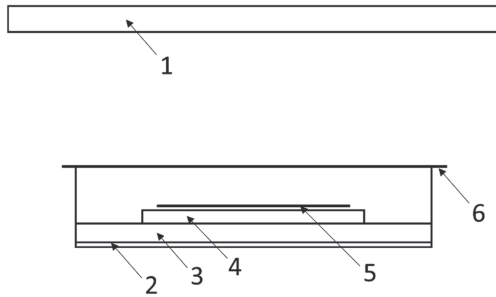


Figure S1. Test setup for antimicrobial testing in a Petri dish. 1- UVA light source, 2- sterile wet filter paper, 3- U-shaped glass rod, 4- 25x25 mm test surface, 5- 20x20x0.05 mm polyethylene cover film, 6- borosilicate moisture preservation glass. For UVA exposures, a self-built fluorescent Hg lamp consisting of 4 fluorescent light bulbs was used. The distance between light bulbs and test surfaces was 55 cm. Light intensity was further attenuated by placing two metal wire grids directly below light bulbs. Light intensity at test surface height was 2.7-3.2 W/m² at 315-400 nm spectral range.

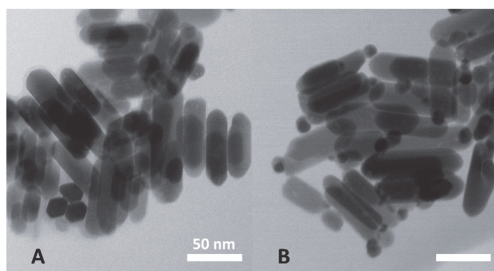


Figure S2. Transmission electron microscopy images of ZnO and ZnO/Ag nanoparticles. A: ZnO nanoparticles, B: 0.6 wt% ZnO/2.7mol% Ag nanoparticles. Scale bars correspond to 50 nm.

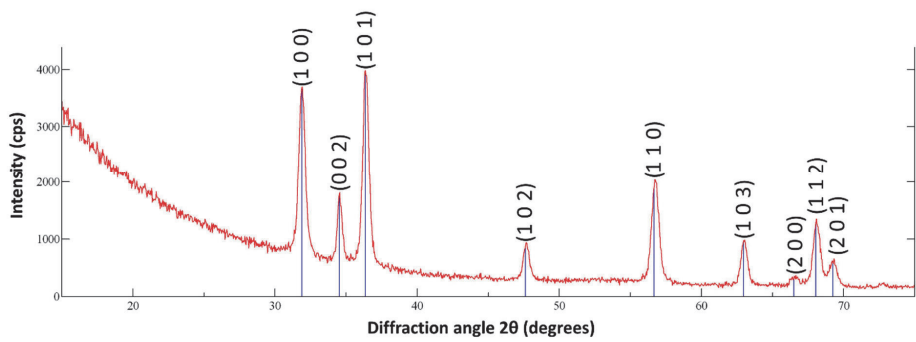


Figure S3. X-ray diffractogram of ZnO/Ag composite nanoparticle coating on silica monocrystal wafer. All detected peaks are characteristic to different crystal lattice planes of ZnO as shown on the graph [ICDD PDF2011, 01-070-8072].

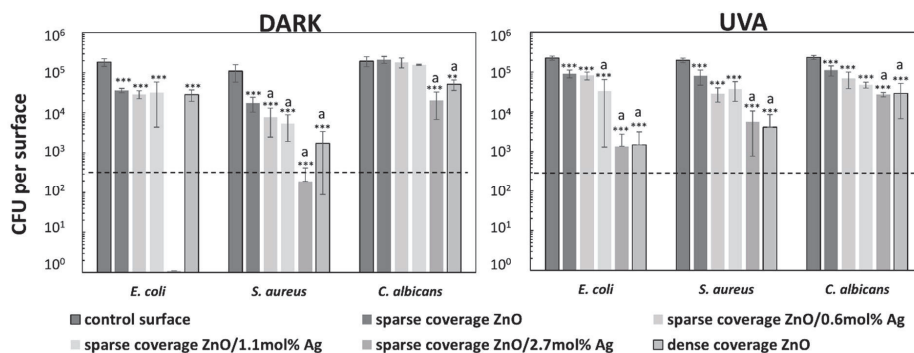


Figure S4. Viability of microorganisms on ZnO and ZnO/Ag surfaces after 60 min incubation in dark conditions and either 15 min (*E. coli*, *S. aureus*) or 60 min (*C. albicans*) under UVA illumination. Decrease statistically significant compared to control surface: *** $p < 0.001$, ** $p < 0.01$. a – decrease statistically significant compared to sparse coverage ZnO surface ($p < 0.05$). Graphs represent averages and standard deviations of three experiments. Dotted line – limit of quantification for CFUs.

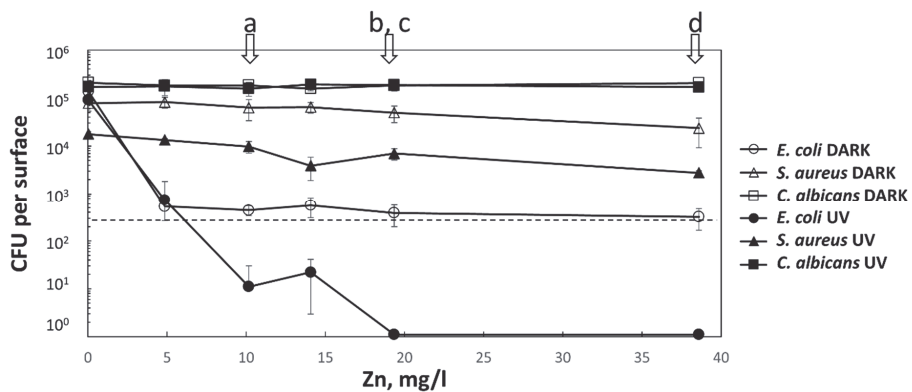


Figure S5. Antimicrobial effect of Zn²⁺ ions after 60 min incubation under UVA illumination or in no illumination conditions. Arrows indicate Zn concentrations representing Zn dissolved after 60 min incubation from sparse covered ZnO surface in dark conditions (a), sparse covered ZnO surface under UVA (b), dense covered ZnO surfaces in dark conditions (c) and dense covered ZnO surface under UVA (d). Graph represents averages and standard deviations of three experiments. Dotted line – limit of quantification for CFUs.

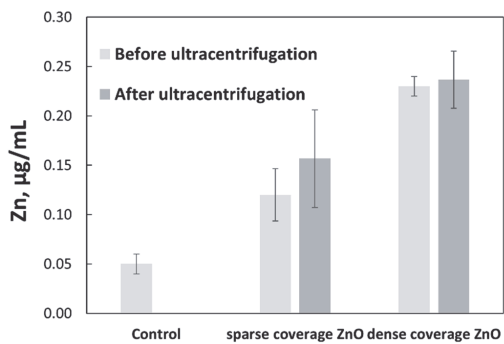


Figure S6. Removal of Zn from washoff from sparse and dense coverage ZnO surfaces after 60 min incubation by ultracentrifugation. Similar Zn content before (light grey bars) and after (dark grey bars) centrifugation indicate that no ZnO particles were released from the surface during testing. Graph represents averages and standard deviations of three experiments.

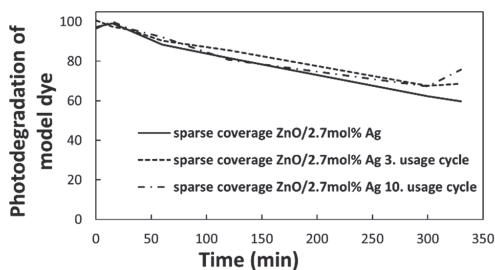


Figure S7. Photocatalytic activity of sparse coverage ZnO/2.7mol% Ag surfaces before and after reuse. X-axis – UVA irradiation time (min). Y-axis – change in characteristic peak area (520-800 nm) of model dye (brilliant blue FCF) (shown as percentage of initial intensity). Particle covered surfaces were coated with a thin layer of 15 mM aqueous dye (brilliant blue FCF) solution using spin-coating (3000 rpm). The photocatalytic reaction was conducted in a climatic chamber (Memmert CTC 256) at 25 °C and 70 RH% under 2.5 W/m² UVA irradiation provided by fluorescent Hg lamp ($\lambda_{\text{max}} = 355$ nm). Prior to irradiation the samples were kept in the climatic chamber in the dark for 1 h to establish adsorption equilibrium of model dye. After given irradiation times the samples were removed from climatic chamber and UV-Vis absorption was measured using UV-Vis spectrophotometer (Cary 5000 UV-Vis-NIR). In dark controls, the surfaces were kept in the climatic chamber without UVA irradiation and pure glass surfaces served as controls without nanoparticle coating. All measurements were done in three parallels. To evaluate photocatalytic degradation, the brilliant blue FCF characteristic UV-Vis absorption peak (520-800 nm) of each sample was measured, spectral background was removed, and absorption peak area was calculated. All spectral areas were normalized respective to initial area before UVA irradiation.

Publication IV

Rosenberg, M.; Visnapuu, M.; Vija, H.; Kisand, V.; Kasemets, K.; Kahru, A.; Ivask, A. (2020). Selective anti-biofilm properties and biocompatibility of nano-ZnO and nano-ZnO/Ag coated surfaces. *Scientific Reports*, 10(1). DOI:10.1038/s41598-020-70169-w

© The Author(s) 2020. This article is licensed under a Creative Commons Attribution 4.0 International License, which permits use, sharing, adaptation, distribution and reproduction in any medium or format, as long as you give appropriate credit to the original author(s) and the source, provide a link to the Creative Commons license, and indicate if changes were made. The images or other third party material in this article are included in the article's Creative Commons license, unless indicated otherwise in a credit line to the material. <https://creativecommons.org/licenses/by/4.0/>



OPEN

Selective antibiofilm properties and biocompatibility of nano-ZnO and nano-ZnO/Ag coated surfaces

M. Rosenberg^{1,2✉}, M. Visnapuu³, H. Vija¹, V. Kisand³, K. Kasemets¹, A. Kahru^{1,4} & A. Ivask^{1,5}

Spread of pathogenic microbes and antibiotic-resistant bacteria in health-care settings and public spaces is a serious public health challenge. Materials that prevent solid surface colonization or impede touch-transfer of viable microbes could provide means to decrease pathogen transfer from high-touch surfaces in critical applications. ZnO and Ag nanoparticles have shown great potential in antimicrobial applications. Less is known about nano-enabled surfaces. Here we demonstrate that surfaces coated with nano-ZnO or nano-ZnO/Ag composites are not cytotoxic to human keratinocytes and possess species-selective medium-dependent antibiofilm activity against *Escherichia coli*, *Staphylococcus aureus* and *Candida albicans*. Colonization of nano-ZnO and nano-ZnO/Ag surfaces by *E. coli* and *S. aureus* was decreased in static oligotrophic conditions (no planktonic growth). Moderate to no effect was observed for bacterial biofilms in growth medium (supporting exponential growth). Inversely, nano-ZnO surfaces enhanced biofilm formation by *C. albicans* in oligotrophic conditions. However, enhanced *C. albicans* biofilm formation on nano-ZnO surfaces was effectively counteracted by the addition of Ag. Possible selective enhancement of biofilm formation by the yeast *C. albicans* on Zn-enabled surfaces should be taken into account in antimicrobial surface development. Our results also indicated the importance of the use of application-appropriate test conditions and exposure medium in antimicrobial surface testing.

Biofilms are by far the preferred lifestyle of bacteria¹, mostly in diverse nutrient-limited environmental niches. Biofilm communities cause biomass buildup on solid surfaces that results in major expenses in marine traffic, water systems maintenance and in the industrial sector. Biofilms can also harbor potential human pathogens in food industry, health-care facilities, drinking water systems and on high-touch surfaces in public spaces. It is estimated that hard to treat pathogenic biofilms account for over 80% of all human microbial infections² with antibiotic-resistant ESKAPE pathogens³ including six nosocomial pathogens commonly associated with multidrug resistance and virulence (*Enterococcus faecium*, *Staphylococcus aureus*, *Klebsiella pneumoniae*, *Acinetobacter baumannii*, *Pseudomonas aeruginosa*, *Enterobacter spp.*) being the most problematic in the field. Biofilms pose a major medical challenge as they can be over 1,000-fold more tolerant to antibiotics than their planktonic counterparts⁴. Spatially heterogeneous natural selection in biofilm milieu also contributes to antibiotic resistance development and transfer^{5,6} as well as producing antibiotic-resistant bacteria that are more fit and not easily outcompeted in the absence of the drug⁷.

Controversially, most of the methods used to assess antimicrobial properties of surface materials, irrespective of their proposed application, either use planktonic cultures or study indirect effects such as release of antimicrobial compounds from the surfaces⁸. Such methods might not correctly report surface efficacy in proposed applications. Even if biofilm formation on material of interest is studied, often-used methods of biofilm viability assessment are prone to critical failures. For example, viability staining with propidium iodide and suitable counterstains can dramatically underestimate viability in both oligotrophic⁹ and growth medium biofilms¹⁰ while colony counts, the gold standard of microbiology, depend on viable cell harvesting efficiency and dispersion of harvested aggregates prior to cultivation^{11,12}.

Susceptibility to metal ions has been demonstrated to be similar for both biofilms and planktonic cultures¹³ which makes antimicrobial metal-based approaches good candidates to prevent pathogen transfer and biofilm

¹Laboratory of Environmental Toxicology, National Institute of Chemical Physics and Biophysics, Tallinn, Estonia. ²Department of Chemistry and Biotechnology, Tallinn University of Technology, Tallinn, Estonia. ³Institute of Physics, University of Tartu, Tartu, Estonia. ⁴Estonian Academy of Sciences, Tallinn, Estonia. ⁵Institute of Molecular and Cell Biology, University of Tartu, Tartu, Estonia. ✉email: rosenbergerm@tut.ee

formation on high-touch surfaces. Silver and copper are good examples of infection prevention and marine antifouling agents historically used even before deeper knowledge of microbes or biofilms was established. Historical use of the former is well reviewed by Lemire et al.¹⁴. Zinc is a later addition to the list after wider use of ZnO nanoparticles. Although zinc is an essential micronutrient being incorporated into 4–10% of proteins across the domains of life¹⁵, it possesses a dose-dependent antibacterial activity at higher concentrations. Zinc toxicity towards microbes is mainly attributable to deactivation of proteins via thiol-disulfide chemistry^{14,16} and protein binding or metal replacement (e.g. manganese starvation^{17,18}) resulting in impaired energy metabolism^{19–21}, higher susceptibility to reactive oxygen species (ROS)²² and eventually loss of membrane potential and membrane permeabilization. Zn tolerance in non-physiological concentrations has been shown to depend on microbial species with *C. albicans* and *P. aeruginosa* being less sensitive to Zn toxicity than *E. coli* or *S. aureus*²³. ZnO nanoparticles have been demonstrated to possess additional antibacterial properties due to direct contact and ROS production²⁴. Nano-specific effects damage bacterial cell membranes and downregulate genes associated with managing oxidative stress in *S. aureus* as well as upregulate genes associated with cation efflux in *E. coli* and *P. aeruginosa* and inhibit biofilm formation by *E. coli*, *S. aureus* and *P. aeruginosa*^{25–30} among other microbes. Addition of silver adds to antimicrobial effects in a variety of mechanisms including membrane and cell wall damage, protein inactivation, impaired energy metabolism, ROS production and DNA damage^{31–39}.

Inhibition of biofilm formation on Zn-based applications can partially be attributed to general Zn toxicity to bacteria above physiological concentrations but also other biofilm-specific mechanisms of action could be involved. For example, it has been proposed that sublethal Zn or Ag concentrations could affect biofilm formation by interfering with quorum sensing^{40–43} or modulate amyloid fibril formation^{44,45}.

Another promising way is the development of antimicrobial surfaces containing photocatalysts that not only induce microbial killing but also degradation of organic matter under specific illumination conditions that could hopefully decrease dry touch-transfer of pathogens or delay moist surface colonization between light exposures. The most popular photocatalyst is TiO₂ but also ZnO is widely used²⁴. In one of our previous studies⁴⁶ we demonstrated that in addition to killing bacterial cells during photocatalysis, TiO₂ surfaces also caused photooxidation of bacterial debris thus, referring to the possibility of extended efficacy of those surfaces.

The idea behind photodegradation is that light with high enough energy to exceed band gap energy of the photocatalytic metal oxide (e.g. 3.37 eV in the case of ZnO) will excite electron–hole pairs. The photogenerated electrons (e⁻) and holes (h⁺) can reduce or oxidize compounds like surface adsorbed O₂ and H₂O to produce ROS. The produced ROS (e.g. superoxide anion radical ‘O₂⁻’ and hydroxyl radical ‘OH’) are able to partially or completely degrade organic contaminants including microbes. It has been claimed that ZnO can produce ROS even without light activation⁴⁷—ROS production via releasing of trapped electrons, so called ‘photocatalysis in the dark’⁴⁸ with respective antimicrobial activity^{49,50}. Therefore, not only metal ions but assumingly also ROS can contribute to the antimicrobial and self-cleaning nature of photocatalytic metal oxide based surfaces in dark conditions. Increased antimicrobial and antibiofilm behavior of nano-ZnO covered dental implant⁵¹ and ZnO thin film covered food-packaging polymer⁵² compared to uncoated controls indicate a promising potential of ZnO-based coatings. The use of nanoparticle-based surfaces increases the potential efficiency and reactivity of such surfaces due to increased specific surface area of nanosized matter.

We have previously reported developing novel multi-effective antimicrobial coatings based on nano-ZnO/Ag composite particles⁵³. The novelty of these coatings rises from a combined and complex effect of different antimicrobial mechanisms: (i) antimicrobial activity of Zn²⁺ ions, (ii) antimicrobial activity of Ag⁺ ions, and (iii) antimicrobial activity of ROS, generated at the surface of nano-ZnO and nano-ZnO/Ag via photocatalytic processes under UV-A illumination. Our coatings also have two additional advantages (i) degradation of organic debris (incl. dead bacteria) by ROS takes place on the surface and (ii) photocatalytic activity of ZnO is enhanced by the formation of nano-ZnO/Ag composite particles (via charge separation process in ZnO/Ag system).

Antimicrobial properties of our previously developed UV-A-induced nano-ZnO and nano-ZnO/Ag composite coated surfaces were evaluated using an in-house protocol based on ISO standards for measurement of antibacterial activity of non-porous surfaces (ISO 22196:2011⁵⁴) and photocatalytic surfaces (ISO 27447:2009⁵⁵), protocols designed to measure antimicrobial action in a thin layer of microbial suspension uniformly spread between test surface and cover film. The nano-ZnO-coated solid surfaces were found to be highly effective under UV-A illumination with over 3 log decrease in planktonic *E. coli* and *S. aureus* viability during 1 h exposure. Photodepositing Ag onto the nano-ZnO increased its photocatalytic activity and acted as an additional antimicrobial agent in the absence of UV-A exposure⁵³.

With the intent to further develop these materials for use on high-touch surfaces in the public spaces, in this study we additionally assessed the efficacy of the surface materials against biofilm formation in application-appropriate oligotrophic environment and in the absence of UV-A exposure. For that we opted for a static model to grow biofilms directly on the studied surfaces and to be able to simultaneously monitor dissolution-driven toxicity to the planktonic cells in a small closed system. A mixed approach combining physical methods (vortexing and ultrasonication) with chemical ones (addition of surfactant, using high salt concentration) was used for biofilm harvesting. Biocompatibility of the surfaces was studied using in vitro skin-relevant human cell growth directly on the nano-enabled surfaces.

Results

To assess both anti-adhesion effect of the coating materials and metal release-associated antimicrobial activity towards planktonic microbes, biofilm formation on the sparsely and densely coated nano-ZnO and sparsely coated nano-ZnO/Ag surfaces as well as viability of planktonic microbes in the test system was studied. Biofilms were either grown in static oligotrophic environment (1:500 diluted nutrient broth in synthetic tap water, not supporting planktonic growth) at room temperature to mimic real-life-like use in moist environments (similar

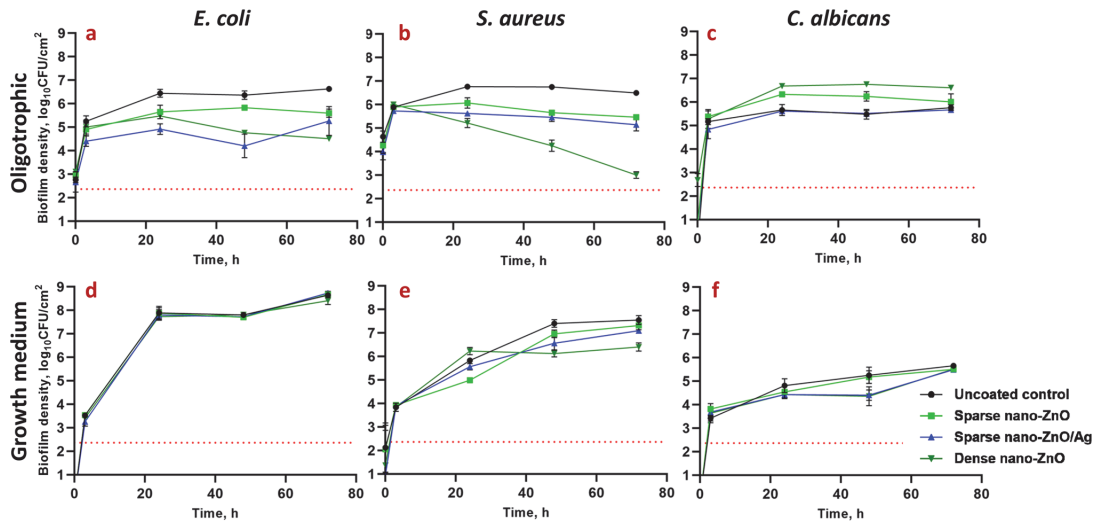


Figure 1. *E. coli* MG1655 (a, d), *S. aureus* ATCC25923 (b, e) or *C. albicans* CA14 (c, f) monospecies biofilms harvested at different time points from nano-ZnO or nano-ZnO/Ag or uncoated surfaces in static oligotrophic environment (1:500 diluted NB in synthetic tap water; a–c) or growth medium (LB; d, e; YPD; f). Biofilm formation was more affected by the nano-enabled coatings in oligotrophic environment than in growth medium with significantly decreased colonization by *E. coli* and *S. aureus* from 24 h onwards while nano-ZnO surfaces selectively enhanced surface colonization by *C. albicans*. Only dense nano-ZnO surfaces demonstrated statistically significant moderate colonization inhibiting effect on *S. aureus* in growth medium 48–72 h post-inoculation. Red dotted line represents the limit of quantification (231 CFU/cm²). Data represents mean \pm SD of 3 independent experiments with 6–9 data points \pm SD.

to previously used standard conditions for planktonic testing⁵³) or in nutrient-rich growth mediums (LB, YPD; supporting exponential growth) resembling classical laboratory approach for studying biofilms⁵⁶. Well described human-relevant biofilm-forming Gram-positive (*S. aureus* ATCC25923) and Gram-negative (*E. coli* MG1655) model bacteria were selected for the experiments. *C. albicans* CA14 was included as a fungal model organism to represent different types of microbes potentially transferred by fomites. The effect of the surfaces on biofilm formation was quantitatively evaluated by harvesting viable adherent cells followed by colony counting or by qualitative epifluorescence microscopy. In parallel, antimicrobial activity towards planktonic cells above the surfaces was analyzed using colony counting.

Biofilm formation on surfaces coated with nano-ZnO or nano-ZnO/Ag. Nano-ZnO inhibited bacterial biofilm formation in a dose-dependent manner in oligotrophic conditions (Fig. 1a, b) reaching maximum of 2.12 and 3.49 log reduction on dense nano-ZnO surface compared to uncoated surface after 72 h for *E. coli* and *S. aureus*, respectively. In growth medium, however, only the dense nano-ZnO surface significantly inhibited biofilm formation of *S. aureus* but not *E. coli* (Fig. 1d, e). It was also evident that while there was rapid surface colonization taking place during the first 3 h of incubation in oligotrophic conditions, regardless of surface type, the surfaces in growth medium were either colonized more slowly or the initial adherence was weaker and adherent cells were more easily washed off during sample preparation.

Addition of Ag to the sparse nano-ZnO surfaces had transient negative effect on *E. coli* biofilm formation in oligotrophic conditions with an additional 0.5–1.6 log reduction in harvested viable cells (3–48 h post-inoculation, respectively) compared with sparse nano-ZnO without added Ag (Fig. 1a). This additional reduction decreased to a non-significant 0.34 log by 72 h. Ag had only a small but statistically significant effect on *S. aureus* biofilm formation in oligotrophic conditions (<0.5 log additional reduction compared to sparse nano-ZnO) indicating better tolerance to silver compared to *E. coli* (Fig. 1b). As expected, addition of Ag to nano-ZnO surfaces had no effect on bacterial biofilm formation in organic-rich growth medium (Fig. 1d, e) due to lower bioavailability of silver.

Surfaces coated with nano-ZnO promoted *C. albicans* biofilm formation in oligotrophic conditions with up to 1.27 log increase in viable attached cells at 48 h time point compared to uncoated surface (Fig. 1c). Silver-containing surfaces had no significant effect on *C. albicans* biofilm formation nor on planktonic viability in oligotrophic conditions compared to uncoated surfaces. However, considering enhanced *C. albicans* biofilm formation on sparse nano-ZnO surfaces and biofilm formation on sparse nano-ZnO/Ag surfaces in oligotrophic conditions demonstrating a significant 0.55–0.72 log reduction compared to sparse nano-ZnO surface during 3–48 h, respectively (Fig. 1c), it could be concluded that silver transiently inhibited *C. albicans* biofilm formation bringing it down to control level. This inhibition was lost 72 h post-inoculation. No biofilm promoting effect was

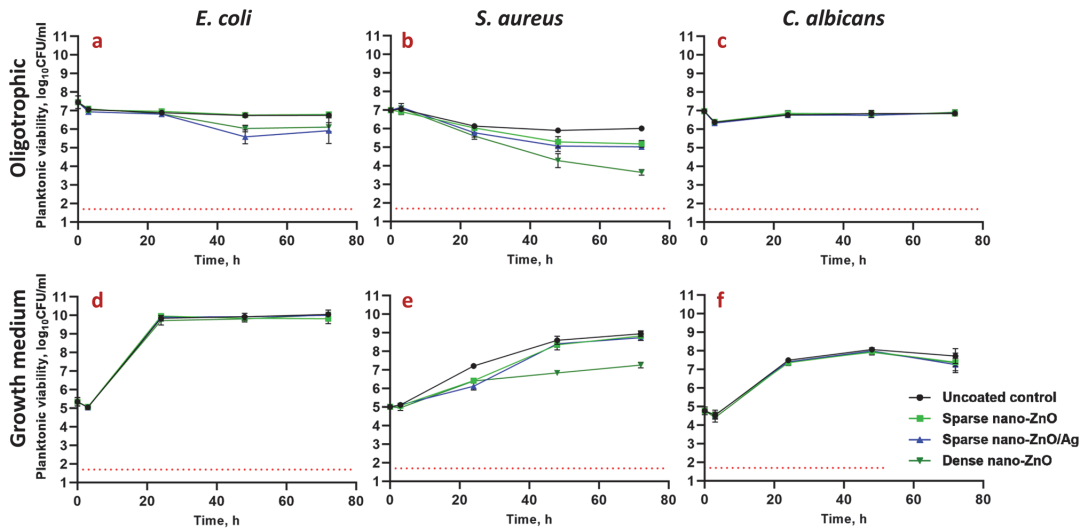


Figure 2. Viability of *E. coli* MG1655 (a, d), *S. aureus* ATCC25923 (b, e) or *C. albicans* CAI4 (c, f) planktonic cells above nano-ZnO, nano-ZnO/Ag or uncoated surfaces in static oligotrophic environment (1:500 diluted nutrient broth in synthetic tap water; a–c) or growth medium (LB: d, e; YPD: f). Planktonic cells were generally more affected by nano-enabled coatings in oligotrophic environment than in growth medium. Red dotted line represents the limit of quantification (50 CFU/mL). Data represents mean \pm SD of 3 independent experiments with 6–9 data points \pm SD.

observed in growth medium where inversely a moderate transient biofilm inhibition on both sparse nano-ZnO/Ag (0.85 log decrease) and dense nano-ZnO (0.89 log decrease) surfaces was observed at 48 h (Fig. 1f). Inhibitory effect of silver was further illustrated by the presence of areas with several flattened “ghost cells” on sparse nano-ZnO/Ag surface in growth medium (Supplementary Fig. 1) accompanying slight decrease in viable biofilm cell count 48 h post-inoculation (Fig. 1f). Similar areas with dead cells were not observed in other conditions and seemed to serve as a matrix for the biofilm to grow on.

Viability of planktonic microbes above the surfaces coated with nano-ZnO or nano-ZnO/Ag. In organics-rich growth media most of the Zn deposited on the nano-ZnO coated surfaces (Fig. 3a–c) was released into the medium already after 24 h whereas in oligotrophic conditions up to 10 times less Zn was released (Fig. 3d–f). Increased Zn release in growth media can be attributed to both, culture acidification and formation of protein complexes driving Zn dissolution from nano-ZnO^{23,57,58}. Higher release of Zn into bacterial growth medium yielded in less biofilm inhibition (Fig. 1d,e) and higher viability of planktonic bacteria (Fig. 2d,e) while in oligotrophic conditions more nano-ZnO remained on the surface resulting in both more effective inhibition of biofilm formation (Fig. 1a,b) and lower planktonic viability (Fig. 2a,b). This can possibly be explained by differences in bioavailability. No statistically significant reduction in viability of planktonic yeast cells was registered, regardless of surface type or test media used (Fig. 2c,f).

Slight decrease in overall planktonic viable counts at 3 h (Fig. 2a–f) can be explained by microbial attachment to solid surfaces, including on the polystyrene well surface which decrease planktonic counts in oligotrophic conditions and is not yet compensated by proliferation during 3 h in growth medium at room temperature.

Zinc release from the dense nano-ZnO surface (Fig. 3c,f) had a small but statistically significant negative effect of 0.63 logs reduction by 72 h on planktonic *E. coli* viability in oligotrophic conditions and no effect in growth medium (Fig. 2a,d) while the same surfaces decreased *S. aureus* planktonic viability in a dose-dependent manner in both oligotrophic conditions and growth medium (Fig. 2b,e) with maximum of 2.37 and 1.69 logs reduction, respectively. This effect can likely be attributed to relative sensitivity of *S. aureus* towards Zn.

Ag from the nano-ZnO/Ag surfaces decreased planktonic viability of *E. coli*, but not *S. aureus* and *C. albicans* in oligotrophic conditions (Fig. 2a–c). Ag from sparse nano-ZnO/Ag had no significant effect on planktonic viability in growth media (Fig. 2d–f) which can be explained by lower bioavailability of released Ag⁺ ions due to complexing proteins and chloride in the medium^{59–61}. Maximum calculated Ag concentration in the test system in case of complete release of Ag from the surface coating was estimated to reach 15.27 ± 2.21 ng/mL (Supplementary Table 1). Actual release could not be reliably measured possibly due to high adsorption of Ag to organic matter in the test medium and/or polystyrene well walls.

Biofilm and cell morphology. Coverage of the surfaces by 48 h biofilm biomass in epifluorescence microscopy (Fig. 4) and higher magnification SEM images of representative microcolonies (Fig. 5) confirmed

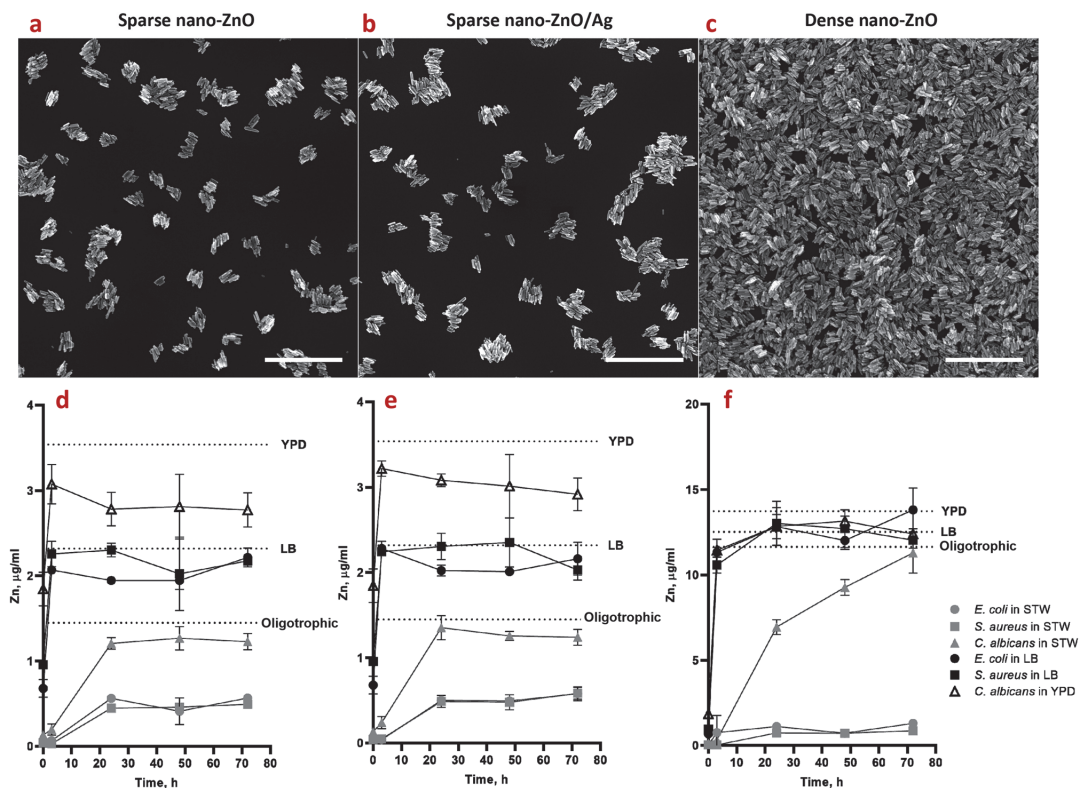


Figure 3. SEM images of sparse nano-ZnO (a), sparse nano-ZnO/Ag (b) and dense nano-ZnO (c) coated surfaces as well as measured Zn release from sparse ZnO (d), sparse ZnO/Ag (e) and dense ZnO (f) surface to the test environments (including the microbes) over time. (a–c) Scale bars represent 1 μm. (d–f) maximum Zn concentration in each test environment (measured Zn background in different media + theoretical total Zn release from ZnO nanoparticles) is marked as a dotted line. Almost total Zn dissolution was reached already at 3 h in growth medium while dissolution equilibrium was much more slowly achieved in oligotrophic conditions and at lower Zn concentration (d–f). The only exception was *C. albicans* that significantly enhanced Zn release to near total dissolution in oligotrophic conditions. Data represents mean ± SD of 3 independent experiments. Total Ag content of 23.56 ± 3.42 ng/cm² in the sparse ZnO/Ag surface was measured which could result in up to 15.27 ± 2.21 ng/mL concentrations in the 5 mL test volume (Supplementary Table 1).

morphological and structural differences between biofilms grown on uncoated surfaces in growth medium and oligotrophic conditions as well as between biofilms on nano-ZnO coated and uncoated surfaces.

In case of *E. coli*, also clear differences in cell surface structure were observed. *E. coli* biofilms in growth medium consisted of cells with smoother surfaces and less extracellular matrix (ECM) extended to solid surface while *E. coli* cells in oligotrophic biofilms had a more coarse surface structure and fibrillar ECM extended to solid surface (Fig. 5 upper panels). These differences occurred despite the fact that surface-associated amyloid fibers (SAFs) in the ECM were found to interconnect individual cells of *E. coli* (Supplementary Figs. 2, 3) and *S. aureus* (Supplementary Figs. 4, 5) biofilms in all growth and exposure conditions used. Although there was less *E. coli* biofilm on nano-ZnO-coated surfaces in oligotrophic conditions compared to uncoated surface (Figs. 1a, 4 upper panels) and cells tended to be shorter in length on nano-ZnO-coated surfaces, cells with normal morphology could be found even in direct contact with ZnO nanoparticles on dense nano-ZnO surfaces (Fig. 5, upper panels). ZnO nanoparticles were dissolved from the nano-ZnO surfaces in growth medium during 48 h incubation, as also confirmed by elemental analysis (Fig. 3f) and were not visible on SEM images (Fig. 5). Adherence of *S. aureus* cells to nanoparticles on dense nano-ZnO surfaces was also observed, although there were more damaged cells and blebbing, generally associated with cellular damage and virulence^{62–64}, occurring on nano-ZnO surfaces in oligotrophic conditions and on dense ZnO surface in growth medium compared to uncoated surfaces (Fig. 5, middle panels).

There were no clear morphological differences between *S. aureus* biofilm cells on uncoated surfaces in growth medium and oligotrophic conditions besides larger cell size in growth medium (Fig. 5, middle panels). Although Zn-enhanced cell-to-cell adherence has been described for *S. aureus*^{65,66}, *S. aureus* tended to preferably form cell

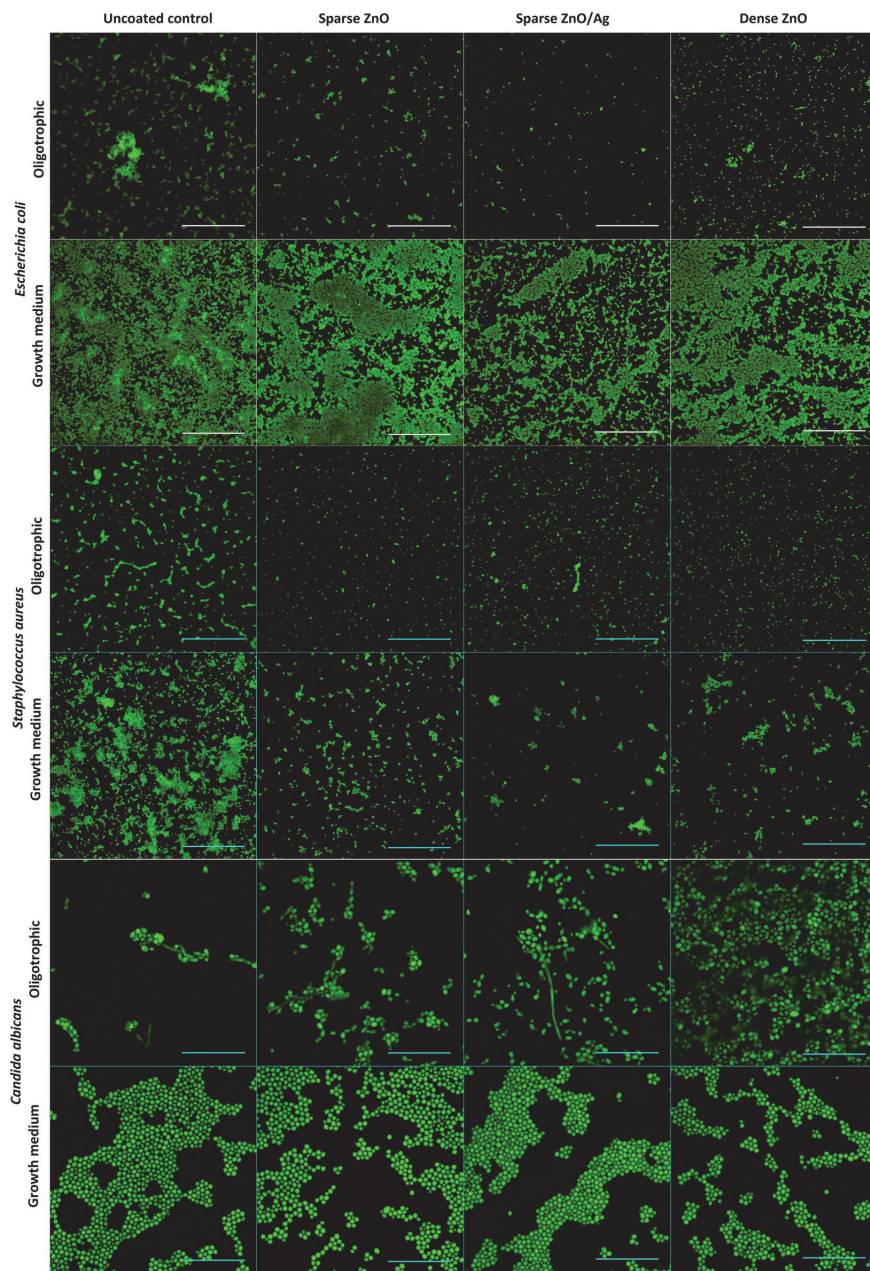


Figure 4. Representative epifluorescence images of *E. coli*, *S. aureus* or *C. albicans* 48 h biofilms on uncoated surfaces or on surfaces coated with nano-ZnO or nano-ZnO/Ag in oligotrophic conditions and growth medium. Fixed biofilms were stained with DNA- and RNA-binding Syto 9. Scale bars represent 50 μm .

aggregates (cell-to-cell adherence) regardless of surface type while *E. coli* tended to cover surface (cell-to-surface adherence) and thereafter form biofilm in height.

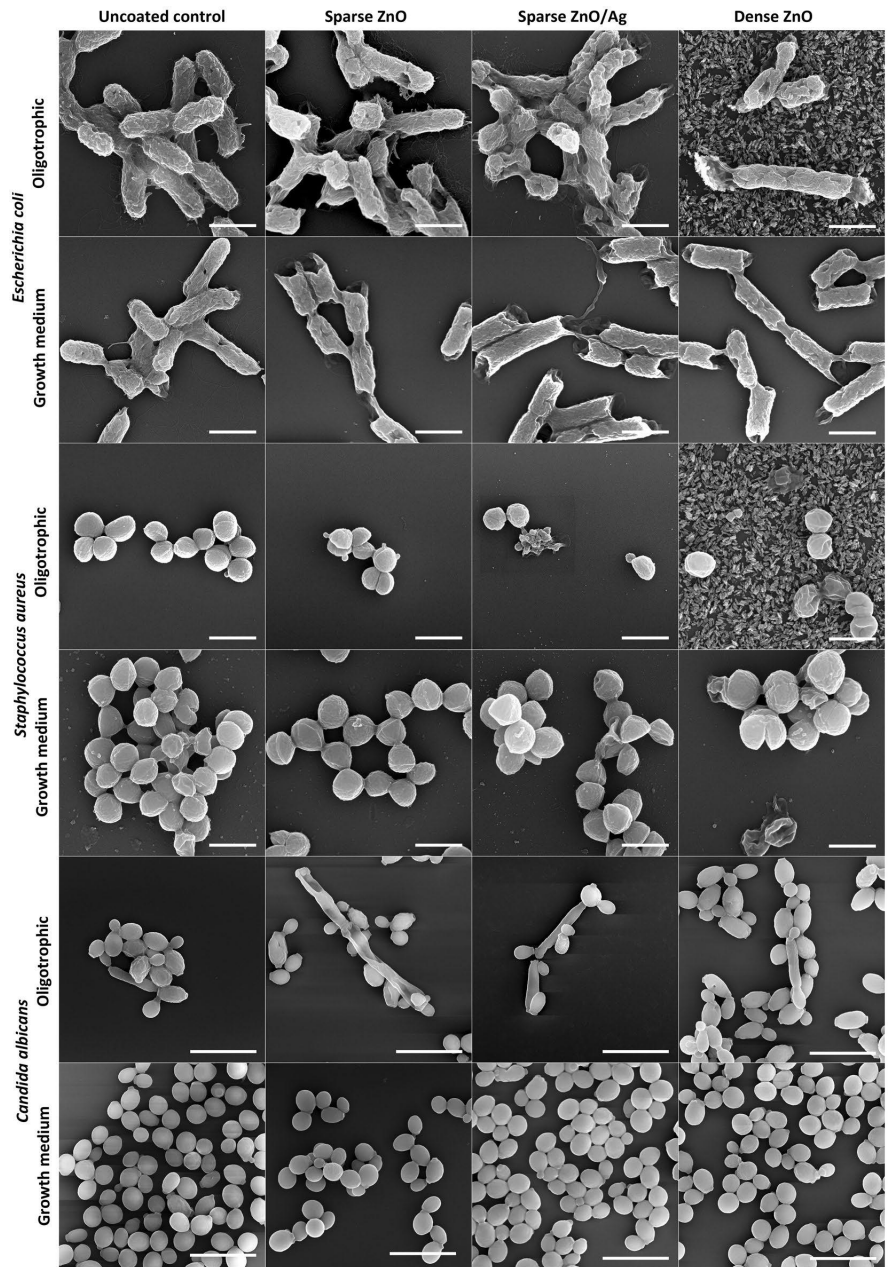


Figure 5. Characteristic SEM images of *E. coli*, *S. aureus* and *C. albicans* cell and microcolony morphology in 48 h biofilm aggregates on uncoated surfaces or on surfaces coated with nano-ZnO or nano-ZnO/Ag in oligotrophic conditions and growth medium. Scale bars represent 1 μm for bacteria and 10 μm for *C. albicans*. For designation of the surface coatings, see Fig. 3a–c.

Pseudohyphal morphology of the dimorphic fungus *C. albicans* was only observed in oligotrophic conditions, where yeast form was qualitatively more dominant on dense nano-ZnO surface (bottom panels in Figs. 4 and 5).

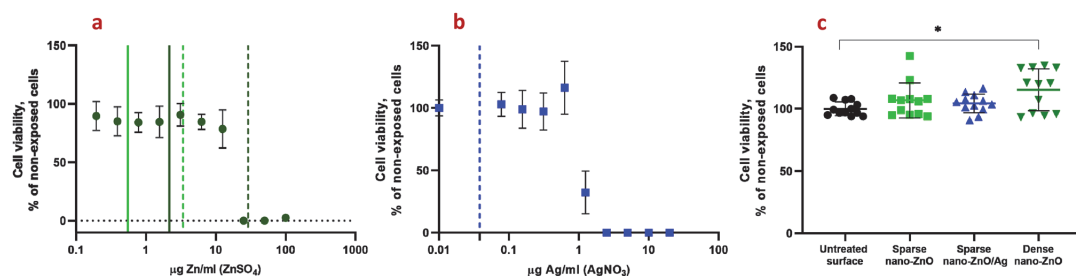


Figure 6. Cytotoxicity of soluble Zn (a) and Ag (b) salts or nano-ZnO and nano-ZnO/Ag coated surfaces (c) to HaCaT keratinocytes after 48 h in standard cell-culture conditions (DMEM high glucose medium supplemented with Na-pyruvate (1 mM), penicillin–streptomycin (100 U/mL;100 µg/mL), fetal bovine serum (10%), 37 °C, 5% CO₂). (a) Viability of HaCaT cells exposed to ZnSO₄. Solid line denotes Zn released into cell culture medium from sparse nano-ZnO (light green) and dense nano-ZnO (dark green) surfaces during 48 h. Dotted lines denote respective maximal theoretical concentration in case of total release of deposited Zn. (b) Viability of HaCaT cells exposed to AgNO₃. Dotted blue line marks theoretical maximum release of Ag into the test environment from sparse nano-ZnO/Ag surface. Actual release could not be reliably measured possibly due to high adsorption of Ag to organic matter in the test medium and/or polystyrene well walls. (c) Cytotoxicity of nano-ZnO and nano-ZnO/Ag coated surfaces to HaCaT keratinocytes cultured directly on the surfaces. No direct cytotoxicity of nano-enabled surfaces was observed. Increased growth of keratinocytes was observed on dense nano-ZnO surfaces. *Denotes statistically significant difference (P < 0.05). Zn release from the surfaces during 48 h did not reach cytotoxic range. Theoretical maximal Zn concentration resulting from total Zn release from the dense nano-ZnO surfaces was in toxic range while total Zn from sparse nano-ZnO and Ag from sparse nano-ZnO/Ag would not have reached toxic concentrations in cell culture medium.

No true hyphae were observed nor expected from this strain in the absence of serum.

In vitro biocompatibility of nano-ZnO and nano-ZnO/Ag surfaces. In order to assess the biocompatibility of nano-ZnO and nano-ZnO/Ag surfaces with human cells, the growth of human keratinocytes directly on the surfaces in standard cell culture conditions was evaluated. Despite the fact that there was enough Zn deposited on dense nano-ZnO surfaces to cause toxicity to the cells in case of total release, amount of Zn released into cell culture medium did not reach cytotoxic concentrations during 48 h (Fig. 6a,b) and normal growth and morphology of human keratinocytes on nano-ZnO coated surfaces was observed (Fig. 7). Total Zn and Ag amount deposited on sparsely coated surfaces was not high enough to cause cytotoxicity even in case of theoretical total release into the medium (Fig. 6a,b). Compared to control surface, slightly enhanced attachment and growth of keratinocytes on dense nano-ZnO surfaces (Fig. 6c) was observed. This observation cannot be explained by differences in surface properties of the different surfaces, e.g., hydrophilicity (see water contact angles on different surfaces in Supplementary Fig. 6).

Discussion

The extracellular matrix (ECM) is an integral part of biofilms and can make up most of the volume of a mature biofilm⁶⁸ but total biomass or biovolume is not a good proxy for total or viable cell count in a biofilm, especially when comparing chemical treatments or carrier surfaces that could potentially affect ECM composition. However, viable microbes are critically needed to establish biofilms de novo and the sole cause of pathogen transfer via high-touch surfaces. Therefore, we chose to quantify viable microbes harvested from 3 to 72 h biofilms to evaluate de novo surface colonization. As harvested CFU counts exclude ECM quantification entirely, we also evaluated the biofilms qualitatively by epifluorescence and electron microscopy. Epifluorescence microscopy was chosen to be performed on 48 h fixed biofilm samples monostained with Syto 9 instead of viable biofilms stained with Syto 9 and propidium iodide (PI) because (i) based on pilot experiments, largest effect was expected at 48 h; (ii) PI is known to underestimate viability in biofilms^{9,10}; (iii) highly variable Syto 9 intensity in viable biofilms depending on viability state and Gram type of the cells^{9,69}; (iv) time limits of working with viable samples to achieve comparable representative results.

It must be noted, however, that adding liquid manipulation steps such as rinsing, fixation and gradual dehydration to the preparation of biofilm samples is likely to affect the appearance of biofilms and cause e.g., loss of biomass in each step. Kragh et al. have recently demonstrated that media removal and rinsing can critically affect quantitative biofilm analysis compared to undisturbed biofilms¹⁰. In addition, we observed that while oligotrophic bacterial biofilms retained their overall microcolony architecture during fixing and dehydration steps, biofilms formed in growth medium lost most of their biomass and surface coverage during dehydration steps prior to SEM. Taking into account also the rapid biofilm formation during the first 3 h in oligotrophic conditions (Fig. 1) we empirically suggest that biofilms formed in oligotrophic conditions are more strongly attached to the substratum.

Reductions in harvested viable counts of bacterial biofilms on nano-ZnO and nano-ZnO/Ag surfaces were accompanied by respective reductions in planktonic viable counts regardless of media used and can therefore

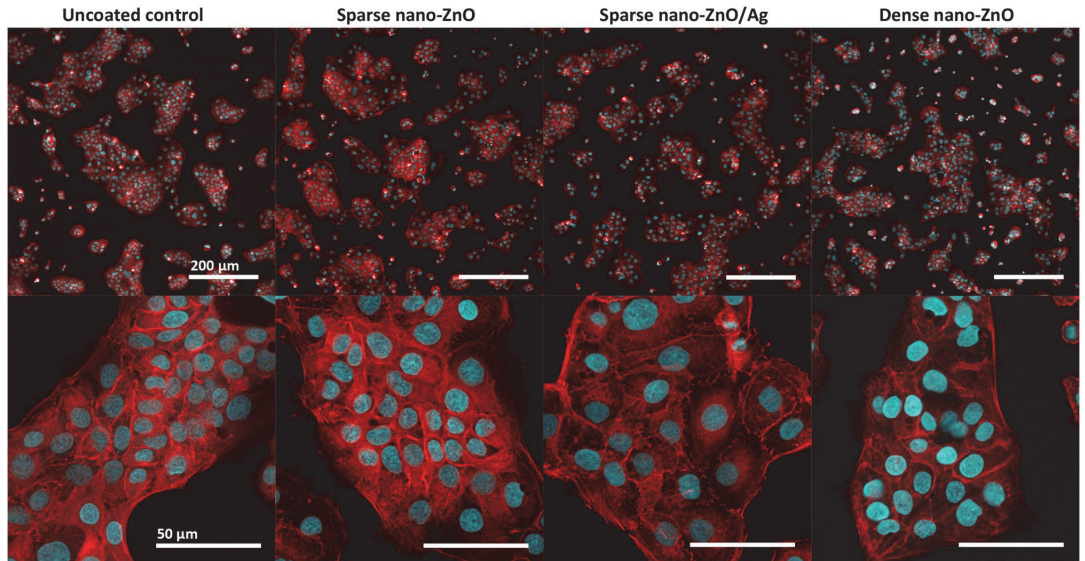


Figure 7. Representative confocal microscopy (CLSM) images of HaCaT keratinocytes on nano-ZnO or nano-ZnO/Ag coated surfaces: upper panel—lower magnification CLSM (scale bar 200 μm), bottom panel—higher magnification CLSM (scale bar 50 μm); nuclei—cyan (Hoechst 33342), cytoskeleton—red (Phalloidin-TRITC). Cells are viable (Fig. 6) and appear normal on all surfaces.

be mostly attributed to general antibacterial activity of the Zn-enabled surfaces and metal dissolution in concordance with previous knowledge^{13,70} and not biofilm-specific mode of action. *S. aureus* was more sensitive to Zn and *E. coli* more sensitive to Ag for both biofilms and planktonic cultures in accordance with our previous results using a planktonic test in oligotrophic conditions⁵³. *S. aureus* cells attached to ZnO-coated surfaces (Fig. 5, middle panels) appeared damaged on SEM micrographs and presented blebs. Blebbing has been described not only for Gram-negative, but also for Gram-positive bacteria and fungi⁶² and appears to have a more general role in stress response, virulence and intercellular communication across the domains of life. Vesicle formation has also been confirmed in case of *S. aureus*⁶³ and can take place for example in response to antibiotic stress thereby increasing virulence⁶⁴.

We have shown previously that choice of media critically affects metal toxicity⁶¹ and indeed, it was evident, that both Zn and Ag were more toxic in oligotrophic conditions compared to no effect on either biofilm or planktonic cells of *E. coli* in growth medium. This can be explained by lower metal bioavailability in organics-rich growth medium^{57–61} but one must acknowledge that also physiology of exponentially growing and starving non-dividing microbes is different. Although classical microbiological culture media are the most used testing environments, their suitability for each application should be evaluated.

Although metal effect to surface associated amyloids (SAFs) in biofilm matrix is yet scarcely studied^{44,45}, we also hypothesized that high Zn concentrations might interfere with bacterial surface-associated amyloid^{71–74} formation as it can negatively affect fibrillar structure of other amyloids^{75–79} and could thereby disrupt SAF-mediated surface colonization. Although cell surface morphology seemed to differ between *E. coli* cells grown on nano-ZnO and uncoated surfaces in oligotrophic conditions (Fig. 5, top panel), we found no substantial qualitative differences in amyloid staining of those biofilms (Supplementary Figs. 2–5). Qualitative results do not strictly rule out smaller Zn-dependent differences, which amyloid signal quantification could possibly discriminate, if present.

While reduction in bacterial biofilm viability was accompanied by respective antibacterial activity against planktonic cells there were clear biofilm-specific effects on *C. albicans* biofilm formation. Although planktonic viable counts were not significantly different from uncoated control surface regardless of surface type or media used, biofilm formation was affected. Enhanced dose-dependent biofilm formation of *C. albicans* on nano-ZnO-coated surfaces in oligotrophic conditions cannot be explained by differences in the hydrophilic properties of nano-ZnO coated and uncoated surfaces (Supplementary Fig. 6). However, *C. albicans* has been demonstrated to possess systems to harvest extracellular Zn and store Zn intracellularly in zincosomes⁸⁰ which enables *C. albicans* to both overcome nutritional immunity in host organism as well as to detoxify Zn²⁺ excess. Active uptake of extracellular Zn could also be the reason, why nano-ZnO was depleted from the surfaces in oligotrophic conditions in the presence of *C. albicans* but not bacteria (Fig. 3d–f). For dense nano-ZnO surfaces this effect was also clearly observable on SEM images (Fig. 5, right column). Interestingly, previously published results on zinc effects on *Candida* biofilm formation are contradictory. For example, Kurakado et al. demonstrated an increase in *C. albicans* biofilm formation as a response to ZnSO₄ and a decrease in response to zinc chelator⁸¹ while several others report Zn-associated biofilm inhibition^{82–84}. These contradictions could be partly due to different average

and local Zn concentrations reached in these studies while we had the nano-ZnO attached to a solid surface resulting in lower average Zn concentration in the test environment or due to growth-related and physiological differences in various oligotrophic and nutrient-rich environments as well as differences in yeast strains used. We also observed that pseudohyphal morphology of *C. albicans*⁶⁷ was only registered in oligotrophic conditions where yeast form was qualitatively more dominant on dense nano-ZnO surface (bottom panels in Figs. 4 and 5). Harrison *et al.* have demonstrated that sub-inhibitory Zn²⁺ concentrations can indeed interrupt yeast to hyphal differentiation in *Candida* biofilms⁸⁵ and it has been suggested that zinc-responsive transcription factor Zap1 is a negative regulator of biofilm matrix accumulation and maturation⁸⁶ also directing the yeast-hypha balance to yeast form⁸⁷. On the other hand, filamentation is not a prerequisite for initial biofilm formation⁸⁸ as can also be seen in our results.

Candida spp is an important cause of nosocomial bloodstream infections⁹⁰. Although we did not look into polymicrobial biofilms, enhancement of *C. albicans* biofilm formation could be especially disadvantageous in biomedical applications as many patients with candidemia tend to present polymicrobial blood cultures⁹¹ and surface colonization by *C. albicans* can in turn enhance polymicrobial biofilm formation or drug tolerance of other potential pathogens^{92–94}. In the light of existing and emergent drug-resistant *Candida* spp⁸⁹ Zn-enhanced *C. albicans* biofilm formation in oligotrophic conditions should be studied further to reveal mechanistic causes of the biofilm-promoting phenomenon.

Zinc oxide is well tolerated by humans and is listed as a generally recognized as safe (GRAS) substance by the US Food and Drug Administration (21CFR182.8991), approved for use in cosmetics in EU for up to 25% concentration in the ready-for-use preparation (Regulation (EC) No 1223/2009) and widely used in topical applications (incl. sunscreens, baby powders, diaper creams, mineral make-up etc.) as well as food additive, corrosion protection, filler/pigment in paints alongside titanium dioxide etc. We would like to emphasize that growing human keratinocytes directly on the surfaces of interest as a measure of biocompatibility was used as a worst-case-scenario during material development phase. In vivo dermal exposure to surface-bound ZnO is expected to be lower due to the lack of fully functional skin barrier in cell culture conditions and shorter exposures by high-touch surfaces. The observed slightly higher viability of human keratinocytes on dense nano-ZnO surfaces is not entirely unexpected as zinc is known to promote wound healing⁹⁵ and has been shown to also promote keratinocyte migration and proliferation as well as to modulate integrin expression needed for adherence to extracellular matrix⁹⁶. However, the lack of cytotoxicity for keratinocytes on ZnO and ZnO/Ag surfaces does not rule out potential sublethal events, e.g., genotoxicity that has been observed at somewhat lower zinc concentrations than cytotoxicity^{97,98} and these specific toxic effects would require further studies.

Conclusion

This study demonstrated that in general, bacterial *E. coli* and *S. aureus* monospecies biofilm formation on nano-ZnO and nano-ZnO/Ag composite-enabled surfaces was inhibited in a dose-dependent manner: sparsely coated nano-ZnO surfaces were less inhibitory than densely coated ones and inhibition of biofilm formation was accompanied by antibacterial activity against planktonic cells. The surfaces were not cytotoxic to human keratinocytes and no significant inhibition of yeast biofilm was observed. On the contrary, enhancement of *C. albicans* biofilm formation was registered on nano-ZnO surfaces in oligotrophic conditions. This observation is certainly disadvantageous considering the emergence of drug-resistant infections of *Candida* spp. and yeast role in polymicrobial biofilms. Our results indicate that best approach to achieve broad-spectrum inhibition of biofilm formation on high-touch surfaces would be the combination of ZnO and silver. It is also important to highlight the role of the test environment. Except for Zn toxicity towards *S. aureus*, all above-mentioned antimicrobial and antibiofilm effects were detected only in oligotrophic environment and not in widely used microbial growth media. Moreover, selection of detection method proved critical in the quality of information acquired as biomass was lost in every liquid manipulation step. Media removal and washing steps have been shown to critically affect quantitative biofilm analysis. We add to that and propose that liquid manipulation steps can also easily introduce compositional biases, e.g. exaggerate biomass differences formed in different conditions.

Methods

Surfaces. The preparation of ZnO and ZnO/Ag nanoparticles is more thoroughly described in our previous work⁵³. Briefly, hydrothermal synthesis was used to prepare ZnO nanoparticles using zinc acetate as a precursor. ZnO/Ag composite particles were created by supplementing ZnO nanoparticles with Ag using UVA-induced photodeposition. ZnO or ZnO/Ag nanoparticles were deposited on 18 × 18 mm square cover glasses (2855-18, Corning) using spin-coating and subsequently annealed to enhance particle surface attachment. Two different coating densities of nano-ZnO were used further referred to as sparse and dense, depicted on Fig. 3a–c). Nano-ZnO/Ag composite particles were used only in sparse coating density. Dense coating resulted in uniformly covered surfaces while sparse coatings exposed glass carrier surface with distance between nanoparticle clusters comparable to bacterial cell size as can be seen on SEM images of the surfaces on Fig. 3. Physical and chemical properties of the nanoparticles used as well photocatalytic and antibacterial activity of the surfaces used in this study have been previously described⁵³. Total Zn content in the nano-coatings was analyzed using TXRF (S2 Picofox, Bruker) and Ag content with AAS (ContrAA 800, Analytic Jena AG) after 1 h treatment in 0.5 mL concentrated HNO₃. The results are shown in Supplementary Table 1.

Biofilm formation, harvesting and quantification. Monospecies biofilms of *E. coli* MG1655, *S. aureus* ATCC25923 and *C. albicans* CA14 were studied. Sterile nano-ZnO, nano-ZnO/Ag or uncoated surfaces were placed into non tissue culture treated 6-well polystyrene plate wells. 5 mL of microbial inoculum was added to each well. To prepare inoculums, overnight cultures of microbes were pelleted by centrifugation (7,000 ×g,

Synthetic tap water (STW; DIN10531), prepared as 5 × stock	300 mg/L NaHCO ₃ , 175 mg/L MgSO ₄ , 300 mg/L CaCl ₂ ; pH 7.5 in 1xSTW
Nutrient broth (ISO 22196)	3 g/L meat extract, 10 g/L peptone, 5 g/L NaCl; pH 6.8–7.2
Lysogeny broth (LB)	5 g/L tryptone, 5 g/L yeast extract, 5 g/L NaCl; pH 6.8–7.2
Yeast extract peptone dextrose medium (YPD) and respective agar	20 g/L peptone, 10 g/L yeast extract, 20 g/L glycerol + 15 g/L agar for plates; pH 6.8–7.2
Phosphate buffered saline (PBS)	8 g/L NaCl, 0.2 g/L KCl, 0.81 g/L Na ₂ HPO ₄ × 2H ₂ O, 0.2 g/L KH ₂ PO ₄ ; pH 7.1
Nutrient agar (ISO 22196)	5 g/L meat extract, 10 g/L peptone, 5 g/L NaCl, 15 g/L agar; pH 7.0–7.2
Soybean casein digest broth with lecithin and polyoxyethylene sorbitan monooleate (SCDLP broth; ISO 22196)	17 g/L casein peptone, 3 g/L soybean peptone, 5 g/L NaCl, 2.5 g/L Na ₂ HPO ₄ , 2.5 g/L glucose, 1.0 g/L lecithin, 7.0 g/L nonionic surfactant; pH 6.8–7.2
Sodium cacodylate buffer, prepared as 0.2 M stock	4.8 g Na(CH ₂) ₂ AsO ₃ × 3 H ₂ O in 100 mL deionized water brought to pH 7.4 with the addition of 5.6 mL 0.2 M HCl

Table 1. Media and buffers.

10 min) and washed twice with deionized water before re-suspension in test medium and density optimization. Initial cell density was about 10⁷ CFU/mL in oligotrophic conditions, i.e., synthetic tap water (STW; Table 1) containing 1:500 diluted nutrient broth (NB; Table 1) and 10⁵ CFU/mL in growth media, i.e., lysogeny broth (LB, Table 1) in case of bacteria and yeast extract-peptone-dextrose medium (YPD, Table 1) in case of yeast. Surfaces were incubated in dark static conditions (covered with aluminum foil) at room temperature (22 °C) to allow biofilm formation. After 0, 3, 24, 48 and 72 h three samples of each surface were dip-rinsed in PBS (Table 1) with sterile forceps, carefully drained from one corner and submerged in 15 mL 0.5 × neutralizing broth (SCDLP; Table 1) with 1.5 M NaCl in 50 mL centrifuge tube, vortexed for 30 s at max speed, ultrasonicated for 15 min in ultrasonic bath (Branson1800) and again vortexed for 30 s. An aliquot of each resulting suspension was serially diluted in PBS and drop-plated on nutrient agar (NA) or yeast growth agar (YPD agar, Table 1) for colony counting. Planktonic fraction in 5 mL media over biofilms in each well was mixed by pipetting, serially diluted and plated for planktonic colony count. To assess Zn release from the surfaces, an aliquot from planktonic fraction (including microbes) in wells above the biofilms was taken for elemental analysis. TXRF (S2 Picofox, Bruker) was used for Zn analysis. Maximum calculated Ag concentration in the test system in case of complete release of Ag from the surface coating was estimated to reach 15.27 ± 2.21 ng/mL (Supplementary Table 1). Actual release could not be measured due to high adsorption of Ag to organic material and well walls.

Viable counts of cells harvested from biofilms were calculated as follows:

$$\frac{\text{CFU}}{\text{cm}^2} = \text{CFUs counted} \times \text{serial dilution factor} \times \frac{\text{sonication volume}(\mu\text{L})}{\text{plated volume}(\mu\text{L})} \times \frac{1}{\text{sample surface area}(\text{cm}^2)}$$

Viable counts of inoculums and planktonic cells were calculated as follows:

$$\text{CFU/ml} = \text{CFUs counted} \times \text{dilution factor} \times \frac{1000(\mu\text{L})}{\text{plated volume}(\mu\text{L})}$$

Ultrasonication protocol. SCDLP (Table 1) was used for toxicity neutralizing properties (ISO 27447) and its surfactant content was expected to enhance releasing biofilms from surfaces. 1.5 M NaCl was used to aid in biofilm harvesting as it has also been successfully used for extracellular matrix removal⁹⁹ and does not influence microbial viability when combined with ultrasonication and vortexing (Supplementary Fig. 7). Staining with 30 μM propidium iodide and 5 μM Syto 9 with subsequent epifluorescence microscopy (see below) was used to evaluate biofilm harvesting efficiency. It was confirmed that adherent cells were removed from the surfaces (data not shown).

Staining and microscopy. Biofilms were stained to visualize total cellular biomass (DNA/RNA), surface-associated amyloid fibers (SAF) and chitin (in case of yeast). Before staining, the biofilms were dip-rinsed in PBS (Table 1) to remove loosely bound cells as described above and fixed by 2-h incubation in 2.0% glutaraldehyde in 0.1 M sodium cacodylate buffer (Table 1) followed by rinsing once in the same buffer. For total cellular biomass visualization, nucleic acids were stained by incubating the fixed cells for 15 min with 5 μM Syto 9. For staining of SAF and chitin (fungal cell wall component), fixed biofilms were incubated for 15 min with 5 μM Syto 9 and 10 μM Congo Red. Stained biofilms were visualized with Olympus CX41 using exciter filter BP475, dichroic mirror DM500, barrier filter O515IF (Syto9 staining) or with Zeiss LSM800 confocal laser scanning microscope (CLSM) using excitation/emission track settings of 488 nm/505–550 nm (Syto 9) and 561 nm/575–700 nm (Congo Red).

Congo Red (CR), used to stain SAFs, also stains cellulose and chitin in fungal cell walls¹⁰⁰ due to structural similarity to cellulose. In this study, we have used CR also to visualize *C. albicans* cells by staining both cell wall and fungal SAFs¹⁰¹. Regarding possible cellulose signal interfering with amyloid staining of *E. coli*, as cellulose is

a known component in ECM of several *Enterobacteriaceae* species, it is known that *E. coli* K-12 strains, including MG1655 have a stop codon mutation in the cellulose operon and do not produce cellulose¹⁰².

To visualize biofilm morphology, electron microscopy was used. For that, fixed biofilms were gradually dehydrated with ethanol, air-dried, coated with 3 nm Au/Pd layer (Polaron Emitech SC7640 Sputter Coater) and visualized with scanning electron microscopy (FEI Helios NanoLab 600).

Cytotoxicity testing. Toxicity of the surfaces was tested on human immortalized HaCaT keratinocytes (ThermoFisher). Cells were maintained in DMEM high glucose medium supplemented with Na-pyruvate (1 mM), penicillin–streptomycin (100 U/mL and 100 µg/mL, respectively) and fetal bovine serum (10%) at 37 °C and 5% CO₂. During maintenance, the cell density was kept between 0.5–1 × 10⁶ cells/mL. Each type of surface in four replicates was placed into a separate well of a 6-well plate and 2 mL of cell suspension (4 × 10⁴ cells/mL) in supplemented DMEM medium was added. Cells were cultivated for 48 h, surfaces were removed using tweezers to a new well of a 6-well plate. An aliquot of the remaining medium was taken for Zn concentration measurement by TXRF (S2 Picofox, Bruker). One replicate of each type of surface was left for microscopy while to the rest of three replicates 0.33% of Neutral Red (Sigma) solution in supplemented DMEM medium was added and incubated at 37 °C and 5% CO₂ for 4 h. After that, the dye solution was removed by double washing with PBS and the dye remaining within viable cells was dissolved over 10 min (gentle shaking) using 1 mL of Neutral Red Assay Solubilization Solution (Sigma). The intensity of Neutral Red dye was measured spectrophotometrically at 540 nm using Fluoroskan plate reader (Thermo). Cell viability on nano-ZnO and nano-ZnO/Ag surfaces was calculated as percentage of viability on uncoated surface. Cell viability assays on surfaces were repeated twice. For microscopy, the surfaces with cells were first covered with 3.7% formaldehyde in 0.1% TritonX-100 solution for 10 min, then with 1 µg/mL solution of Hoechst 33,342 (ThermoFisher) and 1 µg/mL Phalloidin-TRITC (Sigma) in PBS for 30 min. After that, the dye solution was removed and cells were imaged using confocal microscope with filter settings for DAPI and TRITC.

For cytotoxicity assays of respective soluble salts (Fig. 7), exposure to HaCaT cells was carried out in 96-well format and cell viability was assessed using Neutral Red assay, essentially as described above.

Statistical analysis. One- or two-way ANOVA analysis followed by Tukey *post-hoc* test was used to detect significant differences in multiple comparisons at 0.05 significance level using GraphPad Prism 8.3.0. Log-transformed data was used for the analysis of CFU counts. Only statistically significant ($P < 0.05$) differences and log reductions are mentioned in the text unless stated otherwise.

Received: 20 March 2020; Accepted: 6 July 2020

Published online: 10 August 2020

References

- Flemming, H.-C. & Wuertz, S. Bacteria and archaea on Earth and their abundance in biofilms. *Nat. Rev. Microbiol.* **17**(4), 247–260. <https://doi.org/10.1038/s41579-019-0158-9> (2019).
- NIH. *Research on microbial biofilms*: PA Number: PA-03-047 (National Institute of Health, 2002). <https://grants.nih.gov/grant/s/guide/pa-files/PA-03-047.html>.
- Pendleton, J. N., Gorman, S. P. & Gilmore, B. E. Clinical relevance of the ESKAPE pathogens. *Expert Rev. Anti-infect. Ther.* **11**(3), 297–308. <https://doi.org/10.1586/eri.13.12> (2013).
- Ceri, H. *et al.* The Calgary Biofilm Device: new technology for rapid determination of antibiotic susceptibilities of bacterial biofilms. *J. Clin. Microbiol.* **37**(6), 1771–1776 (1999).
- France, M. T., Cornea, A., Kehlet-Delgado, H. & Forney, L. J. Spatial structure facilitates the accumulation and persistence of antibiotic-resistant mutants in biofilms. *Evol Appl* **12**(3), 498–507. <https://doi.org/10.1111/eva.12728> (2019).
- Olsen, I. Biofilm-specific antibiotic tolerance and resistance. *Eur. J. Clin. Microbiol. Infect. Dis.* **34**(5), 877–886. <https://doi.org/10.1007/s10096-015-2323-z> (2015).
- Santos-Lopez, A., Marshall, C. W., Scribner, M. R., Snyder, D. J. & Cooper, V. S. Evolutionary pathways to antibiotic resistance are dependent upon environmental structure and bacterial lifestyle. *Elife* **8**, 13. <https://doi.org/10.7554/eLife.47612> (2019).
- Sjollema, J. *et al.* In vitro methods for the evaluation of antimicrobial surface designs. *Acta Biomater.* **70**, 12–24. <https://doi.org/10.1016/j.actbio.2018.02.001> (2018).
- Rosenberg, M., Azevedo, N. F. & Ivask, A. Propidium iodide staining underestimates viability of adherent bacterial cells. *Sci. Rep.* <https://doi.org/10.1038/s41598-019-42906-3> (2019).
- Kragh, K. N., Alhede, M., Kvich, L. & Bjarnsholt, T. Into the well—A close look at the complex structures of a microtiter biofilm and the crystal violet assay. *Biofilm* <https://doi.org/10.1016/j.biofilm.2019.100006> (2019).
- Mandakhalikar, K. D. *et al.* Extraction and quantification of biofilm bacteria: Method optimized for urinary catheters. *Sci Rep* **8**(1), 8069. <https://doi.org/10.1038/s41598-018-26342-3> (2018).
- Kobayashi, H., Oethinger, M., Tuohy, M. J., Procop, G. W. & Bauer, T. W. Improved detection of biofilm-formative bacteria by vortexing and sonication: a pilot study. *Clin. Orthop. Relat. Res.* **467**(5), 1360–1364. <https://doi.org/10.1007/s11999-008-0609-5> (2009).
- Harrison, J. J., Ceri, H., Stremick, C. A. & Turner, R. J. Biofilm susceptibility to metal toxicity. *Environ. Microbiol.* **6**(12), 1220–1227. <https://doi.org/10.1111/j.1462-2920.2004.00656.x> (2004).
- Lemire, J. A., Harrison, J. J. & Turner, R. J. Antimicrobial activity of metals: mechanisms, molecular targets and applications. *Nat. Rev. Microbiol.* **11**(6), 371–384. <https://doi.org/10.1038/nrmicro3028> (2013).
- Andreini, C., Banci, L., Bertini, I. & Rosato, A. Zinc through the three domains of life. *J. Proteome Res.* **5**(11), 3173–3178. <https://doi.org/10.1021/pr0603699> (2006).
- Harrison, J. J. *et al.* Chromosomal antioxidant genes have metal ion-specific roles as determinants of bacterial metal tolerance. *Environ. Microbiol.* **11**(10), 2491–2509. <https://doi.org/10.1111/j.1462-2920.2009.01973.x> (2009).
- Couñago, R. M. *et al.* Imperfect coordination chemistry facilitates metal ion release in the Psa permease. *Nat Chem Biol* **10**(1), 35–41. <https://doi.org/10.1038/nchembio.1382> (2014).

18. McDevitt, C. A. *et al.* A molecular mechanism for bacterial susceptibility to zinc. *PLoS Pathog* **7**(11), e1002357. <https://doi.org/10.1371/journal.ppat.1002357> (2011).
19. Ong, C. Y., Walker, M. J. & McEwan, A. G. Zinc disrupts central carbon metabolism and capsule biosynthesis in *Streptococcus pyogenes*. *Sci. Rep.* **5**(1), 10799. <https://doi.org/10.1038/srep10799> (2015).
20. Mills, D. A., Schmidt, B., Hiser, C., Westley, E. & Ferguson-Miller, S. Membrane potential-controlled inhibition of cytochrome c oxidase by zinc. *J. Biol. Chem.* **277**(17), 14894–14901. <https://doi.org/10.1074/jbc.M111922200> (2002).
21. Hosler, J. P., Ferguson-Miller, S. & Mills, D. A. Energy transduction: proton transfer through the respiratory complexes. *Annu. Rev. Biochem.* **75**(1), 165–187. <https://doi.org/10.1146/annurev.biochem.75.062003.101730> (2006).
22. Eijkelkamp, B. A. *et al.* Extracellular zinc competitively inhibits manganese uptake and compromises oxidative stress management in *Streptococcus pneumoniae*. *PLoS ONE* **9**(2), e89427. <https://doi.org/10.1371/journal.pone.0089427> (2014).
23. Pasquet, J. *et al.* The contribution of zinc ions to the antimicrobial activity of zinc oxide. *Colloids Surf. A* **457**, 263–274. <https://doi.org/10.1016/j.colsurfa.2014.05.057> (2014).
24. Sirelkhatim, A. *et al.* Review on zinc oxide nanoparticles: antibacterial activity and toxicity mechanism. *Nano-Micro Lett.* **7**(3), 219–242. <https://doi.org/10.1007/s40820-015-0040-x> (2015).
25. Seil, J. T. & Webster, T. J. Reduced *Staphylococcus aureus* proliferation and biofilm formation on zinc oxide nanoparticle PVC composite surfaces. *Acta Biomater.* **7**(6), 2579–2584. <https://doi.org/10.1016/j.actbio.2011.03.018> (2011).
26. Pati, R. *et al.* Topical application of zinc oxide nanoparticles reduces bacterial skin infection in mice and exhibits antibacterial activity by inducing oxidative stress response and cell membrane disintegration in macrophages. *Nanomedicine* **10**(6), 1195–1208. <https://doi.org/10.1016/j.nano.2014.02.012> (2014).
27. Lee, J.-H., Kim, Y.-G., Cho, M. H. & Lee, J. ZnO nanoparticles inhibit *Pseudomonas aeruginosa* biofilm formation and virulence factor production. *Microbiol. Res.* **169**(12), 888–896. <https://doi.org/10.1016/j.micres.2014.05.005> (2014).
28. Lee, L. J., Barrett, J. A. & Poole, R. K. Genome-wide transcriptional response of chemostat-cultured *Escherichia coli* to zinc. *J. Bacteriol.* **187**(3), 1124–1134. <https://doi.org/10.1128/JB.187.3.1124-1134.2005> (2005).
29. Brayner, R. *et al.* Toxicological impact studies based on *Escherichia coli* bacteria in ultrafine ZnO nanoparticles colloidal medium. *Nano Lett.* **6**(4), 866–870. <https://doi.org/10.1021/nl052326h> (2006).
30. Dutta, R. K., Nenavathu, B. P., Gangishetty, M. K. & Reddy, A. V. R. Studies on antibacterial activity of ZnO nanoparticles by ROS induced lipid peroxidation. *Colloids Surf., B* **94**, 143–150. <https://doi.org/10.1016/j.colsurfb.2012.01.046> (2012).
31. Bragg, P. D. & Rainnie, D. J. The effect of silver ions on the respiratory chain of *Escherichia coli*. *Can. J. Microbiol.* **20**(6), 883–889. <https://doi.org/10.1139/m74-135> (1974).
32. Park, H.-J. *et al.* Silver-ion-mediated reactive oxygen species generation affecting bactericidal activity. *Water Res.* **43**(4), 1027–1032. <https://doi.org/10.1016/j.watres.2008.12.002> (2009).
33. Liao, S. Y., Read, D. C., Pugh, W. J., Furr, J. R. & Russell, A. D. Interaction of silver nitrate with readily identifiable groups: relationship to the antibactericidal action of silver ions. *Lett. Appl. Microbiol.* **25**(4), 279–283. <https://doi.org/10.1046/j.1472-765X.1997.00219.x> (1997).
34. Lok, C.-N. *et al.* Silver nanoparticles: partial oxidation and antibacterial activities. *J. Biol. Inorg. Chem.* **12**(4), 527–534. <https://doi.org/10.1007/s00775-007-0208-z> (2007).
35. Russell, A. D. & Hugo, W. B. Antimicrobial activity and action of silver. *Progr. Med. Chem.* **31**, 351–370 (1994).
36. Jung, W. K. *et al.* Antibacterial activity and mechanism of action of the silver ion in *Staphylococcus aureus* and *Escherichia coli*. *AEM* **74**(7), 2171–2178. <https://doi.org/10.1128/AEM.02001-07> (2008).
37. Lok, C.-N. *et al.* Proteomic analysis of the mode of antibacterial action of silver nanoparticles. *J. Proteome Res.* **5**(4), 916–924. <https://doi.org/10.1021/pr0504079> (2006).
38. Feng, Q. L. *et al.* A mechanistic study of the antibacterial effect of silver ions on *Escherichia coli* and *Staphylococcus aureus*. *J. Biomed. Mater. Res.* **52**(4), 662–668. [https://doi.org/10.1002/1097-4636\(20001215\)52:4<662::aid-jbm10>3.0.co;2-3](https://doi.org/10.1002/1097-4636(20001215)52:4<662::aid-jbm10>3.0.co;2-3) (2000).
39. Clement, J. L. & Jarrett, P. S. Antibacterial silver. *Met.-Based Drugs* **1**(5–6), 467–482. <https://doi.org/10.1155/MBD.1994.467> (1994).
40. Gómez-Gómez, B. *et al.* Unravelling mechanisms of bacterial quorum sensing disruption by metal-based nanoparticles. *Sci. Total Environ.* **696**, 133869. <https://doi.org/10.1016/j.scitotenv.2019.133869> (2019).
41. Al-Shabib, N. A. *et al.* Biogenic synthesis of Zinc oxide nanostructures from *Nigella sativa* seed: prospective role as food packaging material inhibiting broad-spectrum quorum sensing and biofilm. *Sci. Rep.* **6**(1), 36761. <https://doi.org/10.1038/srep36761> (2016).
42. García-Lara, B. *et al.* Inhibition of quorum-sensing-dependent virulence factors and biofilm formation of clinical and environmental *Pseudomonas aeruginosa* strains by ZnO nanoparticles. *Lett. Appl. Microbiol.* **61**(3), 299–305. <https://doi.org/10.1111/lam.12456> (2015).
43. Zähringer, F., Lacanna, E., Jenal, U., Schirmer, T. & Boehm, A. Structure and signaling mechanism of a zinc-sensory diguanylate cyclase. *Structure* **21**(7), 1149–1157. <https://doi.org/10.1016/j.str.2013.04.026> (2013).
44. Huma, Z. *et al.* Nanosilver mitigates biofilm formation via FapC amyloidosis inhibition. *Small* <https://doi.org/10.1002/sml.201906674> (2020).
45. Yarovskiy, A. E., Johns, S. L., Schuck, P. & Herr, A. B. The biofilm adhesion protein Aap from *Staphylococcus epidermidis* forms zinc-dependent amyloid fibers. *J. Biol. Chem.* **295**(14), 4411–4427. <https://doi.org/10.1074/jbc.RA119.010874> (2020).
46. Joost, U. *et al.* Photocatalytic antibacterial activity of nano-TiO₂ (anatase)-based thin films: effects on *Escherichia coli* cells and fatty acids. *J. Photochem. Photobiol., B* **142**, 178–185. <https://doi.org/10.1016/j.jphotobiol.2014.12.010> (2015).
47. LakshmiPrasanna, V. & Vijayaraghavan, R. Insight into the mechanism of antibacterial activity of ZnO: surface defects mediated reactive oxygen species even in the dark. *Langmuir* **31**(33), 9155–9162. <https://doi.org/10.1021/acs.langmuir.5b02266> (2015).
48. Sun, H. *et al.* Zinc oxide/vanadium pentoxide heterostructures with enhanced day-night antibacterial activities. *J. Colloid Interface Sci.* **547**, 40–49. <https://doi.org/10.1016/j.jcis.2019.03.061> (2019).
49. Hirota, K. *et al.* Preparation of zinc oxide ceramics with a sustainable antibacterial activity under dark conditions. *Ceram. Int.* **36**(2), 497–506. <https://doi.org/10.1016/j.ceramint.2009.09.026> (2010).
50. Lipovsky, A., Nitzan, Y., Gedanken, A. & Lubart, R. Antifungal activity of ZnO nanoparticles—the role of ROS mediated cell injury. *Nanotechnology* **22**(10), 105101. <https://doi.org/10.1088/0957-4484/22/10/105101> (2011).
51. Abdulkareem, E. H. *et al.* Anti-biofilm activity of zinc oxide and hydroxyapatite nanoparticles as dental implant coating materials. *J. Dent.* **43**(12), 1462–1469. <https://doi.org/10.1016/j.jdent.2015.10.010> (2015).
52. Carvalho, P. *et al.* Influence of thickness and coatings morphology in the antimicrobial performance of zinc oxide coatings. *Appl. Surf. Sci.* **307**, 548–557. <https://doi.org/10.1016/j.apsusc.2014.04.072> (2014).
53. Vissnapuu, M. *et al.* UVA-induced antimicrobial activity of ZnO/Ag nanocomposite covered surfaces. *Colloids Surf. B* **169**, 222–232. <https://doi.org/10.1016/j.colsurfb.2018.05.009> (2018).
54. International Organization for Standardization. “ISO 22196:2011 Measurement of antibacterial activity on plastics and other non-porous surfaces.” International Organization for Standardization. www.iso.org. (2011)
55. International Organization for Standardization. “ISO 27447:2009 Fine ceramics (advanced ceramics, advanced technical ceramics)—Test method for antibacterial activity of semiconducting photocatalytic materials.” International Organization for Standardization. www.iso.org. (2009).

56. O'Toole, G. A. & Kolter, R. Initiation of biofilm formation in *Pseudomonas fluorescens* WCS365 proceeds via multiple, convergent signalling pathways: a genetic analysis. *Mol. Microbiol.* **28**(3), 449–461. <https://doi.org/10.1046/j.1365-2958.1998.00797.x> (1998).
57. Herrmann, R., García-García, F. J. & Reller, A. Rapid degradation of zinc oxide nanoparticles by phosphate ions. *Beilstein J. Nanotechnol.* **5**, 2007–2015. <https://doi.org/10.3762/bjnano.5.209> (2014).
58. Li, M., Zhu, L. & Lin, D. Toxicity of ZnO nanoparticles to *Escherichia coli*: mechanism and the influence of medium components. *Environ. Sci. Technol.* **45**(5), 1977–1983. <https://doi.org/10.1021/es102624t> (2011).
59. Behra, R. et al. Bioavailability of silver nanoparticles and ions: from a chemical and biochemical perspective. *J. R. Soc Interface* **10**(87), 20130396. <https://doi.org/10.1098/rsif.2013.0396> (2013).
60. Xiu, Z.-M., Ma, J. & Alvarez, P. J. J. Differential effect of common ligands and molecular oxygen on antimicrobial activity of silver nanoparticles versus silver ions. *Environ. Sci. Technol.* **45**(20), 9003–9008. <https://doi.org/10.1021/es201918f> (2011).
61. Suppi, S. et al. A novel method for comparison of biocidal properties of nanomaterials to bacteria, yeasts and algae. *J. Hazard. Mater.* **286**, 75–84. <https://doi.org/10.1016/j.jhazmat.2014.12.027> (2015).
62. Brown, L., Wolf, J. M., Prados-Rosales, R. & Casadevall, A. Through the wall: extracellular vesicles in Gram-positive bacteria, mycobacteria and fungi. *Nat. Rev. Microbiol.* **13**(10), 620–630. <https://doi.org/10.1038/nrmicro3480> (2015).
63. Lee, E.-Y. et al. Gram-positive bacteria produce membrane vesicles: proteomics-based characterization of *Staphylococcus aureus*-derived membrane vesicles. *Proteomics* **9**(24), 5425–5436. <https://doi.org/10.1002/pmic.200900338> (2009).
64. Andreoni, F. et al. Antibiotics stimulate formation of vesicles in *Staphylococcus aureus* in both phase-dependent and -independent fashions and via different routes. *Antimicrob. Agents Chemother.* **63**(2), e01439–e1518. <https://doi.org/10.1128/AAC.01439-18> (2018).
65. Formosa-Dague, C., Speziale, P., Foster, T. J., Geoghegan, J. A. & Dufrene, Y. F. Zinc-dependent mechanical properties of *Staphylococcus aureus* biofilm-forming surface protein SasG. *Proc. Natl. Acad. Sci. USA* **113**(2), 410–415. <https://doi.org/10.1073/pnas.1519265113> (2016).
66. Conrady, D. G. et al. A zinc-dependent adhesion module is responsible for intercellular adhesion in staphylococcal biofilms. *Proc. Natl. Acad. Sci. USA* **105**(49), 19456–19461. <https://doi.org/10.1073/pnas.0807717105> (2008).
67. Sudbery, P., Gow, N. & Berman, J. The distinct morphogenic states of *Candida albicans*. *Trends Microbiol.* **12**(7), 317–324. <https://doi.org/10.1016/j.tim.2004.05.008> (2004).
68. Flemming, H.-C. & Wingender, J. The biofilm matrix. *Nat. Rev. Microbiol.* <https://doi.org/10.1038/nrmicro2415> (2010).
69. Stiefel, P., Schmidt-Emrich, S., Maniura-Weber, K. & Ren, Q. Critical aspects of using bacterial cell viability assays with the fluorophores SYTO9 and propidium iodide. *BMC Microbiol.* **15**(1), 36. <https://doi.org/10.1186/s12866-015-0376-x> (2015).
70. Gugal, N., Lemire, J. A. & Turner, R. J. The efficacy of different anti-microbial metals at preventing the formation of, and eradicating bacterial biofilms of pathogenic indicator strains. *J. Antibiot.* **70**(6), 775–780. <https://doi.org/10.1038/ja.2017.10> (2017).
71. Schwartz, K., Syed, A. K., Stephenson, R. E., Rickard, A. H. & Boles, B. R. Functional amyloids composed of phenol soluble modulins stabilize *Staphylococcus aureus* biofilms. *PLoS Pathog.* **8**(6), e1002744. <https://doi.org/10.1371/journal.ppat.1002744> (2012).
72. Barnhart, M. M. & Chapman, M. R. Curli biogenesis and function. *Annu. Rev. Microbiol.* **60**(1), 131–147. <https://doi.org/10.1146/annurev.micro.60.080805.142106> (2006).
73. Taglialegna, A. et al. Staphylococcal bap proteins build amyloid scaffold biofilm matrices in response to environmental signals. *PLoS Pathog.* **12**(6), e1005711. <https://doi.org/10.1371/journal.ppat.1005711> (2016).
74. Dutta, A., Bhattacharyya, S., Kundu, A., Dutta, D. & Das, A. K. Macroscopic amyloid fiber formation by staphylococcal biofilm associated SuhB protein. *Biophys. Chem.* **217**, 32–41. <https://doi.org/10.1016/j.bpc.2016.07.006> (2016).
75. Töugu, V. et al. Zn(II)- and Cu(II)-induced non-fibrillar aggregates of amyloid- β (1–42) peptide are transformed to amyloid fibrils, both spontaneously and under the influence of metal chelators. *J. Neurochem.* **110**(6), 1784–1795. <https://doi.org/10.1111/j.1471-4159.2009.06269.x> (2009).
76. Sarell, C. J., Wilkinson, S. R. & Viles, J. H. Substoichiometric levels of Cu²⁺ ions accelerate the kinetics of fiber formation and promote cell toxicity of amyloid- β from Alzheimer disease. *J. Biol. Chem.* **285**(53), 41533–41540. <https://doi.org/10.1074/jbc.M110.171355> (2010).
77. Abelein, A., Gräslund, A. & Danielsson, J. Zinc as chaperone-mimicking agent for retardation of amyloid β peptide fibril formation. *Proc. Natl. Acad. Sci. USA* **112**(17), 5407–5412. <https://doi.org/10.1073/pnas.1421961112> (2015).
78. Ma, B., Zhang, F., Wang, X. & Zhu, X. Investigating the inhibitory effects of zinc ions on amyloid fibril formation of hen egg-white lysozyme. *Int. J. Biol. Macromol.* **98**, 717–722. <https://doi.org/10.1016/j.ijbiomac.2017.01.128> (2017).
79. Ban, D. K. & Paul, S. Nano zinc oxide inhibits fibrillar growth and suppresses cellular toxicity of lysozyme amyloid. *ACS Appl. Mater. Interfaces* **8**(46), 31587–31601. <https://doi.org/10.1021/acsami.6b11549> (2016).
80. Wilson, D. *Candida albicans*. *Trends Microbiol.* **27**(2), 188–189. <https://doi.org/10.1016/j.tim.2018.10.010> (2019).
81. Kurakado, S., Arai, R. & Sugita, T. Association of the hypha-related protein Pra1 and zinc transporter Zrt1 with biofilm formation by the pathogenic yeast *Candida albicans*: Pra1 and Zrt1 regulate biofilm formation. *Microbiol. Immunol.* **62**(6), 405–410. <https://doi.org/10.1111/1348-0421.12596> (2018).
82. Cierech, M. et al. Significance of polymethylmethacrylate (PMMA) modification by zinc oxide nanoparticles for fungal biofilm formation. *Int. J. Pharm.* **510**(1), 323–335. <https://doi.org/10.1016/j.ijpharm.2016.06.052> (2016).
83. Jalal, M., Ansari, M. A., Ali, S. G., Khan, H. M. & Rehman, S. Anticandidal activity of bioinspired ZnO NPs: effect on growth, cell morphology and key virulence attributes of *Candida* species. *Artif. Cells Nanomed. Biotechnol.* **46**(sup1), 912–925. <https://doi.org/10.1080/21691401.2018.1439837> (2018).
84. Divya, M. et al. Biopolymer gelatin-coated zinc oxide nanoparticles showed high antibacterial, antibiofilm and anti-angiogenic activity. *J. Photochem. Photobiol. B* **178**, 211–218. <https://doi.org/10.1016/j.jphotobiol.2017.11.008> (2018).
85. Harrison, J. J. et al. Metal ions may suppress or enhance cellular differentiation in *Candida albicans* and *Candida tropicalis* Biofilms. *Appl. Environ. Microbiol.* **73**(15), 4940–4949. <https://doi.org/10.1128/AEM.02711-06> (2007).
86. Nobile, C. J. et al. Biofilm matrix regulation by *Candida albicans* Zap1. *PLoS Biol.* **7**(6), e1000133. <https://doi.org/10.1371/journal.pbio.1000133> (2009).
87. Ganguly, S. et al. Zap1 control of cell-cell signaling in *Candida albicans* biofilms. *Eukaryot. Cell* **10**(11), 1448–1454. <https://doi.org/10.1128/EC.05196-11> (2011).
88. Nobile, C. J. & Mitchell, A. P. Regulation of cell-surface genes and biofilm formation by the *C. Albicans* transcription factor Bcr1p. *Curr. Biol.* **15**(12), 1150–1155. <https://doi.org/10.1016/j.cub.2005.05.047> (2005).
89. Forsberg, K. et al. *Candida auris*: the recent emergence of a multidrug-resistant fungal pathogen. *Med. Mycol.* **57**(1), 1–12. <https://doi.org/10.1093/mmy/myy054> (2019).
90. Wisplinghoff, H. et al. Nosocomial bloodstream infections due to *Candida* spp. in the USA: species distribution, clinical features and antifungal susceptibilities. *Int. J. Antimicrob. Agents* **43**(1), 78–81. <https://doi.org/10.1016/j.ijantimicag.2013.09.005> (2014).
91. Klotz, S. A., Chasin, B. S., Powell, B., Gaur, N. K. & Lipke, P. N. Polymicrobial bloodstream infections involving *Candida* species: analysis of patients and review of the literature. *Diagn. Microbiol. Infect. Dis.* **59**(4), 401–406. <https://doi.org/10.1016/j.diagmicrobio.2007.07.001> (2007).
92. Bernard, C. et al. *Candida albicans* enhances initial biofilm growth of *Cutibacterium acnes* under aerobic conditions. *Biofouling* **35**(3), 350–360. <https://doi.org/10.1080/08927014.2019.1608966> (2019).

93. Fox, E. P. *et al.* Anaerobic Bacteria grow within *Candida albicans* biofilms and induce biofilm formation in suspension cultures. *Curr. Biol.* **24**(20), 2411–2416. <https://doi.org/10.1016/j.cub.2014.08.057> (2014).
94. Adam, B., Baillie, G. S. & Douglas, L. J. Mixed species biofilms of *Candida albicans* and *Staphylococcus epidermidis*. *J. Med. Microbiol.* **51**(4), 344–349. <https://doi.org/10.1099/0022-1317-51-4-344> (2002).
95. Lin, P.-H. *et al.* Zinc in wound healing modulation. *Nutrients* **10**(1), 16. <https://doi.org/10.3390/nu10010016> (2017).
96. Tenaud, I., Leroy, S., Chebassier, N. & Dreno, B. Zinc, copper and manganese enhanced keratinocyte migration through a functional modulation of keratinocyte integrins. *Exp Dermatol* **9**(6), 407–416. <https://doi.org/10.1034/j.1600-0625.2000.009006407.x> (2000).
97. Sliwinska, A. *et al.* Genotoxicity and cytotoxicity of ZnO and Al₂O₃ nanoparticles. *Toxicol. Mech. Methods* **25**(3), 176–183. <https://doi.org/10.3109/15376516.2015.1006509> (2015).
98. Uzar, N. K., Abudayyak, M., Akcay, N., Algun, G. & Özhan, G. Zinc oxide nanoparticles induced cyto- and genotoxicity in kidney epithelial cells. *Toxicol. Mech. Methods* **25**(4), 334–339. <https://doi.org/10.3109/15376516.2015.1045654> (2015).
99. Chiba, A., Sugimoto, S., Sato, F., Hori, S. & Mizunoe, Y. A refined technique for extraction of extracellular matrices from bacterial biofilms and its applicability: Extraction of ECM from bacterial biofilms. *Microb. Biotechnol.* **8**(3), 392–403. <https://doi.org/10.1111/1751-7915.12155> (2015).
100. Slifkin, M. & Cumbie, R. Congo red as a fluorochrome for the rapid detection of fungi. *J. Clin. Microbiol.* **26**(5), 827–830 (1988).
101. Lipke, P. N. *et al.* Strengthening relationships: amyloids create adhesion nanodomains in yeasts. *Trends Microbiol.* **20**(2), 59–65. <https://doi.org/10.1016/j.tim.2011.10.002> (2012).
102. Serra, D. O., Richter, A. M. & Hengge, R. Cellulose as an architectural element in spatially structured *Escherichia coli* biofilms. *J. Bacteriol.* **195**(24), 5540–5554. <https://doi.org/10.1128/JB.00946-13> (2013).

Acknowledgements

We thank Arvo Tõnisoo for help with SEM imaging and Dr Nuno F. Azevedo for consulting on biofilms. This work was supported by the Estonian Research Council Grants IUT 23-5, PUT 748, EAG20, PRG749, European Regional Development Fund projects “Emerging orders in quantum and nanomaterials (TK134)” and “Advanced materials and high-technology devices for sustain-able energetics, sensorics and nanoelectronics (TK141)” and ERDF project Centre of Technologies and Investigations of Nanomaterials (NAMUR+, project number 2014-2020.4.01.16-0123).

Author contributions

M.R. designed and executed biofilm experiments, analyzed the data and wrote the manuscript. M.V. designed and prepared the surfaces. A.I. designed and executed the cell culture experiments, assisted in experimental design, participated in writing and amending the manuscript. H.V. consulted on and executed elemental analysis. K.K. consulted regarding yeast biology and assisted in writing the manuscript. V.K. designed the surfaces, assisted in experimental design, participated in writing and amending the manuscript. A.K. consulted on general microbiology and critically edited the manuscript.

Competing interests

The authors declare no competing interests.

Additional information

Supplementary information is available for this paper at <https://doi.org/10.1038/s41598-020-70169-w>.

Correspondence and requests for materials should be addressed to M.R.

Reprints and permissions information is available at www.nature.com/reprints.

Publisher's note Springer Nature remains neutral with regard to jurisdictional claims in published maps and institutional affiliations.



Open Access This article is licensed under a Creative Commons Attribution 4.0 International License, which permits use, sharing, adaptation, distribution and reproduction in any medium or format, as long as you give appropriate credit to the original author(s) and the source, provide a link to the Creative Commons license, and indicate if changes were made. The images or other third party material in this article are included in the article's Creative Commons license, unless indicated otherwise in a credit line to the material. If material is not included in the article's Creative Commons license and your intended use is not permitted by statutory regulation or exceeds the permitted use, you will need to obtain permission directly from the copyright holder. To view a copy of this license, visit <http://creativecommons.org/licenses/by/4.0/>.

© The Author(s) 2020

Selective antibiofilm properties and biocompatibility of nano-ZnO and nano-ZnO/Ag coated surfaces

M. Rosenberg*^{1,2}, M. Visnapuu³, H. Vija¹, V. Kisand³, K. Kasemets¹, A. Kahru^{1,4}, A. Ivask^{1,5}

¹ Laboratory of Environmental Toxicology, National Institute of Chemical Physics and Biophysics, Tallinn, Estonia

² Department of Chemistry and Biotechnology, Tallinn University of Technology, Tallinn, Estonia

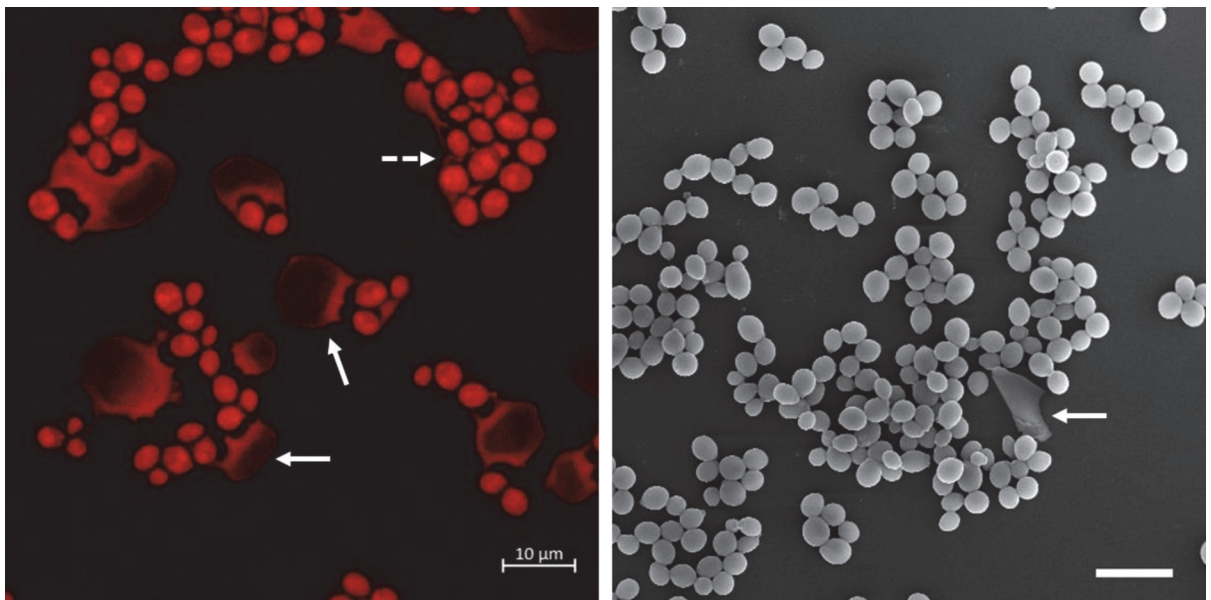
³ Institute of Physics, University of Tartu, Tartu, Estonia

⁴ Estonian Academy of Sciences, Tallinn, Estonia

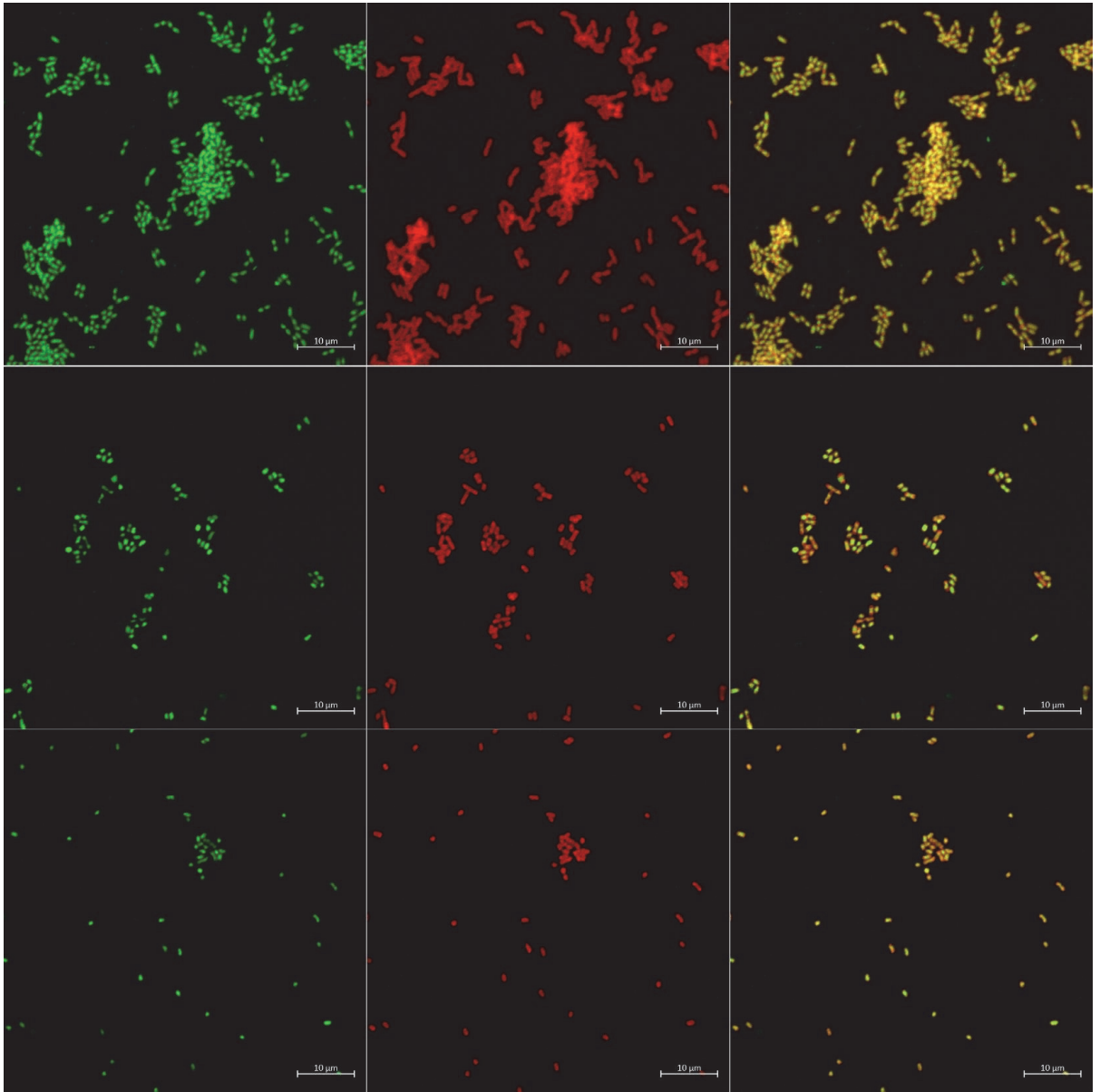
⁵ Institute of Molecular and Cell Biology, University of Tartu, Tartu, Estonia

* rosenbergmerilin@gmail.com

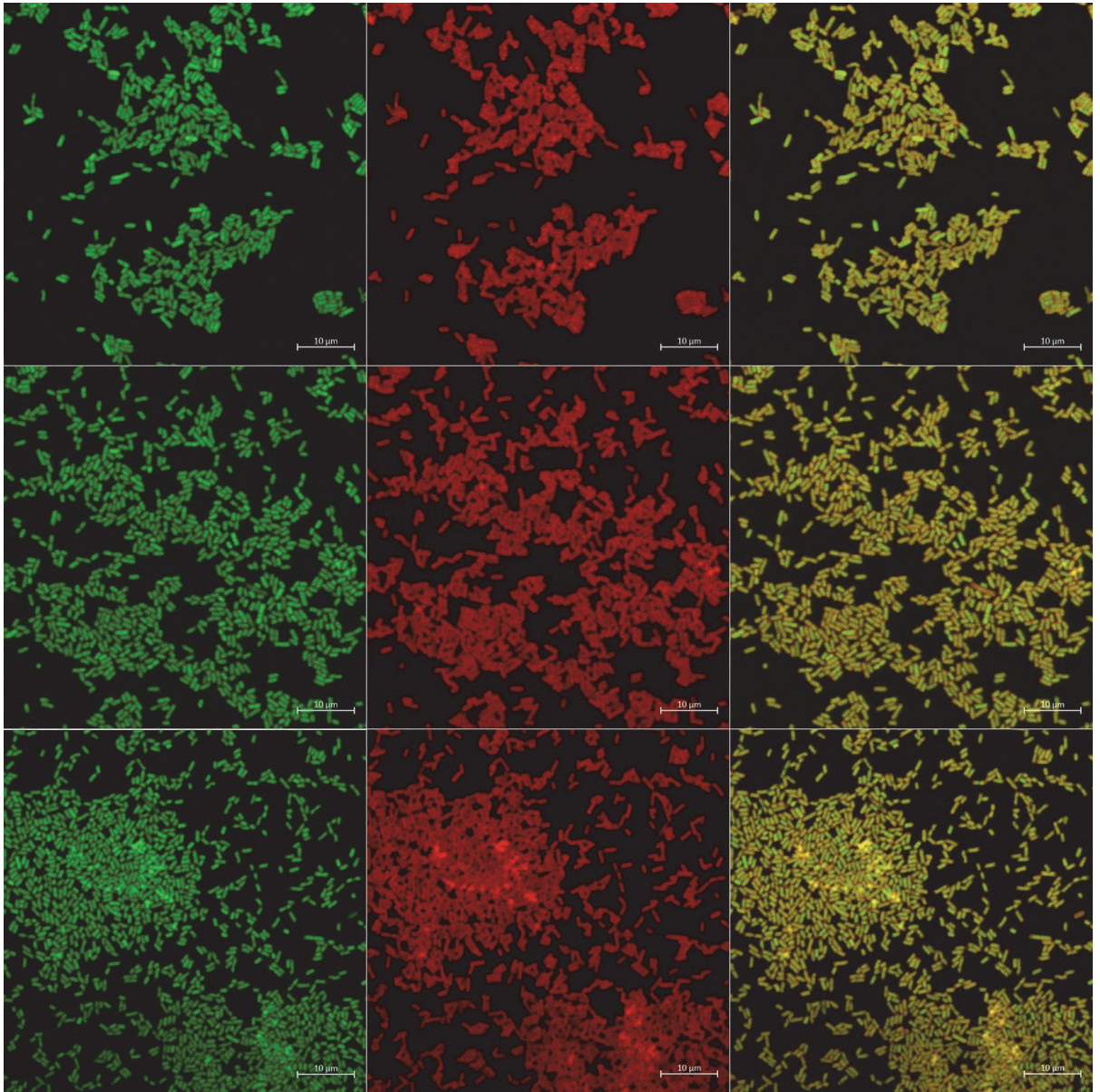
Supplementary figures



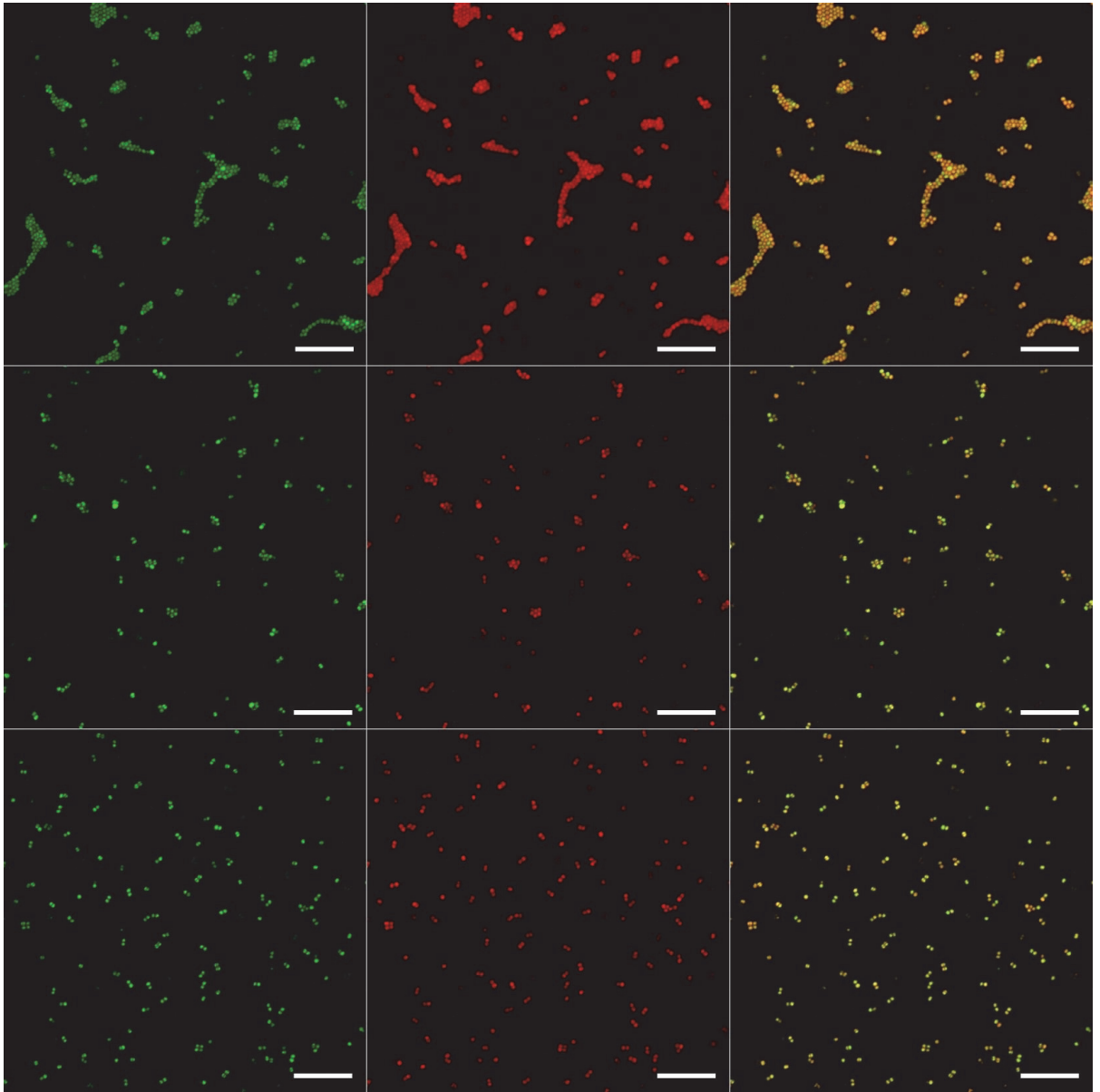
Supplementary Figure 1. 48 h *C. albicans* biofilm on sparse ZnO/Ag surface in growth medium: CLSM maximal orthogonal projection with cell walls stained red with Congo red (left) and SEM image (right). White arrows indicate flattened dead “ghost cells” that occur in patches on nano-ZnO/Ag surfaces and seem to act as a carrier for biofilm cells (dotted arrow). Most “ghost cells” are laterally detached from neighboring cells during several liquid manipulation steps in the fixing protocol and are mostly lost in SEM images. Scale bars represent 10 μm .



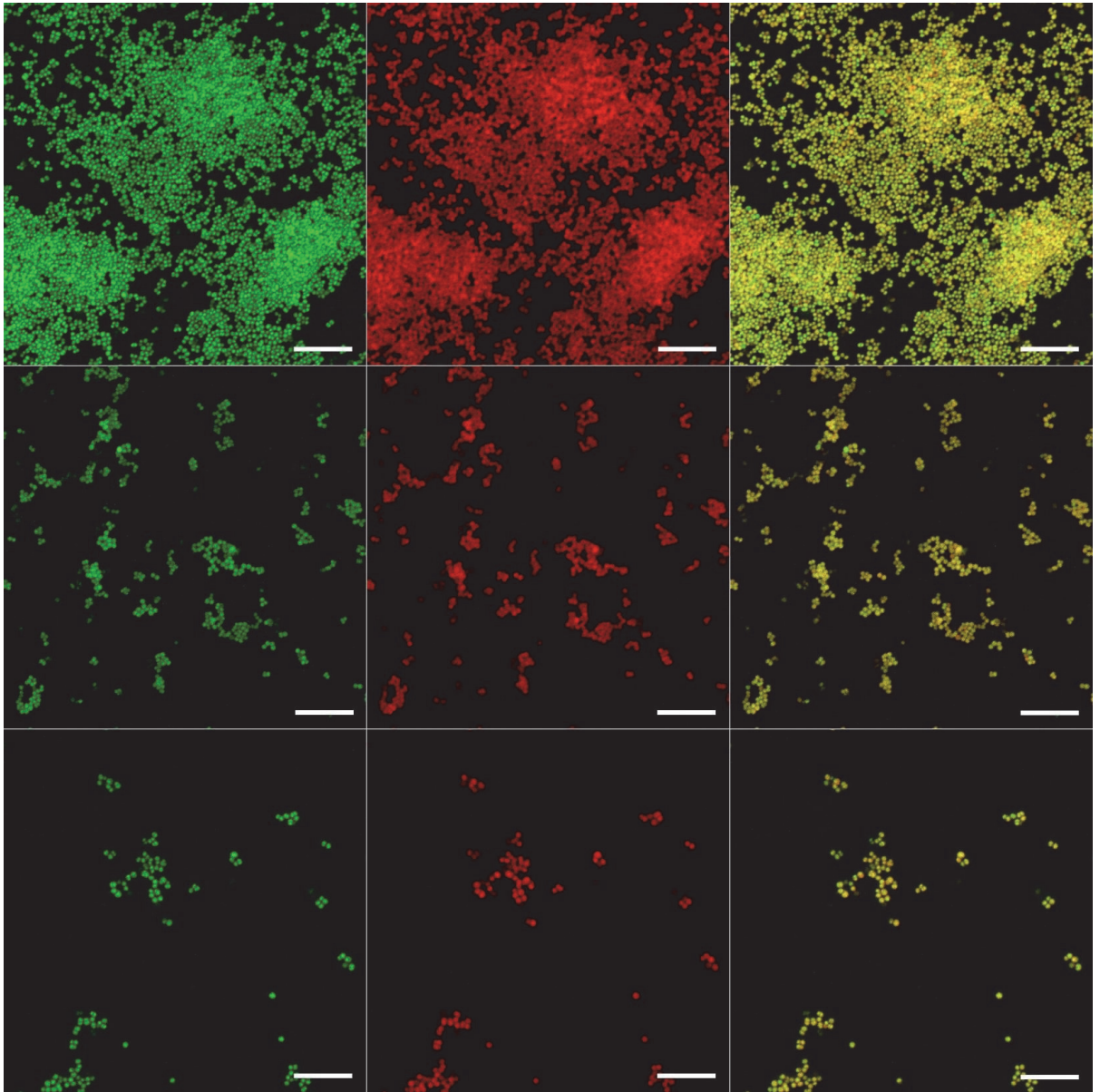
Supplementary Figure 2. Maximal orthogonal projections of representative CLSM images of fixed 48 h oligotrophic *E. coli* biofilm on uncoated surface (upper panel), sparse nano-ZnO surface (middle panel) and dense nano-ZnO (bottom panel). DNA/RNA stained with Syto9 (green channel, left column) and surface-associated amyloid fibers stained with Congo Red (red channel, middle column). Combined channel view in right column. Scale bars represent 10 μm.



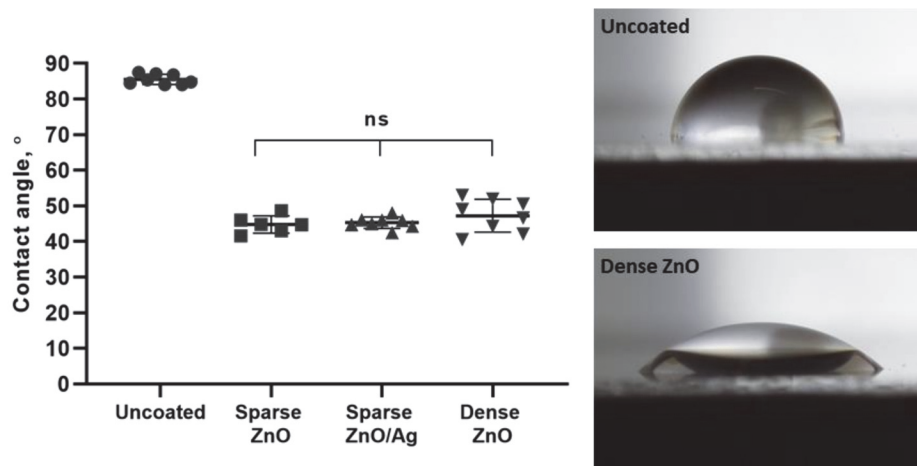
Supplementary Figure 3. Maximal orthogonal projections of representative CLSM images of fixed 48 h growth medium *E. coli* biofilm on uncoated surface (upper panel), sparse nano-ZnO surface (middle panel) and dense nano-ZnO (bottom panel). DNA/RNA stained with Syto9 (green channel, left column) and surface-associated amyloid fibers stained with Congo Red (red channel, middle column). Combined channel view in right column. Scale bars represent 10 µm.



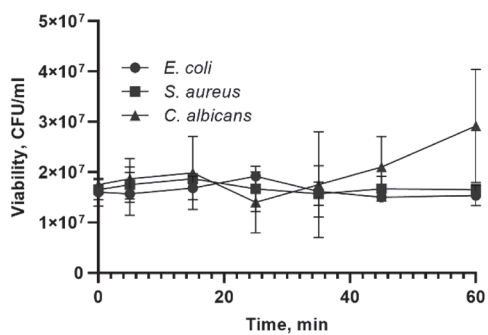
Supplementary Figure 4. Maximal orthogonal projections of representative CLSM images of fixed 48 h oligotrophic *S. aureus* biofilm on uncoated surface (upper panel), sparse nano-ZnO surface (middle panel) and dense nano-ZnO (bottom panel). DNA/RNA stained with Syto9 (green channel, left column) and surface-associated amyloid fibers stained with Congo Red (red channel, middle column). Combined channel view in right column. Scale bars represent 10 μm.



Supplementary Figure 5. Maximal orthogonal projections of representative CLSM images of fixed 48 h growth medium *S. aureus* biofilm on uncoated surface (upper panel), sparse nano-ZnO surface (middle panel) and dense nano-ZnO (bottom panel). DNA/RNA stained with Syto9 (green channel, left column) and surface-associated amyloid fibers stained with Congo Red (red channel, middle column). Combined channel view in right column. Scale bars represent 10 μm .



Supplementary Figure 6. Water contact angles of uncoated, nano-ZnO and nano-ZnO/Ag surfaces. The angles were measured from photos taken 5 sec after pipetting 5 μ l of water to each surface, using Contact Angle plugin (author Marco Brugnara) in ImageJ software [1]. ns – not statistically significant



Supplementary Figure 7. Microbial viability in biofilm harvesting medium (0.5x SCDLP with 1.5M NaCl, Table 1). 15 ml microbial was vortexed for 30 sec, sonicated for 0-60 min, vortexed again for 30 sec, serially diluted and plated for counting. Harvesting protocol in 0.5x SCDLP with high salt concentration did not significantly affect microbial viability after 15 min sonication compared to the initial suspension ($P \geq 0.05$).

Supplementary Table 1. Zn and Ag content in the nano-ZnO and nano-ZnO/Ag surfaces; theoretical maximum release into 5 ml microbial test medium. ND denotes “not detected”.

Surface coating	Zn μg/cm ²	SD	Max Zn release into 5 ml, μg/ml	SD	Ag ng/cm ²	SD	Max Ag release into 5 ml, ng/ml	SD
Uncoated	0.02	0.00	0.01	0.00	ND	ND	ND	ND
Sparse nano-ZnO	2.12	0.12	1.36	0.08	ND	ND	ND	ND
Sparse nano-ZnO/Ag	2.39	0.10	1.54	0.07	23.56	3.42	15.27	2.21
Dense nano-ZnO	18.00	0.70	11.65	0.45	ND	ND	ND	ND

References

- [1] C. A. Schneider, W. S. Rasband, and K. W. Eliceiri, “NIH Image to ImageJ: 25 years of image analysis,” *Nat Methods*, vol. 9, no. 7, pp. 671–675, Jul. 2012, doi: 10.1038/nmeth.2089.

Curriculum vitae

Personal data

Name: Merilin Rosenberg (previously Truusa)
Date and place of birth: 18.03.1984, Estonia
Citizenship: Estonian

Contact data

E-mail: rosenbergmerilin@gmail.com
Phone: +372 5268384

Education

2016–... PhD student (chemistry and biotechnology), Tallinn University of Technology
2005–2009 MSc (genetic engineering), University of Tartu
2002–2005 BSc (genetic engineering), University of Tartu
1991–2002 High school, Tallinn School No 21

Special courses

02.–13.04.2017 Study visit: “Assessment of the role of Cu ion release in efficacy of antimicrobial activity of copper-based surfaces”, University of Southampton, Southampton, UK
16.–19.05.2017 Course: “Alternative Approaches for Risk Assessment”, JRC (EURL ECVAM), Ispra, Italy
18.–22.09.2017 Course: “Nanotoxicology - potential risks of engineered nanomaterials to human health and the environment”, Karolinska Institutet, Stockholm, Sweden
20.11–19.12.2017 Study visit supported by COSTi Action CA15114 “AMiCl”: “Assessment of anti-biofilm activity of antimicrobial surfaces based on ZnO/Ag heterostructures”, University of Porto, Porto, Portugal
07.10.2018 Workshop: “Imaging and Quantifying Biofilms” preceding the 8th ASM Biofilms conference, Washington DC, USA
08.–12.04.2019 Course: “COST AMiCl and PRINT-AID ETN Training School: Antimicrobial Coatings”, University of Amsterdam, Amsterdam, Netherlands
03.09.2019 Workshop: “In vitro biofilm methods” preceding the Eurobiofilms 2019 conference, Glasgow, UK.

Professional employment

2021–... University of Tartu, Institute of Molecular and Cell Biology, specialist (antimicrobial surface coatings)
2018–2021 National Institute of Chemical Physics and Biophysics, Laboratory of environmental toxicology, junior researcher

2011–2012	Health Board, Laboratory of Infectious Diseases, head of laboratory
2008–2011	Tallinn University of Technology, Faculty of Science, Centre for Biology of Integrated Systems, engineer (environmental metagenomics)
2008–2011	BiotaP OÜ, specialist (environmental metagenomics), head of laboratory
2007–2008	Veterinary and Food Laboratory, chief specialist (molecular diagnostics), head of department of molecular analysis

List of publications

Vihodceva, S.; Šutka, A.; Sihtmäe, M.; **Rosenberg, M.**; Otsus, M.; Kurvet, I.; Smits, K.; Bikse, L.; Kahru, A.; Kasemets, K. (2021). Antibacterial activity of positively and negatively charged hematite (α -Fe₂O₃) nanoparticles to *Escherichia coli*, *Staphylococcus aureus* and *Vibrio fischeri*. *Nanomaterials*, 11(3), 652. DOI:10.3390/nano11030652

Spiridonova, J.; Mere, A.; Krunk, M.; **Rosenberg, M.**; Kahru, A.; Danilson, M.; Krichevskaya, M.; Oja Acik, I. (2020). Enhanced visible and ultraviolet light-induced gas-phase photocatalytic activity of TiO₂ thin films modified by increased amount of acetylacetone in precursor solution for spray pyrolysis. *Catalysts*, 10 (9). DOI:10.3390/catal10091011

Rosenberg, M.; Visnapuu, M.; Vija, H.; Kisand, V.; Kasemets, K.; Kahru, A.; Ivask, A. (2020). Selective anti-biofilm properties and biocompatibility of nano-ZnO and nano-ZnO/Ag coated surfaces. *Scientific Reports*, 10(1). DOI:10.1038/s41598-020-70169-w

Rosenberg, M.; Ilić, K.; Juganson, K.; Ivask, A.; Ahonen, M.; Vinković Vrček, I.; Kahru, A. (2019). Potential ecotoxicological effects of antimicrobial surface coatings: a literature survey backed up by analysis of market reports. *PeerJ*, 7 (e6315). DOI: 10.7717/peerj.6315.

Rosenberg, M.; Azevedo, N.F.; Ivask, A. (2019). Propidium iodide staining underestimates viability of adherent bacterial cells. *Scientific Reports*, 9(1). DOI: 1038/s41598-019-42906-3.

Rahmani, R.; **Rosenberg, M.**; Ivask, A.; Kollo, L. (2019). Comparison of mechanical and antibacterial properties of TiO₂/Ag ceramics and Ti6Al4V-TiO₂/Ag composite materials using combined SLM-SPS techniques. *Metals*, 9 (874). DOI: 10.3390/met9080874.

Visnapuu, M.; **Rosenberg, M.**; Truska, E.; Nõmmiste, E.; Šutka, A.; Kahru, A.; Rähn, M.; Vija, H.; Orupõld, K.; Kisand, V.; Ivask, A. (2018). UVA-induced antimicrobial activity of ZnO/Ag nanocomposite covered surfaces. *Colloids and Surfaces B: Biointerfaces*, 169, 222–232. DOI: 10.1016/j.colsurfb.2018.05.009.

Rosenberg, M.; Vija, H.; Kahru, A.; Keevil, C. W.; Ivask, A. (2018). Rapid *in situ* assessment of Cu-ion mediated effects and antibacterial efficacy of copper surfaces. *Scientific Reports*, 8 (8172). DOI: 10.1038/s41598-018-26391-8

Moor, M.; Berger, S.; Davison, J.; Öpik, M.; Bommarco, R.; Bruelheide, H.; Kühn, I.; Kunin, W.E.; Metsis, M.; Rortais, A.; Vanatoa, A.; Vanatoa, E.; Stout, J.C.; **Truusa, M.**; Westphal, C.; Zobel, M.; Walther, G.-R. (2011). Alien plants associate with widespread generalist arbuscular mycorrhizal fungal taxa: evidence from a continental-scale study using massively parallel 454 sequencing. *Journal of Biogeography*, 38 (7), 1305–1317. DOI: 10.1111/j.1365-2699.2011.02478.x.

Elulookirjeldus

Isikuandmed

Nimi: Merilin Rosenberg (end. Truusa)
Sünniaeg ja -koht: 18.03.1984, Eesti
Kodakondsus: Eesti

Kontaktandmed

E-post: rosenbergmerilin@gmail.com
Tel.: +372 5268384

Hariduskäik

2016–... doktoriõpe (keemia ja biotehnoloogia), Tallinna Tehnikaülikool
2005–2009 MSc (geenitehnoloogia), Tartu Ülikool
2002–2005 BSc (geenitehnoloogia), Tartu Ülikool
1991–2002 Keskkharidus, Tallinna 21. Kool

Täiendusõpe

02.–13.04.2017 Laborivisiit: “Assessment of the role of Cu ion release in efficacy of antimicrobial activity of copper-based surfaces”, Southamptoni Ülikool, Southampton, Suurbritannia
16.–19.05.2017 Kursus: “Alternative Approaches for Risk Assessment”, JRC (EURL ECVAM), Ispra, Itaalia
18.–22.09.2017 Kursus: “Nanotoxicology - potential risks of engineered nanomaterials to human health and the environment”, Karolinska Ülikool, Stockholm, Rootsi
20.11–19.12.2017 Laborivisiit COSTi tegevuse CA15114 “AMiCI” raames: “Assessment of anti-biofilm activity of antimicrobial surfaces based on ZnO/Ag heterostructures”, Porto Ülikool, Porto, Portugal
07.10.2018 Töötuba: “Imaging and Quantifying Biofilms” 8th ASM Biofilms konverentsi raames, Washington DC, Ameerika Ühendriigid
08.–12.04.2019 Kursus: “COST AMiCI and PRINT-AID ETN Training School: Antimicrobial Coatings”, Amsterdami Ülikool, Amsterdam, Holland
03.09.2019 Töötuba: “In vitro biofilm methods” Eurobiofilms 2019 konverentsi raames, Glasgow, Suurbritannia.

Teenistuskäik

2021–... Tartu Ülikool, molekulaar- ja rakubioloogia instituut, antimikroobsete pinnakatete spetsialist
2018–2021 Keemilise ja Bioloogilise Füüsika Instituut, keskkonnatoksikoloogia labor, nooremteadur
2011–2012 Terviseamet, nakkushaiguste labor, labori juhataja

2008–2011	Tallinna Tehnikaülikool, loodusteaduskond, integreeritud süsteemide bioloogia keskus, insener (keskkonna metagenoomika)
2008–2011	BiotaP OÜ, spetsialist (keskkonna metagenoomika), laborijuhataja
2007–2008	Veterinaar- ja Toidulaboratoorium, peaspetsialist (molekulaardiagnostika), molekulaaranalüüsi osakonna juhataja

Publikatsioonid

Vihodceva, S.; Šutka, A.; Sihtmäe, M.; **Rosenberg, M.**; Otsus, M.; Kurvet, I.; Smits, K.; Bikse, L.; Kahru, A.; Kasemets, K. (2021). Antibacterial activity of positively and negatively charged hematite (α -Fe₂O₃) nanoparticles to *Escherichia coli*, *Staphylococcus aureus* and *Vibrio fischeri*. *Nanomaterials*, 11(3), 652. DOI:10.3390/nano11030652

Spiridonova, J.; Mere, A.; Krunks, M.; **Rosenberg, M.**; Kahru, A.; Danilson, M.; Krichevskaya, M.; Oja Acik, I. (2020). Enhanced visible and ultraviolet light-induced gas-phase photocatalytic activity of TiO₂ thin films modified by increased amount of acetylacetone in precursor solution for spray pyrolysis. *Catalysts*, 10 (9). DOI:10.3390/catal10091011

Rosenberg, M.; Visnapuu, M.; Vija, H.; Kisand, V.; Kasemets, K.; Kahru, A.; Ivask, A. (2020). Selective anti-biofilm properties and biocompatibility of nano-ZnO and nano-ZnO/Ag coated surfaces. *Scientific Reports*, 10(1). DOI:10.1038/s41598-020-70169-w

Rosenberg, M.; Ilić, K.; Juganson, K.; Ivask, A.; Ahonen, M.; Vinković Vrček, I.; Kahru, A. (2019). Potential ecotoxicological effects of antimicrobial surface coatings: a literature survey backed up by analysis of market reports. *PeerJ*, 7 (e6315). DOI: 10.7717/peerj.6315.

Rosenberg, M.; Azevedo, N.F.; Ivask, A. (2019). Propidium iodide staining underestimates viability of adherent bacterial cells. *Scientific Reports*, 9(1). DOI: 1038/s41598-019-42906-3.

Rahmani, R.; **Rosenberg, M.**; Ivask, A.; Kollo, L. (2019). Comparison of mechanical and antibacterial properties of TiO₂/Ag ceramics and Ti₆Al₄V-TiO₂/Ag composite materials using combined SLM-SPS techniques. *Metals*, 9 (874). DOI: 10.3390/met9080874.

Visnapuu, M.; **Rosenberg, M.**; Truska, E.; Nõmmiste, E.; Šutka, A.; Kahru, A.; Rähn, M.; Vija, H.; Orupõld, K.; Kisand, V.; Ivask, A. (2018). UVA-induced antimicrobial activity of ZnO/Ag nanocomposite covered surfaces. *Colloids and Surfaces B: Biointerfaces*, 169, 222–232. DOI: 10.1016/j.colsurfb.2018.05.009.

Rosenberg, M.; Vija, H.; Kahru, A.; Keevil, C. W.; Ivask, A. (2018). Rapid *in situ* assessment of Cu-ion mediated effects and antibacterial efficacy of copper surfaces. *Scientific Reports*, 8 (8172). DOI: 10.1038/s41598-018-26391-8

Moor, M.; Berger, S.; Davison, J.; Öpik, M.; Bommarco, R.; Bruelheide, H.; Kühn, I.; Kunin, W.E.; Metsis, M.; Rortais, A.; Vanatoa, A.; Vanatoa, E.; Stout, J.C.; **Truusa, M.**; Westphal, C.; Zobel, M.; Walther, G.-R. (2011). Alien plants associate with widespread generalist arbuscular mycorrhizal fungal taxa: evidence from a continental-scale study using massively parallel 454 sequencing. *Journal of Biogeography*, 38 (7), 1305–1317. DOI: 10.1111/j.1365-2699.2011.02478.x.

ISSN 2585-6901 (PDF)
ISBN 978-9949-83-795-3 (PDF)